NOTICE

The quality of this microform is heavily dependent upon the quality of the original thesis submitted for microfilming. Every effort has been made to ensure the highest quality of reproduction possible.

If pages are missing, contact the university which granted the degree.

Some pages may have indistinct print especially if the original pages were typed with a poor typewriter ribbon or if the university sent us an inferior photocopy.

Previously copyrighted materials (journal articles, published tests, etc.) are not filmed.

Reproduction in full or in part of this microform is governed by the Canadian Copyright Act, R.S.C. 1970, c. C-30.

AVIS

La qualité de cette microforme dépend grandement de la qualité de la thèse soumise au microfilmage. Nous avons tout fait pour assurer une qualité supérieure de reproduction.

S'il manque des pages, veuillez communiquer avec l'université qui a conféré le grade.

La qualité d'impression de certaines pages peut laisser à désirer, surtout si les pages originales ont été dactylographiées à l'aide d'un ruban usé ou si l'université nous a fait parvenir une photocopie de qualité inférieure.

Les documents qui font déjà l'objet d'un droit d'auteur (articles de revue, tests publiés, etc.) ne sont pas microfilmés.

La reproduction, même partielle, de cette microforme est soumise à la Loi canadienne sur le droit d'auteur, SRC 1970, c. C-30.

Canada

DYNAMIC INTERFACIAL TENSION OF FINITE REACTIVE SYSTEMS RELATED TO ENHANCED OIL RECOVERY

by

CHRIS I. CHIWETELU

A Thesis submitted in partial fulfillment of the requirement

for the degree of DOCTOR OF PHILOSOPHY

in the

DEPARTMENT OF CHEMICAL ENGINEERING,

UNIVERSITY OF OTTAWA.

OTTAWA , CANADA , 1988

ISBN 0-315-46740-1

UNIVERSITÉ D'OTTAWA
UNIVERSITY OF OTTAWA

Abstract

In enhanced oil recovery by caustic waterflooding , carboxylic acids present in the crude oil react with the caustic reagents of the flood water resulting in the in-situ formation of surface active soap anions. The formation of the active soap species , its accumulation at the interface and subsequent desorption to the bulk oleic and aqueous phases are all influenced by the age of the interface . This accounts for the fact that such reactive systems exhibit the so-called dynamic interfacial tension phenomenon . In order to understand precisely the mechanisms that govern the interaction of carboxylic acids with caustic reagents , we must have a precise and accurate method of measuring dynamic interfacial tension (IFT) . To this end , we have developed a novel experimental scheme , namely , photo-micropendography . Tensions in the range of 1–40 mN/m were readily measured by this experimental scheme for dilute solutions of oleic and lauric acids in hexadecane contacted with a spectrum of NaOH solutions up to 250 mM . A comparison of data obtained by micropendography with those obtained by spinning drop and ring tensiometries suggested that the former gave the most reliable and consistent IFT over a wide range of values . In particular, tension measurements could be made at interfacial ages as low as 5 seconds and as high as 30 minutes .

Long chain fatty acids are practically insoluble in neutral water . As a result , conventional methods for determining acid ionization constants are inapplicable . The proposed equilibrium model for the interaction of single acids with various caustic solutions enables such important

ionization properties to be determined with the aid of nonlinear regression analysis . In addition , a precise estimate of the equilibrium constant governing the formation of the non-dissociated , inactive soap complex could be obtained from the proposed equilibrium model . In order to explain the dynamic interfacial behaviour associated with single acids reacting with a range of various aqueous caustic solutions , a diffusive-kinetic model has been proposed . The model details the important interfacial reactions as well as the predominant interfacial species . Species transport from the bulk to the interface was modelled by the Nernstian theory . For interfacial sorption kinetics , use was made of the Langmuirian theory complemented by Gouy-Chapman's electrical double layer model . The dynamic model equations consisted of a set of coupled , nonlinear ordinary differential equations supplemented with another set of global , algebraic relationships all of which had to be solved simultaneously for the applicable surfactant surface concentration . Good estimates of the adsorption rate constants which were the model parameters , were obtained by correlating the experimental IFT data with the aid of a sensitivity analysis of the problem .

Armed with the pertinent parameters from the single component equilibrium and dynamic models , a generalized dynamic model has been advanced in order to rationalize the interaction of a multi-component acid mixture contacting a spectrum of NaOH solutions . A detailed analysis for binary mixtures of oleic and lauric acids reacting with a range of different caustic concentrations has been carried out in order to demonstrate the validity of the proposed multi-component model . Parameter values were determined for each constituent acid from separate equilibrium and dynamic single component studies . By using these values in the solution of the multi-component model equations , it was possible to obtain theoretical values of the dynamic IFT of the mixture . Such model predictions were compared with experimental data and the agreement was generally satisfactory . The unifying approach to the study of the dynamic interfacial tension in reactive systems

which has been adopted in this work coupled with the close agreement between model predictions and experimental data constitutes a significant contribution in the on-going efforts to understand how crude oil acids interact with caustic reagents to effect drastic lowering of the oil/water interfacial tension. We are now confident that if the dominant acids present in the crude oil can be quantitatively identified , models such as those proposed in this work can be used to design caustic slugs that will be effective throughout the duration of the flood .

Acknowledgement

Very many people both within and outside the university made important contributions to this work . It is extremely difficult for me to mention everyone of these people without adding a second volume to the text . I am particularly overwhelmed by the immense support and encouragement provided by the professors , support staff and students of the chemical engineering department . My two supervisors , namely , Drs. G. Neale and V. Hornof , worked tirelessly throughout the various phases of the project . Their support and encouragement contributed immensely to the successful completion of the work . Dr. W. Hayduk provided an early and timely clue to the maze of experimental difficulties that we encountered early in the project , while Dr. D. McLean spent valuable time reviewing the models and offering constructive suggestions . Our able technical support team of Messrs Gasperetti , Lefebvre and Bonaldo worked feverishly for several months as we tried to perfect the experimental scheme .

Outside the department , help has also come from different sources . Messrs Ed Hearn of the Department of Geology , and Ken Ginn of Bill's Camera Craft Ltd. assisted me a lot in solving some optical problems associated with the experimental scheme . Emeritus Prof. K. Laidler of the Department of Chemistry , and Prof. M. Kates of the Biochemistry Department provided useful information on the ionization properties of fatty acids . From outside the University of Ottawa, the author acknowledges with gratitude the assistance of Dr. Y. Rotenberg of the Department

of Mechanical Engineering , University of Toronto , in promptly sending me a copy of the RBN algorithm . Prof. C.J. Radke of the University of California , Berkeley , gave me very useful leads in tackling the modelling aspects of the work . Prof. D.T. Wasan and Dr. R. Borwankar both of Illinois Institute of Technology , Chicago , provided prompt replies to some questions that I raised with regards to their work on crude oil -caustic systems .

Financial support for this work was provided by the Natural Sciences and Engineering Research Council of Canada (NSERC) , and the University of Ottawa ; the latter being in the form of an entrance/research scholarship . I am also grateful to the government of Ontario for two consecutive OGS awards . Finally , I wish to thank my wife Vic and our three kids for their invaluable support and encouragement throughout the programme .

Contents

List of Tables

List of Figures

Nomenclature

a	capillary constant appearing in Adams-Bashforth formula (Equation 6.3)
a_c	activity ratio defined in the Cratin Equation (Equation 4.5)
A	surface area per molecule, $Å^2$
A_o	minimum surface area per molecule, $Å^2$
A_s	surface area , m^2
b	radius of curvature at the drop's apex
B	adsorption or desorption rate constants
c, C	molar concentrations
d^*	drop diameter of the spinning drop
d_e	drop diameter at the equator
d_s	drop diameter at height, $Z = d_e$
D_{AB}	diffusion coefficient, cm^2/s
D_c	dielectric constant of water
D_i	diffusion coefficient, m^2/hr
e	error function defined in the RBN algorithm
E	objective function
EQUBR	equilibrium

f	surface coverage by the adsorbed species
f_c	species mole fraction defined in the Cratin Equation (Equation 4.5)
$\vec{h}$	vector of differential equations
H	Hessian matrix of partial derivatives
H_n	drop shape parameter
H_c	Henry's law constant
HD	Hexadecane
J	Jacobian matrix
k	Boltzman constant
k_i	sorptive rate constants
$K_{a,c}, K_{b,c}$	equilibrium constants in the Cratin equation
K_{ap}	cell constant of the Anton Parr densimeter
K_a	acid dissociation constant
K_D	salt distribution ratio water/oil
K_i	sorptive equilibrium constants
K_g	global equilibrium parameter of the deZabala's model
K_p	acid distribution ratio oil/water
K_s	equilibrium constant associated with species, NaA
K_{s1}	inactive soap dissociation constant
K_{s2}	inactive soap distribution ratio
K_w	ionic product of water

l	number of run replicates
M	molecular weight
M_s	total number of components in the mixture
n_c	number of CH_2 groups in the hydrocarbon chain
N	Avogadro number
$\vec{Q}$	vector of dimensionless parameters in the RBN algorithm
r	radius of sphere of same volume as the oil droplet
R	universal gas constant
R_1, R_2	principal radii of curvature of a drop
$R_{(a,i)}$	net rate of adsorption/desorption of species,i
s	arc length parameter of the RBN algorithm
$\vec{s}$	vector of state variables
$\vec{s_o}$	vector of initial values of state variables
S	shape parameter
t	time
T	temperature in K
u	run number
v	velocity
V	phase volume, droplet volume
V_A, V_b	solute molar volumes
V_c	solute critical volumes
w	desorption energy per mole.per CH_2 group
W	total energy of desorption per mole

x	horizontal coordinate in the RBN algorithm
$\vec{x}$	vector of independent variables
X	mole fraction
$\mathcal{X}_o$	width dimension in spinning drop tensiometry
$\mathcal{Y}_o$	length dimension in spinning drop tensiometry
z	ionic valency

SUBSCRIPTS

HC	hydrocarbon
HX	acid species
i	phase identity, mixture constituents
NaX	inactive soap species or salt
o	intial state, oleic phase
r	electrical repulsion
s	sub-layer, steric
w,W	water, aqueous phase
x, X	anion , surfactant

GREEK LETTERS

α	association parameter defined in the dynamic model
β	shape parameter of the Adams-Bashforth formula
δ	Nernstian film thickness
η	dynamic viscosity
ϵ, ϵ^*	exponents of the Hayduk-Minhas correlations
ε	electronic charge
γ	interfacial tension, mN/m
Γ	surface concentration of adsorbed species
Γ_{max}	saturation adsorption, mole/m^2
λ	rate parameters of the Rubin-Radke model
μ	chemical potential
ν^*	kinematic viscosity
ν	degrees of freedom of the T and F distributions
ω	angular velocity of rotating drop
ω_d	association parameter in the Wilke-Chang correlation
ϕ	turning angle in the Adams-Bashforth formula
ψ_G	the Gouy surface potential, mV
ψ_o	interfacial potential, mV
Π	surface pressure, mN/m
ρ	density
σ	surface charge density
θ	parameters of the regression problem
θ_c	contact angle
ζ	electrophoretic mobility

Chapter 1

Introduction

1.1 Enhanced Oil Recovery Practice

The production of medium to low viscosity crude oils from sub-terranean reservoirs is conventionally carried out by drilling wells right down to the oil bearing zone . The large pressure difference between the formation and the well head is often sufficient to ensure continued flow of oil for several years . However , as more and more of the oil and the associated formation water are produced , the reservoir pressure is reduced to the point where additional forces are needed to induce flow . At this point , waterflooding is initiated in what are generally referred to as secondary recovery[1,2] operations . Secondary waterflooding may achieve an additional 5 to 10% recovery of the original oil in place . Thus, well over 50% of the oil initially saturating the reservoir remains unproduced even after waterflooding . In order to overcome the large capillary forces trapping the oil in the reservoir matrix , surfactants are added to the flood water thus giving rise to the so-called Micellar[2] processes . Micellar processes are usually conducted as tertiary recovery operations[1,2] (following secondary waterflooding) . The efficacy of the micellar flood is greatly improved by injecting a polymer solution immediately after the surfactant slug . The polymer buffer bank provides the

necessary mobility control which ensures an efficient sweep of the reservoir .

Despite high oil recoveries from micellar floods in laboratory tests , actual field trials have been largely disappointing . It is now very doubtful if such recovery processes can be economical at current world oil prices . Besides , surfactant floods are limited to moderately viscous crudes and fairly high permeabilities . Canadian crude oil reserves are largely in the form of very viscous heavy oils and tar sands. Heat is required in order to initiate flow of heavy oils and this is achieved by hot water/steam injection or by in-situ combustion . Heavy crudes generally contain significant amounts of carboxylic acids and other reactive agents . Thus by adding simple caustic reagents to the flood water , surfactant soap species are produced in-situ , by the reaction between the acids and the caustic agents . It is the presence of such in-situ produced surfactants that accounts for the proven efficacy of caustic waterflooding of heavy oil reservoirs .

1.2 Dynamic Interfacial Tension and Oil Recovery

Surfactants in general are adsorbed at the oil-water interface and can thus reduce the interfacial tension (IFT) . A significantly reduced interfacial tension is required to overcome the capillary forces retaining residual oil within the reservoir matrix . Recent laboratory studies have shown that the IFT arising from the interaction of acids in the crude oil with caustic reagents in the flood water exhibits a marked dependence on the time of contact between the two phases , as well as on the composition of the crude oil and the caustic concentration of the flood water . Oftentimes , the IFT starts off low , but rises subsequently to much higher values as the interface ages . To date , the exact mechanism of dynamic interfacial tension in reactive systems is poorly understood . Yet, this basic knowledge is fundamental to the successful design of caustic floods and thus deserves a considerable degree of research effort .

1.3 Objectives of this Study

The first task in seeking to understand the phenomenon of dynamic interfacial tension is to develop an accurate and reliable method for its measurement . This is the primary objective of this study . Because the identity of interfacially active acids present in crude oils is yet to be firmly established, this investigation deals primarily with artificial oleic phases in which long chain fatty acids , namely C12 and C18 , have been dissolved . The working oleic solvent was hexadecane and a broad spectrum of caustic concentrations up to 250 mM formed the aqueous phase . This working concentration range was selected based on average caustic levels employed in actual field trials as well as all possible effective concentrations as the flood progresses through the reservoir . It is envisaged that the initial caustic level of the flood water would be reduced by as much as 70% due to dilution by the connate water , reaction with reservoir fluids and adsorption and ion exchange with matrix minerals .

In Part I of this report , we summarize current theories and models of crude/caustic interactions. Details of the experimental system which has been developed are presented in Part II . Part III deals with the proposed equilibrium and dynamic models governing the interaction of single acid species with a spectrum of caustic concentrations . The extension of the dynamic model to the case of multicomponent acid mixtures is treated in Part IV . Part V discusses the experimental data and model predictions .

Part I

Literature Review

Chapter 2

The Role of Caustic Reagents in Enhanced Oil Recovery

2.1 Caustic Reagents and IFT Reduction

Campbell[3,4] stated that sodium silicate , sodium hydroxide , sodium carbonate and sodium phosphate are the most widely-used reagents for alkaline waterflooding . In some instances , these reagents are used merely as a preflush in the removal of multivalent cations from the reservoir matrix . However , in the majority of cases[5] , alkaline agents are added to the flood water with a view to achieving additional oil recovery by the interaction of the alkali with the carboxylic acids present in the crudes . Because of the higher alkalinity associated with sodium hydroxide and sodium orthosilicate , these are the prevalent alkaline flood reagents . Several researchers[6–9] have reported IFT values below 0.01 mN/m when crudes were contacted with caustic solutions. Consequently , it was suggested that ultra-low IFT was necessary for enhanced oil recovery by caustic waterflooding . Cooke et al. [10] opined that the IFT should at least be below 2.0 mN/m for additional oil to be recovered from a caustic flood .

Recent investigations[11–17] have shown that the IFT of acidic crude oil-caustic systems varies both with time and temperature . Indeed , according to Castor et al. [11] an ultra-low IFT might not be attainable under actual reservoir conditions . They suggested a most probable IFT range of 1–10 mN/m . This recent assertion of Castor et al. , fuelled the controversy among researchers as to the correct interpretation of laboratory IFT data . Some workers argue that equilibrium IFT data are valid in actual field situations , while others contend that the minimum IFT obtained in dynamic measurements is the most applicable value . deZabala [18,19] obtained IFT data from multiple contacting of a fixed alkaline solution with fresh acidic crude oil . These IFT values were much lower than in the single contact case , but the minima were closer to those of the single contact runs . deZabala thus concluded that dynamic IFT minima most closely represent actual field situations .

2.2 Mechanisms of Crude-Caustic Interactions

In a recent review , Johnson [20] outlined the various mechanisms which have been postulated for enhanced oil recovery by caustic waterflooding . These include:-

1 Emulsification and Entrainment[21].

2 Emulsification and Entrapment[8].

3 Wettability Reversal(oil wet to water wet)[22,23].

4 Wettability Reversal(water wet to oil wet) [10,24].

Recently , Castor et al. [11] added three more mechanisms ;

5 Partial Wettability Reversal from water wet to oil wet ,

6 Chromatographic Wettability Reversal ,

7 Emulsification and Coalescence.

These various mechanisms have been amply discussed in the literature . Two dominant concepts emerge from a rational evaluation of all these proposed mechanisms . The first one is that emulsification is necessary for the release of the oil ganglia from the reservoir matrix . Secondly , the wettability of the reservoir has to be altered in the direction which ensures that the released oil can be efficiently mobilized . It is important to stress that while emulsification is desirable in caustic waterflooding , too stable an emulsion is counter-productive . The oil droplets entrained in the emulsion must coalesce to form a stable oil bank , and this is only possible where the emulsion breaks up fairly easily . Pasquarelli and Wasan [17] found that asphaltenes in crude oils gave rise to rigid films . Dodd et al. [25] identified metalliferous substances in the form of pophyrin-metal complexes as the species responsible for surface film stability . Castor et al. [11] made a significant contribution in the area of the stability of emulsions formed by the interaction of caustic reagents with acidic crudes . They reported that alkaline $Ca(OH)_2$ produced as much as 44% of the waterflood residual oil , and this they attributed to the enhanced instability of the in-situ formed emulsion . Before this significant finding , divalent cations have been associated with poor oil recoveries due mainly to severe caustic losses following the exchange of the Na^+ ions in the flood water with the Ca^+, Mg^+ ions of the reservoir matrix . Bunge and Radke [26] discussed in detail the mechanisms of simultaneous ion exchange and multivalent cation precipitation . They concluded that such phenomena could indeed enhance oil recovery by substituting monovalent cations for the divalent ones present in the reservoir rock surfaces. Dormani [27] obtained significant additional oil recoveries when small amounts of divalent salts were added to the injected aqueous phase .

2.3 Salinity Effects

The role of salinity in caustic waterflooding has been extensively investigated [7,8-10,14-16,28-31]. Cooke et al. [10] surmised that the presence of brine was required for oil recovery by the wettability reversal (water wet to oil wet) mechanism . On the contrary, wettability reversal from oil wet to water wet is favored in low salinity environments . As far as IFT reduction goes , high salinity has been consistently shown to be detrimental . The only good effect of salinity at low concentrations is that it reduces the amount of caustic required to achieve the same reduction in IFT . Beyond a very narrow concentration range , salinity may increase IFT by several orders of magnitude . The optimum salinity according to Bansal et al. [30] corresponds to the maximum in the surface charge density . At higher NaCl levels , the surface charge density drops , IFT increases as the surface active species are desorbed in the form of undissociated soap . Chan and Yen [28,29,31] came to similar conclusions following several laboratory investigations . Bansal et al. [30] also found that excessive levels of caustic have similar unfavorable effects as high salinity . On the basis of these findings , we believe that salinity considerations may be safely excluded in laboratory investigations aimed at gaining an insight into the mechanisms of crude- caustic interactions .

Chapter 3

Ionization and Interfacial Properties of Fatty Acids

3.1 Crude Oil Carboxylic Acids

A knowledge of crude oil carboxylic acid chemistry is obviously desirable if the complex interactions occurring between these acids and caustic reagents are to be properly understood . We need to know with certainty the identity of these acids and especially that of the dominant surface-active species . Additionally , we have to be able to understand at least the interfacial properties of such acids both individually and as mixtures . Some work has been done in this area but a lot more is still needed . Lochte[32] articulated the available information on crude oil acids and stated that both phenols and fatty acids were present . The fatty acids themselves comprised of small and long chain aliphatic components , as well as C5 naphthenic acids . Credit for the in-depth elucidation of crude oil fatty acid chemistry must go to Seifert and his co-workers[33–37]. These workers employed the state-of-the art analytical techniques such as UV , IR and high resolution mass spectrometry as well as column and gel-permeation chromatography , in their extensive analyses of Californian crude

oils. They identified both straight and branched aliphatic acids among several other classes of acids. The molecular weight of the interfacially-active acids ranged from 200-700 . Seifert and Teeter[33] positively identified mono and poly-cyclic naphthenic acids as well as aromatic components . Also positively identified were C18 acids both straight and branched , and to a less extent hetero-cyclics.

Jang et al. [38] also contributed to our present knowledge of crude oil acid chemistry . They found that aliphatic acids both saturated and unsaturated of chain length in the range C8 -C18 were present as well as naphthenics and di-aromatics . Dunning et al. [39] positively correlated crude oil interfacial activity with Ni-porphyrin complexes often associated with asphaltenes . Khulbe et al. [15] found significant interfacial activity even with the maltene fractions . The latter authors concluded that asphaltenes per se were not responsible for all of the interfacial phenomena associated with crude oil-caustic systems . Indeed , the study of asphaltenes and maltenes provides only a rough indication of the amount of polar species present in the crude . There does not appear to be a better alternative to the rigorous and painstaking approach adopted by Seifert and his co-workers, for the unequivocal identification of the surface active species that are involved in crude/caustic interactions .

3.2 The Ionization and Interfacial Behaviour of Fatty Acids

Much of what is known today about the properties of fatty acids has been well documented in the series edited by Markley[40] . Fatty acids in general exhibit marked variation in physical properties with increasing chain length and increasing degree of unsaturation . Although hundreds of naturally occurring fatty acids have been identified , their physical properties are not available in the literature except for the shorter chain , aliphatic acids whose chain lengths are less than 10 CH_2 groups . For caustic enhanced oil recovery , longer chain paraffinics and naphthenics are

more relevant , but regrettably , very little is reported on important physical characteristics such as solubility , viscosity , vapor pressures and boiling points . Even where such information is reported, the data are oftentimes misleading.

3.2.1 Interfacial Properties

Fatty acid monolayers have been extensively studied especially for the C10–C18 straight, paraffinic subclass [41–48] . In general , films of unsaturated fatty acids spread either on air-water , or oil-water interfaces are more expanded than their saturated counterparts . For films of monolayers of C18 fatty acids , Welles[45] reported that expansion increases in the order ;

saturated < trans-ethylenic < cis-ethylenic < acetylenic . Welles also found that the degree of expansion was influenced (though to a lesser extent) by the position of the double and triple bonds of ethylenic and acetylenic acids, respectively . Terminal double or triple bonds tend to enhance the spreading of the acid in water and this has been explained by the dominance of chain-water over chain-chain interactions . Depending on the structure of the acid , these chain-chain and chain-solvent interactions may result in significant aggregation when the film is compressed . Tanford [41] opined that fatty acids tend to associate into dimers both in the organic phase and as anionic aggregates in alkaline solutions .

3.2.2 Ionization of Fatty Acids

Ionization of acids generally is quantified in terms of a dissociation or ionization constant (usually a pK value) . Such parameters are determined by potentiometric titrations of aqueous solutions of the acid using standardized HCl or KOH [49,50] . Beyond the pK_a range of 2–11 , Albert and Serjeant [50] recommend the use of spectrophotometric or conductometric methods . Other methods for measuring the ionization constant of fatty acids include Raman and magnetic resonance

spectroscopy as well as thermometric titrations . Despite the availability of these analytical methods, only pK_a values of paraffinic acids up to C10 are readily available in the literature . Higher chain acids are practically insoluble in water, thus making the use of the above analytical methods unworkable . Consequently , the usual recourse is to estimate the K_a values from surface pressure data obtained by spreading the acid on an oleic-alkaline aqueous interface .

Patil et al.[46] studied the interfacial behaviour of palmitic and oleic acids spread at constant pressures in buffered alkaline solutions kept at a constant ionic strength . They reported apparent pK_a for the acids in the range of 8.6–9.9 , and further showed that the pK_a value was influenced by the electrical field strength of the acid film as well as by H , pH and the ionic strength of the aqueous solution . Ramakrishnan and Wasan [51] developed an equilibrium model with which they obtained pK_a values for crude oil acids in the range of 10–12 . They maintained that their predicted K_a values were in the range suggested by deZabala and Radke [19] . Trujillo [13] employed the Cratin correlation [52] and obtained much higher pK_a values (11–13) for the crude oil system which he studied . Hejl and Levorova [53] studied the ionization of oleic acid at concentrations ranging from 10^{-1} to 5.0×10^{-3} N . They reported K_a values of the order of 10^{-10} to 10^{-11} , but they added that the K_a values depended on pH and the oleate concentration . Chan and Yen[31] adduced that the probable pK_a of crude oil acids is 9 ; a much lower value than the figures quoted by the above-named authors . Since the identity of the interfacially-active acids in the crude oils used by these authors was not established , the predicted K_a values must be treated with some reservation, especially when such predictions are made by assuming that one single , yet ill-defined species is to be representative of the acids present in the given crude . In such complex systems like crude oil , multi-component models are likely to yield more meaningful K_a values . The controversy surrounding the pK_a of crude oil acids or indeed of higher fatty acids in general , is far from being

resolved . Definitive theories that can adequately handle the complex chain-chain and chain-solvent interactions as well as interactions among various head groups are needed .

Chapter 4

Mechanisms and Models of Crude-Caustic Interactions

4.1 Models for the Transfer of Surfactants across Liquid-Liquid Interfaces

England and Berg[54] pioneered the recent efforts at quantitatively explaining the mechanisms of surfactant transport across the interface separating two immiscible liquid phases . Their analyses, though applicable to non-reacting liquid phases of infinite extent , showed that interfacial resistances signified by sorptive barriers were largely responsible for the phenomenon of dynamic interfacial tension . Mass transfer per se had relatively small effects on the observed IFT behaviour . The authors' use of Fickian diffusion to model what is essentially a convective diffusion problem is questionable , especially when Sherwood and Wei[55] had demonstrated the inadequacy of the simple diffusion theory in situations where convection currents were involved . Other researchers[56-59] have shed more light on the phenomenon of convective diffusion , the most notable contribution

being the treatise by Sawistowiski[58] . Sternling and Scriven[59] outlined very clearly the conditions under which interfacial convection would influence inter-phase mass transfer . The conditions are as follows :

1. solute transfer out of phase of higher viscosity ,
2. solute transfer out of phase of lower viscosity ,
3. situations where large differences in kinematic viscosity exist between the phases ,
4. cases where steep concentration gradients exist near the interface ,
5. when both phases have low diffusivities and viscosities ,
6. when surface-active species are absent from the interface ,
7. when the interfaces are of large extent .

In reacting systems such as the ones we have investigated ,all of the above conditions (except 6 above) are present. Under such conditions , Marangoni instabilities[58] are generated in the interface. Additionally, temperature gradients between the top and bottom parts of the measurement chamber reinforce the incidence of convective diffusion resulting in greatly increased mass transfer rates.

Rubin and Radke [60] extended the analyses of England and Berg[54] to the important case of phases of finite extent . This latter model did not address reactive systems , but the use of Nernstian theory[65] to model convective diffusion was particularly significant . Rubin and Radke[60] examined in detail the occurence of IFT minima in dynamic measurements of crude oil/caustic systems for cases in which the interfacial area and phase volumes remained unchanged. In a follow-up paper[61], the authors allowed for areal variations of the oil droplet spinning in

the capillary tube of the spinning drop tensiometer . Given the popularity of the spinning drop tensiometer[62-64] for dynamic IFT measurement , the work of Rubin and Radke[60,61] set the stage for modelling of crude/ caustic interactions using IFT data determined with the spinning drop tensiometer .

4.2 Equilibrium Models of Crude/Caustic Interactions

4.2.1 The Cratin Equation

Cratin [52] studied the variation of IFT with pH for crude oil asphaltenes and resins in acidic and alkaline aqueous media . He noted that significant IFT reduction occurred at both the low and high pH regimes . Consequently , Cratin proposed that a zwitter-ionic species (represented by $Z^{\pm}$), was the surfactant species involved. The zwitterion is itself not surface active but can be made so by hydrolysis as follows:

$$HZ^{+} + OH^{-} = Z^{\pm} + H_2O \tag{4.1}$$

with an associated equilibrium constant $K_{b,c}$. A second reaction occurs at low pH involving the anionic species , Z^{-} formed at high pH as follows:

$$Z^{-} + H^{+} = Z^{\pm} \tag{4.2}$$

The equilibrium constant , $K_{a,c}$, applies to equation 4.2 . Two other variables were defined by Cratin[52] as follows ;

a species-mole fraction , $f_{c,i}$, given by ;

$$f_{c,i} = \frac{[Z]_i}{[Z]_t} \tag{4.3}$$

where

$$Z_t = [Z^{-}] + [Z^{+}] + [Z^{\pm}] \tag{4.4}$$

and an interfacial activity , a_c , defined as ;

$$a_c = \frac{\gamma_o - \gamma_i}{\gamma_o} = \sum_{i=1}^{3} a_{c,i} f_{c,i} \tag{4.5}$$

Substituting for the various concentration and activity terms in equation 4.5 , followed by algebraic manipulations , Cratin[52] obtained the equation ;

$$\frac{\gamma_i}{\gamma_o} = 1.0 - \frac{a_-}{\left[1.0 + \frac{[H^+]}{K_{a,c}}\right]} \tag{4.6}$$

Equation 4.6 results from the vanishing of $a_\pm$, and the fact that at high pH , $K_{b,c} \rightarrow 0$. This was the form of the Cratin equation employed by Trujillo[13] in his equilibrium model .

4.2.2 The Equilibrium model of Chan and Yen

Chan and Yen [29] hypothesized that the spectrum of crude oil acids could be represented by a single (though ill-defined) species designated by **HA** . They associated a dissociation constant , K_a with this hypothetical acid , and further proposed an equilibrium constant , K_s , governing the formation of the tight , inactive soap species , NaA . A conservation equation for the active species, A^- , led to the final working equation , namely ;

$$[A^-] = \frac{[HA]_o}{\left(\frac{[H^+]}{K_a} + \frac{C_{Na^+}}{K_s} + 1\right)} \tag{4.7}$$

Chan and Yen suggested that K_s should be in the range of 10^{-2} to 1 , but they did not give any probable range for K_a .

4.2.3 The Equilibrium Chemical Model of deZabala

deZabala [18] used the HA concept proposed by Chan and Yen but he allowed for the partitioning of the acid between the oleic and aqueous bulk phases . The formation and subsequent dissociation

of the tight soap species , namely , NaA , was not considered by the author in the development of his model . Rather , deZabala[18] used a charge balance in the aqueous phase to relate C_A and the global equilibrium parameter , K_g , defined by

$$K_g = K_p K_w K_a;$$

with the final equation as follows ;

$$C_{A^-} = \frac{1}{2}\frac{C_{Na^+}}{\left(1+\frac{K_g}{(C_{HA})_o}\right)} + \frac{1}{2}\sqrt{\left(\frac{C_{Na^+}}{\left(1+\frac{K_g}{(C_{HA})_o}\right)}\right)^2 + \frac{4K_w(C_{HA})_o}{K_g}} \tag{4.8}$$

At high pH , equation 4.8 reduces to the following ;

$$C_{A^-} = \frac{C_{Na^+}}{\left(1+\frac{K_g}{(C_{HA})_o}\right)} \tag{4.9}$$

deZabala[18] suggested that K_p could be in the range of 10^3 to 10^4 , while K_a took values ranging from 10^{-10} to 10^{-12} .

4.2.4 The Equilibrium Model of Ramakrishnan and Wasan

The model proposed by Ramakrishnan and Wasan[51] was the only one of its kind to deal with the electrical properties of the interface . While retaining the HA acid representation of Chan and Yen[29] , these authors considered that the acid was initially partitioned to the aqueous side of the interface from where it ionized reversibly to give the active soap anions . They further proposed the following mechanism for the formation of the undissociated soap species NaA , and its subsequent partitioning to the oleic phase , viz ;

$$Na^+ + A^- \rightleftharpoons NaA_w \tag{4.10}$$

with an associated equilibrium constant K_{s1}, given by ;

$$K_{s1} = \frac{C_{Na^+}C_{A^-}}{C_{NaAw}} \tag{4.11}$$

The partitioning of NaA favours the oleic phase thus resulting in a distribution ratio given by ;

$$K_{s2} = \frac{C_{NaAw}}{C_{NaAo}} \ll 1 \tag{4.12}$$

By combining Equations 4.11 and 4.12 , a global constant K_s , was defined as follows :-

$$K_s = K_{s1}K_{s2} = \frac{C_{Na+}C_{A-}}{C_{NaAo}} \tag{4.13}$$

This seemingly radical treatment of the undissociated soap species appears to have been corroborated by the recent experimental results of Borwankar[66] . Earlier on , Sharma et al. [67] had argued on the basis of the work done by Lucassen[68] , that the undissociated soap species remained essentially in the interface with little tendency to desorb either to the oleic phase or to the aqueous medium .

4.3 . Dynamic Models of Crude-Caustic Interactions

4.3.1 Trujillo's Dynamic Model

Trujillo[13] proposed a dynamic model for the interaction of acidic crudes with caustic reagents which leaned heavily on the diffusive-kinetic analysis of England and Berg[54] . His IFT data were obtained with the aid of the spinning drop tensiometer but for times in excess of one hour . Trujillo argued that thermal and mechanical equilibrium of the oil droplet in the tensiometer would not be achieved at times earlier than one hour . The attainment of mechanical equilibrium in a reacting oil/water system is difficult to ascertain , but from published IFT data of crude/caustic systems , equilibrium is generally attained within 15 minutes of spinning in the tensiometer . The standard instruction[69] for the use of the spinning drop tensiometer for IFT measurement stipulates at least one hour of spinning . However , it must be remembered that the formation of the surface-active soap species and its subsequent kinetic-diffusive transfer to and from the interface are expected

to be reasonably fast . Trujillo may indeed have missed the important transient phase of the crude/caustic interactions .

In dealing with the interfacial reactions themselves , the author assumed quite rightly that the rates were several orders of magnitude greater than the rates of physical adsorption . Literature on the rates of dissociation of carboxylic acids[70–72] does indeed confirm this postulate . Hammett[70] stated that the rates of proton-transfer reactions were in the range of 10^{10} to 10^{11} l/mole-sec . Nuernberg and Duerbeck[70] affirmed that carboxylic acid recombination reactions are diffusion controlled and that the rate constants for such reactions should be of the order of 4×10^{10} l/mole-sec . Laidler[73] agreed with the latter assertion . The desorption rate constants predicted by Trujillo[13] were very much pH dependent . This too is hard to justify on the basis of conventional theories of chemical kinetics[74–77] .

4.3.2 The Model of Sharma , Jang and Yen

In their own treatment of dynamic IFT in crude/caustic systems , Sharma et al. [67] incorporated essentially all the requisite ingredients , such as convective diffusion , electrical interfacial effects and sorption kinetics . The problem with the model was that it included the relatively fast acid ionization steps to the detriment of the slower and thus rate determining sorptive kinetic steps . In addition , species interphase mass transfer was modelled as pseudo first-order reactions each with its own reversible rate constants . The result was a highly multi-parameter system of first order differential equations which were solved only by assigning arbitrary parameter values .

An obvious over-simplification of the problem was the use of the electrophoretic mobility [42,43], ζ , to represent the double layer potential ψ_o . According to Davies and Rideal[43], the ratio $\frac{\zeta}{\psi_o}$, can in the best of situations be about 0.5 , and in some specific cases is much less .

4.3.3 The Dynamic Model of Borwankar and Wasan

Borwankar and Wasan[78] studied the dynamic IFT behaviour of a Californian crude in various aqueous caustic solutions using the spinning drop tensiometer . They employed the equilibrium parameters determined earlier by Ramakrishnan and Wasan[51] in the formulation of their phenomenological model . In a follow-up paper[79] , the authors extended their analysis to incorporate flowing liquid phases such as occurs in a linear displacement of oil with an alkaline solution . The authors accounted rigorously for the variation of the surface area of the spinning drop with time. Their analyses of the physical and chemical mechanisms governing the interaction of the crude oil acids with NaOH contained all the pertinent diffusive-kinetic considerations . In particular, adequate attention was paid to the electrical nature of the interface . The predicted sorptive rate constants appeared to correlate the experimental data quite well . The equilibrium constants used by Borwankar and Wasan were derived from a consideration of a hypothetical acid HA , representing the largely unknown crude oil surface active acids . Under such circumstances , the predicted rate constants have to be treated with caution simply because of the fact that the IFT manifested by the crude oil is a complex sum of the contributions from a number of acids whose widely different interfacial characteristics are influenced by pH as well as the interfacial potential .

Part II

Experimental Aspects

Chapter 5

Design and Elements of the Photo-Micropendographic System

5.1 Experimental Design

5.1.1 Selection of the Working System

Since naphthenic and aromatic acids are probably the most surface-active of the numerous crude oil acids, these should the target of in-depth laboratory studies in order to determine their ionization behaviour. Unfortunately, these acids are not commercially available in sufficiently high purities. Additionally, such acids do not readily dissolve in simple organic solvents such as paraffinic hydrocarbons. In view of these difficulties,we decided to restrict our attention to C10–C18 fatty acids . Having selected the working acids, the next step was to pick an appropriate solvent for the oleic phase . Such a solvent would have adequate solvating power for the designated acids . In addition , modelling considerations necessitated the solvent to be uni-component , and of the highest purity possible . This latter requirement was in order that important transport properties such as

diffusivity and viscosity could be determined with minimum uncertainty . Indeed , there are no reliable correlations in standard texts[75,80,81] for the estimation of diffusivity in multi-component solvent systems . Even for single solvents , the best correlations are those developed for paraffinic hydrocarbons[82] . Another criterion for selecting the working solvent was its viscosity . Preliminary trials showed that the viscosity of the solvent had to be substantially greater than that of water in order to dampen the contraction and elongation of the experimental oil drop as the IFT changed with time . In the end, the selected solvent was hexadecane, and this was further purified by vacuum distillation.

As for the fatty acids themselves , we considered several fatty acids above C12. Saturated acids such as stearic and palmitic have limited solubilities in the working solvent, and the purity of the commercially available samples was considered too low. Finally, lauric and oleic acids were picked and the working concentrations were 0.02 M for lauric, and 0.10-1.0 mM for oleic.

5.1.2 Experimental Strategies

The main objective of this study was to obtain accurate dynamic IFT data for single acids dissolved in the oleic phase and contacted with a broad spectrum of aqueous NaOH solutions . Such data would be used to obtain precise parameter estimates from the various models which would also be developed at latter stages of the work . In addition , dynamic IFT measurements would be made for binary mixtures of lauric and oleic acids against a spectrum of caustic concentrations in the aqueous phase . Parameters determined from the single acid component models would be used in the solution of the multi-component model equations in order to predict the applicable IFT values. The adequacy of all the proposed models would then be verified by comparing the experimental with the predicted IFT values .

Strategy for Single Acid Experiments

step1: Preliminary runs to determine suitable working acid concentration , oil droplet volume and the exposure time necesary to attain equilibrium .

step2: Actual IFT measurements in replicates using the pre-determined acid strength in the oleic phase and various NaOH solutions .

step3: Determination of equilibrium IFT values .

step4: Data Analysis and development of the equilibrium and dynamic models .

Strategy for the Binary Mixture Studies

step1: Formulate binary mixtures of the two acids , namely , lauric and oleic , maintaining the same lauric acid concentration in the mixture as was used in the single component studies . The effective oleic acid concentration in the mixture would be systematically increased up to a maximum of 10 mole% consistent with the range of IFTs measurable with the experimental apparatus .

step2: Perform blank runs with the actual oleic acid concentration in the mixture as was done for the single component studies .

step3: Perform single component model analysis for the reference oleic acid systems in order to determine all pertinent parameters .

step4: Carry out dynamic IFT measurements for the binary mixtures using a range of caustic concentrations .

step5: Develop the generalized dynamic model for a multi-component acid mixture . Formulate the model equations which apply in the case of a binary acid mixture and solve them using the parameter values determined from the individual single component studies .

Table 1 gives the specification of the reagents used in this study , while Table 2 details the formulation of the binary acid mixtures .

Table 1 : Specifications of Reagents Used

NAME	SPECIFICATION	REMARKS
Sodium Hydroxide	Fisher Certified,ACS,Pellets	used as supplied
Hexadecane	Fisher Certified	redistilled under 0.1 mm Hg vacuum , with a rotavapor kit
Toluene	Fisher Certified , ACS	used as supplied
Lauric Acid	Fisher reagent, 99$^+$ mole%	used as supplied
Oleic Acid	Fisher reagent, 99 mole%	used as supplied
Water	Double distilled and deionized	none

5.2 Choice of Dynamic IFT Measurement System

Spinning drop tensiometry[62–64] has emerged as the most popular technique for tension measurements. Indeed, it is currently the only proven technique for ultra-low tension work. The governing equation for spinning drop tensiometry involves the balance (at gyro-static equilibrium) between capillary and centrifugal forces acting on an oil droplet retained in a cylindrical capillary tube filled

Table 2: Formulation of Binary Acid Mixtures: Material Balances

Mixture Designation	M1	M2	M3	M4	M5
Mole % oleic acid in mixture	0.50	0.99	1.54	2.97	4.76
Effective oleic acid concentration in mixture, mM	0.10	0.20	0.3125	0.6125	1.00
Volume of 0.04 M lauric acid needed, ml	50.0	50.0	50.0	50.0	50.0
Volume of 0.01 M oleic acid needed, ml	1.00	2.00	3.13	6.13	10.00
Volume of make-up hexadecane, ml	49.0	48.00	46.87	43.87	40.00
Total Volume of mixture, ml	100.0	100.0	100.0	100.0	100.0

with the aqueous phase,viz ;

$$\Delta P = \gamma [1/R_1 + 1/R_2] = \frac{2\gamma}{R_o} - \frac{\Delta\rho\omega^2 y^2}{2} \tag{5.1}$$

When the length to width ratio of the spinning drop exceeds 4, Vonnegut[62,63] obtained a solution to equation 5.1 for the applicable tension as follows;

$$\gamma = \frac{\Delta\rho\omega^2 y_o^2}{4} \tag{5.2}$$

Equation 5.2 is very convenient for calculating IFT from the measured droplet diameter, the angular velocity and the densities of the oleic and aqueous phases.

From an experimental point of view, spinning drop tensiometry is relatively simple,fast and accurate. However, there are lingering doubts concerning the true meaning of tension measurements carried out by this technique. For instance, it is difficult to determine precisely the age of the interface associated with a given dynamic tension measurement. Also, additional shear stresses in the fluids due to the spinning action enhance mass transfer and subsequently the magnitude of the interfacial tension. In some instances, the magnitude of the angular velocity is known to affect

the measured tension. Even the measurements of the linear dimensions of the droplet may be in serious error when the droplet tends to drift from one end of the tube to the other. There is also a considerable heat generated by the rotor assembly and this tends to make temperature control rather difficult.

In view of these inherent problems of the spinning drop technique, we decided to adopt a different measurement approach which would attempt to remedy the above-named problems while maintaining the same or better precision and accuracy. One such technique involves the use of pendant oil droplets immersed in a static aqueous phase. This technique has been shown to be capable of giving very accurate tension values especially for reacting systems. A detailed discussion of the pendant drop technique will be presented in the next chapter.

5.3 Elements of the Photo-Micropendographic System

The experimental technique which has been developed for this work is hereafter referred as photo-micropendography. Essentially, the technique is based on freezing the experimental pendant oil droplet photographically, and then making coordinate measurements from high quality negatives. These linear measurements are then used for the calculation of the boundary tension. The hardware structure of the micropendographic experimental system consists of the following elements :

1. The Ramé-Hart contact angle goniometer equipped with standard accessories for pendant drop measurements .

2. The Scherr-Tumico optical comparator model 20-4200 which also has direct digital x, z scales accurate to 0.001 mm .

3. A precise temperature control system for the measurement chamber .

4. A precise interfacial age monitoring system .

5. Bulk property measurement apparatus such as the densimeter , the Cannon-Fenske viscometer and the pH meter .

The principal software employed for data analysis was the algorithm of Rotenberg , Boruvka and Neumann (RBN)[83] , which will be discussed in some detail in the next chapter . Other software routines were taken from IMSL[84] and SAS[85] libraries that were supported on the University of Ottawa's Amdahl 470 main frame computer .

5.3.1 Details of the Goniometer Measurement System

The standard components of the goniometer included the microscope and 35 mm camera units, together with the specimen stage assembly , the environmental chamber and the micro-syringe attachment . Modifications were effected on the goniometer in two key areas , namely , the addition of the 'pendo' cell with its associated housing unit , and the adaptation of the micro syringe to enable upwards pendant drops to be formed . Fig. 1 is the schematic of the modified goniometer as an integral component of the micropendographic experimental system . Fig. 2 shows the details of the micro-syringe and the modified oil forming needle . Design details of the pendo cell and the pendo cell housing are given in Fig. 3 .

The pendo cell and its associated housing is the heart of the micro-pendographic measurement system . The cell itself is a rectangular , optically flat glass vessel with a holding volume of 1 mL. This particular unit was designed to hold the requisite amount of the aqueous phase together with the oil droplet suspended from the tip of the micro-syringe assembly . The pendant oil drop would be completely immersed in the aqueous phase but fully exposed to the optical system of the goniometer . It was also desirable to enclose the entire pendo cell unit within the original

environmental chamber of the goniometer in order to eliminate as far as possible external convection currents . Working with a much reduced cell volume enabled us to keep the phase volume ratio within the 100– 1000 range typical in spinning drop tensiometry[62,63] . The hub of the stainless steel needle was made of teflon in order to provide an air-tight fit of the drop forming needle to the main micro-syringe assembly (see Fig. 2) .

5.3.2 The Temperature Control System

The environmental chamber within which the experiments were conducted was kept at a temperature of 25 ±0.1° C , by the continuous circulation of cooling water from a Haake F3 precision temperature bath . As can be seen from Fig. 1. , a heat absorbing glass (heat shield) was installed ahead of the measurement chamber but on the optical axis , in order to reduce the excessive radiant heat from the hot tungsten lamp . The actual temperature of the measurement cell was monitored with a type K thermocouple and displayed on a Thermo-electric digital read-out .

5.3.3 The Density Measurement System

The Anton Parr Precision densimeter model DMA 02C was used for the measurement of the densities of all working solutions . The temperature of this unit was controlled to 25 ±0.01°C by means of a Techneurop Programmable temperature controller in series with a Neslab RTE-4 Endocal refrigerated circulating bath . The densimeter cell temperature was displayed on a digital Hewlett Packard model 2801A quartz thermometer . An on-line Commodore PET model 4032 computer hooked to model 4040 disk drive and an Integral Data Systems model 560 printer was used to calculate the densities from the experimentally determined cell periods .

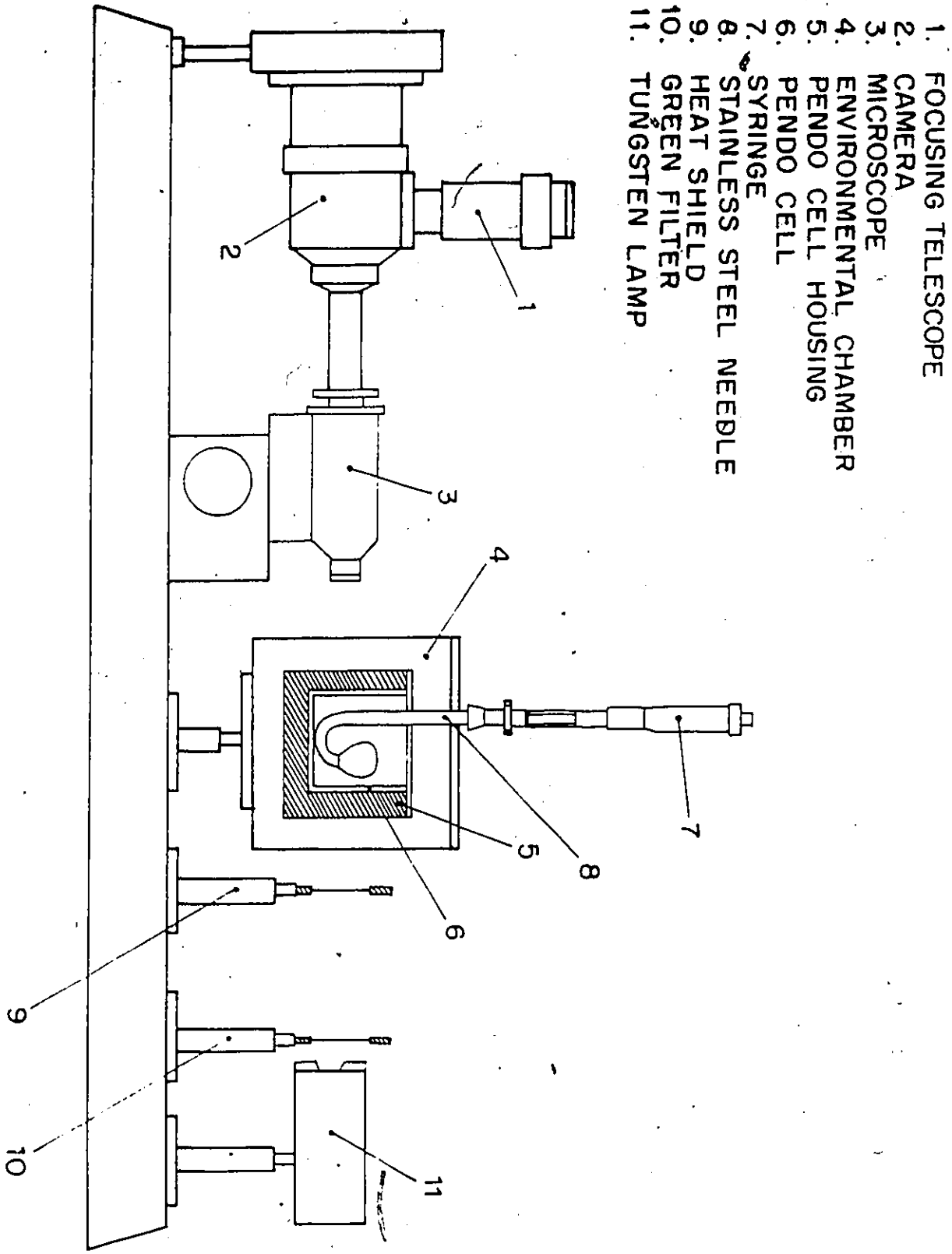

Figure 1 : Schematics of the Micropendographic System

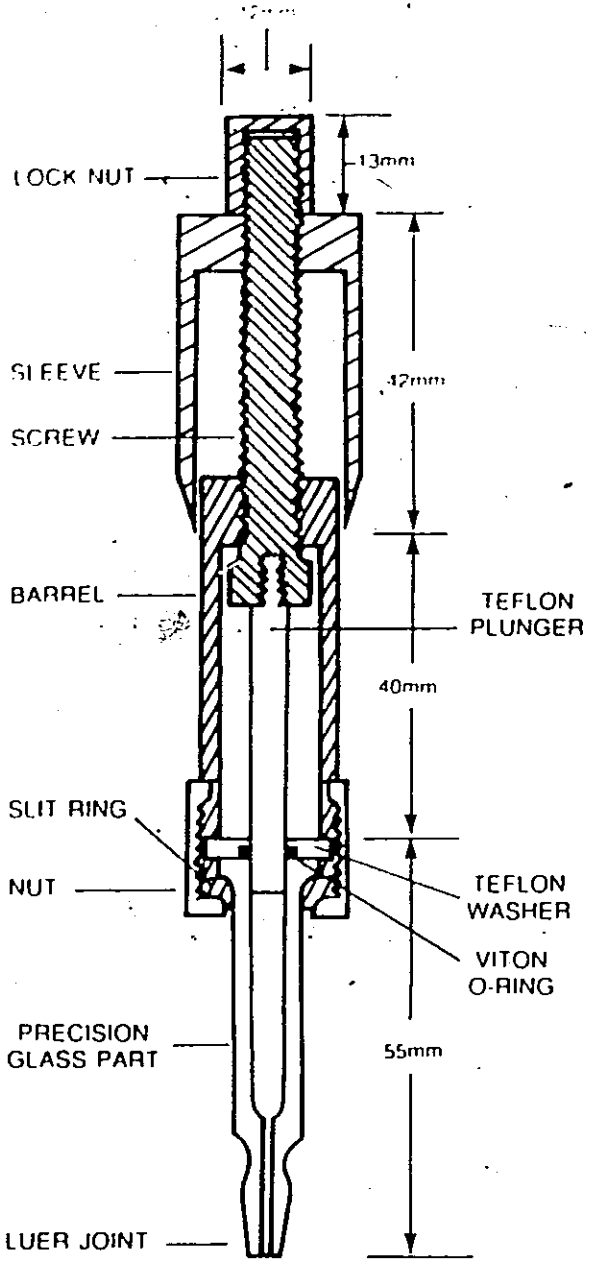

Figure 2.1 : Micro-Syringe Details

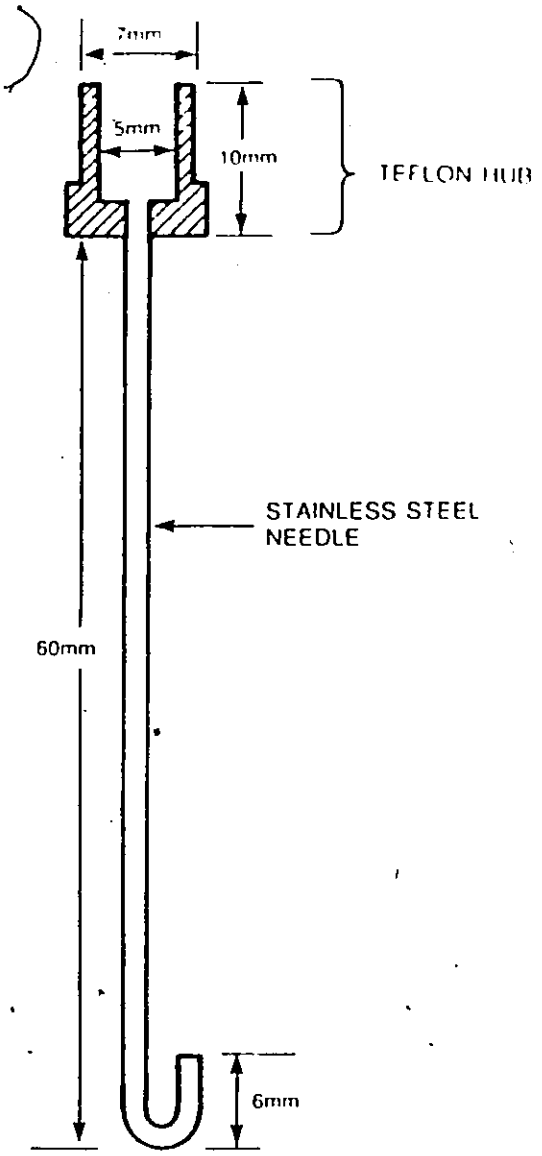

Figure 2.2 : Modified Drop Forming Needle

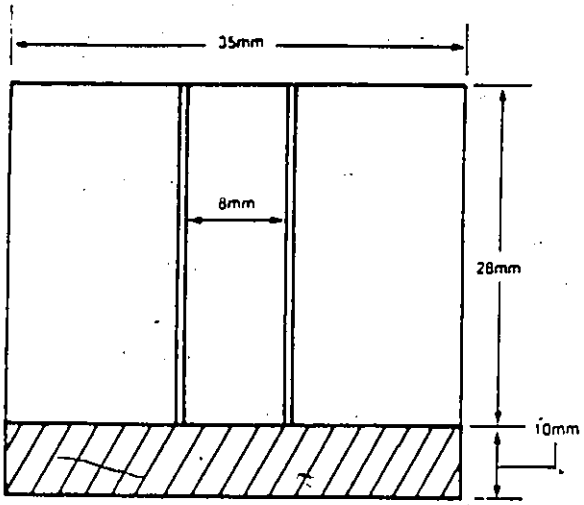

SECTION A-A

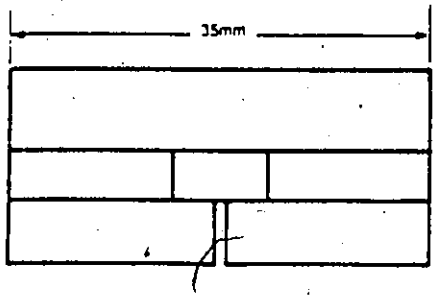

Figure 3.2 : Pendo Cell Cover

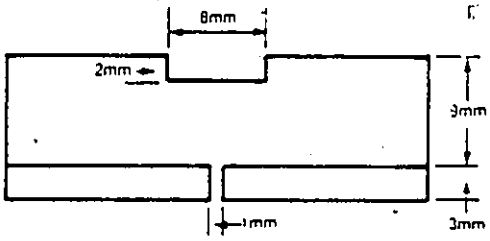

Figure 3.1 : Pendo Cell Housing

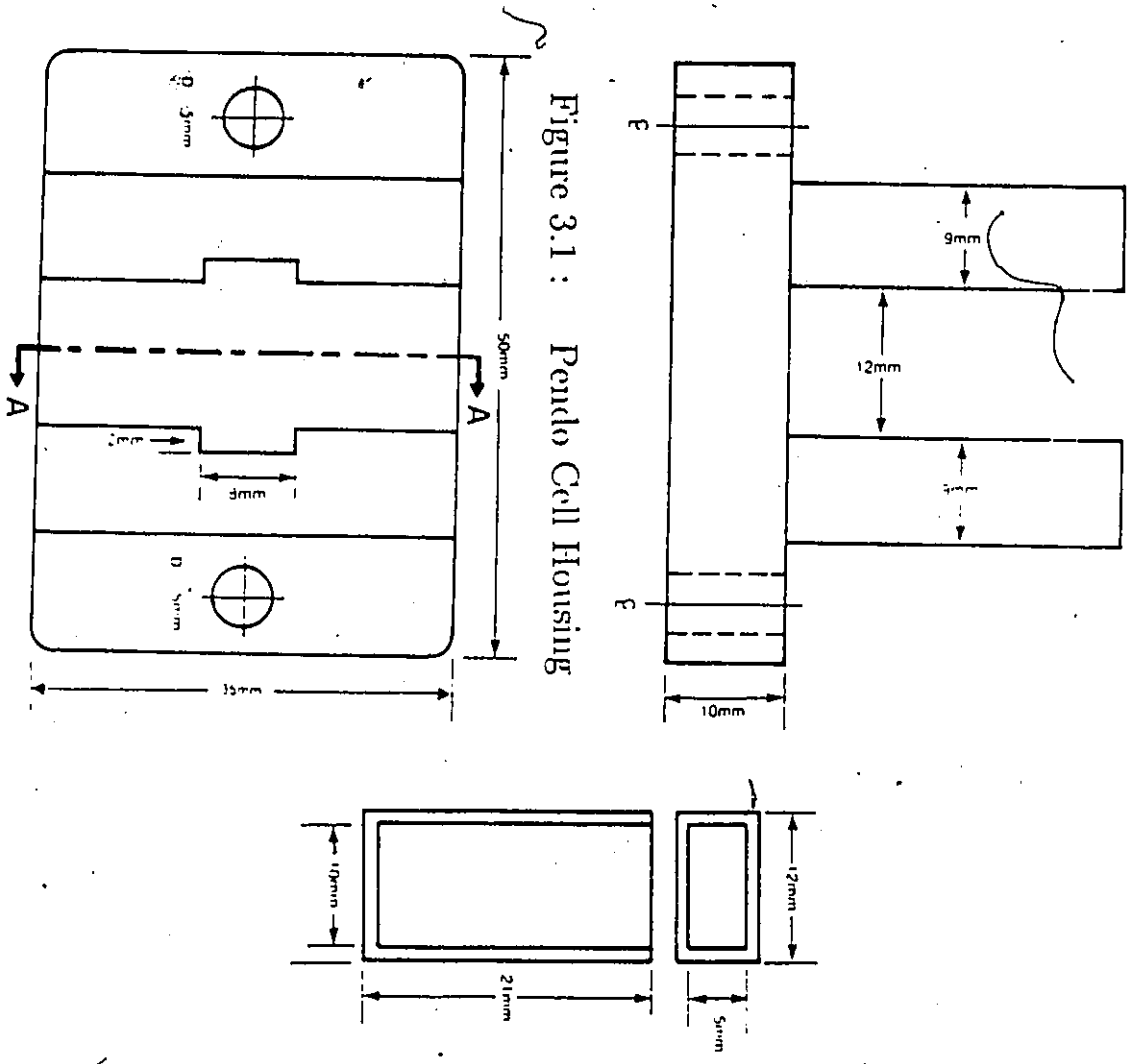

Figure 3.3 : Pendo Cell Details

5.3.4 The Precision Timing System

The age of the oil-water interface and hence the progress of the dynamic experiments was monitored by the use of a Gralab model 625 programmable timer/intervalometer . The programme loaded in the intervalometer dictated the frequency at which the photographs of the oil droplet would be taken in the course of a given experiment . In order to determine the entire duration of the experiment , a Precision Scientific timer was connected in series with the Gralab intervalometer .

5.3.5 pH and Viscosity Measurement

Viscosity measurements were made with pre-calibrated Cannon-Fenske viscometers at 25° C . The pH of the aqueous solutions was determined with the Orion Research digital ionalyzer model 501 using the Fisher Scientific's high pH glass electrode in series with a calomel reference electrode .

Chapter 6

Experimental Procedure

6.1 Preparation of Working Solutions

The double distilled and deionized water used in preparing the caustic solutions was deaerated under 0.1 mm Hg vacuum for 15 minutes . In most cases , a stock solution of 250 mM NaOH was prepared from which diluents were made to arrive at the required NaOH concentrations . The entire solution preparation exercise was carried out under nitrogen . For the oleic phase , the stock solution was 0.01 M for oleic acid , and for lauric acid , it was 0.04 M . Freshly prepared caustic solutions were used for all experiments .

6.2 Pre-run Trials

For the given acid concentration in the oleic phase and for each working NaOH solution , a preliminary run was required in order to select the most appropriate needle out of three different sizes , namely , gauges 22 , 25 and 28 with internal diameters of 0.0406 , 0.0254 and 0.01524 cm respectively . It was also necessary to know in advance the optimum size of an oil drop which would have appropriate shapes over the entire duration of the run . One criterion which we used to assess

the appropriateness of the drop was the ability to measure both d_e, and d_s as originally specified by Andreas et al. [86] , and illustrated in Fig. 4 . The other criterion was that the drop would not approach a spherical geometry at any stage of the dynamic experiment . Another important information to be derived from the trial runs was the operational oil droplet volumes , the proper selection of microscope lenses , and the expected duration of the transient IFT phenomena .

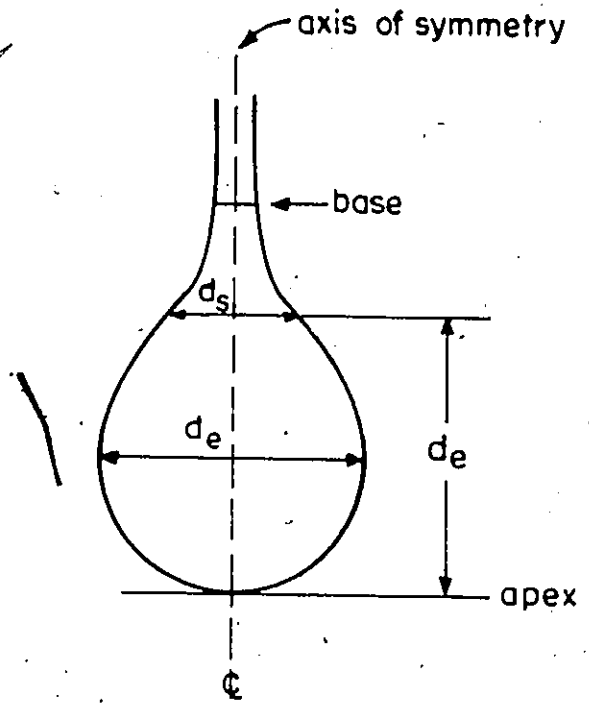

Figure 4 : Shape Determining Parameters of Andreas et al.

6.3 Cleaning and Goniometer Assembly

A rigorous cleaning procedure for all vessels , glassware , needles and syringes that come in contact with either of the two phases was mandatory . The procedure consisted of initial washing with copious amounts of water , then followed by ethanol and finally acetone . All glassware were further cleaned with hot chromic acid and thoroughly rinsed with water . Drying of the cells, syringes and glassware was effected with air followed by nitrogen.

The oil syringe was carefully filled with the oleic phase ensuring that all the air trapped in the syringe and needle was expelled . Thereafter the micro-syringe sub-assembly was mounted on a support attached to the micropendographic system . Exactly 0.87 mL of the appropriate NaOH solution was pipetted into the pendo cell which was subsequently covered. Next , the pendo cell was placed inside the pendo cell housing and the entire unit positioned under the drop forming needle. All residual oil on the needle tip was carefully wiped off before the needle was then lowered into the aqueous phase . The cover plate of the environmental chamber,through which the needle would have been passed before its insertion into the pendo cell , was then also lowered to contact the pendo cell cover . Finally , the environmental chamber cover was secured to the pendo cell housing by means of two long bolts . After assembly , the pendo cell housing with the drop forming needle and the cover plate was then carefully lowered into the environmental chamber of the goniometer. In order to position the drop exactly on the optical axis , the pendo cell had to be lowered to the bottom of the environmental chamber by manipulating the supporting bolts while at the same time lowering the microsyringe sub-assembly .

6.3.1 Goniometer Assembly

The combination of microscope objective and eye-piece lenses necessary to achieve the desired magnification of the experimental drop was fixed to the microscope . The 35 mm camera back was then loaded with the special Kodak Technical Pan TP 135-36 film . It was found from pre-run trials that the camera had to be operated at 200 ASA for shutter speeds as high as 1/250 seconds to be utilized . The alignment of the optical axis was then checked using the focusing telescope attached to the manual exposure body of the camera unit . Simultaneously , the illumination of the image plane was adjusted by varying the voltage applied to the tungsten lamp . The temperature control system of the goniometer was then set to achieve the desired working temperature . Finally, the intervalometer was programmed for the run and all necessary adjustments made on the optical system in order that very sharp images of the experimental drop would be obtained .

6.4 Measurement Procedure

6.4.1 Photographic Technique

The experiment was started by delivering a pre-determined volume of oil by means of the micro-syringe unit and thereby forming a pendant drop immersed in the aqueous phase which was in turn contained in the pendo cell . Simultaneously , the intervalometer was started and the experimental drop was photographed at the pre-set intervals dictated by the intervalometer . The experimental oil droplets had equatorial diameters in the range of 1–3 mm ,while the height of the drop was in the range of 2–5 mm. Such relatively small drops did not suffer from any appreciable optical distortion from the imaging lens. In the case of the Ramé-Hart goniometer, the use of the flat-field eye piece eliminated almost all of the optical distortion associated with the microscope system.

6.4.2 Drop Coordinate Measurement

Readying the Comparator

With the completion of a set of experiments and having exhausted the roll of films , the latter was then processed into negatives . The numbers appearing on the different frames of the negative were matched against those assigned by the frame counter of the camera in the course of the experiment. Each frame to be measured had to be laid flat on specially fabricated , acrylic frame holders . The dimensional details of the frame holders are shown in Fig. 5 . The selected frame was first

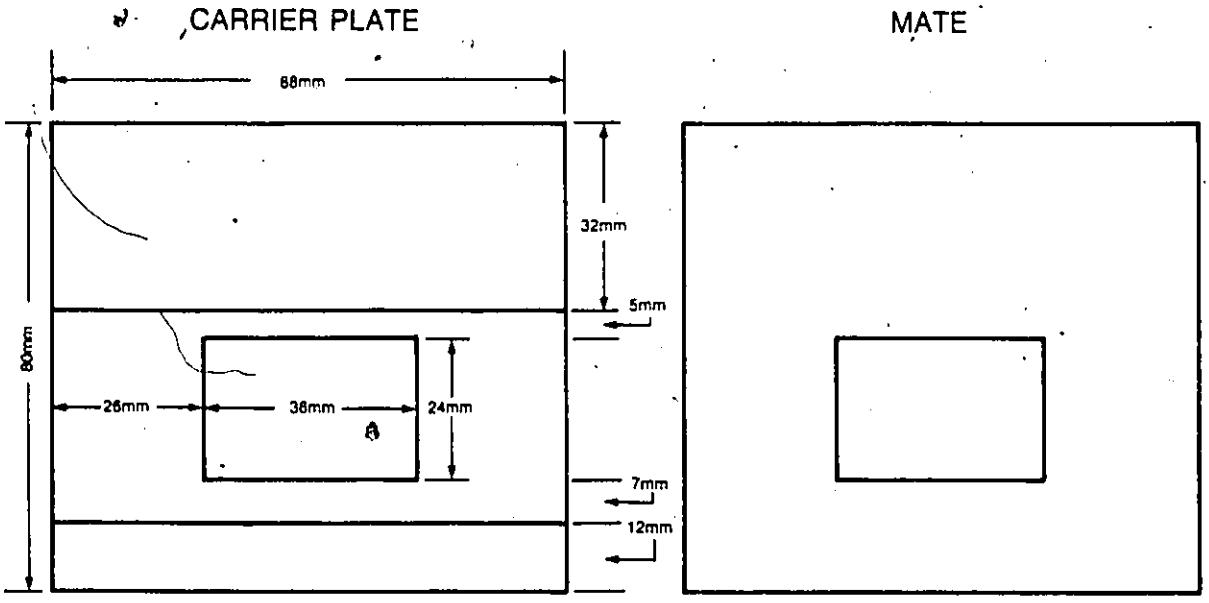

Figure 5 : Details of Negative Frame Holders

centered on the carrier plate (see Fig. 5) and secured by strips of double sided cellotape paper at the four corners of the frame . The covering frame holder was then placed over the carrier plate and their top edges were secured by means of a Hoffman clip . The other end of the pair of frame holders was fixed to the vise attached to the optical comparator . The enlarged image of the drop was then focused on the screen of the comparator in such a way as to reveal the entire profile of the drop including the extremity of the stainless steel needle .

Coordinate Measurement

The axis of symmetry of the drop was determined by measuring the horizontal distances to both edges of the drop , namely , XXL and XXR (see Fig. 6) , for every 2.0 mm vertical movement away from the apex of the drop until the base was reached . In all cases , the appropriate axis corresponded to that setting in which pairs of values of XXR and XXL for all values of Z , did not differ by more than 0.02 mm . Having determined the axis of symmetry and the origin of the coordinate system , the dimensions XXL and XXR were then very carefully measured for each 0.50 mm vertical movement up to and including the base . Both horizontal measurements as well as the corresponding vertical coordinate were duly recorded . Usually about 30 pairs of coordinate measurements were sufficient to span the entire profile of the drop . In all cases , the data set included the point with a vertical coordinate value of d_e . This additional point enabled the same set of data to be used to calculate IFT with the aid of the Tables developed by Andreas et al. [86] and Stauffer[87] . The coordinate dimensions measured with the aid of the comparator correspond to those of the experimental drop magnified by the optical system of the goniometer . This magnification factor had to be determined accurately , and we achieved that by photographing a precision glass-etched scale (obtained from Gaertner Corporation) placed at the same object plane as the drop .

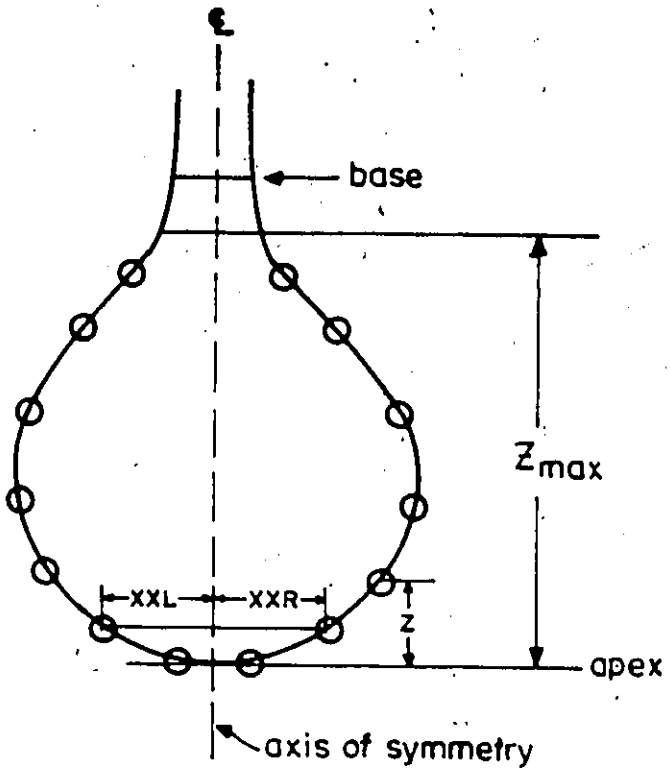

Figure 6 : Typical Drop Coordinate Measurements for use with the RBN Algorithm

6.4.3 Preliminary Data Processing

An average X-coordinate value was calculated from each pair of values of XXR and XXL (see Fig. 6). These X-coordinate values together with the corresponding Z-coordinate measurements constituted the data set for the working oleic/ caustic system at the interfacial age corresponding to the experimental frame number. Before the data set was finally entered into the input file of the data analysis programme , the measured dimensions were scaled down to the actual size of the droplet by dividing with the magnification factor of the optical system . Two additional input parameters , namely , the densities of both liquid phases , and the local gravitational acceleration were also required . The former was calculated by using a software package run on a Commodore

micro-computer which converts the periods indicated on the Anton Parr (AP) densimeter directly to densities using high purity water as the reference liquid , according to the equation :

$$\rho_1 - \rho_2 = K_{ap}[T_1^2 - T_2^2] \tag{6.1}$$

The local gravitational acceleration was the value in our laboratory as determined by specialists from Energy , Mines and Resources of Canada (EMR)..

6.5 Determination of Interfacial Parameters with the RBN Algorithm

6.5.1 Principles of IFT Determination from Shapes of Pendant Drops

The classical equation of Young and Laplace[42,43,86-89] is given by :

$$\Delta P = \gamma[\frac{1}{R_1} + \frac{1}{R_2}] \tag{6.2}$$

Bashforth and Adams[88] solved equation 6.2 for the case of a figure of revolution in which the two radii of curvature at the apex were equal using numerical integration . For such geometry , equation 6.2 becomes :

$$\gamma[1/R_1 + 1/R_2] = \Delta\rho gz + 2\gamma/b \tag{6.3}$$

By defining a dimensionless parameter , β , equation 6.3 becomes :

$$\frac{1}{\left\{(R_1/b) + \frac{\sin\phi}{(x/b)}\right\}} = \beta(z/b) + 2 \tag{6.4}$$

The parameter β is defined as follows ;

$$\begin{aligned} \beta &= \frac{\Delta\rho g b^2}{\gamma} \\ &= \frac{2b^2}{a^2} \end{aligned} \tag{6.5}$$

Bashforth and Adams obtained solutions to equation 6.4 and equation 6.5 in the form of tables of (x/b) , and (z/b) for various values of β , and ϕ . Andreas et al. [86] were the first to extend the solution of Bashforth and Adams specifically to the case of axisymmetrical pendant drops , thus laying the foundation for the determination of boundary tensions by this technique . Ambwani and Tomlinson[89] have recently reviewed the various improvements to the classical solution of Andreas et al. Although equation 6.4 could not be solved analytically for the pendant drop geometry by Andreas et al. [86] , they proposed a solution scheme which they credited with 99% accuracy in the calculated IFT values . A shape parameter , S, (see Fig. 4) was defined by the authors as follows ;

$$S = \frac{d_s}{d_e} \tag{6.6}$$

They defined yet another function H_s , as follows ;

$$H_s = \beta\left(\frac{d_e}{b}\right)^2 \tag{6.7}$$

and finally obtained the following expression relating γ, H_s and S , thus ;

$$\begin{aligned} \gamma &= \frac{g(\Delta\rho)b^2}{\beta} \\ &= \frac{g(\Delta\rho)d_e^2}{H_s} \end{aligned} \tag{6.8}$$

By using H_s values determined from photographs of drops of special conductivity water of known γ, Andreas et al. [86] produced the famous H-S Tables for the calculation of IFT . Stauffer[87] recently extended these tables to smaller S values such as would be obtained in low tension studies.

In recent times , the availability of better optical systems coupled with powerful numerical integration schemes have greatly improved the accuracy of axisymmetrical drop techniques for the determination of boundary tensions . Rotenberg et al. [83] developed an algorithm for calculating boundary tensions using either sessile or pendant drops. Vos and Los[90] used the striascopic

imaging technique in order to improve the accuracy of the coordinate measurements . Girault et al. [91,92] produced a micro-computer oriented routine for digitizing video images of pendant drops. The latter authors claimed that very accurate coordinate measurements over small point spacings could be made by using the digitizing technique .

6.5.2 The Algorithm of Rotenberg , Boruvka and Neumann

The RBN algorithm[83] enables the IFT , interfacial area and droplet volume to be determined from the same coordinate data set . It does this by fitting a Laplacian curve through the measured X , Z coordinate points as illustrated in Fig. 6 .

Formulation of the Objective Function

By considering the meridian section of an axisymmetric pendant drop , Rotenberg et al. [83] reformulated the Young-Laplace equation in terms of x, s ,and z as follows :

$$x = \mathrm{x(s)}, \tag{6.9}$$

$$z = \mathrm{z(s)} \tag{6.10}$$

from geometrical considerations , it follows that ;

$$\frac{dx}{ds} = \cos\phi \tag{6.11}$$

$$\frac{dz}{ds} = \sin\phi \tag{6.12}$$

$$\frac{1}{R_1} = \frac{d\phi}{ds} \tag{6.13}$$

all the above equations can be combined to give ;

$$\frac{d\phi}{ds} = 2/R_o + \frac{\Delta\rho g z}{\gamma} - \frac{\sin\phi}{x} \tag{6.14}$$

Equation 6.14 is the transformed Young-Laplace equation in terms of the variables x, z, s and ϕ. The linear coordinates are made dimensionless as follows :

$$X = \frac{x}{R_o} \tag{6.15}$$

$$S = \frac{s}{R_o} \tag{6.16}$$

$$Z = \frac{z}{R_o} \tag{6.17}$$

Suppose a calculated Laplacian curve , $v = \mathrm{v(s)}$, differs from the experimental points , u_n , by the normal distance $d(u_n, v)$, then the objective function is given by ;

$$\mathbf{E} = \frac{1}{2}\sum_{n=1}^{N}[d(u_n, v)]^2$$

with parameters , $\vec{Q} = (q_1, q_2, q_3, q_4)$, defined by ;

$$q_1 = X_o \tag{6.18}$$

$$q_2 = Z_o \tag{6.19}$$

$$q_3 = R_o \tag{6.20}$$

$$q_4 = \frac{\Delta\rho g R_o^2}{\gamma} \tag{6.21}$$

so that in terms of $\vec{Q}$, $\vec{\mathbf{E}}$, becomes ;

$$\mathbf{E}(q_1, q_2, q_3, q_4) = \sum_{n=1}^{N} e_n(q_1, q_2, q_3, q_4) \tag{6.22}$$

where

$$e_n = 1/2d(u_n, v)^2 \tag{6.23}$$

thus for a single datum point ,

$$e = 1/2\Big[(q_3 X(S_m, q_4) \pm (q_1 - X_e))^2 + (q_3 Z(S_m, q_4) + (q_2 - Z_e))^2\Big] \tag{6.24}$$

such that :

$$q_3 X(S_m, q_4) = x \tag{6.25}$$

$$q_3 Z(S_m, q_4) = z \tag{6.26}$$

with x, z representing the coordinates of a point on the Laplacian curve closest to the experimental coordinate (X_e, Z_e) , while S_m is the corresponding value of the arc length parameter , s , at that point . Because S_m varies with $\vec{Q}$, it follows that ;

$$c = e(S_m(q_1, q_2, q_3, q_4), q_1, q_2, q_3, q_4)$$

and the conditions for extremum using equation 6.22 becomes ;

$$\frac{\delta \mathbf{E}}{\delta q_k} = \sum_{n=1}^{N} \frac{\delta e_n}{\delta q_k} = 0, \qquad k = 1, 2, 3, 4 \tag{6.27}$$

and the quotient , $\frac{\delta e}{\delta q_k}$, will be given by the relationship , thus ;

$$\frac{\delta e}{\delta q_k} = (\frac{\delta e}{\delta S_m}) \frac{\delta S_m}{\delta q_k} + (\frac{\delta e}{\delta q_k}) \tag{6.28}$$

and from equation 6.27 , equation 6.28 becomes ,

$$\frac{\delta \mathbf{E}}{\delta q_k} = \sum_{n=1}^{N} (\frac{\delta e_n}{\delta q_k}) = 0 \tag{6.29}$$

Solving the System of Equations

In order to solve equation 6.29 for the parameters , $\vec{Q}$, RBN[83] used the Newton-Raphson technique moderated by incremental loading of revised parameter estimates . To this end , a Hessian matrix of partial derivatives had to be formulated in terms of the parameters as follows ;

$$\frac{\delta^2 \mathbf{E}}{\delta q_k \delta q_l} = \sum_{n=1}^{N} \frac{\delta^2 e_n}{\delta q_k \delta q_l} \tag{6.30}$$

Additionally , the authors employed the Euler integration procedure in the calculation of values of S starting from zero to S_m for each datum point until Z_{max} . The complete solution of the regression problem features in the first instance , a subroutine that initially fits an approximate circular arc through the data points in order to obtain initial values of $\vec{Q}$. Next , the objective function and the Jacobian with Hessian matrices of partial derivatives are defined . For each datum point , the coordinates of the calculated Laplacian curve closest to the experimental point are found by using a very stiff convergence criterion ,viz :

$$\frac{|E_o - E|}{E} < 10^{-9} \tag{6.31}$$

$$\left|\vec{E}\right| < 10^{-9} \tag{6.32}$$

Once the final converged value of $\vec{Q}$ has been found , γ is obtained from q_4 using the definition ;

$$\gamma = \frac{\Delta\rho g R_o^2}{q_4}$$

Calculating Interfacial Parameters with the RBN Algorithm

A listing of the above algorithm was obtained from the authors and modified for the VS Fortran Compiler of the University of Ottawa Amdahl computer. As a further check on the accuracy of the predicted IFT , values of d_e, d_s taken from the coordinate measurements data set were used to calculate S and the corresponding IFT was determined with the aid of the H-S Tables of Andreas et al. [86] and Stauffer[87] . Tension values arising from highly elongated oil droplets could not be calculated by the RBN algorithm . The failure of the algorithm when applied to drops with an irregular profile stems from the requirement that a circular arc has to pass through all data points to start the curve fitting routine . In such situations , tension values were readily and accurately determined by the use of the H-S Tables .

Part III

Development of Models for Single Component Systems

Chapter 7

Development of the Equilibrium Model

7.1 Qualitative Model Description

In any diffusive-kinetic analysis of chemical interactions involving species present in two or more phases in contact , a geometrical model of the interface is very helpful . The geometrical model, although a hypothetical concept, facilitates the delineation of the extent of diffusive phenomena from those associated with sorption kinetics . Fig. 7 gives the salient features of the proposed geometrical model . The oleic and aqueous sub-layers provide a path for the reacting species to reach the interface from the respective bulk phases . In order to handle the electrical nature of the adsorbed surfactant anions at the interface , the geometrical model also allows for the existence of an electric double layer with an associated potential .

Our proposed equilibrium model takes into account the partitioning of the fatty acid between the oleic and aqueous sub-layers subject to the applicable distribution coefficient . The acid ionizes at the aqueous side of the interface forming the surface-active soap anions . The adsorption of the

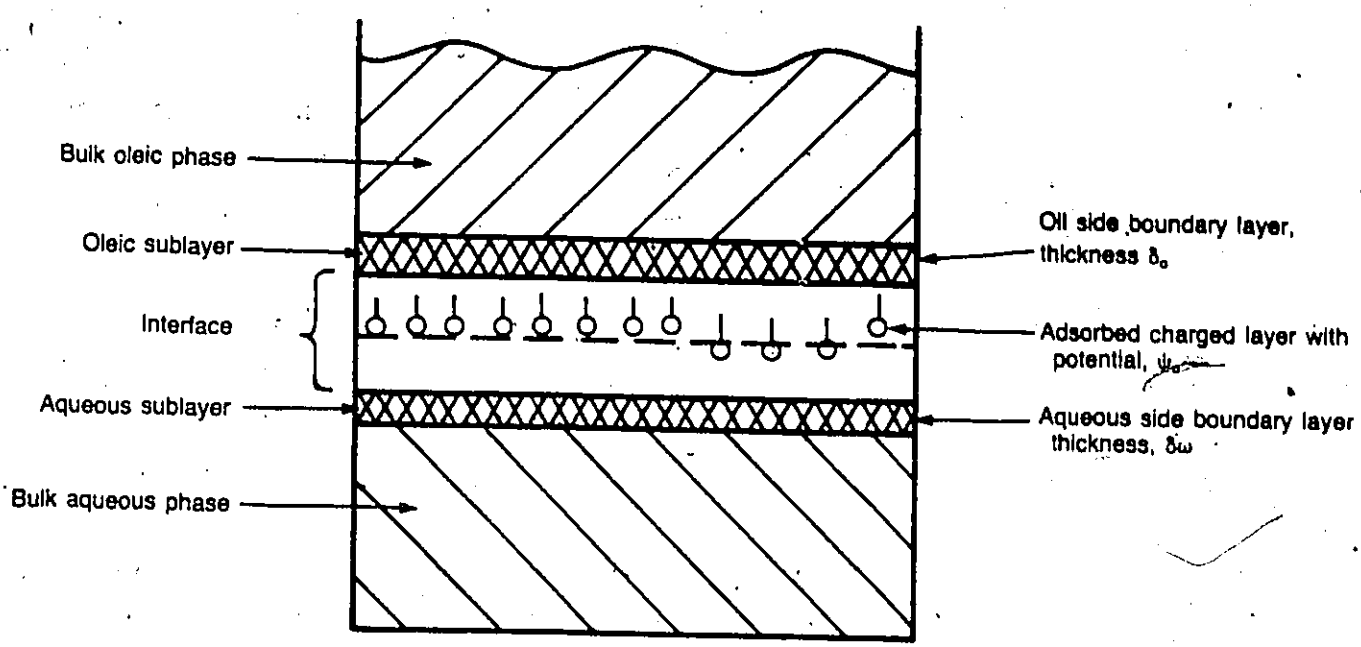

Figure 7 : A Geometrical Model of the Interface

anionic soap species results in the formation of an electrical double layer . However, the surface concentration of the anion decreases firstly by desorption to the aqueous phase , and secondly through the formation of the undissociated sodium salt . We adopt here the notion proposed by Ramakrishnan and Wasan[51] , that this surface inactive soap complex partitions preferentially to the oleic phase . The focus of the equilibrium model then is the determination of the pertinent parameters such as the acid dissociation constant , and the equilibrium constant governing the formation of the inactive soap with its subsequent removal to the oleic phase . The detailed development of the model is presented in the following sections .

7.2 Interfacial Reactions and Equilibria Relationships

1. Partitioning of the acid , HX , to the aqueous sublayer ;

$$HX_o \rightleftharpoons HX_w \tag{7.1}$$

Reaction 7.1 is governed by the partition coefficient , K_p , which is given by ;

$$K_p = \frac{C_{HX_o}}{C_{HX_w}} \gg 1 \tag{7.2}$$

2. Dissociation of the acid at the aqueous side of the interface according to the reaction ;

$$HX \rightleftharpoons H^+ + X^- \tag{7.3}$$

The ionization constant for reaction 7.3 , is given by ;

$$K^D_{HX} = \frac{C_{H^+} C_{X^-}}{C_{HX_w}} \tag{7.4}$$

The equilibrium ionic concentrations are influenced by the ionic product of water as follows ;

$$K_w = C_{H^+} C_{OH^-} \tag{7.5}$$

3. Formation of the surface inactive soap complex at the aqueous side of the interface in accordance with the reaction ;

$$Na^+ + X^- \rightleftharpoons NaX_w \tag{7.6}$$

and this too has an associated equilibrium constant defined as ;

$$K'_{NaX_w} = \frac{C_{Na^+} C_{X^-}}{C_{NaX_w}} \tag{7.7}$$

4. Partitioning of the soap complex to the oleic phase with the distribution ratio given as follows ;

$$K_D = \frac{C_{NaX_w}}{C_{NaX_o}} \ll 1 \tag{7.8}$$

By combining equations 7.7 and 7.8 , we can define a global equilibrium parameter for the desorption of X^- to the oleic phase thus ;

$$K^D_{NaX} = K'_{NaX_w} K_D$$
$$= \frac{C_{Na+} C_{X-}}{C_{NaX_o}} \quad (7.9)$$

7.3 Equilibrium Model Equations

7.3.1 Relating Anion Concentration to the Equilibrium Parameters

Conservation equations for the surface active species are written as follows ;

i Mass balance for X^- ;

$$V_w C_{HX_w} + V_w C_{X-} + V_o C_{HX_o} + V_o C_{NaX_o} = V_o (C_{HX_o})_o \quad (7.10)$$

ii Mass balance for Na^+ ;

$$V_w C_{Na+} + V_o C_{NaX_o} = V_w (C_{OH})_o \quad (7.11)$$

iii Charge balance in the aqueous phase ;

$$C_{Na+} + C_{H+} = C_{OH-} + C_{X-} \quad (7.12)$$

For the working aqueous phase pH , C_{H+} is negligible and C_{X-} is small compared to C_{OH-}. Equation 7.12 simplifies to ;

$$C_{Na+} = C_{OH-} \quad (7.13)$$

By combining equations 7.9 , and 7.11 , and using equation 7.13 , we obtain the following :

$$C_{Na+} = C_{OH-}$$
$$= \frac{(C_{OH-})_o}{\left[1 + \frac{V_o}{V_w} \frac{C_{X-}}{K^D_{NaX}}\right]} \quad (7.14)$$

From equations 7.2 and 7.4 , we may write ;

$$\frac{K_p}{K_{HX}^D} = \frac{C_{HX_o}}{C_{H+}C_{X-}} \tag{7.15}$$

We now use equation 7.5 , to eliminate C_{H+} from equation 7.15 and the result is as follows ;

$$C_{HX_o} = \frac{K_w K_p C_{X-}}{K_{HX}^D C_{OH-}} \tag{7.16}$$

Finally we substitute for C_{NaX_o} using equation 7.9 , C_{HX_w} using equation 7.4, and for C_{HX_o} using equation 7.16 all in equation 7.10 . The result is the following ;

$$C_{X-} = \frac{(C_{HX_o})_o}{\left[\left(\frac{V_w}{V_o}(1 + \frac{K_w}{K_{HX}^D C_{OH-}})\right) + \frac{K_w K_p}{K_{HX}^D C_{OH-}} + \frac{C_{OH-}}{K_{NaX}^D}\right]} \tag{7.17}$$

At the relatively high working NaOH concentration range (ie. pH > 10) , the following relationship will be generally valid , viz :

$$\frac{K_w}{K_{HX}^D C_{OH-}} \ll 1,$$

then equation 7.17 simplifies to the following ;

$$C_{X-} = \frac{(C_{HX_o})_o}{\left[\frac{V_w}{V_o} + \frac{K_w K_p}{K_{HX}^D C_{OH-}} + \frac{C_{OH-}}{K_{NaX}^D}\right]} \tag{7.18}$$

7.3.2 Relating Anion Concentration to IFT

We adopt an approach similar to that of Davies and Rideal[43] , and write down the rates of adsorption and desorption for the anionic surfactant employing Langmuirian kinetics , viz :

1. Rate of adsorption of X^- from the aqueous sublayer is given by ;

$$\frac{d\Gamma_x}{dt} = B_1 C_{X-}(1 - f) \tag{7.19}$$

2. Rate of desorption of surfactant to the aqueous sublayer according to the following ;

$$-\frac{d\Gamma_x}{dt} = B_2 \Gamma_x \exp(-\frac{W}{RT}) \tag{7.20}$$

3. Using the Poisson-Boltzmann relationship,the sublayer concentration , $C_{X_s^-}$, is written in terms of the bulk concentration , C_{X^-} , as follows :

$$C_{X_s^-} = C_{X^-} \exp(-\frac{z_x \psi_o \epsilon N}{RT}) \tag{7.21}$$

4. At equilibrium , the rates of adsorption and desorption are equal , thus equation 7.19 is combined with equations 7.20 and 7.21 , and the result is as follows ;

$$C_{X^-} = \frac{(B_2/B_1)\Gamma_x \exp(-\frac{W}{RT})}{\left\{(1 - \frac{\Gamma_x}{\Gamma_{max}}) \exp(-\frac{z_x \psi_o \epsilon N}{RT})\right\}} \tag{7.22}$$

5. The Gouy-Chapman model is used to calculate the double layer potential as follows ;

$$\psi_G = -\frac{2kT}{\epsilon} \sinh^{-1}\left\{\frac{\sigma}{\sqrt{C_i}}\sqrt{\left[\frac{500\pi}{D_c RT}\right]}\right\} \tag{7.23}$$

At the working temperature of 25° C , the values of the other physical constants , namely , k, R , ϵ , and D_c , are substituted into equation 7.23 and the result is as follows ;

$$\psi_G = -51.4 \sinh^{-1}\left(\frac{136.9}{A\sqrt{C_i}}\right) \tag{7.24}$$

6. Relating Γ_x to the equilibrium surface pressure

Langmuir[93] proposed an equation of state for neutral species adsorbing at the oil/water interface . Frumkin and Volmer[43,93] modified the Langmuirian equation of state to account for the fact that the species are adsorbed at fixed sites on the interface . The resulting equation then becomes ;

$$\Pi_s = \frac{kT}{A_o} \ln(\frac{A}{A - A_o}) \tag{7.25}$$

If the interface is charged , Davies [94] proposed an additional electrical repulsion term , Π_r. Hachisu [95] confirmed the validity of the Davies equation and thus settled once and for all

the controversy which had surrounded it for a while . The result which we now refer to as the Frumkin-Volmer-Davies- Hachisu (FVDH) equation of state becomes ;

$$\begin{aligned} \Pi &= \Pi_s + \Pi_r \\ &= \gamma_o - \gamma \\ &= \frac{kT}{A_o}\ln\left(\frac{A}{A - A_o}\right) + \sqrt{\left(\frac{8D_c NC(kT)^3}{10^3\varepsilon^2}\right)}\left[\cosh\left(\frac{\varepsilon\psi_o}{2kT}\right) - 1.0\right] \end{aligned} \tag{7.26}$$

if Γ is expressed in moles per m^2 , then A is evaluated (in $Å^2$) as follows ;

$$A = \frac{1}{\Gamma_x N 10^{-16}} \tag{7.27}$$

$$A_o = \frac{1}{\Gamma_{max} N 10^{-16}} \tag{7.28}$$

7.4 Summary of the Equilibrium Model Equations

The equilibrium chemical model that describes the interaction of a fatty acid dissolved in the oleic phase and NaOH present in the aqueous phase can be summarized as the following coupled system of non-linear , algebraic equations :

(i) The equilibrium caustic concentration in the aqueous phase as per equation 7.14 ;

$$C_{OH^-} = \frac{(C_{OH^-})_o}{\left[1 + \frac{V_o}{V_w}\frac{C_{X^-}}{K^D_{NaX}}\right]} \tag{7.29}$$

(ii) The equilibrium aqueous phase concentration of the surfactant species (equation 7.18) ;

$$C_{X^-} = \frac{(C_{HX_o})_o}{\left[\frac{V_w}{V_o} + \frac{K_w K_p}{K^D_{HX} C_{OH^-}} + \frac{C_{OH^-}}{K^D_{NaX}}\right]} \tag{7.30}$$

(iii) The surfactant surface concentration as obtained in equation 7.22 ;

$$C_{X^-} = \frac{B_2/B_1\Gamma_x \exp(-\frac{W}{RT})}{\left\{(1 - \frac{\Gamma_x}{\Gamma_{max}})\exp(-\frac{z_x\psi_o\epsilon N}{RT})\right\}} \tag{7.31}$$

(iv) The interfacial double layer potential arising from the adsorbed anionic surfactant species (equation 7.24) ;

$$\psi_o = -51.4 \sinh^{-1}\left[\frac{136.9}{A\sqrt{C_i}}\right] \tag{7.32}$$

(v) The FVDH equation of state (equation 7.26) ;

$$\Pi = \frac{KT}{A_o}\ln\left(\frac{A}{A - A_o}\right) + \sqrt{\left(\frac{8D_cNC(kT)^3}{10^3\varepsilon^2}\right)}\left[\cosh\left(\frac{\varepsilon\psi_o}{2kT}\right) - 1.0\right] \tag{7.33}$$

7.5 Solution of the Equilibrium Model Equations

7.5.1 Specification of the Regression Problem

Values of C_{X^-} are expected to be quite low. In addition , preliminary experimental data showed that the working phase volume ratios , V_o/V_w , are also quite low ; such that the following relationship may be assumed to be generally valid , viz :

$$\frac{V_o}{V_w}\frac{C_{X^-}}{K^D_{NaX}} \ll 1.0$$

With this assumption , equation 7.29 simplifies to the trivial case :

$$C_{OH^-} = (C_{OH^-})_o$$

In regression analysis[96–98] , a specification of the variables of the regression problem is warranted. For this problem therefore , the independent variables which are also experimentally-determined are , C_{OH^-} , (V_w/V_o) and $(C_{HX_o})_o$. The dependent variable is Π , while K^D_{HX} and K^D_{NaX} constitute the parameters to be estimated . The remaining variables , namely , W, K_p, B_2/B_1, and Γ_{max} are considered as model constants. Standard nonlinear regression analysis[96–98] requires that the dependent variable be explicitly related to one or more functions of the independent variables together with the model parameters . A closer inspection of the structure of the

proposed model equations shows that this requirement cannot be satisfied, since equation 7.26 in which the dependent variable is expressed does not contain any terms in any of the independent variables nor of the model parameters . Thus, what we have is indeed a unique regression problem.

7.5.2 Calculation of the Model Constants

These so-called model constants are evaluated based on information available from the literature. Since this information is often of a more general nature , the accuracy of the calculated values is questionable . Ideally , the constants should be estimated together with the designated model parameters . However , this would lead to multiparametization , and as has been amply demonstrated by Bard[98] , precise parameter estimates may not be realised, and even when possible, such estimates may turn out to be quite inaccurate . McLean[99] agrees with Bard that parsimonious parametization is probably the only way to go in order to arrive at realistic solutions .

Determination of K_p

Tanford [41] proposed that at sufficiently dilute acid concentrations (when activity coefficients are close to one) , the following relationship holds ;

$$\mu^{\circ}_{HC} - \mu^{\circ}_{W} = RT \ln \frac{X_W}{X_{HC}} \tag{7.34}$$

Tanford[41] also found that the term $(\mu^{\circ}_{HC} - \mu^{\circ}_{W})$ was a linear function of the chain length , and for saturated fatty acids in the range C8–C22 , this linear relationship was roughly as follows ;

$$\mu^{\circ}_{HC} - \mu^{\circ}_{W} = 4260 - 825n_c \tag{7.35}$$

By combining equations 7.34 and7.35 and converting to SI units , we obtain the following ;

$$\begin{aligned} RT \ln \frac{X_W}{X_{HC}} &= -RT \ln K_p \\ &= 17807 - 3449n_c \end{aligned} \tag{7.36}$$

Equation 7.36 applies strictly to saturated , straight chain paraffinic acids which were studied by Tanford . Indeed , data reported in Ref. 41 for oleic and linoleic acids indicated that the equation would not be quite appropriate for unsaturated acids . However , Traube's Rule[42] makes an exception for the presence of a double bond in the hydrocarbon chain . In fact , we found excellent agreement in n_c values applicable in Equation 7.35 with similar values calculated by the use of Traube's Rule . Thus , in order to use equation 7.36 to calculate the partition coefficient for the oleic acid system , the value of n_c has to be 17 as recommended by Traube's Rule . For lauric acid, n_c takes the value of 12 .

Evaluation of W and B_2/B_1

Davies and Rideal [43] analysed the adsorption-desorption phenomena associated with ionic surfactants and concluded that the ratio , B_1/B_2 is independent of the hydrodynamics of the adsorption process. They assigned the value of 20 Å to this ratio based on considerations for the thickness of the adsorbed film .

Another relationship developed by Davies and Rideal[43] enables W to be evaluated as follows;

$$W = n_c w \tag{7.37}$$

For the oil-water interface , w takes the value of 810 cals (3385 J) , and n_c is evaluated by the use of Traube's Rule .

Determination of Γ_{max}

There are wide differences in the values of Γ_{max} or alternatively , A_o , that have been proposed in the literature . For example , reported A_o values for oleic acid or sodium oleate range from 22 to 35 $Å^2$ per molecule . In this study , we have used 30$Å^2$ per ion for the minimum area of the oleate

ion . van Voorst Vader[100] found the A_o value for sodium laurate at the heptane-water interface to be 45Å^2 per ion . This value was also used for the laurate ion in this study .

7.5.3 The Solution Methodology

One of the most powerful nonlinear parameter estimation routines is the algorithm of Levenberg and Marquardt[101,102] . This algorithm is also widely used and that accounts for the fact that it is readily available through various software vendors . The IMSL routine ZXSSQ[84] does not require analytical derivatives and was thus very convenient for this estimation problem . As in all parameter estimation problems , good initial guesses are warranted . Kittrell et al. [103] discussed various ways of obtaining good initial guesses including the use of grid searches and linearizing the equations . However , due to the complexity of the problem , classical parameter search techniques could not be used . Rather , it was far more efficient to obtain good initial guesses by solving the model equations manually using a trial and error approach .

The outline of the solution procedure adopted is roughly as follows : Manual calculations provided starting parameter values as well as initial guesses for A , and ψ_o . Input data included the pertinent NaOH concentrations , the initial acid concentration in the oleic phase , the experimentally determined surface pressures as well as the phase volume ratios and the model constants . For any given acid/ caustic system , all relevant input data are supplied from a data file . The main programme reads the data and then initiates a call to the routine ZXSSQ. For each pair of values of C_{OH} and Π, the appropriate value of ψ_o has to be calculated as a first step in the solution of the model equations. To this end, equations 7.24 and 7.26 are solved simultaneously by means of a Newton-Raphson iteration technique and executed in a separate subroutine . Thereafter , the model equations were then solved strictly in the following order ; equation 7.18 , 7.22 and 7.26

in order to obtain new estimates of the surface pressure for each and every data point. Finally, the residuals are evaluated as well as the sum of the squares of the residuals. In the next and subsequent iterations, ZXSSQ seeks to minimize SSR by automatic adjustment of the parameter values until convergence is achieved . The convergence criteria were a difference of 10^{-5} between successive residual sum of squares , and an agreement in successive parameter estimates up to the fifth significant digit .

Chapter 8

Development of the Dynamic Model

8.1 General Model Formulation Principles

Since species transport from the bulk to the interface and vice versa must be accounted for in a dynamic model , the geometrical model of Fig. 7 was particularly useful. The diffusion boundary layers shown in Fig. 7 represent the path for convective diffusion in accordance with Nernstian theory . All interfacial reactions occur between the two sub-layers . The model which is detailed below consists of the following elements :

(i) Transport of the reacting species from the bulk phases to the interface by convective diffusion;

(ii) Interfacial reactions and associated equilibria leading to the formation of the surface active soap species ;

(iii) Transfer of reaction products from the interface to the bulk phases by convective diffusion ;

(iv) Surfactant adsorption and desorption resulting in time dependent changes in surface excess concentration and consequently the interfacial tension .

8.2 Interfacial Kinetics and Sorptive Equilibria

The chemical reactions of interest are essentially those outlined in the last chapter. However,the reactions per se are reasonably fast and thus are not rate limiting. The rate limiting reactions are the sorptive ones. These and the associated equilibria are outlined as follows :

(1) Adsorptive dissociation of acid in accordance with the following equation ;

$$HX_{o,s} \overset{K_{HX_o}}{\rightleftharpoons} H^+ + X^-_{ads} \tag{8.1}$$

(2) Desorption of X^- to the aqueous sublayer as follows ;

$$X^-_{ads} \overset{K_X}{\rightleftharpoons} X^-_{w,s} \tag{8.2}$$

(3) Removal of X^- to the oleic sublayer as the inactive complex NaX_o , thus ;

$$X^-_{ads} + Na^+ \overset{K_{NaX}}{\rightleftharpoons} NaX_{o,s} \tag{8.3}$$

(4) Desorption of X^- to the aqueous sublayer as HX_w in accordance with the reaction ;

$$X^-_{ads} + H^+ \overset{K_{HX_w}}{\rightleftharpoons} HX_{w,s} \tag{8.4}$$

8.3 Sorption Kinetic Rate Equations

We employ Langmuirian sorption kinetics to describe the adsorption and desorption of the surface active anion to and from the interface in accordance with the reactions outlined in the preceding section .

(a) Net rate of adsorption of X^- from the aqueous sublayer in accordance with equation 8.2 ;

$$R_{(a,X)} = k_1 C_{X_s} \exp\left(\frac{\varepsilon\psi_o}{kT}\right)\left(1 - \frac{\Gamma}{\Gamma_{max}}\right) - k_{-1}\Gamma \tag{8.5}$$

A rearrangement of equation 8.5 results in the following ;

$$R_{(a,X)} = \frac{k_1}{\Gamma_{max}}\left[C_{X_s} \exp\left(\frac{\varepsilon\psi_o}{kT}\right)(\Gamma_{max} - \Gamma) - \frac{k_{-1}\Gamma_{max}}{k_1}\Gamma\right] \tag{8.6}$$

Equation 8.6 suggests that the adsorption rate constant , k_1 , and the sorptive equilibrium constant , K_X may be reexpressed as follows ;

$$k_X = k_1/\Gamma_{max} \tag{8.7}$$

$$K_X = k_1/k_{-1}\Gamma_{max} \tag{8.8}$$

In terms of these newly-defined rate constants , equation 8.6 becomes the following ;

$$R_{(a,X)} = k_X\left[C_{X_s} \exp\left(\frac{\varepsilon\psi_o}{kT}\right)(\Gamma_{max} - \Gamma) - \frac{\Gamma}{K_X}\right] \tag{8.9}$$

(b) Net rate of adsorption of HX_o from the oleic sublayer in accordance with equation 8.1 . Using a similar argument as in part(a) , we can write ;

$$R_{(a,HX_o)} = k_{HX_o}\left[C_{HX_{o,s}}(\Gamma_{max} - \Gamma) - \frac{\Gamma}{K_{HX_o}}C_{H^+} \exp -\left(\frac{\varepsilon\psi_o}{kT}\right)\right] \tag{8.10}$$

(c) Adsorption of HX_w from the aqueous sublayer in accordance with reaction 8.4 ;

$$R_{(a,HX_w)} = k_{HX_w}\left[C_{HX_{w,s}}(\Gamma_{max} - \Gamma) - \frac{\Gamma}{K_{HX_w}}C_{H^+} \exp -\left(\frac{\varepsilon\psi_o}{kT}\right)\right] \tag{8.11}$$

(d) Adsorption of NaX_o from the oleic sublayer according to equation 8.3 ;

$$R_{(a,NaX_o)} = k_{NaX}\left[C_{NaX_{o,s}}(\Gamma_{max} - \Gamma) - \frac{\Gamma}{K_{NaX}}C_{Na^+} \exp -\left(\frac{\varepsilon\psi_o}{kT}\right)\right] \tag{8.12}$$

It has been suggested [66] that an equilibrium exists in the aqueous phase between the acid and the anion in accordance with the ionization reaction and its associated equilibrium constant , viz ;

$$HX_w \overset{K^D_{HX}}{\rightleftharpoons} H^+ + X^-_w \tag{8.13}$$

The fact that reaction 8.13 occurs rather rapidly gives credence to the above proposition . In view of this relationship , we can combine the rate expressions for X^- and HX_w by means of an association parameter[66] , α , given by ;

$$\alpha = 1 + \frac{C_{H+}}{K^D_{HX}} \tag{8.14}$$

Firstly , equation 8.9 is rearranged as follows ;

$$R_{(a,X)} \exp(\frac{\varepsilon\psi_o}{kT}) = k_X \left[C_{X,s}(\Gamma_{max} - \Gamma) - \frac{\Gamma}{K_X} \exp -(\frac{\varepsilon\psi_o}{kT}) \right] \tag{8.15}$$

Next , equation 8.15 is multiplied by $\frac{C_{H+}}{K^D_{HX}}$, and the result is the following ;

$$\begin{aligned} R_{(a,X)} \exp -(\frac{\varepsilon\psi_o}{kT}) \frac{C_{H+}}{K^D_{HX}} &= R_{(a,HX_w)} \\ &= k_X \left[C_{HX_w,s}(\Gamma_{max} - \Gamma) - \frac{\Gamma C_{H+}}{K_{HX_w}} \exp -(\frac{\varepsilon\psi_o}{kT}) \right] \end{aligned} \tag{8.16}$$

Finally, combining equations 8.15 and 8.16 leads to the joint sorption rate equation for X^- and HX_w as follows ;

$$\begin{aligned} R_{(a,X+HX_w)} &= R_{(a,X)} \exp -(\frac{\varepsilon\psi_o}{kT}) \alpha \\ &= k_X \alpha \left[C_{X,s}(\Gamma_{max} - \Gamma) - \frac{\Gamma}{K_X} \exp -(\frac{\varepsilon\psi_o}{kT}) \right] \end{aligned} \tag{8.17}$$

8.4 Species Bulk Transport by Convective Diffusion

Following the analysis of Levich[65] , a general expression for the transport of any species from the interior of the bulk phase to the sublayer by Nernstian convective diffusion may be written as follows ;

$$V_i \frac{dC_i}{dt} = -\frac{A_s D_i}{\delta_i}(C_i - C_{i,s}) \tag{8.18}$$

Equation 8.18 can then be expanded for all the relevant interfacial species of the dynamic system as follows, :

1. Transport of HX_o ,

$$V_o \frac{dC_{HX_o}}{dt} = -\frac{A_s D_{HX_o}}{\delta_o}(C_{HX_o} - C_{HX_{o,s}}) \tag{8.19}$$

2. For the transport of X_w^- ,

$$V_w \frac{dC_{X_w}}{dt} = -\frac{A_s D_{X_w}}{\delta_w}(C_{X_w} - C_{X_{w,s}}) \tag{8.20}$$

3. Similarly for the transport of HX_w ,

$$V_w \frac{dC_{HX_w}}{dt} = -\frac{A_s D_{HX_w}}{\delta_w}(C_{HX_w} - C_{HX_{w,s}}) \tag{8.21}$$

4. And lastly for the transport of NaX_o ,

$$V_o \frac{dC_{NaX_o}}{dt} = -\frac{A_s D_{NaX_o}}{\delta_w}(C_{NaX_o} - C_{NaX_{o,s}}) \tag{8.22}$$

Equations 8.20 and 8.21 can be combined by means of the α parameter defined in the previous section ; this gives the combined bulk transport equation for X_w^- and HX_w as follows :

$$V_w \alpha \frac{dC_X}{dt} = -\frac{A_s \alpha D_w}{\delta_w}(C_{X_w} - C_{X_{w,s}}) \tag{8.23}$$

where

$$D_w = D_X = D_{HX} \tag{8.24}$$

8.5 Differential Equations of the Dynamic Model

If there is to be no net species accumulation in the sublayers , then the following relationship must hold , viz :

$$R_{(s,i)} = \frac{D_i}{\delta_i}(C_i - C_{i,s}) \tag{8.25}$$

Equation 8.25 can now be used together with each of the sorptive kinetic rate expressions to solve for the sublayer concentrations , namely , $C_{HX_{o,s}}$, $C_{NaX_{o,s}}$, and C_{X_s} . Thereafter , the expressions for the sublayer concentrations are substituted into equations 8.19 , 8.22 and 8.23 respectively . The resulting differential equations are as follows :

(i) Diffusive-kinetic equation for HX_o ;

$$V_o\frac{dC_{HX_o}}{dt} = -\frac{D_{HX_o}A_s k_{HX_o}}{[k_{HX_o}\delta_o(\Gamma_{max}-\Gamma)+D_{HX_o}]}\left\{C_{HX_o}(\Gamma_{max}-\Gamma)-\frac{\Gamma}{K_{HX}}C_{H^+}\exp-(\frac{\varepsilon\psi_o}{kT})\right\} \tag{8.26}$$

(ii) Diffusive-kinetic equation for species NaX_o ;

$$V_o\frac{dC_{NaX_o}}{dt} = -\frac{D_{NaX_o}A_s k_{NaX}}{[k_{NaX}\delta_o(\Gamma_{max}-\Gamma)+D_{NaX_o}]}\left\{C_{NaX_o}(\Gamma_{max}-\Gamma)-\frac{\Gamma}{K_{NaX}}C_{Na^+}\exp-(\frac{\varepsilon\psi_o}{kT})\right\} \tag{8.27}$$

(iii) Diffusive-kinetic equation for $(X_w^- + HX_w)$;

$$V_w\frac{dC_X}{dt} = -\frac{D_w A_s k_X}{\left[k_X\delta_w(\Gamma_{max}-\Gamma)+D_w\exp-(\frac{\varepsilon\psi_o}{kT})\right]}\left\{C_X(\Gamma_{max}-\Gamma)-\frac{\Gamma}{K_X}\exp-(\frac{\varepsilon\psi_o}{kT})\right\} \tag{8.28}$$

(iv) Diffusive-kinetic equation governing surfactant surface concentration , Γ :-

An overall mass balance for all species transferring from the bulk phases to the interface leads to the following equation , viz :-

$$\frac{d\Gamma}{dt} = \sum_i^N \frac{D_i}{\delta_i}(C_i - C_{i,s}) \tag{8.29}$$

We now expand the above equation for the various interacting species to obtain the following;

$$\frac{d\Gamma}{dt} = \frac{D_{HX_o}}{\delta_o}(C_{HX_o}-C_{HX_{o,s}})+\frac{D_{NaX_o}}{\delta_o}(C_{NaX_o}-C_{NaX_{o,s}})+\frac{D_w\alpha}{\delta_w}(C_X-C_{X_s}) \tag{8.30}$$

When the previously obtained expressions for the sublayer concentrations are substituted into equation 8.30 , the resulting equation gives the dynamic surface concentration as a function of the concentrations of the various interacting species as follows ;

$$\frac{d\Gamma}{dt} = \frac{D_{HX_o} k_{HX_o}}{[k_{HX_o}\delta_o(\Gamma_{max} - \Gamma) + D_{HX_o}]} \left\{ C_{HX_o}(\Gamma_{max} - \Gamma) - \frac{\Gamma}{K_{HX_o}} C_{H^+} \exp -(\frac{\varepsilon\psi_o}{kT}) \right\}$$
$$+ \frac{D_{NaX} k_{NaX}}{[k_{NaX}\delta_o(\Gamma_{max} - \Gamma) + D_{NaX}]} \left\{ C_{NaX}(\Gamma_{max} - \Gamma) - \frac{\Gamma}{K_{NaX}} C_{Na^+} \exp -(\frac{\varepsilon\psi_o}{kT}) \right\}$$
$$+ \frac{D_w \alpha k_X}{\left[k_X\delta_w(\Gamma_{max} - \Gamma) + D_w \exp -(\frac{\varepsilon\psi_o}{kT})\right]} \left\{ C_X(\Gamma_{max} - \Gamma) - \frac{\Gamma}{K_X} \exp -(\frac{\varepsilon\psi_o}{kT}) \right\} \quad (8.31)$$

In order to complete the model , Γ has to be related to the dynamic surface pressure . We make the assumption that the instantaneous surface concentration of the anionic surfactant is in quasi-equilibrium with the prevailing surface pressure . Under such circumstances , the FVDH equation of state for charged monolayers will apply . Also , the interfacial potential , ψ_o , will be given by the Gouy-Chapman equation (see equation 7.24) . Thus the system consisting of equations 8.26, 8.27 , 8.28, 8.31, 7.24, and 7.26 is the proposed dynamic model .

Chapter 9

Solution of the Dynamic Model Equations

9.1 Specification of the Model Parameters

As outlined in the preceding chapter , we have a system of four coupled nonlinear ordinary differential equations(equations 8.26 to 8.28) , which must be solved simultaneously along with the algebraic equations 7.24 and 7.26 : The parameters of the regression problem are the adsorption rate constants , k_{HX_o} , k_{NaX_o} and k_X . The specification of the other variables in the model is as follows :

(a) Independent (experimentally determined) variables , namely , V_o , V_w , A_s , C_{H+} , C_{OH-}, and C_{Na+} .

(b) Model constants Type 1 , namely , the equilibrium parameters , such as K_{HX_o} , K_{NaX} , K_X and K^R_{HX} .

(c) Model constants Type 2 , (the boundary layer thicknesses) , which are δ_o and δ_w .

(d) Model constants Type 3 , the Fickian diffusion coefficients , namely , D_{HX_o} , D_{NaX_o} and D_w .

The independent variables , C_{H+} , C_{Na+} , and C_{OH-} are known from the aqueous phase caustic composition and the ionic product of water . Other independent variables are the interfacial area and droplet volume which are determined from the analysis of the experimental data with the RBN algorithm . The theories underlying the calculation of the various model constants are presented in the following sections .

9.2 Calculation of Diffusion Coefficients

According to Reid et al. [81] , the best known correlations for the estimation of liquid-liquid diffusivities are the following ;

(i) the correlation of Wilke and Chang [104] ,

(ii) the correlation of Hayduk and Minhas [105],

(iii) the correlation of Tyn and Calus [106] .

In Chapter 3 of Ref. [107] , Hayduk reviewed the currently available correlations for the estimation of diffusivities in liquids. He also considers the correlations named above to be the best general ones that can be used for both polar and non-polar systems . All the above-named correlations require a good estimate of solute molar volume at the normal boiling point . The correlation of Tyn and Calus[106] requires surface tension data of dilute solutions of the solutes in the working solvents to be provided . Since such surface tension data were not measured in this work , only the first two named correlations were considered .

9.2.1 Determination of Solute Molar Volumes

Three slightly different methods were used for the estimation of solute molar volumes . These were recommended by Reid et al. [81] and are as follows :

1. the additive method of Schroeder ,
2. the method of Le Bas ,
3. and the correlation of Tyn and Calus .

The correlation of Tyn and Calus for the estimation of solute molar volumes was the one that was strongly recommended by Reid et al. [81] . Besides , the molar volumes calculated by the use of the method of Schroeder differed substantially from the figures obtained when the method of Le Bas was employed (see Appendix C). As a result of this discrepancy , the correlation of Tyn and Calus was used for the determination of solute molar volumes , and the applicable relationship is as follows ;

$$V_b = 0.285 V_c^{1.048} \tag{9.1}$$

In order to obtain critical volumes required in equation 9.1 , use was made of Vetere's method [81].

9.2.2 Estimation of Diffusivities

(a) Diffusivities in hexadecane :

The generalized Wilke-Chang correlation[104] can be written as follows ;

$$D^{\circ}_{AB} = \frac{7.4 \times 10^{-8} \sqrt{(\omega_d M_B)} T}{\eta V_A^{0.6}} \tag{9.2}$$

and for non-associated solvents , ω_d assumes the value of 1.0 .

The Hayduk-Minhas correlation valid for solutions in normal paraffinic solvents[105] is given

by ;

$$D^{\circ}_{AB} = \frac{13.3 \times 10^{-8} T^{1.47} \eta_B^{\epsilon}}{V_A^{0.71}} \tag{9.3}$$

where

$$\epsilon = \frac{10.2}{V_A^{-0.791}} \tag{9.4}$$

(b) Diffusivities in water :

The Wilke-Chang correlation namely equation 9.2, retains the same form when water is the solvent . The only thing that changes is ω_d for which the value of 2.6 was assigned by the authors . A different correlation was proposed by Hayduk and Minhas for aqueous solutions as follows ;

$$D^{\circ}_{AB} = 1.25 \times 10^{-8} (V_A^{-0.19} - 0.292) T^{1.52} \eta_w^{\epsilon*} \tag{9.5}$$

where

$$\epsilon* = \frac{9.58}{V_A} - 1.12 \tag{9.6}$$

9.3 Calculation of the Equilibrium Sorptive Rate Constants

It can be shown that once the equilibrium parameters , namely , K^D_{HX} , and K^D_{NaX} as well as the constants Γ_{max} and K_p are determined from the equilibrium model , all the equilibrium sorptive rate constants can be calculated starting from K_X . The mathematical analysis leading to the calculation of these equilibrium rate constants is presented below :

9.3.1 Calculation of K_X

In chapter 8 , K_X had been defined according to equation 8.8 . From equation 8.2 , K_X can also be expressed in concentration terms as follows ;

$$K_X = \frac{[X^-_{Ads}]}{[X^-_{w,s}]} \tag{9.7}$$

. Close inspection of equations 7.19 and 7.20, leads to the following ;

$$\begin{aligned} K'_X &= \left[\frac{\Gamma\Gamma_{max}}{C_{X^-_s}(\Gamma_{max}-\Gamma)}\right]_{eq} \\ &= \frac{B_1}{B_2 \exp(-\frac{W}{RT})} \end{aligned} \tag{9.8}$$

By comparing equations 8.8 and 9.8 , we see that K_X can be expressed in terms of previously determined constants as follows ;

$$K_X = \frac{(\frac{B_1}{B_2})\exp(\frac{W}{RT})}{\Gamma_{max}} \tag{9.9}$$

9.3.2 Calculation of K_{HX_o}

Following a procedure similar to that used in the preceding section , we write in accordance with equation 8.1, the following relationship for K_{HX_o} ;

$$K_{HX_o} = \frac{[H^+][X^-_{Ads}]}{[HX_{o,s}]} \tag{9.10}$$

By definition , K^D_{HX} is simply the following ;

$$K^D_{HX} = \frac{[X^-_w][H^+]}{[HX_w]} \tag{9.11}$$

and for K_p , the definition is as follows ;

$$K_p = \frac{[HX_o]}{[HX_w]} \tag{9.12}$$

By combining equations 9.10 – 9.12, we obtain the following ;

$$\frac{K_{HX_o}K_p}{K^D_{HX}} = \frac{[X^-_{ads}]}{[X_{w,s}]} = K_X \tag{9.13}$$

It follows from equation 9.13 that K_{HX_o} is given by :

$$K_{HX_o} = \frac{K_X K^D_{HX}}{K_p} \tag{9.14}$$

9.3.3 Determination of K_{NaX_o}

Similarly , using equation 8.10 , an expression for K_{NaX_o} may be written as follows ;

$$K_{NaX_o} = \frac{[X^-_{ads}][Na^+]}{[NaX_o]} \tag{9.15}$$

recalling the definition of K^D_{NaX} , thus ;

$$K^D_{NaX} = \frac{[Na^+][X^-]}{[NaX_o]} \tag{9.16}$$

then the combination of equations 9.15 and 9.16 leads to the following relationship , viz ;

$$\frac{K_{NaX_o}}{K^D_{NaX}} = \frac{[X^-_{ads}]}{[X^-_w]} = K_X \tag{9.17}$$

and the expression for K_{NaX_o} becomes ;

$$K_{NaX_o} = K^D_{NaX}K_X \tag{9.18}$$

9.4 Calculation of the Boundary Layer Thicknesses

The general convective diffusion equation can be written as follows ;

$$\frac{\delta c}{\delta t} + \vec{v}\cdot \text{grad}c = D\nabla^2 c \tag{9.19}$$

For a uni-dimensional diffusion boundary layer , Levich[65] showed that at steady state , the convective-diffusion equation becomes ;

$$v_x \frac{\delta c}{\delta x} + v_y \frac{\delta c}{\delta y} = D \frac{\delta^2 c}{\delta y^2} \tag{9.20}$$

By making some simplifying assumptions , Levich obtained an approximate solution to equation 9.20 which is valid for a flat plate. For such a geometry, the diffusion boundary layer thickness δ , is given as ;

$$\delta \approx D^{\frac{1}{3}} \nu^{*\frac{1}{6}} \sqrt{\frac{x}{U_\infty}} \tag{9.21}$$

Nernst[65] had suggested that the convective diffusional flux could be represented by an equation similar to equation 8.25 . He however gave no clues as to how the boundary layer thickness could be calculated a priori . The analysis of the convective diffusion problem by Levich[65] not only justified the classical equation of Nernst but went further to show the variables that influence the magnitude of δ . An expression similar to equation 9.21 has been derived for δ in a rather different context[108] .

It follows therefore from equation 9.21 that in a static system , δ will be given roughly as follows;

$$\delta \propto D^{\frac{1}{3}} \nu^{*\frac{1}{6}} \tag{9.22}$$

It is pertinent to note that equation 9.22 has also be shown to be valid even for a spherical geometry. Thus , this relationship (equation 9.22), can be used to calculate δ for any given system , provided that the value for a reference system (with known values of D and ν^*) is available . The reference system used in this study was the crude oil system studied by deZabala[18]. The mathematical analysis leading to the evaluation of pertinent variables was developed on the basis of the work done by deZabala[18] as well as Rubin and Radke[60] . The detailed calculations for the boundary layer thicknesses are shown in Appendix C .

9.5 Solving the Modelling Problem

9.5.1 General Concepts

The dynamic model being considered here consists of a set of four coupled , nonlinear differential equations alongside four other algebraic relationships . At the same time , there are three model parameters to be estimated . In essence , we have a non-linear regression problem involving ordinary differential equations as well as algebraic relationships which must be solved in order to obtain satisfactory parameter estimates . Ideally , the procedure for dealing with such a problem is to solve the differential equations and estimate the parameters thereafter . Such an approach does not work for the problem at hand , since the parameters must be known in order to solve the equations . Under such circumstances , one would then try to solve the equations and at the same time estimate the parameters . To date , there are no proven algorithms that can successfully execute such a task . We attempted to combine a differential equation solving routine with a non-linear parameter estimation one . While the solution of the differential equations was successful, the parameter estimation aspect was a failure , thus rendering that approach unworkable for the problem at hand.

After a careful examination of the structure of the model equations as well as the experimental data set , it became clear that the primary objective had to be the accurate solution of the differential equations . This then meant that the parameters would be estimated by a trial and error approach . A further complication was the fact that good initial estimates of the parameters were not available . Worse still , there is inadequate theory in the literature to determine what range of parameter values are applicable for the systems under consideration . The only way that satisfactory parameter estimates could be achieved under the circumstances was to perform a sensitivity analysis of the problem . For this aspect of the work , we relied entirely on the procedure

outlined by Bard[98] , and the detailed formulation of the sensitivity equations is given in the next subsection .

9.5.2 Sensitivity Analysis of the Dynamic Problem

We employ Bard's notation[98] and write;

$\vec{\theta}$ = [k_{HX} k_{NaX} k_X], a vector of the 3 model parameters ,

$\vec{s}$ = [C_{HX_o} C_{NaX_o} C_X Γ], a vector of 4 state variables ,

$\vec{s_o}$ = [$(C_{HX_o})_o$ 0.0 0.0 0.0], a vector of initial values of the state variables .

The above definition implies that 12 sensitivity equations need to be formulated and then solved simultaneously with the 4 original ordinary differential equations . The original differential equations can be written in terms of the recently-defined variables as ;

$$\frac{d\vec{s}}{dt} = \vec{h}(t \quad \vec{x} \quad \vec{s} \quad \vec{\theta}) \tag{9.23}$$

By differentiating equation 9.23 with respect to $\vec{\theta}$ employing the chain rule , the following relationship is obtained , viz;

$$\frac{d}{dt}\left(\frac{\delta\vec{s}}{\delta\vec{\theta}}\right) = \frac{\delta\vec{h}}{\delta\vec{\theta}} + \frac{\delta\vec{h}}{\delta\vec{s}}\frac{\delta\vec{s}}{\delta\vec{\theta}} \tag{9.24}$$

The sensitivity equations now follow from the expansion of equation 9.24 as follows :

$$\begin{aligned}
\frac{d}{dt}\left(\frac{\delta s_1}{\delta\theta_1}\right) &= \frac{d}{dt}\left(\frac{\delta C_{HX_o}}{\delta k_{HX_o}}\right) \\
&= -\frac{D_{HX_o}^2 A_s}{V_o\left[k_{HX_o}\delta_o(\Gamma_{max}-\Gamma)+D_{HX_o}\right]^2}\left\{C_{HX_o}(\Gamma_{max}-\Gamma)\right\} \\
&+ \frac{D_{HX_o}^2 A_s}{V_o\left[k_{HX_o}\delta_o(\Gamma_{max}-\Gamma)+D_{HX_o}\right]^2}\left\{\frac{\Gamma}{K_{HX_0}}C_{H^+}\exp-\left(\frac{\varepsilon\psi_o}{kT}\right)\right\} \\
&- \left(\frac{\delta C_{HX_o}}{\delta k_{HX_o}}\right)\frac{D_{HX_o}A_s k_{HX_o}(\Gamma_{max}-\Gamma)}{V_o\left[k_{HX_o}\delta_o(\Gamma_{max}-\Gamma)+D_{HX_o}\right]} \\
&+ \left(\frac{\delta\Gamma}{\delta k_{HX_o}}\right)\frac{C_{HX_o}D_{HX_o}A_s k_{HX_o}}{V_o\left[k_{HX_o}\delta_o(\Gamma_{max}-\Gamma)+D_{HX_o}\right]}\left\{1-\frac{k_{HX_o}\delta_o(\Gamma_{max}-\Gamma)}{\left[k_{HX_o}\delta_o(\Gamma_{max}-\Gamma)+D_{HX_o}\right]}\right\}
\end{aligned} \tag{9.25}$$

$$+\left(\frac{\delta\Gamma}{\delta k_{HX_o}}\right)\frac{C_{H^+}\exp-(\frac{e\psi_o}{kT})D_{HX_o}A_s k_{HX_o}}{V_o[k_{HX_o}\delta_o(\Gamma_{max}-\Gamma)+D_{HX_o}]K_{HX_o}}\left\{1+\frac{\Gamma k_{HX_o}\delta_o}{[k_{HX_o}\delta_o(\Gamma_{max}-\Gamma)+D_{HX_o}]}\right\}$$

$$\frac{d}{dt}(\frac{\delta s_2}{\delta\theta_1})=\frac{d}{dt}(\frac{\delta C_{NaX_o}}{\delta k_{HX_o}})$$
$$=-\frac{D_{NaX_o}A_s k_{NaX}(\Gamma_{max}-\Gamma)}{V_o[k_{NaX}\delta_o(\Gamma_{max}-\Gamma)+D_{NaX_o}]}(\frac{\delta C_{NaX_o}}{\delta k_{HX_o}})$$
$$+\left(\frac{\delta\Gamma}{\delta k_{HX_o}}\right)\frac{D_{NaX_o}A_s k_{NaX}C_{NaX_o}}{V_o k_{NaX}\delta_o(\Gamma_{max}-\Gamma)}\left\{1-\frac{k_{NaX}\delta_o(\Gamma_{max}-\Gamma)}{[k_{NaX}\delta_o(\Gamma_{max}-\Gamma)+D_{NaX_o}]}\right\} \qquad (9.26)$$
$$+\left(\frac{\delta\Gamma}{\delta k_{HX_o}}\right)\frac{D_{NaX_o}A_s k_{NaX}C_{Na^+}\exp-(\frac{e\psi_o}{kT})}{V_o[k_{NaX}\delta_o(\Gamma_{max}-\Gamma)+D_{NaX_o}]K_{NaX}}\left[1+\frac{\Gamma\delta_o k_{NaX}}{[k_{NaX}\delta_o(\Gamma_{max}-\Gamma)+D_{NaX_o}]}\right]$$

$$\frac{d}{dt}(\frac{\delta s_3}{\delta\theta_1})=\frac{d}{dt}(\frac{\delta C_X}{\delta k_{HX_o}})$$
$$=-\frac{D_w A_s k_X(\Gamma_{max}-\Gamma)}{V_w\left[k_X\delta_w(\Gamma_{max}-\Gamma)+D_w\exp-(\frac{e\psi_o}{kT})\right]}(\frac{\delta C_X}{\delta k_{HX_o}}) \qquad (9.27)$$
$$+\left(\frac{\delta\Gamma}{\delta k_{HX_o}}\right)\frac{D_w A_s k_X C_X}{V_w\left[k_X\delta_w(\Gamma_{max}-\Gamma)+D_w\exp-(\frac{e\psi_o}{kT})\right]}\left\{1-\frac{K_w\delta_w(\Gamma_{max}-\Gamma)}{\left[k_X\delta_w(\Gamma_{max}-\Gamma)+D_w\exp-(\frac{e\psi_o}{kT})\right]}\right\}$$
$$+\left(\frac{\delta\Gamma}{\delta k_{HX_o}}\right)\frac{D_w A_s k_X\exp-(\frac{e\psi_o}{kT})}{V_w\left[k_X\delta_w(\Gamma_{max}-\Gamma)+D_w\exp-(\frac{e\psi_o}{kT})\right]K_X}\left[1+\frac{\Gamma k_X\delta_w}{\left[k_X\delta_w(\Gamma_{max}-\Gamma)+D_w\exp-(\frac{e\psi_o}{kT})\right]}\right]$$

$$\frac{d}{dt}(\frac{\delta s_4}{\delta\theta_1})=\frac{d}{dt}\left(\frac{\delta\Gamma}{\delta k_{HX_o}}\right)$$
$$=\frac{D^2_{HX_o}}{[k_{HX_o}\delta_o(\Gamma_{max}-\Gamma)+D_{HX_o}]^2}[C_{HX_o}(\Gamma_{max}-\Gamma)]$$
$$-\frac{D^2_{HX_o}}{[k_{HX_o}\delta_o(\Gamma_{max}-\Gamma)+D_{HX_o}]^2}\left[\frac{\Gamma C_{H^+}\exp-(\frac{e\psi_o}{kT})}{K_{HX_o}}\right]$$
$$+\frac{D_{HX_o}k_{HX_o}(\Gamma_{max}-\Gamma)}{[k_{HX_o}\delta_o(\Gamma_{max}-\Gamma)+D_{HX_o}]}(\frac{\delta C_{HX_o}}{\delta k_{HX_o}})$$
$$+\frac{D_{NaX_o}k_{NaX_o}(\Gamma_{max}-\Gamma)}{[k_{NaX}\delta_o(\Gamma_{max}-\Gamma)+D_{NaX_o}]}(\frac{C_{NaX_o}}{\delta k_{HX_o}})$$
$$+\frac{D_w k_X\alpha(\Gamma_{max}-\Gamma)}{\left[k_X\delta_w(\Gamma_{max}-\Gamma)+D_w\exp-(\frac{e\psi_o}{kT})\right]}(\frac{\delta C_X}{\delta k_{HX_o}})$$
$$+\left(\frac{\delta\Gamma}{\delta k_{HX_o}}\right)\frac{D_{HX_o}k_{HX_o}C_{HX_o}}{[k_{HX_o}\delta_o(\Gamma_{max}-\Gamma)+D_{HX_o}]}\left\{\frac{k_{HX_o}\delta_o(\Gamma_{max}-\Gamma)}{[k_{HX_o}\delta_o(\Gamma_{max}-\Gamma)+D_{HX_o}]}-1.0\right\}$$
$$-\left(\frac{\delta\Gamma}{\delta k_{HX_o}}\right)\frac{D_{HX_o}k_{HX_o}C_{H^+}\exp-(\frac{e\psi_o}{kT})}{[k_{HX_o}\delta_o(\Gamma_{max}-\Gamma)+D_{HX_o}]K_{HX_o}}\left\{1.0+\frac{\Gamma k_{HX_o}\delta_o}{[k_{HX_o}\delta_o(\Gamma_{max}-\Gamma)+D_{HX_o}]}\right\}$$
$$+\left(\frac{\delta\Gamma}{\delta k_{HX_o}}\right)\frac{D_{NaX_o}k_{NaX}C_{NaX_o}}{[k_{NaX}\delta_o(\Gamma_{max}-\Gamma)+D_{NaX_o}]}\left\{\frac{k_{NaX}\delta_o(\Gamma_{max}-\Gamma)}{[k_{NaX}\delta_o(\Gamma_{max}-\Gamma)+D_{NaX_o}]}-1.0\right\}$$

$$- \left(\frac{\delta\Gamma}{\delta k_{HX_o}}\right) \frac{D_{NaX_o} k_{NaX} C_{Na+} \exp -(\frac{e\psi_o}{kT})}{[k_{NaX}\delta_o(\Gamma_{max}-\Gamma)+D_{NaX_o}]\,K_{NaX_o}} \left\{1.0 + \frac{\Gamma k_{NaX}\delta_o}{[k_{NaX}\delta_o(\Gamma_{max}-\Gamma)+D_{NaX_o}]}\right\} \quad (9.28)$$

$$+ \left(\frac{\delta\Gamma}{\delta k_{HX_o}}\right) \frac{D_w k_w \alpha C_X}{\left[k_X\delta_w(\Gamma_{max}-\Gamma)+D_w \exp -(\frac{e\psi_o}{kT})\right]} \left\{\frac{K_w\delta_w(\Gamma_{max}-\Gamma)}{\left[k_X\delta_w(\Gamma_{max}-\Gamma)+D_w \exp -(\frac{e\psi_o}{kT})\right]} - 1.0\right\}$$

$$- \left(\frac{\delta\Gamma}{\delta k_{HX_o}}\right) \frac{D_w k_w \alpha \exp -(\frac{e\psi_o}{kT})}{\left[k_X\delta_w(\Gamma_{max}-\Gamma)+D_w \exp -(\frac{e\psi_o}{kT})\right] K_X} \left\{1.0 + \frac{\Gamma k_X\delta_w}{\left[k_X\delta_w(\Gamma_{max}-\Gamma)+D_w \exp -(\frac{e\psi_o}{kT})\right]}\right\}$$

$$\frac{d}{dt}(\frac{\delta s_1}{\delta\theta_2}) = \frac{d}{dt}(\frac{\delta C_{HX_o}}{\delta k_{NaX_o}})$$

$$= -\frac{D_{HX_o}A_s k_{HX_o}(\Gamma_{max}-\Gamma)}{V_o[k_{HX_o}\delta_o(\Gamma_{max}-\Gamma)+D_{HX_o}]}(\frac{\delta\Gamma}{\delta k_{NaX}})$$

$$+ \left(\frac{\delta\Gamma}{\delta k_{NaX}}\right) \frac{D_{HX_o}A_s k_{HX_o}C_{HX_o}}{V_o[k_{HX_o}\delta_o(\Gamma_{max}-\Gamma)+D_{HX_o}]} \left\{1.0 - \frac{k_{HX_o}\delta_o(\Gamma_{max}-\Gamma)}{[k_{HX_o}\delta_o(\Gamma_{max}-\Gamma)+D_{HX_o}]}\right\} \quad (9.29)$$

$$+ \left(\frac{\delta\Gamma}{\delta k_{NaX}}\right) \frac{D_{HX_o}A_s k_{HX_o}C_{H+} \exp -(\frac{e\psi_o}{kT})}{V_o[k_{HX_o}\delta_o(\Gamma_{max}-\Gamma)+D_{HX_o}]\,K_{HX_o}} \left\{1.0 + \frac{\Gamma k_{HX_o}\delta_o}{[k_{HX_o}\delta_o(\Gamma_{max}-\Gamma)+D_{HX_o}]}\right\}$$

$$\frac{d}{dt}(\frac{\delta s_2}{\delta\theta_2}) = \frac{d}{dt}(\frac{\delta C_{NaX_o}}{\delta k_{NaX}})$$

$$= -\frac{A_s D^2_{NaX_o}}{V_o[k_{NaX}\delta_o(\Gamma_{max}-\Gamma)+D_{NaX_o}]^2} \left\{C_{NaX_o}(\Gamma_{max}-\Gamma) - \frac{\Gamma C_{Na+} \exp -(\frac{e\psi_o}{kT})}{K_{NaX_o}}\right\}$$

$$- \frac{D_{NaX_o}A_s k_{NaX}(\Gamma_{max}-\Gamma)}{V_o[k_{NaX}\delta_o(\Gamma_{max}-\Gamma)+D_{NaX_o}]}(\frac{\delta C_{NaX_o}}{\delta k_{NaX}})$$

$$+ \left(\frac{\delta\Gamma}{\delta k_{NaX}}\right) \frac{D_{NaX_o}A_s k_{NaX}C_{NaX_o}}{V_o[k_{NaX}\delta_o(\Gamma_{max}-\Gamma)+D_{NaX_o}]} \left\{1.0 - \frac{k_{NaX}\delta_o(\Gamma_{max}-\Gamma)}{[k_{NaX}\delta_o(\Gamma_{max}-\Gamma)+D_{NaX_o}]}\right\} \quad (9.30)$$

$$+ \left(\frac{\delta\Gamma}{\delta k_{NaX}}\right) \frac{D_{NaX_o}A_s k_{NaX}C_{Na+} \exp -(\frac{e\psi_o}{kT})}{V_o[k_{NaX}\delta_o(\Gamma_{max}-\Gamma)+D_{NaX_o}]\,K_{NaX_o}} \left\{1 + \frac{\Gamma\delta_o k_{NaX}}{[k_{NaX}\delta_o(\Gamma_{max}-\Gamma)+D_{NaX_o}]}\right\}$$

$$\frac{d}{dt}(\frac{\delta s_3}{\delta\theta_2}) = \frac{d}{dt}(\frac{\delta C_X}{\delta k_{NaX}})$$

$$= -\frac{D_w A_s k_X(\Gamma_{max}-\Gamma)}{V_w\left[k_X\delta_w(\Gamma_{max}-\Gamma)+D_w \exp -(\frac{e\psi_o}{kT})\right]}(\frac{\delta C_X}{\delta k_{NaX}})$$

$$+ \left(\frac{\delta\Gamma}{\delta k_{NaX}}\right) \frac{D_w A_s k_X C_X}{V_w\left[k_X\delta_w(\Gamma_{max}-\Gamma)+D_w \exp -(\frac{e\psi_o}{kT})\right]} \left\{1.0 - \frac{K_w\delta_w(\Gamma_{max}-\Gamma)}{\left[k_X\delta_w(\Gamma_{max}-\Gamma)+D_w \exp -(\frac{e\psi_o}{kT})\right]}\right\}$$

$$+ \left(\frac{\delta\Gamma}{\delta k_{NaX}}\right) \frac{D_w A_s k_X \exp -(\frac{e\psi_o}{kT})}{V_w\left[k_X\delta_w(\Gamma_{max}-\Gamma)+D_w \exp -(\frac{e\psi_o}{kT})\right] K_X} \quad (9.31)$$

$$+ \left(\frac{\delta\Gamma}{\delta k_{NaX}}\right) \frac{D_w A_s k_X \exp -(\frac{e\psi_o}{kT})}{V_w\left[k_X\delta_w(\Gamma_{max}-\Gamma)+D_w \exp -(\frac{e\psi_o}{kT})\right] K_X} \left\{\frac{\Gamma k_X\delta_w}{\left[k_X\delta_w(\Gamma_{max}-\Gamma)+D_w \exp -(\frac{e\psi_o}{kT})\right]}\right\}$$

$$\frac{d}{dt}\left(\frac{\delta s_4}{\delta\theta_2}\right) = \frac{d}{dt}\left(\frac{\delta\Gamma}{\delta k_{NaX}}\right)$$

$$= \frac{D_{NaX_o}^2}{[k_{NaX}\delta_o(\Gamma_{max}-\Gamma)+D_{NaX_o}]^2}\{C_{NaX_o}(\Gamma_{max}-\Gamma)\}$$

$$- \frac{D_{NaX_o}^2}{[k_{NaX}\delta_o(\Gamma_{max}-\Gamma)+D_{NaX_o}]^2}\left\{\frac{\Gamma C_{Na+}\exp-(\frac{\epsilon\psi_o}{kT})}{K_{NaX_o}}\right\}$$

$$+ \frac{D_{HX_o}k_{HX_o}(\Gamma_{max}-\Gamma)}{[k_{HX_o}\delta_o(\Gamma_{max}-\Gamma)+D_{HX_o}]}\left(\frac{\delta C_{HX_o}}{\delta k_{NaX}}\right)$$

$$+ \frac{D_{NaX_o}k_{NaX}(\Gamma_{max}-\Gamma)}{[k_{NaX}\delta_o(\Gamma_{max}-\Gamma)+D_{NaX_o}]}\left(\frac{\delta C_{NaX_o}}{k_{NaX}}\right)$$

$$+ \frac{D_w k_X\alpha(\Gamma_{max}-\Gamma)}{\left[k_X\delta_w(\Gamma_{max}-\Gamma)+D_w\exp-(\frac{\epsilon\psi_o}{kT})\right]}\left(\frac{\delta C_X}{\delta k_{NaX}}\right)$$

$$+ \left(\frac{\delta\Gamma}{\delta k_{NaX}}\right)\frac{D_{HX_o}k_{HX_o}C_{HX_o}}{[k_{HX_o}\delta_o(\Gamma_{max}-\Gamma)+D_{HX_o}]}\left\{\frac{k_{HX_o}\delta_o(\Gamma_{max}-\Gamma)}{[k_{HX_o}\delta_o(\Gamma_{max}-\Gamma)+D_{HX_o}]}-1.0\right\}$$

$$- \left(\frac{\delta\Gamma}{\delta k_{NaX}}\right)\frac{D_{HX_o}k_{HX_o}C_{H+}\exp-(\frac{\epsilon\psi_o}{kT})}{[k_{HX_o}\delta_o(\Gamma_{max}-\Gamma)+D_{HX_o}]K_{HX_o}}\left\{1.0+\frac{\Gamma k_{HX_o}\delta_o}{[k_{HX_o}\delta_o(\Gamma_{max}-\Gamma)+D_{HX_o}]}\right\}$$

$$+ \left(\frac{\delta\Gamma}{\delta k_{NaX}}\right)\frac{D_{NaX_o}k_{NaX}C_{NaX_o}}{[k_{NaX}\delta_o(\Gamma_{max}-\Gamma)+D_{NaX_o}]}\left\{\frac{k_{NaX}\delta_o(\Gamma_{max}-\Gamma)}{[k_{NaX}\delta_o(\Gamma_{max}-\Gamma)+D_{NaX_o}]}-1.0\right\}$$

$$- \left(\frac{\delta\Gamma}{\delta k_{NaX}}\right)\frac{D_{NaX_o}k_{NaX}C_{Na+}\exp-(\frac{\epsilon\psi_o}{kT})}{[k_{NaX}\delta_o(\Gamma_{max}-\Gamma)+D_{NaX_o}]K_{NaX_o}}\left\{1.0+\frac{\Gamma k_{NaX}\delta_o}{[k_{NaX}\delta_o(\Gamma_{max}-\Gamma)+D_{NaX_o}]}\right\}$$

$$+ \left(\frac{\delta\Gamma}{\delta k_{NaX}}\right)\frac{D_w k_w\alpha C_X}{\left[k_X\delta_w(\Gamma_{max}-\Gamma)+D_w\exp-(\frac{\epsilon\psi_o}{kT})\right]}\left\{\frac{K_w\delta_w(\Gamma_{max}-\Gamma)}{\left[k_X\delta_w(\Gamma_{max}-\Gamma)+D_w\exp-(\frac{\epsilon\psi_o}{kT})\right]}\right\}$$

$$- \left(\frac{\delta\Gamma}{\delta k_{NaX}}\right)\frac{D_w k_w\alpha C_X}{\left[k_X\delta_w(\Gamma_{max}-\Gamma)+D_w\exp-(\frac{\epsilon\psi_o}{kT})\right]}$$

$$- \left(\frac{\delta\Gamma}{\delta k_{NaX}}\right)\frac{D_w k_w\alpha\exp-(\frac{\epsilon\psi_o}{kT})}{\left[k_X\delta_w(\Gamma_{max}-\Gamma)+D_w\exp-(\frac{\epsilon\psi_o}{kT})\right]K_X}\left\{\frac{\Gamma k_X\delta_w}{\left[k_X\delta_w(\Gamma_{max}-\Gamma)+D_w\exp-(\frac{\epsilon\psi_o}{kT})\right]}\right\}$$

$$- \left(\frac{\delta\Gamma}{\delta k_{NaX}}\right)\frac{D_w k_w\alpha\exp-(\frac{\epsilon\psi_o}{kT})}{\left[k_X\delta_w(\Gamma_{max}-\Gamma)+D_w\exp-(\frac{\epsilon\psi_o}{kT})\right]K_X} \tag{9.32}$$

$$\frac{d}{dt}\left(\frac{\delta s_1}{\delta\theta_1}\right) = \frac{d}{dt}\left(\frac{\delta C_{HX_o}}{\delta k_X}\right)$$

$$= -\frac{D_{HX_o}A_s k_{HX_o}(\Gamma_{max}-\Gamma)}{V_o[k_{HX_o}\delta_o(\Gamma_{max}-\Gamma)+D_{HX_o}]}\left(\frac{\delta C_{HX_o}}{\delta k_X}\right)$$

$$+ \left(\frac{\delta\Gamma}{\delta k_X}\right)\frac{D_{HX_o}A_s k_{HX_o}C_{HX_o}}{V_o[k_{HX_o}\delta_o(\Gamma_{max}-\Gamma)+D_{HX_o}]}\left\{1.0-\frac{k_{HX_o}\delta_o(\Gamma_{max}-\Gamma)}{[k_{HX_o}\delta_o(\Gamma_{max}-\Gamma)+D_{HX_o}]}\right\}$$

$$+ \left(\frac{\delta\Gamma}{\delta k_X}\right)\frac{D_{HX_o}A_s k_{HX_o}C_{H+}\exp-(\frac{\epsilon\psi_o}{kT})}{V_o[k_{HX_o}\delta_o(\Gamma_{max}-\Gamma)+D_{HX_o}]K_{HX_o}}\left\{\frac{\Gamma k_{HX_o}\delta_o}{[k_{HX_o}\delta_o(\Gamma_{max}-\Gamma)+D_{HX_o}]}\right\}$$

$$+\left(\frac{\delta\Gamma}{\delta k_X}\right)\frac{D_{HX_o}A_s k_{HX_o}C_{H^+}\exp-(\frac{e\psi_o}{kT})}{V_o\left[k_{HX_o}\delta_o(\Gamma_{max}-\Gamma)+D_{HX_o}\right]K_{HX_o}} \tag{9.33}$$

$$\begin{aligned}\frac{d}{dt}(\frac{\delta s_2}{\delta\theta_3}) &= \frac{d}{dt}(\frac{\delta C_{NaX_o}}{\delta k_X})\\ &= -\frac{D_{NaX_o}A_s k_{NaX}(\Gamma_{max}-\Gamma)}{V_o\left[k_{NaX}\delta_o(\Gamma_{max}-\Gamma)+D_{NaX_o}\right]}(\frac{\delta C_{NaX_o}}{\delta k_X})\\ &+\left(\frac{\delta\Gamma}{\delta k_X}\right)\frac{D_{NaX_o}A_s k_{NaX}C_{NaX_o}}{V_o\left[k_{NaX}\delta_o(\Gamma_{max}-\Gamma)+D_{NaX_o}\right]}\left\{1.0-\frac{k_{NaX}\delta_o(\Gamma_{max}-\Gamma)}{\left[k_{NaX}\delta_o(\Gamma_{max}-\Gamma)+D_{NaX_o}\right]}\right\}\\ &+\left(\frac{\delta\Gamma}{\delta k_X}\right)\frac{D_{NaX_o}A_s k_{NaX}C_{Na^+}\exp-(\frac{e\psi_o}{kT})}{V_o\left[k_{NaX}\delta_o(\Gamma_{max}-\Gamma)+D_{NaX_o}\right]K_{NaX_o}}\left\{1.0+\frac{\Gamma\delta_o k_{NaX}}{\left[k_{NaX}\delta_o(\Gamma_{max}-\Gamma)+D_{NaX_o}\right]}\right\}\end{aligned} \tag{9.34}$$

$$\begin{aligned}\frac{d}{dt}(\frac{\delta s_3}{\delta\theta_3}) &= \frac{d}{dt}(\frac{\delta C_X}{\delta k_X})\\ &= -\frac{D_w^2 A_s\exp-(\frac{e\psi_o}{kT})}{V_w\left[k_X\delta_w(\Gamma_{max}-\Gamma)+D_w\exp-(\frac{e\psi_o}{kT})\right]}\left\{C_X(\Gamma_{max}-\Gamma)-\frac{\Gamma\exp-(\frac{e\psi_o}{kT})}{K_X}\right\}\\ &-\frac{D_w A_s k_X(\Gamma_{max}-\Gamma)}{V_w\left[k_X\delta_w(\Gamma_{max}-\Gamma)+D_w\exp-(\frac{e\psi_o}{kT})\right]}(\frac{\delta C_X}{\delta k_X})\\ &-\left(\frac{\delta\Gamma}{\delta k_X}\right)\frac{D_w A_s k_X C_X}{V_w\left[k_X\delta_w(\Gamma_{max}-\Gamma)+D_w\exp-(\frac{e\psi_o}{kT})\right]}\left\{\frac{K_w\delta_w(\Gamma_{max}-\Gamma)}{\left[k_X\delta_w(\Gamma_{max}-\Gamma)+D_w\exp-(\frac{e\psi_o}{kT})\right]}\right\}\\ &+\left(\frac{\delta\Gamma}{\delta k_X}\right)\frac{D_w A_s k_X C_X}{V_w\left[k_X\delta_w(\Gamma_{max}-\Gamma)+D_w\exp-(\frac{e\psi_o}{kT})\right]}\\ &+\left(\frac{\delta\Gamma}{\delta k_X}\right)\frac{D_w A_s k_X\exp-(\frac{e\psi_o}{kT})}{V_w\left[k_X\delta_w(\Gamma_{max}-\Gamma)+D_w\exp-(\frac{e\psi_o}{kT})\right]K_X}\left\{\frac{\Gamma k_X\delta_w}{\left[k_X\delta_w(\Gamma_{max}-\Gamma)+D_w\exp-(\frac{e\psi_o}{kT})\right]}\right\}\\ &+\left(\frac{\delta\Gamma}{\delta k_X}\right)\frac{D_w A_s k_X\exp-(\frac{e\psi_o}{kT})}{V_w\left[k_X\delta_w(\Gamma_{max}-\Gamma)+D_w\exp-(\frac{e\psi_o}{kT})\right]K_X}\end{aligned} \tag{9.35}$$

$$\begin{aligned}\frac{d}{dt}(\frac{\delta s_4}{\delta\theta_3}) &= \frac{d}{dt}\left(\frac{\delta\Gamma}{\delta k_X}\right)\\ &= \frac{D_w^2\alpha\exp-(\frac{e\psi_o}{kT})}{\left[k_X\delta_w(\Gamma_{max}-\Gamma)+D_w\exp-(\frac{e\psi_o}{kT})\right]^2}\{C_X(\Gamma_{max}-\Gamma)\}\\ &-\frac{D_w^2\alpha\exp-(\frac{e\psi_o}{kT})}{\left[k_X\delta_w(\Gamma_{max}-\Gamma)+D_w\exp-(\frac{e\psi_o}{kT})\right]^2}\left\{\frac{\Gamma\exp-(\frac{e\psi_o}{kT})}{K_X}\right\}\\ &+\frac{D_{HX_o}k_{HX_o}(\Gamma_{max}-\Gamma)}{\left[k_{HX_o}\delta_o(\Gamma_{max}-\Gamma)+D_{HX_o}\right]}(\frac{\delta C_{HX_o}}{\delta k_X})\\ &+\frac{D_{NaX_o}k_{NaX}(\Gamma_{max}-\Gamma)}{\left[k_{NaX}\delta_o(\Gamma_{max}-\Gamma)+D_{NaX_o}\right]}(\frac{\delta C_{NaX_o}}{\delta k_X})\end{aligned}$$

$$
+\frac{D_w k_X \alpha \exp_{\cdot}-(\frac{\epsilon\psi_o}{kT})}{\left[k_X\delta_w(\Gamma_{max}-\Gamma)+D_w\exp-(\frac{\epsilon\psi_o}{kT})\right]}(\frac{\delta C_X}{\delta k_X})
$$

$$
+\left(\frac{\delta\Gamma}{\delta k_X}\right)\frac{D_{HX_o}k_{HX_o}C_{HX_o}}{[k_{HX_o}\delta_o(\Gamma_{max}-\Gamma)+D_{HX_o}]}\left\{\frac{k_{HX_o}\delta_o(\Gamma_{max}-\Gamma)}{[k_{HX_o}\delta_o(\Gamma_{max}-\Gamma)+D_{HX_o}]}\right\}
$$

$$
-\left(\frac{\delta\Gamma}{\delta k_X}\right)\frac{D_{HX_o}k_{HX_o}C_{HX_o}}{[k_{HX_o}\delta_o(\Gamma_{max}-\Gamma)+D_{HX_o}]}
$$

$$
-\left(\frac{\delta\Gamma}{\delta k_X}\right)\frac{D_{HX_o}k_{HX_o}C_{H^+}\exp-(\frac{\epsilon\psi_o}{kT})}{[k_{HX_o}\delta_o(\Gamma_{max}-\Gamma)+D_{HX_o}]K_{HX_o}}\left\{\frac{\Gamma k_{HX_o}\delta_o}{[k_{HX_o}\delta_o(\Gamma_{max}-\Gamma)+D_{HX_o}]}\right\}
$$

$$
-\left(\frac{\delta\Gamma}{\delta k_X}\right)\frac{D_{HX_o}k_{HX_o}C_{H^+}\exp-(\frac{\epsilon\psi_o}{kT})}{[k_{HX_o}\delta_o(\Gamma_{max}-\Gamma)+D_{HX_o}]K_{HX_o}}
$$

$$
+\left(\frac{\delta\Gamma}{\delta k_X}\right)\frac{D_{NaX_o}k_{NaX}C_{NaX_o}}{[k_{NaX}\delta_o(\Gamma_{max}-\Gamma)+D_{NaX_o}]}\left\{\frac{k_{NaX}\delta_o(\Gamma_{max}-\Gamma)}{[k_{NaX}\delta_o(\Gamma_{max}-\Gamma)+D_{NaX_o}]}\right\}
$$

$$
-\left(\frac{\delta\Gamma}{\delta k_X}\right)\frac{D_{NaX_o}k_{NaX}C_{NaX_o}}{[k_{NaX}\delta_o(\Gamma_{max}-\Gamma)+D_{NaX_o}]}
$$

$$
-\left(\frac{\delta\Gamma}{\delta k_X}\right)\frac{D_{NaX_o}k_{NaX}C_{Na^+}\exp-(\frac{\epsilon\psi_o}{kT})}{[k_{NaX}\delta_o(\Gamma_{max}-\Gamma)+D_{NaX_o}]K_{NaX_o}}\left\{\frac{\Gamma k_{NaX}\delta_o}{[k_{NaX}\delta_o(\Gamma_{max}-\Gamma)+D_{NaX_o}]}\right\}
$$

$$
-\left(\frac{\delta\Gamma}{\delta k_X}\right)\frac{D_{NaX_o}k_{NaX}C_{Na^+}\exp-(\frac{\epsilon\psi_o}{kT})}{[k_{NaX}\delta_o(\Gamma_{max}-\Gamma)+D_{NaX_o}]K_{NaX_o}}
$$

$$
+\left(\frac{\delta\Gamma}{\delta k_X}\right)\frac{D_w k_X\alpha C_X}{\left[k_X\delta_w(\Gamma_{max}-\Gamma)+D_w\exp-(\frac{\epsilon\psi_o}{kT})\right]}\left\{\frac{K_w\delta_w(\Gamma_{max}-\Gamma)}{\left[k_X\delta_w(\Gamma_{max}-\Gamma)+D_w\exp-(\frac{\epsilon\psi_o}{kT})\right]}\right\}
$$

$$
-\left(\frac{\delta\Gamma}{\delta k_X}\right)\frac{D_w k_X\alpha C_X}{\left[k_X\delta_w(\Gamma_{max}-\Gamma)+D_w\exp-(\frac{\epsilon\psi_o}{kT})\right]}
$$

$$
-\left(\frac{\delta\Gamma}{\delta k_X}\right)\frac{D_w k_X\alpha\exp-(\frac{\epsilon\psi_o}{kT})}{\left[k_X\delta_w(\Gamma_{max}-\Gamma)+D_w\exp-(\frac{\epsilon\psi_o}{kT})\right]K_X}\left\{\frac{\Gamma k_X\delta_w}{\left[k_X\delta_w(\Gamma_{max}-\Gamma)+D_w\exp-(\frac{\epsilon\psi_o}{kT})\right]}\right\}
$$

$$
-\left(\frac{\delta\Gamma}{\delta k_X}\right)\frac{D_w k_X\alpha\exp-(\frac{\epsilon\psi_o}{kT})}{\left[k_X\delta_w(\Gamma_{max}-\Gamma)+D_w\exp-(\frac{\epsilon\psi_o}{kT})\right]K_X} \tag{9.36}
$$

9.5.3 Solution Procedure

There are a total of 16 nonlinear , coupled differential equations (12 sensitivity , and 4 state) which must be solved simultaneously for the sensitivity coefficients , namely , $\frac{\delta\Gamma}{\delta k_X}$, $\frac{\delta\Gamma}{\delta k_{NaX}}$, and $\frac{\delta\Gamma}{\delta k_{HX_o}}$. The IMSL routine DGEAR[84] was used for the solution of these equations , but in view of the stiffness of the problem , an analytical Jacobian matrix of partial derivatives is required . This matrix of partial derivatives is obtained by differentiating equation 9.24 with respect to each state

variable , i. e. , we seek partial derivatives of the form :

$$\frac{\delta}{\delta \vec{s^*}} \left[\frac{d}{dt} \left(\frac{\delta \vec{s}}{\delta \vec{\theta}} \right) \right]$$

where the vector , $\vec{s^*}$, includes the 12 sensitivity coefficients in addition to the 4 state variables . Thus , the Jacobian matrix of partial derivatives consists of 256 (16 × 16) differential equations .

For the solution of the sensitivity equations , all the afore-mentioned input data such as the various model constants , the initial parameter estimates and the independent variables were supplied. At each experimentally determined time interval , the routine DGEAR[84] was called and the calculated values of the relevant sensitivity coefficients as well as the state variables were recorded.

Once the sensitivity coefficients were available , it was then possible to see which parameters influenced Γ more than the others, and at the same time , one could determine the direction in which any parameter affected the state variables for any given caustic concentration and initial acid concentration . The programme written for the purpose of solving the sensitivity equations was then modified so as to calculate the surface pressure corresponding to each experimental time interval . The parameters were adjusted in order to minimize the difference between the calculated and experimental surface pressures at each and every time interval for the given initial caustic and acid concentrations .

Part IV

Dynamic Model for

Multi-Component Systems

Chapter 10

Development of a Dynamic Model for Multi-Component Systems

We now seek to extend the single component dynamic model of chapter 8 to cases of a mixture of several acids in the oleic phase interacting with a spectrum of aqueous NaOH solutions .

10.1 Basic Assumptions

There are a number of basic assumptions which underly the development of the single component models presented in part III . In formulating the multi-component model equations , additional assumptions must be made , some of which are the following :

(i) Surface coverage is limited to a monolayer.

(ii) Ideal behaviour for all interacting species in the bulk phases and the interface .

This means that the concentrations of all surface-active species both in the respective bulk phases and in the interface are so dilute that steric and coulombic forces of repulsion between

particles of the different species are minimal .

(iii) Each acid species present in the mixture undergoes the various interfacial reactions discussed in chapter 8 without any interference from other acidic constituents .

(iv) Transport and sorption kinetic rate parameters determined from the single component equilibrium and dynamic models will be valid for any given mixture constituent and its associated surface active species .

(v) In keeping with Nernstian convective diffusion theory , each acid in the mixture together with its associated surface active species sets up unique diffusion boundary layers which are not influenced by those of other mixture constituents .

10.2 Generalized Sorption Kinetic Rate Equations

The interfacial reactions outlined in section 8.3 are valid for each acid in the mixture . We can write down the rate expressions for any given acid component , i , using the arguments presented in chapter 8 as follows ;

(a) Adsorptive dissociation of acid from oleic sub-layer;

$$R_{(a,HX_{o,i})} = k_{HX_{o,i}}\left[C_{HX_{o,i,s}}(\Gamma_{max} - \Gamma) - \frac{\Gamma_i}{K_{HX_{o,i}}} C_{H^+} \exp -(\frac{\varepsilon\psi_o}{kT})\right] \qquad (10.1)$$

(b) Adsorption of X_i^- from the aqueous sublayer ;

$$R_{(a,X_i^-)} = k_{X_i}\left[C_{X_{i,s}}(\frac{\varepsilon\psi_o}{kT})(\Gamma_{max} - \Gamma) - \frac{\Gamma_i}{K_{X_i}}\right] \qquad (10.2)$$

(c) Adsorption of $NaX_{o,i}$ from the oleic sublayer ;

$$R_{(a,NaX_{o,i})} = k_{NaX_i}\left[C_{NaX_{o,i,s}}(\Gamma_{max} - \Gamma) - \frac{\Gamma_i}{K_{NaX_{o,i}}} C_{Na^+} \exp -(\frac{\varepsilon\psi_o}{kT})\right] \qquad (10.3)$$

(d) Adsorption of $HX_{w,i}$ from the aqueous sublayer ;

$$R_{(a,HX_{w,i})} = k_{HX_{w,i}}\left[C_{HX_{w,i,s}}(\Gamma_{max} - \Gamma) - \frac{\Gamma_i}{K_{HX_{w,i}}} C_{H+} \exp -(\frac{\varepsilon\psi_o}{kT})\right] \qquad (10.4)$$

We combine equations 10.2 and 10.4 by the use of the α parameter defined in chapter 8 , and the result is as follows ;

$$\begin{aligned} R_{(a,X_i^- + HX_{w,i})} &= R_{(a,X_i^-)} \exp -(\frac{\varepsilon\psi_o}{kT})\left[1 + \frac{C_{H+}}{K^D_{HX_i}}\right] \\ &= k_{X_i}\alpha_i\left[C_{X_{i,s}}(\Gamma_{max} - \Gamma) - \frac{\Gamma_i}{K_{X_i}} \exp -(\frac{\varepsilon\psi_o}{kT})\right] \end{aligned} \qquad (10.5)$$

10.3 Species Bulk Transport Equations

The Nernstian convective diffusion theory is used to obtain the bulk transport equations for all relevant species of the multi-component system in accordance with equation 8.16 as follows :

(i) Transport of $HX_{o,i}$ to the oleic sublayer ;

$$V_o\frac{dC_{HX_{o,i}}}{dt} = -\frac{D_{HX_{o,i}}A_s}{\delta_{o,i}}\left[C_{HX_{o,i}} - C_{HX_{o,i,s}}\right] \qquad (10.6)$$

(ii) Transport of $NaX_{o,i}$ to the oleic sublayer ;

$$V_o\frac{dC_{NaX_{o,i}}}{dt} = -\frac{D_{NaX_{o,i}}A_s}{\delta_{o,i}}\left[C_{NaX_{o,i}} - C_{NaX_{o,i,s}}\right] \qquad (10.7)$$

(iii) Transport of X_i^- to the aqueous sublayer ;

$$V_w\frac{dC_{X_i^-}}{dt} = -\frac{D_{X_i^-}A_s}{\delta_{w,i}}\left[C_{X_i^-} - C_{X_{i,s}^-}\right] \qquad (10.8)$$

(iv) Transport of $HX_{w,i}$ in accordance with the following equation ;

$$V_w\frac{dC_{HX_{w,i}}}{dt} = -\frac{D_{HX_{w,i}}A_s}{\delta_{w,i}}\left[C_{HX_{w,i}} - C_{HX_{w,i,s}}\right] \qquad (10.9)$$

Equations 10.8 and 10.9 are then combined using α_i , and the result becomes ;

$$V_w \alpha_i \frac{dC_{X_i^-}}{dt} = -\frac{D_{w,i} A_s \alpha_i}{\delta_{w,i}} \left[C_{X_i^-} - C_{X_{i,s}^-} \right] \qquad (10.10)$$

10.4 The Equations of the Multi-Component Dynamic Model

Following the procedure adopted for the single component analyses , we solve for the various sublayer concentrations and then resubstitute the same into the bulk transport equations . The resulting diffusive-kinetic equations are as follows :

1. for the species $HX_{o,i}$;

$$V_o \frac{dC_{HX_{o,i}}}{dt} = -\frac{D_{HX_{o,i}} A_s k_{HX_{o,i}}}{\left[k_{HX_{o,i}} \delta_{o,i} (\Gamma_{max} - \Gamma) + D_{HX_{o,i}} \right]} \left[C_{HX_{o,i}} (\Gamma_{max} - \Gamma) - \frac{\Gamma_i}{K_{HX_{o,i}}} C_{H^+} \exp -(\frac{\varepsilon \psi_o}{kT}) \right] \qquad (10.11)$$

2. for the species $NaX_{o,i}$;

$$V_o \frac{dC_{NaX_{o,i}}}{dt} = -\frac{D_{NaX_{o,i}} A_s k_{NaX_{o,i}}}{\left[k_{NaX_{o,i}} \delta_{o,i} (\Gamma_{max} - \Gamma) + D_{NaX_{o,i}} \right]} \left[C_{NaX_{o,i}} (\Gamma_{max} - \Gamma) \right] + \frac{D_{NaX_{o,i}} A_s k_{NaX_{o,i}}}{\left[k_{NaX_{o,i}} \delta_{o,i} (\Gamma_{max} - \Gamma) + D_{NaX_{o,i}} \right]} \left[\frac{\Gamma_i}{K_{NaX_{o,i}}} C_{Na^+} \exp -(\frac{\varepsilon \psi_o}{kT}) \right] \qquad (10.12)$$

3. for the combined aqueous phase species ; $(X^- + HX)_{w,i}$, the equation becomes ;

$$V_w \frac{dC_{X_i}}{dt} = -\frac{D_{w,i} A_s k_{X_i}}{\left[k_{X_i} \delta_{w,i} (\Gamma_{max} - \Gamma) + D_{w,i} \exp -(\frac{\varepsilon \psi_o}{kT}) \right]} \left[C_{X_i} (\Gamma_{max} - \Gamma) - \frac{\Gamma_i}{K_{X_i}} \exp -(\frac{\varepsilon \psi_o}{kT}) \right] \qquad (10.13)$$

4. an overall species mass balance equation can be written thus ;

$$\frac{d\Gamma_i}{dt} = \sum_{i=1}^{M} R_{(a,i,j)} \quad , j = 1, 2 \qquad (10.14)$$

The expansion of equation 10.14 leads to an expression for each individual Γ_i , as follows ;

$$\begin{aligned}\frac{d\Gamma_i}{dt} = & \frac{D_{HX_{o,i}} k_{HX_{o,i}}}{\left[k_{HX_{o,i}}\delta_{o,i}(\Gamma_{max}-\Gamma)+D_{HX_{o,i}}\right]}\left\{C_{HX_{o,i}}(\Gamma_{max}-\Gamma)-\frac{\Gamma_i}{K_{HX_{o,i}}}C_{H^+}\exp-(\frac{\varepsilon\psi_o}{kT})\right\} \\ & + \frac{D_{NaX_{o,i}} k_{NaX_{o,i}}}{\left[k_{NaX_{o,i}}\delta_{o,i}(\Gamma_{max}-\Gamma)+D_{NaX_{o,i}}\right]}\left\{C_{NaX_{o,i}}(\Gamma_{max}-\Gamma)\right\} \\ & - \frac{D_{NaX_{o,i}} k_{NaX_{o,i}}}{\left[k_{NaX_{o,i}}\delta_{o,i}(\Gamma_{max}-\Gamma)+D_{NaX_{o,i}}\right]}\left\{\frac{\Gamma_i}{K_{NaX_{o,i}}}C_{Na^+}\exp-(\frac{\varepsilon\psi_o}{kT})\right\} \qquad (10.15) \\ & + \frac{D_{w,i}\alpha_i k_{X_i}}{\left[k_{X_i}\delta_{w,i}(\Gamma_{max}-\Gamma)+D_{w,i}\exp-(\frac{\varepsilon\psi_o}{kT})\right]}\left\{C_{X_i}(\Gamma_{max}-\Gamma)-\frac{\Gamma_i}{K_{X_i}}\exp-(\frac{\varepsilon\psi_o}{kT})\right\}\end{aligned}$$

In addition to the above differential equations , the following global algebraic relationships characterize the overall interfacial behaviour of the multi-component system , viz :

(a) The overall surfactant surface concentration , Γ , which is given by ;

$$\Gamma = \sum_{i=1}^{M_s}\Gamma_i \qquad (10.16)$$

(b) The surfactant surface concentration expressed in units of $Å^2$ per ion as follows ;

$$A = \frac{1.6603\times10^{-8}}{\Gamma\times10^{-4}} \qquad (10.17)$$

(c) The global interfacial potential , ψ_o , given by the Gouy-Chapman model as follows ;

$$\psi_o = -51.4\sinh^{-1}\left[\frac{136.9}{A\sqrt{C_{OH}}}\right] \qquad (10.18)$$

(d) And finally, the Frumkin-Volmer-Davies-Hachisu (FVDH) equation of state ;

$$\begin{aligned}\Pi &= \gamma_o-\gamma \\ &= \frac{kT}{A_o}\ln(\frac{A}{A-A_o})+\sqrt{\left(\frac{8D_cNC(kT)^3}{10^3\varepsilon^2}\right)}\left[\cosh(\frac{\varepsilon\psi_o}{2kT})-1.0\right] \qquad (10.19)\end{aligned}$$

Chapter 11

Solution of the Model Equations for a Binary Mixture

In order to test the validity of the generalized dynamic model proposed in the last chapter , we now examine the case of a binary mixture of oleic and lauric acids in hexadecane . These same acids were used in the single component studies .

11.1 Specification of the System of Equations

According to the analyses presented in chapter 10 , we have two components , hence $M_n = 2$. Thus , 8 diffusive-kinetic equations are necessary in order that all relevant surface active species of the mixture are considered . The relevant equations are obtained simply by writing each of equations 10.11, 10.12 , 10.13 , and 10.15 twice , (one each for each mixture component and its associated surface active species) . Additionally , the four global relationships , namely , equations 10.16–10.19 must be solved simultaneously with the 8 differential equations .

11.2 Solving the Equations for the Binary Mixture

In comparison to the single component dynamic model , there are now twice the number of differential equations . However , since no parameter estimation is required , sensitivity analysis is not necessary . Thus , we have a smaller number of partial differential equations to handle . The partial differential equations arise from the analytic Jacobian matrix of partial derivatives which must be supplied to the IMSL routine DGEAR[84] .

The eight state variables of the problem are as follows ; $C_{HX_{o,oleic}}$, $C_{HX_{o,lauric}}$, $C_{NaX_{o,oleic}}$, $C_{NaX_{o,lauric}}$, $C_{X_{oleic}}$, $C_{X_{lauric}}$, Γ_{oleic} , Γ_{lauric} . The Jacobian matrix of partial derivatives is obtained by differentiating each of the eight differential equations with respect to each of the eight state variables . The number of equations involved comes to 64 . One important property of the equations is the fact that Γ is a function of Γ_i and must be so treated in taking the partial derivatives . The size of the Jacobian matrix prohibits the listing of the pertinent equations in the text .

A computer program written for the purpose of solving the model equations starts by supplying the values of the relevant equilibrium and dynamic parameters which would have been determined from the single component models . Initial values of the state variables are also specified . Because the parameter ψ_o must be available in order to solve any of the differential equations , we had to compute its value from equations 10.16–10.18 , for each and every step size utilised in the solution scheme . Finally , at each desired time interval , the global value of Γ is calculated in accordance with equation 10.16 . The surface pressure , Π , corresponding to that value of Γ is determined from equation 10.19 . Subsequently , the dynamic interfacial tension for the system at the desired interfacial age can be easily determined once Π is known .

Part V

Results, Discussion and Conclusions

Chapter 12

Physical Properties of Working Solutions

12.1 Properties of the Aqueous Solutions

Physical characteristics such as pH , density , and viscosity were measured for all the aqueous solutions involved in this study . Table A1 of Appendix A lists the property values for the solutions in question . Similar data for the various oleic solutions can be found in Table A2 . Table A1 shows that at NaOH concentration of 0.25 mM , the bulk phase pH was 10.34 . Neutral water used in preparing the caustic solutions had a pH of 7.06 . Spink[47] working with fatty acids of chain length in the range of C14–C18 , found that the ionization of the acid generally commenced at a pH in the range of 9–10 . Thus one can expect a considerable degree of ionization even in the presence of NaOH concentrations as low as 0.25 mM . The data presented in Table A1 also shows that the pH increases with higher caustic concentrations in the aqueous phase . The actual experimental pH values are quite close to the theoretical ones based on the ionic product of water at ambient

conditions . For example , at 25° C , the ionic product of water is given as follows ;

$$K_w = [H^+][OH^-] = 10^{-14} \qquad (12.1)$$

Thus at 250 mM NaOH , equation 12.1 yields the pH of the solution as follows ;

$$-\log[H^+] = pH = 13.40$$

The experimental pH value at this caustic concentration was 13.17, which attests to the accuracy of the solution preparation scheme as well as the pH measurement procedure itself.

The density data also given in Table A1 were all close to the value for neutral water . The small but definite increasing trend in the density values with increase in NaOH concentration is also expected . The viscosity data also followed a trend similar to that of density . At the highest caustic concentration used in the study , the viscosity increased by just 10% relative to that of neutral water. The increase in density was even smaller , a mere 1% . These physical measurements confirm that the aqueous solutions were indeed dilute . If we should adopt Hildebrand's[109] definition of an ideal solution as one in which no heat of mixing or change in total volume occurs , then we could also claim that the aqueous solutions were ideal .

12.2 Physical Property of Oleic Solutions

The density and viscosity data for the various oleic solutions including the binary mixture systems are listed in Table A2 . The densities of the single acid solutions in hexadecane differed only slightly from that of the solvent. However , for the oleic acid solutions , there was a significant increase in density as the acid concentration was raised . For example , the density of 0.10 mM oleic acid was 770.1109 kg/m^3 , while the corresponding value for 1.00 mM acid solution was 770.1715 kg/m^3. As can also be seen from Table A2 , the density of 20 mM lauric acid solution in hexadecane was

770.6251 kg/m^3 . This explains why the densities of the binary acid mixtures were all close to the value measured for 0.02 M lauric acid solution . Even with the mixture systems , we find also an increasing trend in the densities with the increase in the oleic acid content. Mixture M1, which contained only 0.50 mole% of oleic acid , had a density of 770.6250 kg/m^3 , while M5 with an oleic acid content of about 5 mole% had a density of 770.6733 kg/m^3 .

The viscosity data for the oleic solutions were also quite consistent as can be seen from Table A2 . Again , in the case of the single acid solutions , the viscosities were all close to the value measured for hexadecane . With the oleic acid solutions , the increasing trend in the viscosities as the acid concentration was raised is also apparent from the data of Table A2 . It is important to note the difference in the viscosities of 10 mM oleic and lauric acids respectively . The former had a viscosity of 3.0434 mPa. s , while the corresponding value for the latter was 3.0213 mPa. s . From Ref. 40 , the viscosity of oleic acid at 25° C was given as 27.6 mPa. s , and for lauric acid at 70° C, the value was 7.3 mPa. s . Such a large difference in the viscosity of the two acids means that even in very dilute systems, oleic acid solutions should be more viscous than lauric acid solutions of comparable concentrations . As was the case for the binary acid mixture densities , the viscosities differed only slightly from the value determined for 20 mM lauric acid . Additionally , a small increase in the viscosities of these mixtures with increase in oleic acid content can also be noticed in the data of Table A2 . The fact that the mixture properties did not differ substantially from those of the constituent acid solutions showed that no irregular behaviour or synergistic tendencies were manifested .

Chapter 13

Single Component Equilibrium Studies

13.1 Interfacial Data of the Oleic Acid Systems

In most cases , the equilibrium interfacial data were determined by running dynamic measurements until steady state conditions prevailed . Where it was not possible to establish the exact time to equilibrium , additional runs were then made within the vicinity of the anticipated equilibrium point. A final check was carried out by independent IFT measurements using the ring and spinning drop tensiometers . Because of the procedure used to obtain most of the equilibrium data , we have included the equilibrium IFT data among those obtained in the course of the dynamic studies , the latter appearing in a series of Tables in Appendix B as EQUBR values.

The pertinent interfacial data for 0.3125 mM oleic acid in hexadecane in contact with various NaOH solutions are given in Table 3 . The NaOH concentrations as well as the phase volume ratios and the surface pressures for each experimental run are all included in Table 3. By definition (see equation 7.26), Π is the difference between columns 1 and 4 entries for the first experimental drop

(drop no. 1) , while for the second experimental drop, Π is obtained by subtracting column 7 from column 1. From Table 3, we see that even at NaOH concentration of 0.25 mM , the IFT dropped by as much as 11 mN/m from the neutral water tension of 36.5 mN/m . As expected , the IFT dropped as the NaOH concentration was increased , resulting in tensions of about 7 mN/m at caustic concentration of 25 mM . Measurements at higher caustic levels were not carried out due to the instability of the pendant oil droplets in such high caustic environment. We also see in

Table 3: Equilibrium Data for 0.3125 mM Oleic Acid in Hexadecane/Caustic Systems

Oil/Water	NaOH	DROP NO 1			DROP NO 2		
IFT	Conc	V_w/V_o	Oil/NaOH	Surf Press	V_w/V_o	Oil/NaOH	Surf Press
(mN/m)	(mM)	ml/ml	IFT (mN/m)	Π (mN/m)	ml/ml	IFT (mN/m)	Π (mN/m)
36.56	0.25	62.14	25.57	10.99	58.00	25.44	11.12
36.56	1.25	72.50	21.63	14.93	72.50	21.64	14.92
36.56	2.50	217.50	21.48	15.08	217.50	21.03	15.53
36.56	12.50	290.0	9.33	27.23	290.0	9.62	26.94
36.56	25.0	1087.5	6.97	29.59	966.7	7.63	28.93

Table 3 , that the phase volume ratio increased from a value of 62 at NaOH concentration of 0.25 mM to about 1000 at the caustic concentration of 25 mM . That this is a direct consequence of the decrease in IFT with the rise in aqueous caustic concentration can be demonstrated as follows : We recall the Adams-Bashforth equation (equation 6.3) which for a pendant drop becomes ;

$$\Delta P = \Delta\rho g z - \frac{2\gamma}{R_o}. \qquad (13.1)$$

Considering the apex of the drop , at which $\Delta P = 0$, we then find from equation 13.1 that ;

$$\gamma = \frac{R_o \Delta \rho g z}{2} \qquad (13.2)$$

Hence , $\gamma \propto R_o$; thus , a decrease in γ means the size of the pendant drop decreases .

The IFT of hexadecane with neutral water was found to be 43 mN/m . This value was also confirmed by the use of the ring tensiometer. At the initial stages of this study, the literature values for the IFT of both benzene and toluene in neutral water had been well reproduced by our experimental system . However, work carried out by Neumann[110] on a series of paraffins ranging from heptane to tetradecane indicated that the IFT of pure hexadecane in pure water should be about 52 mN/m. The relatively lower value of 43 mN/m indicates the presence of impurities in the solvent. For the purpose of this investigation, it was only necessary to verify that the impurities were inert to caustic within the working NaOH concentrations employed in our studies. For the 0.3125 mM oleic acid solution in hexadecane contacted with neutral water , the drop in IFT was as much as 6.5 mN/m , an indication of the effectiveness of the acid as a surfactant even at such low concentrations . From a practical point of view , it can be deduced that even trace amounts of highly surface-active acids in crude oils contacted with a mildly alkaline flood water may be sufficient to effect significant additional oil recoveries .

Additional equilibrium interfacial studies were carried out with the reference oleic acid solutions for the binary mixture experiments . Data for each applicable oleic acid concentration in the various alkaline media have also been compiled and they appear in appropriate tables of Appendix B . The trend in both IFT and phase volume for these other oleic acid solutions was similar to that found for 0.3125 mM system . For example , the IFT in neutral water obtained with 0.10 mM and 0.20 mM oleic acid solutions was about 41.5 mN/m , substantially higher than the 36.5 mN/m measured at the acid concentration of 0.3125 mM . However , the neutral water IFT was lower when the oleic

acid concentration was increased above 0.3125 mM . Data taken from Appendix B gives the neutral water IFT for 0.6125 mM and 1.00 mM oleic acid as 36.8 and 34.2 mN/m respectively . For these same oleic acid solutions , the equilbrium IFT at 25 mM NaOH was 5.4 and 3.9 mN/m respectively.

13.2 Interfacial Data for the Lauric Acid Systems

Only one single working concentration of 0.02 M was used for the lauric acid single component study , as well as the binary mixture experiments . The equilibrium interfacial data for this acid system are given in Table 4 . Information contained in Table 4 is of the same form as the one given in Table 3 for the oleic acid system . Other experimental details can be found in the relevant tables of Appendix B . Two different values for the IFT in neutral water were given in Table 4 , namely , 32.63 and 34.43 mN/m . The difference in the tension values arose from a slight variation in the chemical composition of the distilled water used during the earlier part of the study from that used at the latter stage . This difference in water quality was as a result of repair work that was carried out on the distillation apparatus . Table 4 shows that the phase volume ratio for this acid system also increased as the NaOH concentration of the aqueous phase was raised . However, the increase in the phase volume ratio was smaller when compared to the values obtained for the oleic acid system . For example , at NaOH concentration of 0.25 mM , V_w/V_o was 45 , and at the caustic level of 25 mM , the ratio increased to 217 . The corresponding values for the oleic acid system , (Table 3) were 62 and 1000 . Consistent with this modest increase in the phase volume ratio, we find that the IFT dropped only marginally even at very high NaOH concentrations . For example , in contrast with the 1.1 mN/m drop in IFT found with the 0.3125 mM oleic acid system at the caustic level of 0.25 mM, the drop in IFT for the lauric acid system at the same NaOH

Table 4: Equilibrium Data for 0.02 M Lauric Acid in Hexadecane/Caustic Systems

Oil/Water	NaOH	DROP NO ONE			DROP NO TWO		
IFT	Conc	V_w/V_o	Oil/NaOH	Surf Press	V_w/V_o	Oil/NaOH	Surf Press
(mN/m)	(mM)	ml/ml	IFT (mN/m)	II (mN/m)	ml/ml	IFT (mN/m)	II (mN/m)
32.63	0.25	45.08	30.77	1.86	45.08	31.21	1.42
32.63	1.25	62.14	24.15	8.48	62.14	25.14	7.49
32.63	2.50	62.14	24.45	8.18	62.14	22.83	9.80
32.63	12.50	174.0	22.66	9.97	174.0	22.44	10.19
34.43	25.0	217.5	22.19	12.24	290.0	22.20	12.23
34.43	100.0	435.0	18.27	16.16	-	-	-
34.43	125.0	-	-	-	511.8	15.64	18.79
34.43	150.0	669.2	13.44	20.99	669.2	13.01	21.42
34.43	200.0	870.0	9.72	24.71	870.0	9.97	24.46
34.43	250.0	790.9	9.98	24.45	-	-	-

concentration was just 1 mN/m. When the caustic concentration was increased to 250 mM , the equilibrium IFT was a mere 10 mN/m , which is substantially higher than the 7 mN/m obtained for the 0.3125 mM oleic acid at NaOH concentration of 25 mM . It should be noted that the working lauric acid concentration of 0.02 M is 64 times the oleic acid concentration of 0.3125 mM. That large concentration ratio , notwithstanding , did not compensate for the poorer surfactancy behaviour of lauric acid compared to oleic acid as evident from the IFT data of Tables 3 and 4 .

13.3 Parameter Estimates from the Equilibrium Model

The single component equilibrium model was discussed in chapter 7 . The development of the model equations was based on the acid ionization reaction together with its associated equilibrium constant. Additionally , we also considered the interfacial reactions leading to the formation of the inactive soap species and its subsequent desorption to the oleic phase , all of which are governed by a salt dissociation constant . As a result , we chose the equilibrium constants associated with the acid and the inactive salt , namely , K^D_{HX} , and K^D_{NaX} respectively , as the model parameters to be precisely estimated by non-linear regression . Table 5 lists the values of these two parameters for all the single component acid systems involved in the study . Parameter values for the lauric acid system were included in Table 5 , but it must be pointed out that precise estimates could not be obtained for this acid because of the dominance of the independent variables over the model parameters . In order to demonstrate this peculiar problem , we reexamine the relationship between the anion concentration and the model parameters given earlier as equation 7.18 . This equation is reproduced as follows ;

$$C_{X^-} = \frac{(C_{HX_o})_o}{\left\{\frac{V_w}{V_o} + \frac{K_w K_p}{K^D_{HX} C_{OH^-}} + \frac{C_{OH^-}}{K^D_{NaX}}\right\}} \qquad (13.3)$$

In equation 13.3 , the value of K_p for lauric acid was 1.36×10^4 , by far smaller than the corresponding value for oleic acid , which was 1.43×10^7 . The result was that the phase volume ratio completely dominated the denominator of equation 13.3 for all values of C_{OH^-} , thus making the other terms statistically insignificant . When the experimental data for this acid system were analysed with the non-linear regression routine , namely ZXSSQ[84], the parameter estimates were highly unrealistic . Because the preliminary parameter estimates which were found by a manual solution of the model equations were quite close to the final values obtained by regression analysis for the oleic acid systems , we believe that the figures for the lauric acid system given in Table 5

are as precise as can be expected given the peculiar nature of the model equations as well as the constants for the acid in question.

Table 5: Parameter Estimates from the Equilibrium Model

System Identity	NaOH Conc. (mM)	K^D_{HX} ($M \times 10^7$)	K^D_{NaX}, ($M \times 10^4$)
0.10 mM Oleic in HD/NaOH	0.25–200.0	5.70	0.67
0.20 mM Oleic in HD/NaOH	0.25–125.0	7.74	0.55
0.3125 mM Oleic in HD/NaOH	0.25 –25.0	2.14	1.16
0.6125 mM Oleic in HD/NaOH	0.25– 25.0	1.21	1.57
1.00 mM Oleic in HD/NaOH	0.25 – 25.0	1.62	0.94
0.02 M Lauric in HD/NaOH	0.25– 2.50	0.01	2.00
0.02 M Lauric in HD/NaOH	2.50–250.0	0.0005	2.00

13.3.1 Parameter Estimates for the Oleic Acid Systems

The parameter values which are listed in Table 5 were estimated by the use of the Levenberg-Marquardt algorithm [101,102] . This algorithm was available as the IMSL routine ZXSSQ[84] . Both parameters were estimated simultaneously and the final estimates were those that resulted in the minimum sum of squares of residuals , as well as satisfying the convergence criteria which had been given earlier in chapter 7 . A further check in the precision of the estimates was made by using starting values which were within 95% of the final estimates and verifying that in every case the final converged parameter value remained unchanged . It was also desirable to verify the usual assumption of constant variance[97] associated with least square analysis. This was done by residual plots as shown in Figs. 8–17, and these plots provided an additional check on the adequacy of the proposed model. As shown in Appendix C , the covariance matrix was also calculated in

order to obtain standard errors of the parameter estimates at the 95% confidence interval .

In Table 5, the predicted dissociation constant of oleic acid varied markedly with the initial acid concentration of the oleic phase . The value of K^D_{HX} for the 0.10 mM and 0.20 mM oleic acid solutions in hexadecane was 5.7 $\times 10^{-7}$ and 7.7 $\times 10^{-7}$ M , respectively . For 0.3125 mM oleic acid , the estimated dissociation constant was 2.14 $\times 10^{-7}$ M , substantially lower than the values obtained at lower acid concentrations . The dissociation constant dropped even further at higher oleic acid concentrations , viz ; 1.21 $\times 10^{-7}$ at acid concentration of 0.6125 mM , and 1.62 $\times 10^{-7}$ at 1.0 mM . The equilibrium constant associated with the inactive salt , K^D_{NaX} , did not exhibit such a dramatic concentration dependence as the acid dissociation constant . However , the data of Table 5 show a small but significant increase in the salt equilibrium constant with the increase in oleic acid concentration. Ramakrishnan and Wasan[51] were the first to assign an equilibrium constant to the formation of the inactive salt and its subsequent partitioning to the oleic phase . In view of the paucity of reported data on this equilibrium constant , it is difficult to say what its true value should be . Indeed , additional theoretical work will be necessary in order to establish the true nature of this equilibrium constant . Consequently , our estimates of the salt equilibrium constants had to be constrained to the range of the values reported by Ramakrishnan and Wasan[51] from their study of crude oil-caustic systems .

When the acid ionization constants are interpreted in terms of pK_a , we find that at lower oleic acid concentrations (ie. below 0.3125 mM) , the pK_a was about 6 , but at higher concentrations, the value was closer to 7 . Several researchers[13,51,53] working mostly with crude oils reported pK_a values in the range of 11–13 . Chen and Yen[31] were the only ones to suggest that the pK_a of crude oil acids might not be as high as were being reported . They opined that the pK_a value

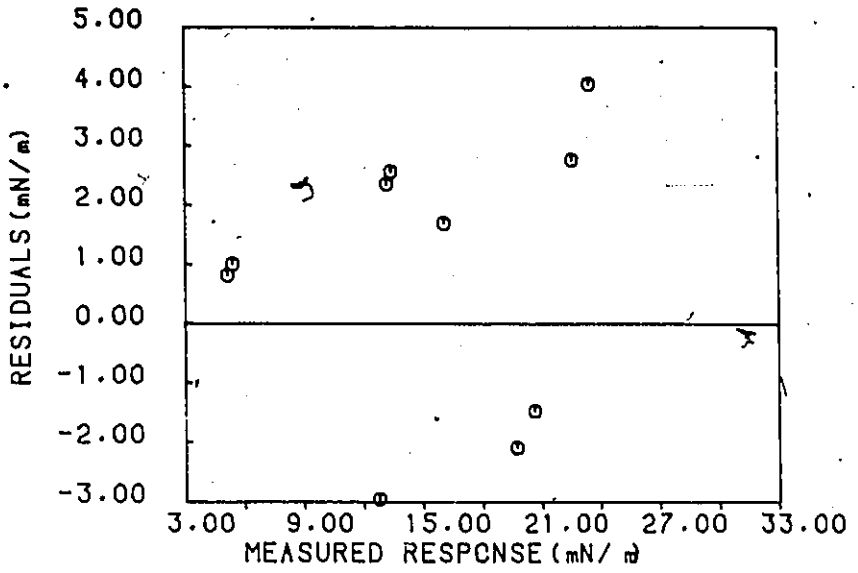

Figure 8 : Residual Vs Measured Response
System : 0.10 mM Oleic in HD/NaOH

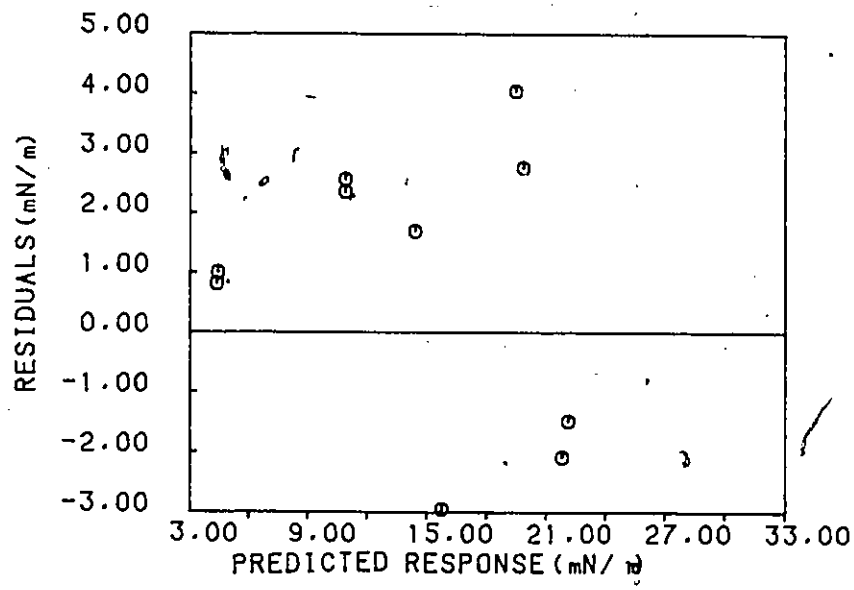

Figure 9 : Residual Vs Predicted Response
System : 0.10 mM Oleic in HD/NaOH

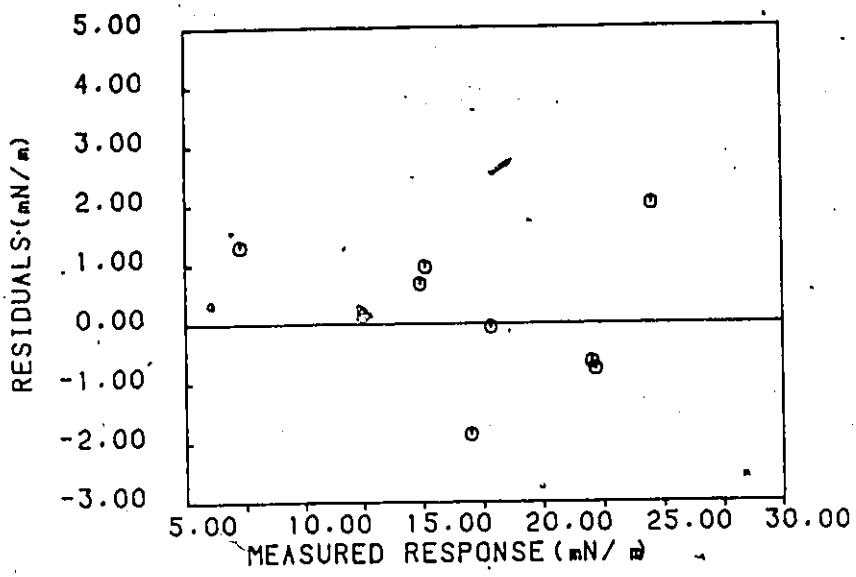

Figure 10 : Residual Vs Measured Response
System : 0.20 mM Oleic in HD/NaOH

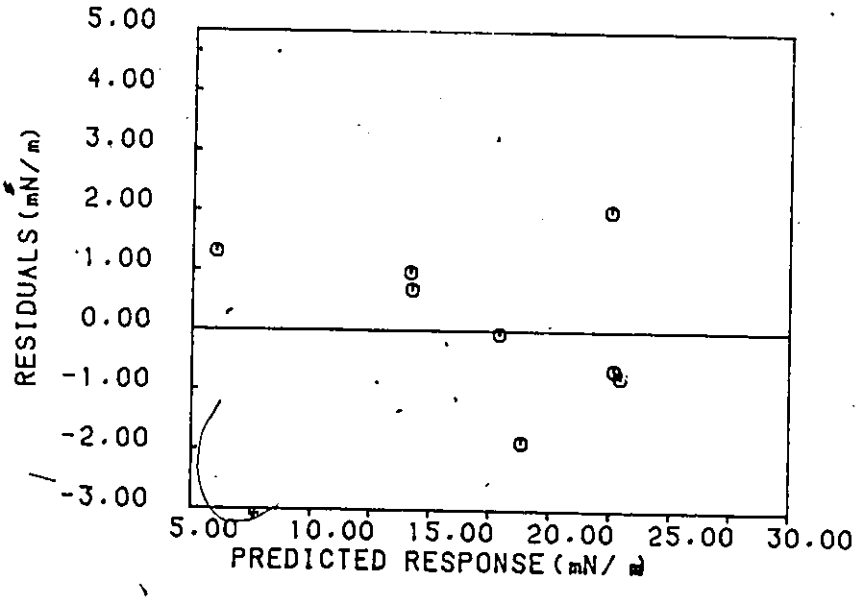

Figure 11 : Residual Vs Predicted Response
System : 0.20 mM Oleic in HD/NaOH

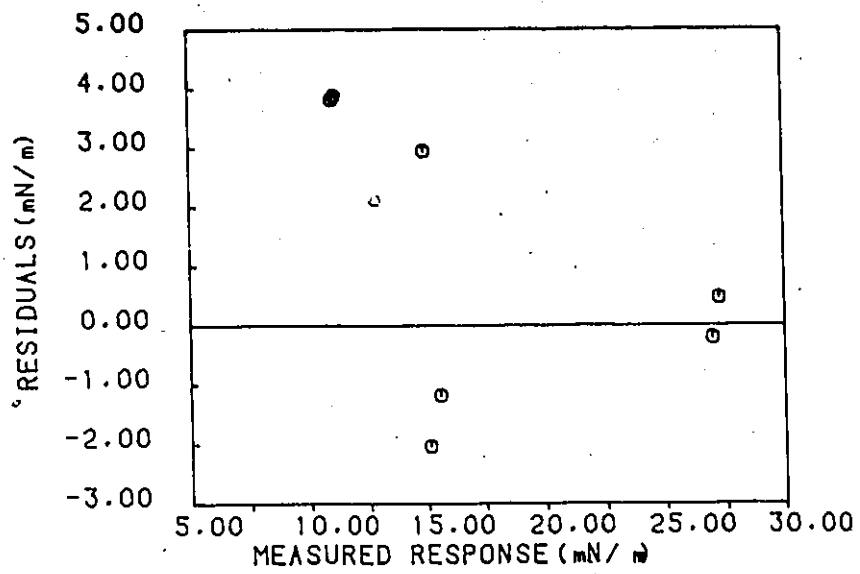

Figure 12 : Residual Vs Measured Response
System : 0.3125 mM Oleic in HD/NaOH

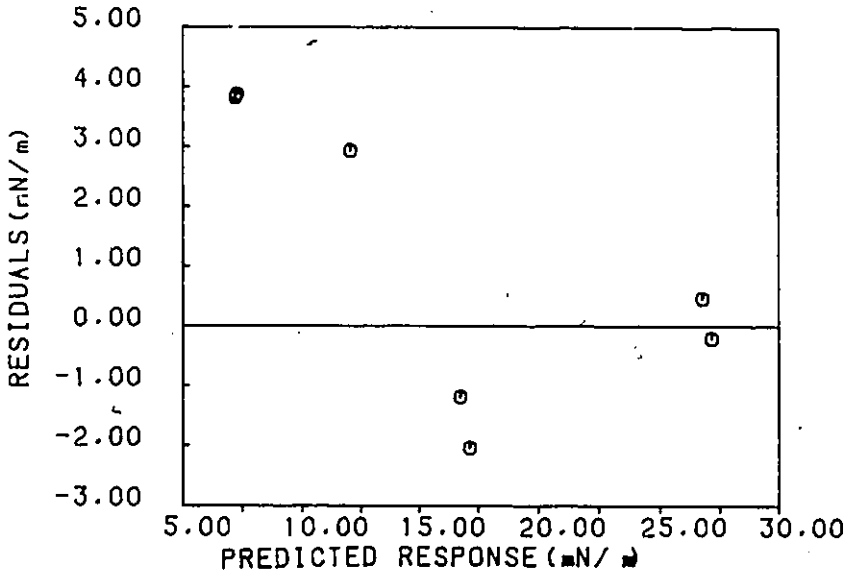

Figure 13 : Residual Vs Predicted Response
System : 0.3125 mM Oleic in HD/NaOH

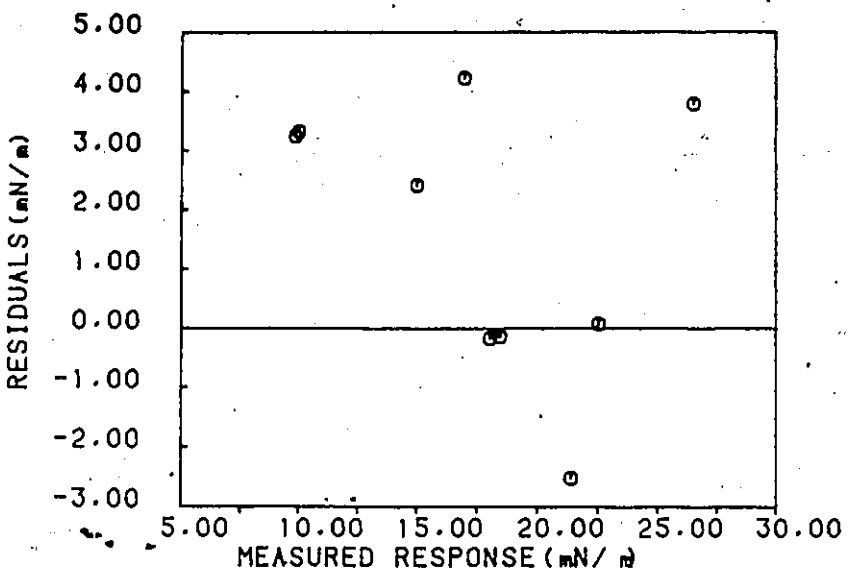

Figure 14 : Residual Vs Measured Response
System : 0.6125 mM Oleic in HD/NaOH

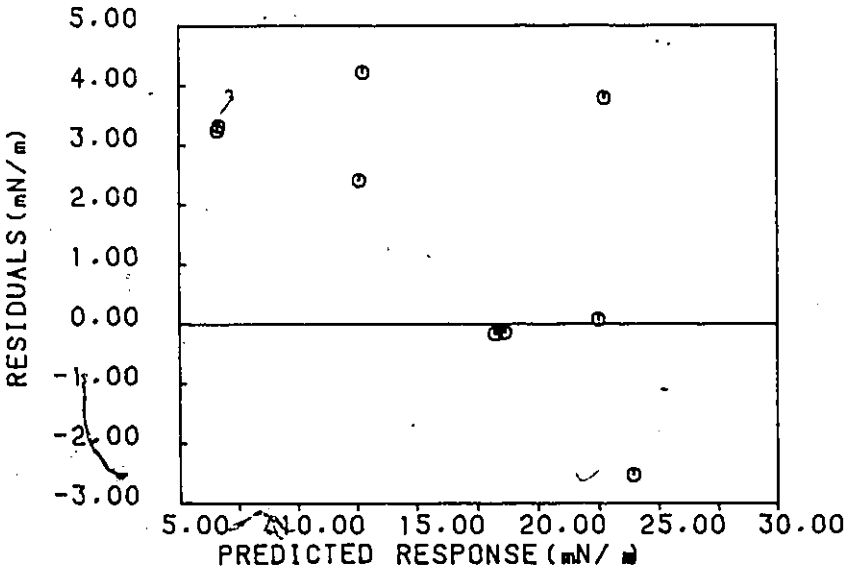

Figure 15 : Residual Vs Predicted Response
System : 0.6125 mM Oleic in HD/NaOH

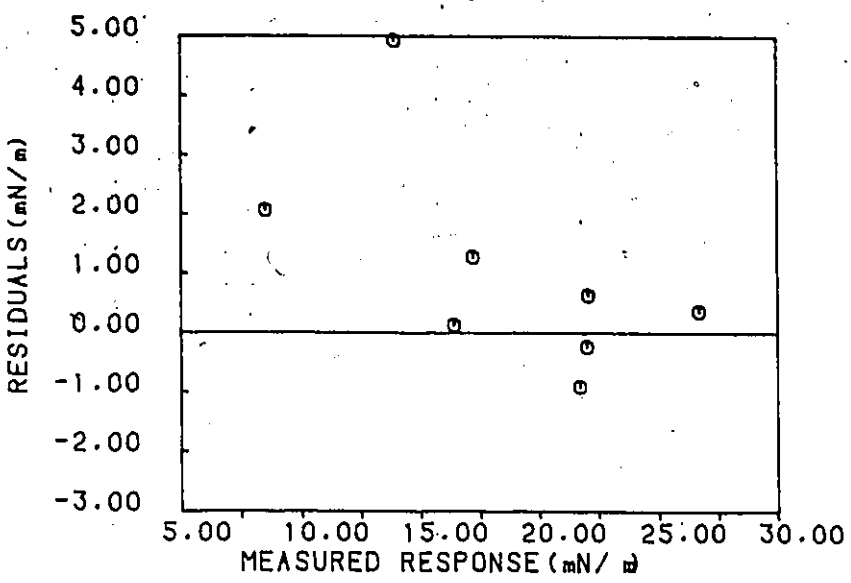

Figure 16 : Residual Vs Measured Response
System : 1.00 mM Oleic in HD/NaOH

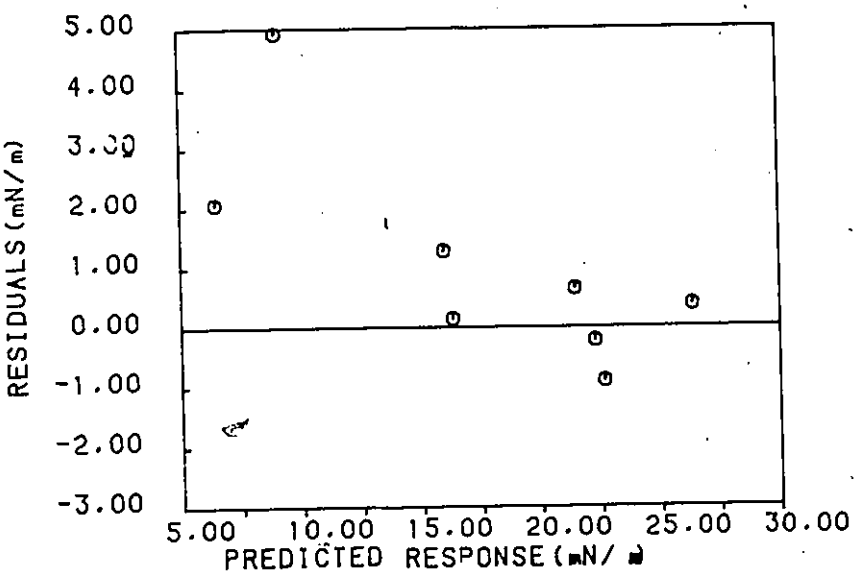

Figure 17 : Residual Vs Predicted Response
System : 1.00 mM Oleic in HD/NaOH

could be no more than 9 . Patil et al. [46] also estimated the pK_a of C14-C18 fatty acids to be in the range of 8-9 , but pointed out that the value depended on the applied surface pressure as well as the field strength of the aqueous phase . The data presented in Table 5 for the oleic acid systems corroborate the assertion of Patil et al. [51] and are also in agreement with the data published by Hejl and Levorova[53] .

With regards to the estimates for the salt equilibrium constant K^D_{NaX} , the trend evident in Table 5, in which higher K^D_{NaX} were obtained at higher oleic acid concentrations , is an important factor in the interpretation of the equilibrium tension data . While the pK_a values increased at higher acid levels in the oleic phase , the higher values of K^D_{NaX} were needed to prevent the reduced amount of active anions from desorbing to the oleic phase in the form of undissociated soap . In this way, it was possible to get lower IFT values at increased acid concentrations despite the reduced ionization potential .

13.3.2 Parameter Estimates for the Lauric Acid System

In Table 5 , the pK_a value for lauric acid at NaOH concentration below 2.50 mM is roughly 9 , but that increases to 10 at higher caustic levels . We now get closer to the range of pK_a values reported earlier by Trujillo [13] , also by Ramakrishnan and Wasan[51] . It is also important to note that the above authors worked at the higher caustic concentration range , namely , 2.50-250 mM. The reason that wide differences exist in predicted values of the dissociation constant of fatty acids is because of differences in the modelling of the interaction of the acid with alkaline reagents. Additionally , the interfacial data for various crude oil/caustic systems differ substantially with the result that conflicting parameter estimates are almost imperative , while the true value of the dissociation constant remains elusive . It does not appear that we can eliminate the effects of

the acid concentration nor the caustic concentration (employed for the IFT or surface pressure measurements) , on the estimated dissociation constants for any given acid system . Tanford [41] asserted that fatty acids and their associated anions tend to aggregate in both the oleic and aqueous environments , and that the higher the species concentration , the more will be the degree of aggregation . Greater degree of aggregation at higher concentrations will lead to lower ionization constants as we find for the two acids investigated here . It seems logical then that the true pK_a value for long chain fatty acids can only be obtained by working at low acid concentrations and by using the appropriate level of alkalinity in the aqueous phase for the generation of experimental IFT data . The determination of the true value of the dissociation constant of crude oil acids is therefore contingent upon a proper identification and quantization of the constituent acids .

13.4 Interfacial Potential and Equilibrium IFT

As stated in chapter 7 , the interfacial potential , ψ_o , at each caustic concentration , has been calculated by the use of the Gouy-Chapman double layer theory . The Gouy equation (equations 7.23, 7.24) , relates the prevailing potential to the surface concentration of the surfactant anion and the total electrolyte concentration . In the solution of the equilibrium model equations , we found that in general , ψ_o , gradually decreased from about 200 mv at 0.25 mM NaOH to about 160 mv at 25 mM NaOH . The reason for this trend lies in the complex functional relationship between ψ_o and both Γ and C_{OH^-} as can be seen from equation 7.24 . Low initial anion surface concentration at low caustic levels , results in high values of ψ_o in the absence of any other swamping electrolytes . Bansal et al. [30] measured electrophoretic mobility in crude oil/caustic systems and found that the zeta potential increased with increase in the caustic concentration to a maximum around 250 mM NaOH and then decreased thereafter . The authors showed that the maximum in electrophoretic

mobility coincided with the minimum in IFT and consequently the maximum surfactant adsorption . Within the caustic concentration range covered in this investigation , we did not find any cyclic trends in the values of the interfacial potential . Bansal et al. [30] also contended that low initial surface potentials would favour additional surfactant adsorption at the interface. At higher concentrations of the adsorbed surfactant , the formation of the non-dissociated soap species would reduce surfactant adsorption ,resulting in an increase in IFT . From our analysis , it appears that the initially high interfacial potential does not inhibit surfactant adsorption . The reason for this is that at the shear plane , the value of the potential falls off very rapidly to the extent that anion accumulation at the interface is still possible . However at high concentrations of the adsorbed anions , a combination of steric and coulombic repulsion forces will force some of the surfactant ions back to the bulk . The formation of the non-dissociated soap species will also accelerate the removal of excess adsorbed anions from the interface . The overall effect is an increase in IFT until an equilibrium is established . It has to be emphasized that the electrophoretic mobility and the interfacial potential are not exactly identical and should not be confused in the analysis of the electrical phenomena associated with reacting systems .

Chapter 14

Single Component Dynamic Studies

Part I: Interfacial Data

14.1 Interfacial Data for the Oleic Acid Systems

As with the equilibrium studies , the interfacial variables of interest are the IFT , the interfacial area and droplet volume for each working acid concentration and any given caustic solution . All the above information was simultaneously obtained by the use of the micropendographic measurement system . The complete set of interfacial data for all the oleic acid solutions and for each working NaOH solution is presented in the various tables of Appendix B . In the case of 0.3125 mM oleic acid solution in hexadecane , the IFT data have been plotted as a function of interfacial age as shown in Figs. 18–23 . Other oleic acid concentrations were investigated only as part of the binary mixture studies . Consequently , the resulting IFT vs time plots appear in Figs. 57–61 along with the data for the various mixtures .

Fig. 18 gives the dynamic IFT plot when 0.3125 mM oleic acid is exposed to double distilled water . In this figure , as well as in other similar plots , the data points are the average values from

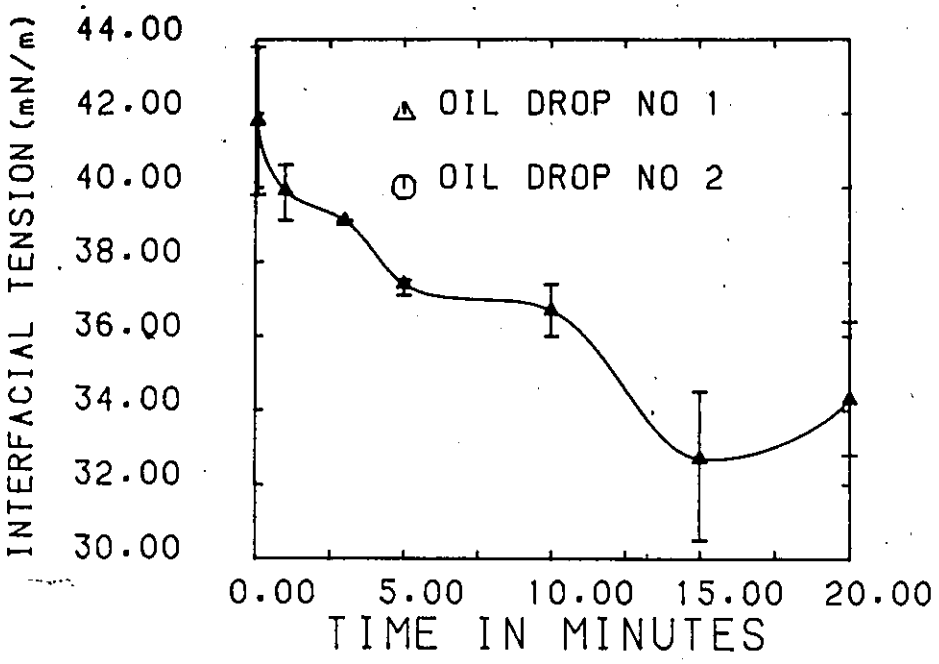

Figure 18 : IFT Vs Time for 0.3125 mM Oleic Acid in HD Vs Double Distilled Water

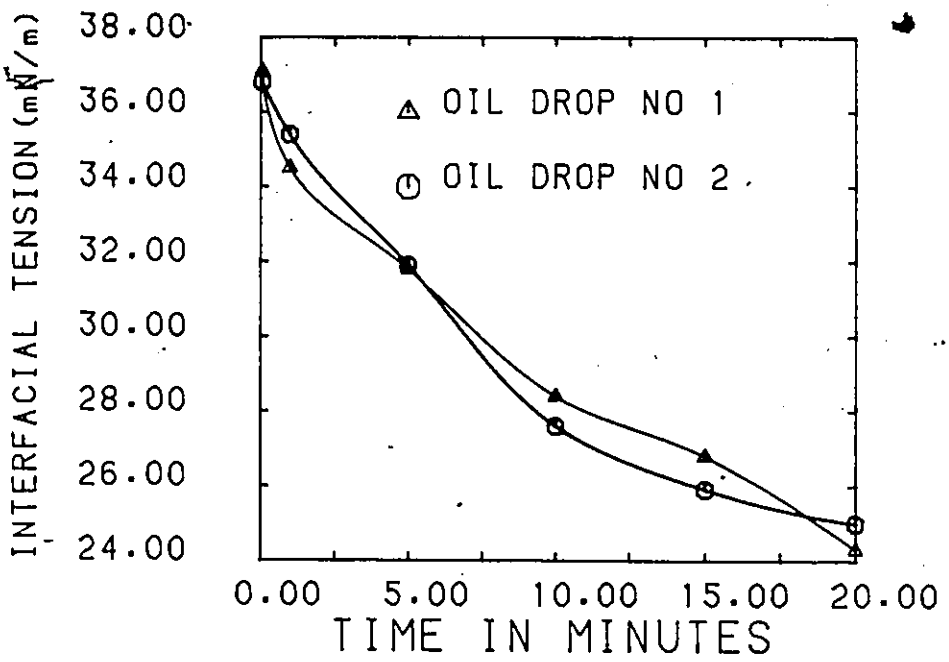

Figure 19 : IFT Vs Time for 0.3125 mM Oleic Acid in HD Vs 0.25 mM NaOH

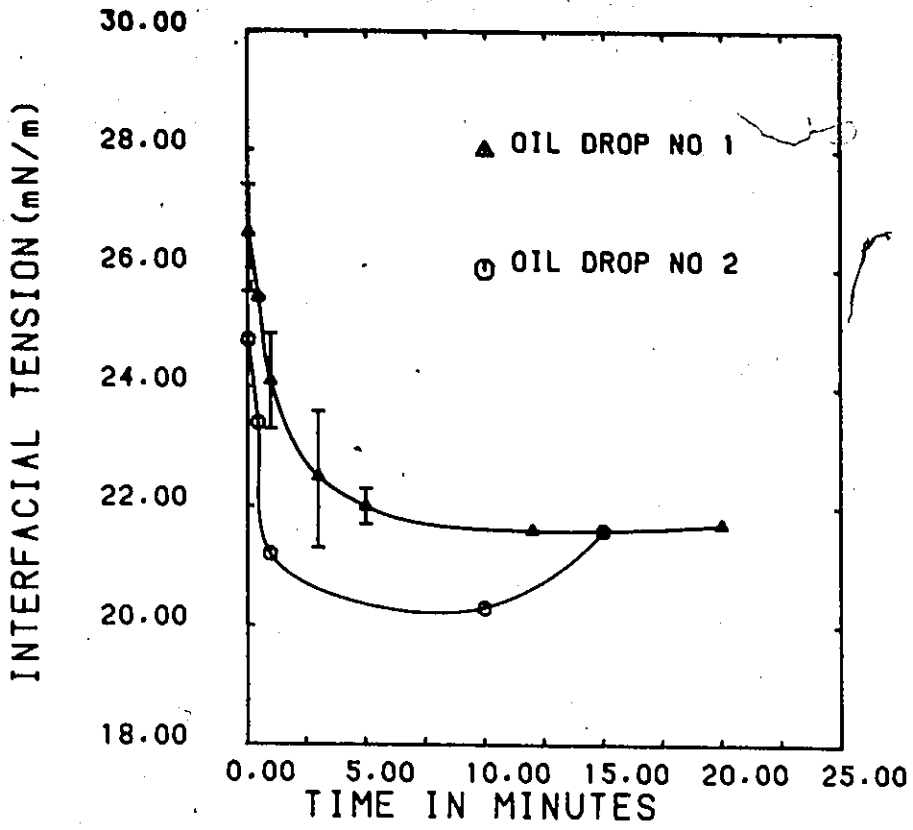

Figure 20 : IFT Vs Time for 0.3125 mM Oleic Acid in HD Vs 1.25 mM NaOH

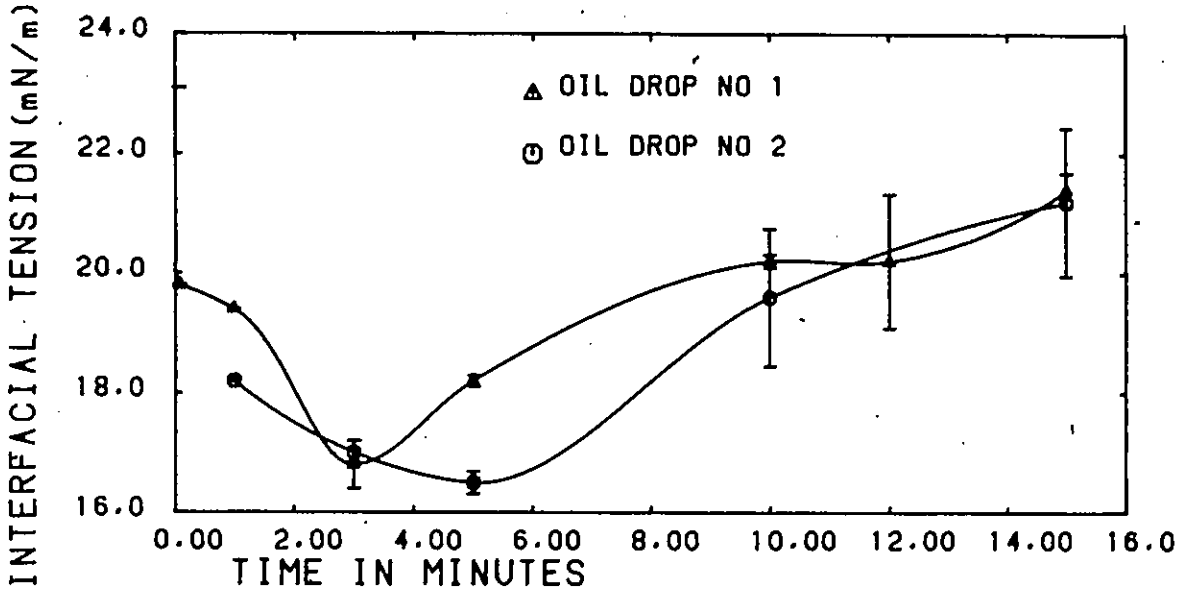

Figure 21 : IFT Vs Time for 0.3125 mM Oleic Acid in HD Vs 2.50 mM NaOH

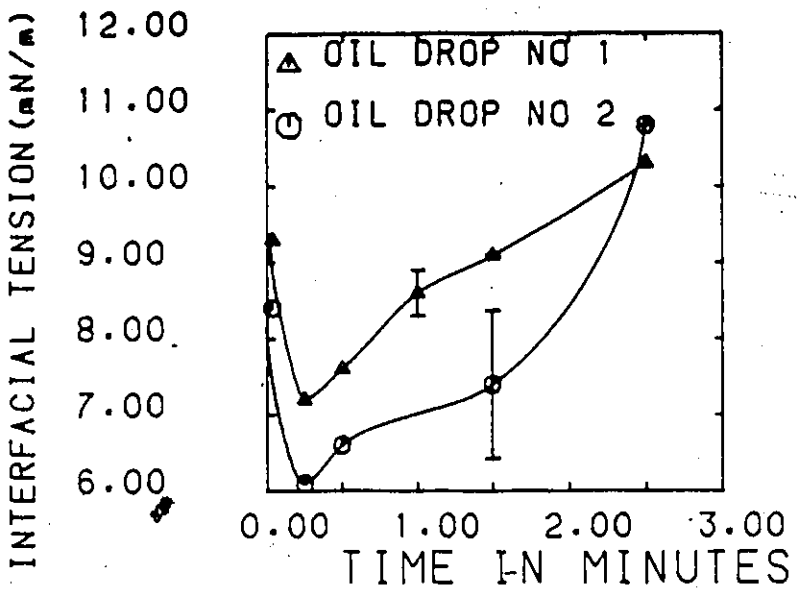

Figure 22 : IFT Vs Time for 0.3125 mM Oleic Acid in HD Vs 12.50 mM NaOH

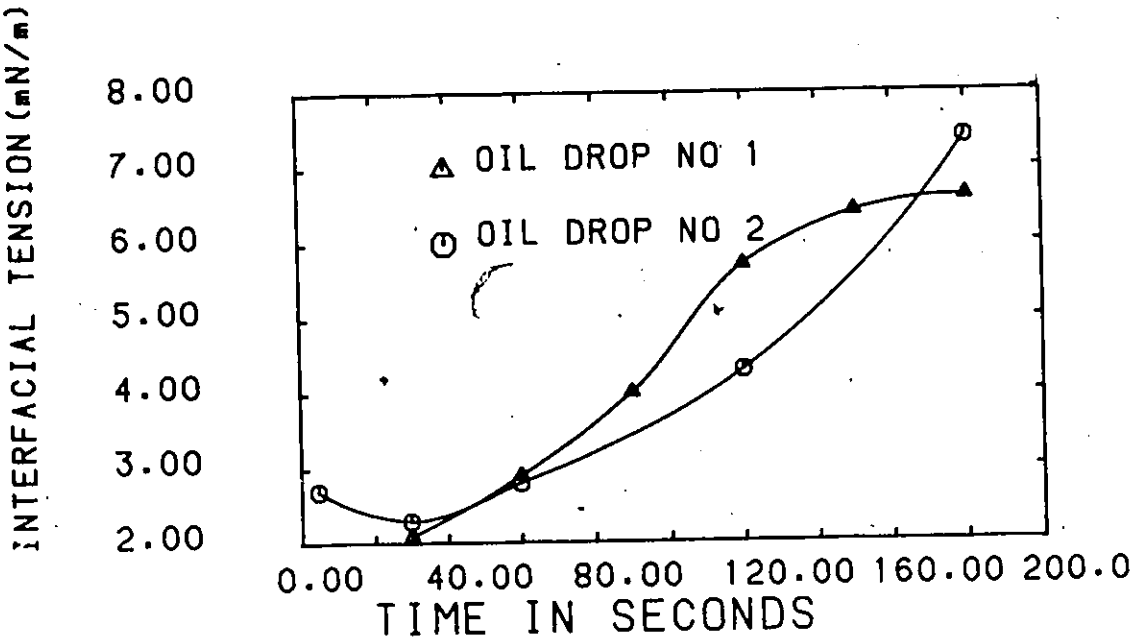

Figure 23 : IFT Vs Time for 0.3125 mM Oleic Acid in HD Vs 25.00 mM NaOH

at least two replicate experiments and/or repeat coordinate measurements . Flags in the plots are indicative of the range of values associated with any given data point . In Fig. 18 , the IFT at an interfacial age of 5 seconds was about 42 mN/m , but with extended contact time , the IFT dropped monotonically to an equilibrium value of 33.6 mN/m attained in an interfacial age of 15 minutes. At the caustic concentration of 0.25 mM , we find in Fig. 19, a similar decreasing trend in IFT until the equilibrium value of 24 mN/m was attained . When the caustic concentration was raised to 1.25 mM , Fig. 20 shows that the minimum in IFT dropped to 21 mN/m but this was attained much sooner , at an interfacial age of 5 minutes . In Fig. 21 , the working NaOH concentration was 2.50 mM , the IFT goes through a characteristic minimum reached just after 3 minutes of phase contact . Thereafter , the boundary tension slowly increased to about 21 mN/m after 15 minutes contact time . With a further increase in the caustic concentration to 12.5 mM (see Fig. 22) , the IFT minimum dropped to 9 mN/m and was reached at an interfacial age of just 30 seconds . Beyond this minimum , the rise in the tension value was rather sharp . At a caustic concentration of 25 mM , no IFT minimum was observed as can be seen from Fig. 23. The IFT after 5 seconds of phase contact was only 2 mN/m but it rose slowly but steadily to values around 10 mN/m at the interfacial age of about 3 minutes .

In neutral water , at the oleic acid concentration of 0.1 mM , Fig. 57(a) shows that the IFT remained nearly constant at 42 mN/m . In Fig. 57 (b), for this oleic acid concentration contacted with 0.25 mM NaOH , a small drop in IFT was manifested as the equilibrium value of 35 mN/m was reached after 20 minutes contact time . It was only when the caustic concentration rose to 2.50 mM , that we found a sharp drop in IFT to a minimum of 21.5 mN/m , reached after 3 minutes of phase contact . Beyond that interfacial age , the IFT again rose very sharply (see Fig. 57 (d)) . At a caustic concentration of 12.5 mM , the IFT again exhibited a minimum after a contact time

of one minute but the subsequent rise in the interfacial tension was more gradual than in Fig. 57 (d) . For this acid concentration , an increasing IFT trend was manifested at NaOH levels beyond 25 mM similar to the behaviour of 0.3125 mM oleic acid at NaOH concentration of 25 mM . In particular , as can be seen from Fig. 57(g) , the IFT remained fairly constant at about 3 mN/m in the presence of 200 mM NaOH .

For the 0.2 mM oleic acid system , the dynamic IFT vs time data are plotted within the collection of sub-plots depicted in Fig. 58 . There were no significant differences in tension values at this acid concentration from those found for 0.1 mM acid strength for all working NaOH concentrations. It took a much higher acid concentration , namely 0.6125 mM , for the IFT at the caustic concentration of 0.25 mM to attain values close to 20 mN/m at an interfacial age beyond 10 minutes (see Fig. 60) . The IFT dropped to 2 mN/m for this oleic acid concentration exposed to 12.5 mM NaOH solution at an interfacial age of about 20 seconds and showed only a small rise at longer times . The trend observed for the 0.6125 mM acid concentration was basically repeated when the level of acid in the oleic phase rose to 1.0 mM .

14.2 Interfacial Data for the Lauric Acid Systems

Tables B2.1–B2.10 of Appendix B contain the relevant experimental dynamic interfacial data for 0.02 M lauric acid contacting several aqueous NaOH solutions . The corresponding IFT vs time plots are given as Figs. 24–32 . In neutral water , as can be seen from Fig. 24 , the IFT remained high and relatively constant at about 33 mN/m . In contrast with 0.3125 mM oleic acid in the same neutral water , the drop in IFT with time was quite significant . There was hardly any drop in IFT for the lauric acid in contact with 0.25 mM NaOH solution , and the dynamic IFT values were little changed from the figures obtained for neutral water . Even at a caustic level of 1.25

mM, the IFT at an interfacial age of 5 seconds was still as high as 28 mN/m as can be seen in Fig. 26.

In Fig. 27 , the working NaOH concentration was 2.50 mM . We observe a shallow drop in tension to a minimum value of 20 mN/m at an interfacial age of 3 minutes . Beyond this contact time , the IFT rose gradually . No characteristic minimum in IFT was apparent at the caustic concentration of 12.5 mM as can be seen from Fig. 28 . The boundary tension rose continually from an initial value of 13 mN/m to an equilibrium value of 25 mN/m . A similar trend was also oberved at a caustic concentration of 25 mM (see Fig. 29) . In Fig. 31 , the caustic concentration used was 150 mM , and the IFT after 5 seconds of contact between the two phases dropped to 7 mN/m . Thereafter , the IFT rose continually to about 15 mN/m after an exposure time of 5 minutes . There was practically no difference in the IFT data obtained with 200 mM NaOH from the tension data using 150 mM NaOH , and the trends in both sets of data were very similar .

It is apparent from the IFT data obtained for the oleic acid systems in comparison to those found for the lauric acid solutions , that at all working caustic solutions the oleic acid was a superior surfactant generator than lauric acid . The fact that the working lauric acid concentration was 64 times that of 0.3125 mM oleic acid did not improve the interfacial effectiveness of the former in the alkaline aqueous systems used in this study . One may thus infer from these rather qualitative results , that oleic acid may have a higher acid dissociation constant or that the oleate anion once adsorbed at the oil-water interface is not readily desorbed to the bulk phases . From this observation , it may be inferred that in any given acidic crude oil system , unsaturated long chain acids are most likely to be interfacially more effective than saturated acids of the same or shorter chain , when the oil is contacted with an alkaline aqueous medium .

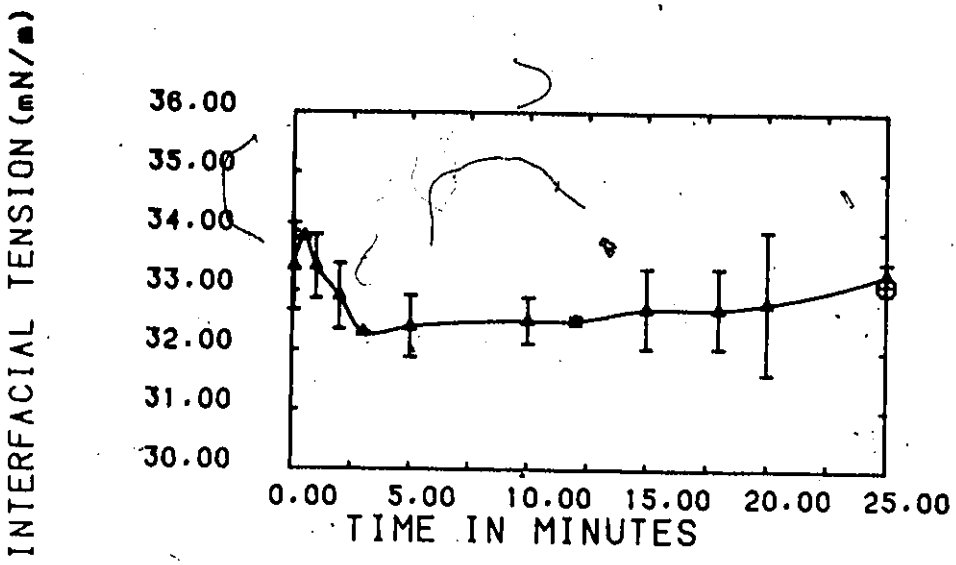

Figure 24 : IFT Vs Time for 0.02 M Lauric Acid in HD Vs Double Distilled Water

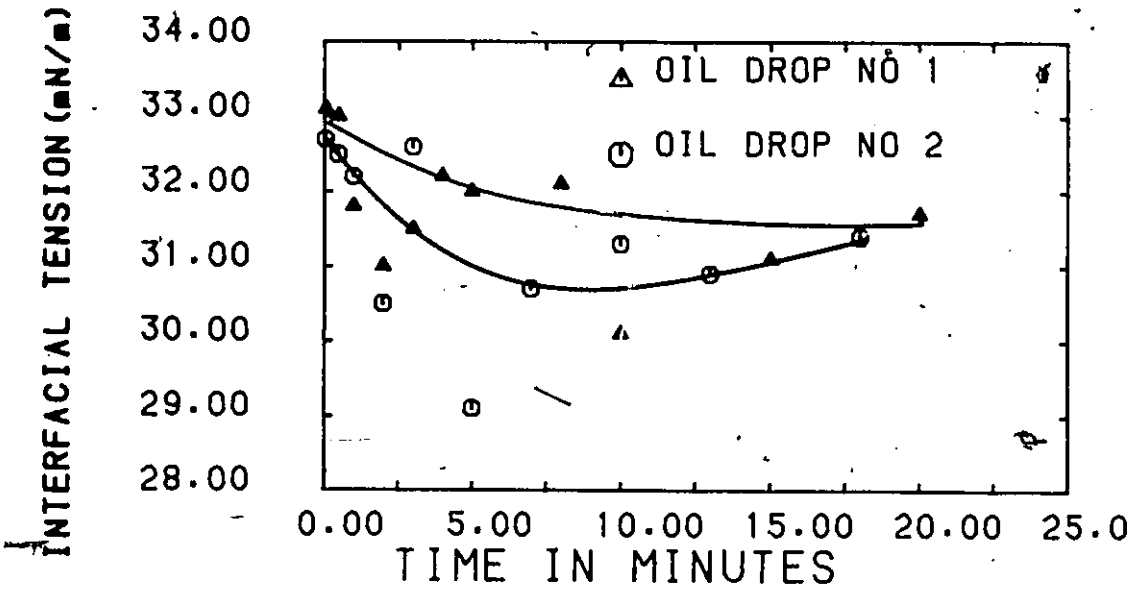

Figure 25 : IFT Vs Time for 0.02 M Lauric Acid in HD Vs 0.25 mM NaOH

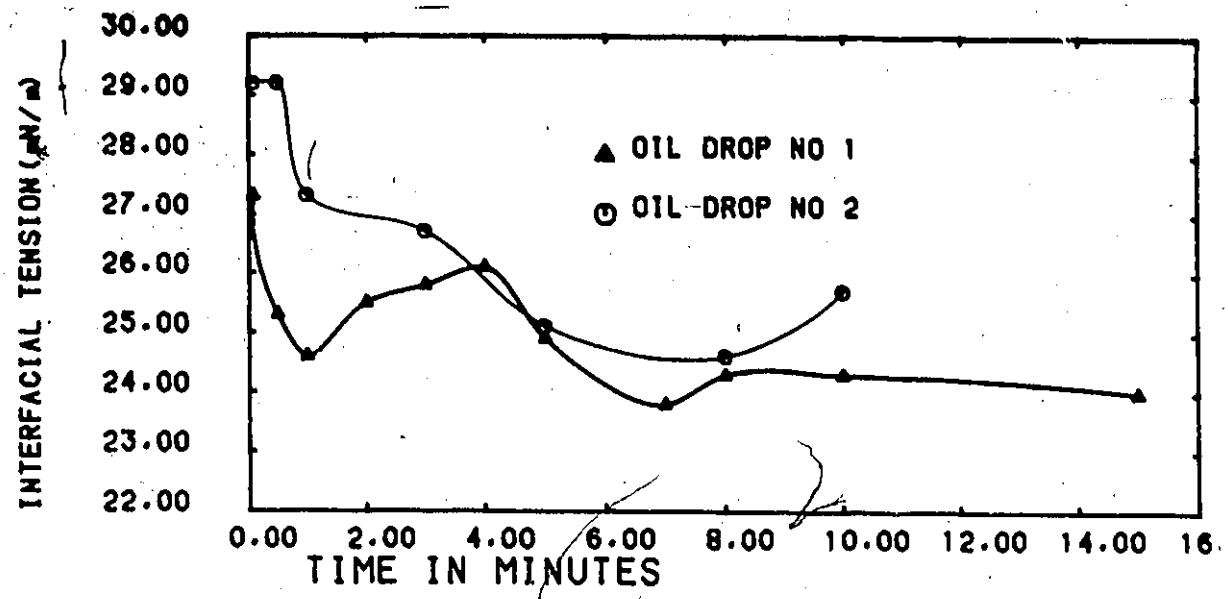

Figure 26 : IFT Vs Time for 0.02 M Lauric Acid in HD Vs 1.25 mM NaOH

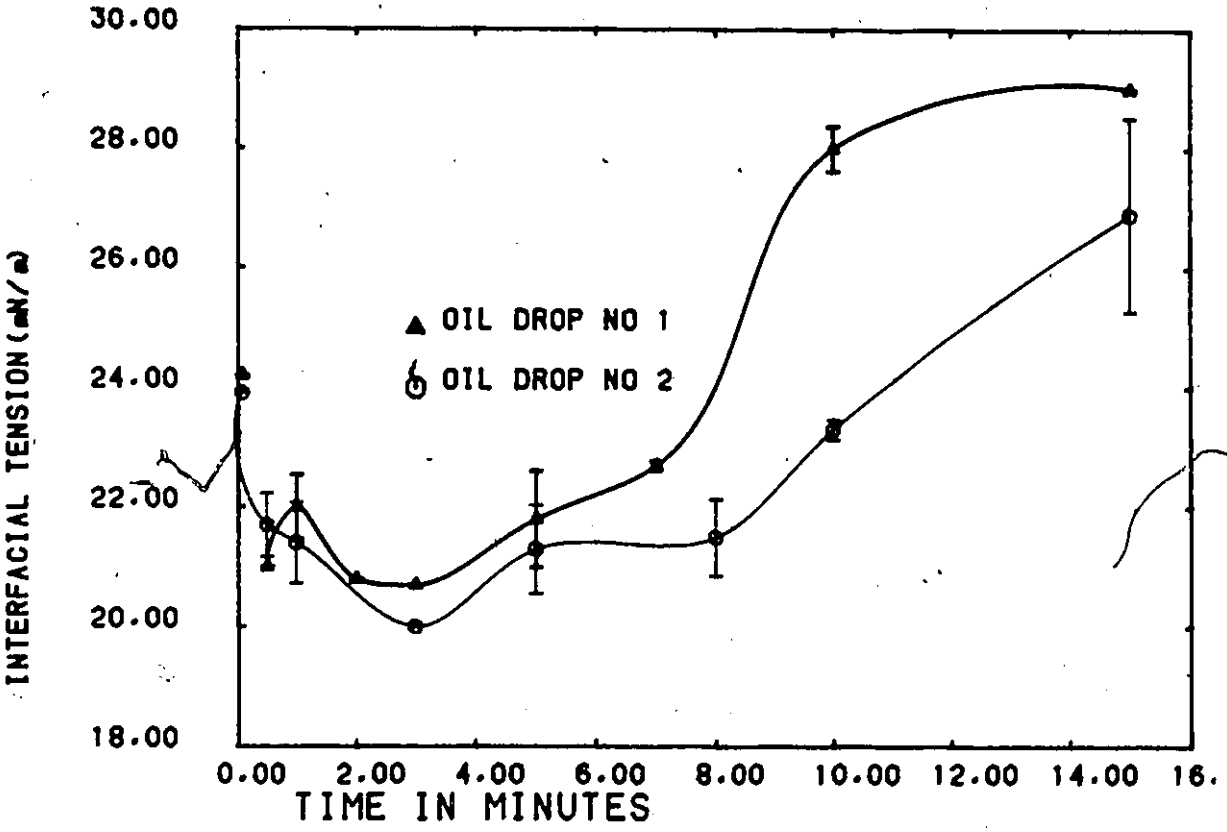

Figure 27 : IFT Vs Time for 0.02 M Lauric Acid in HD Vs 2.50 mM NaOH

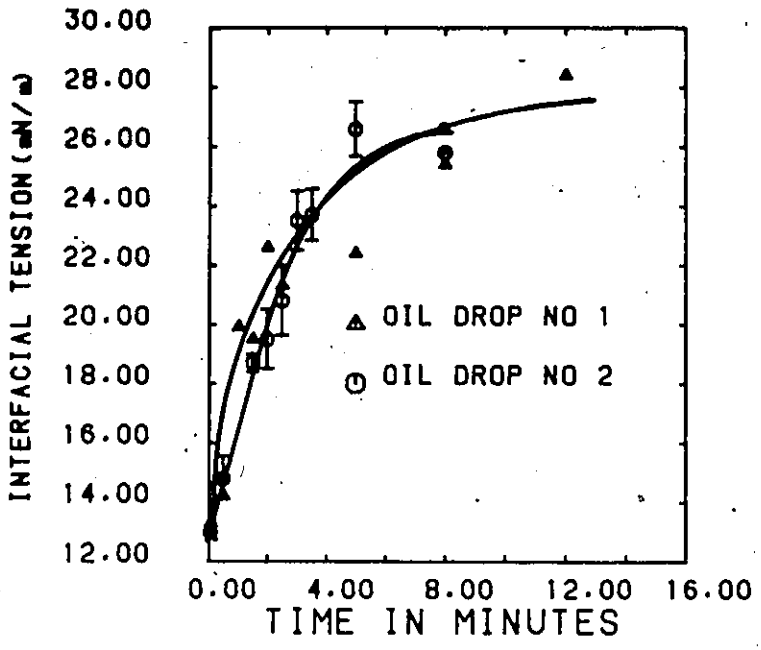

Figure 28 : IFT Vs Time for 0.02 M Lauric Acid in HD Vs 12.50 mM NaOH

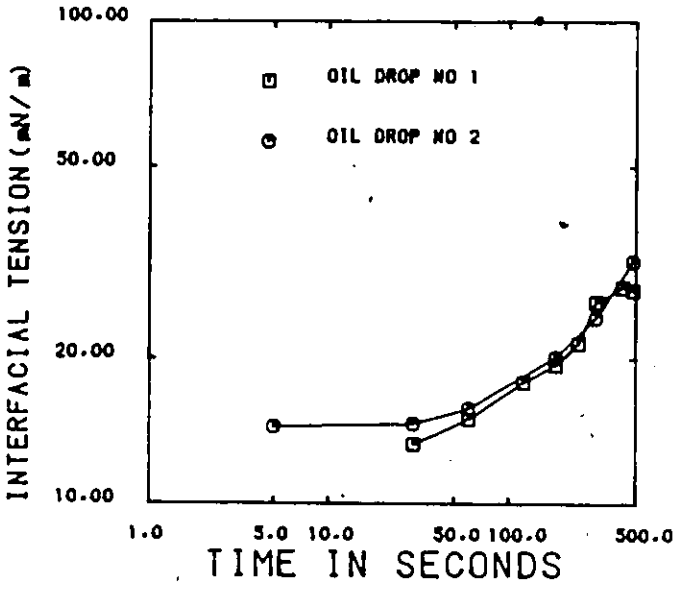

Figure 29 : IFT Vs Time for 0.02 M Lauric Acid in HD Vs 25.00 mM NaOH

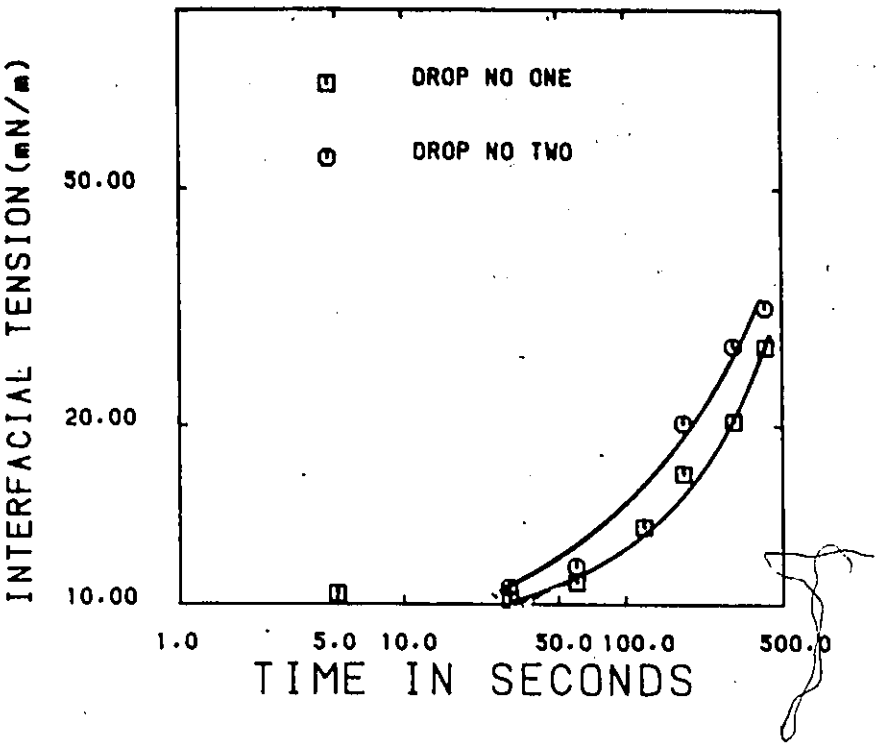

Figure 30 : IFT Vs Time for 0.02 M Lauric Acid in HD Vs 50.00 mM NaOH

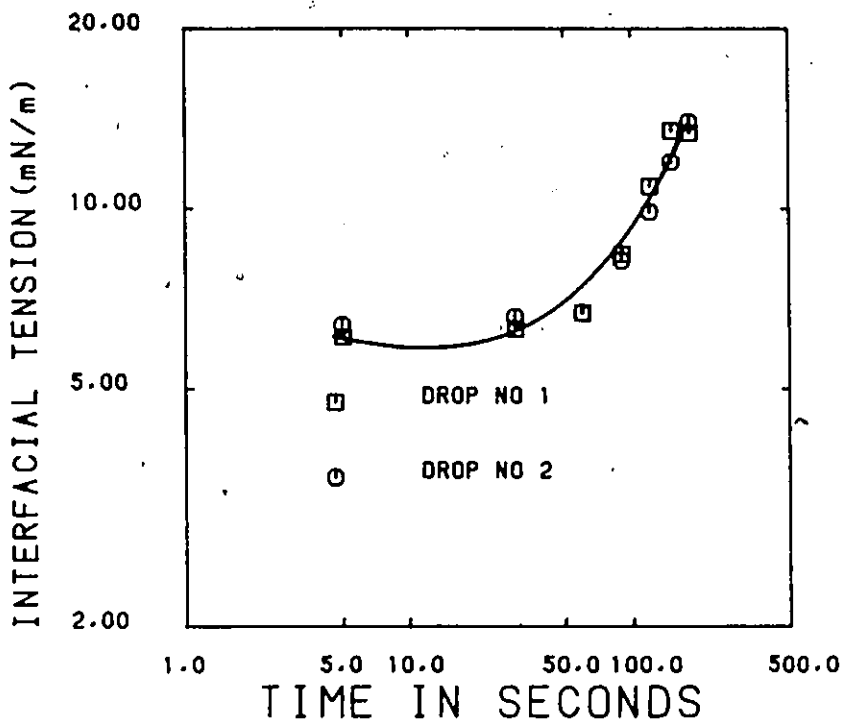

Figure 31 : IFT Vs Time for 0.02 M Lauric Acid in HD Vs 150.00 mM NaOH

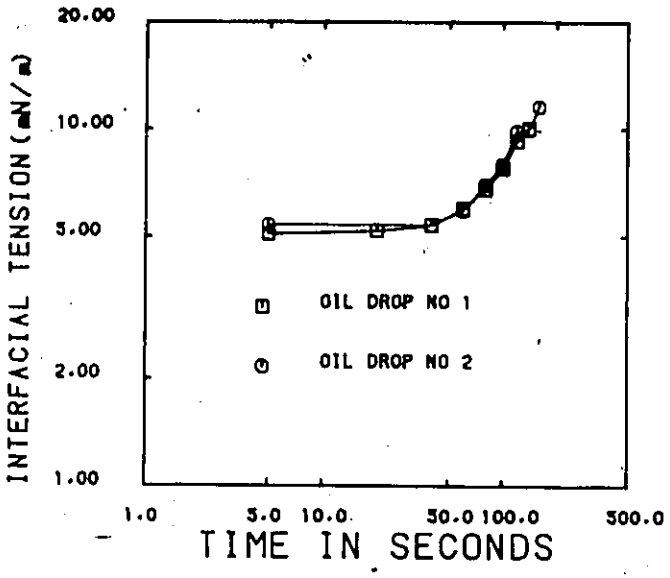

Figure 32 : IFT Vs Time for 0.02 M Lauric Acid in HD Vs 200.00 mM NaOH

14.3 Dynamic IFT Data by Ring and Spinning Drop Tensiometries

Dynamic IFT measurements were carried out for the 0.3125 mM oleic acid/ caustic systems using two additional but independent methods , namely , ring and spinning drop tensiometries . The aim of this supplementary study was to check the accuracy of the data obtained by the micropendographic technique . The Fisher's model 215 ring auto-tensiomat was used and the general procedure for IFT measurements by this technique had been described elsewhere[1] . The only notable differ-

ence in the experimental procedure for these dynamic measurements was that the oleic and aqueous phases were not pre-equilibrated prior to actual measurements . For the spinning drop tensiometer (SDT) , the University of Texas model 500 instrument was used , and the procedure for dynamic tension measurement with the instrument was recently outlined by Reive[111] . No SDT tension data were obtained when the acidic solution was contacted with neutral water . The oil droplet remained firmly attached to the wall of the capillary tube and could not be readily dislodged . Comparative IFT data for the 0.3125 mM oleic acid in hexadecane with various caustic solutions arising from these independent measurements were plotted as shown in Fig. D1 of Appendix D. In Fig. D1 (a) as well as in other sub-plots of Fig. D1 , we find that there are no IFT values determined by ring tensiometry for contact times less than two minutes . The reason for that was the finite time required for the ring to contact the interface and then be pulled through it into the oleic phase. SDT tension data plotted in Fig. D1 were calculated by using various solution schemes which included the following :

(i) The Vonnegut's solution [62] , which is strictly valid for infinitely long droplets ;

$$\gamma = \frac{\Delta\rho\omega^2 y_o^2}{4} \qquad (14.1)$$

Gardner and Hayes[69] proposed that the droplet width as measured with the spinning drop tensiometer should be corrected for the refractive index of the aqueous phase (usually water). Following this recommendation , Reive[111] modified equation 14.1 as follows ;

$$\gamma = \frac{0.522\Delta\rho d^{*3}}{T^2} \qquad (14.2)$$

(ii) For finite drops (ie. length to width ratio less than 4.0) , Slattery and Chen[64] proposed their widely used equation 32 of reference 64 . On the introduction of the refractive index

correction factor , this equation becomes the following ;

$$\gamma = 0.5 \left(\frac{d^*}{2r^*_{max}} \right)^3 \frac{\Delta\rho}{1.33^3} \omega^2 \qquad (14.3)$$

(iii) Princen et al. [62] proposed a series of equations in addition to Table 1 of reference 62 for calculating IFT from SDT data for finite and semi-infinite drops . However , despite the elegance of their work , the authors' proposed solution scheme is not widely used for the simple reason that there was no systematic method for utilizing the various equations in order to quickly calculate IFT . It is not even clear from their paper which experimental data will be required to successfully calculate the boundary tension .

The spinning drop tensiometer experimental data and the IFT calculated by these alternative solution schemes are listed in Tables D1–D3 of Appendix D .

For the 0.3125 mM oleic acid in neutral water , the tension data obtained by ring tensiometry were quite close to the values determined by micropendography . In Fig. D1 (a) for the NaOH concentration of 0.25 mM , we find that the ring tensiometer data were lower but showed a similar trend to that obtained by micropendography . On the other hand , the solution scheme of Slattery and Chen[64] provided the closest agreement with the micropendographic data at this NaOH concentration . However , the trend in the IFT values obtained by spinning drop tensiometry at longer contact times was different from that of the micropendographic tension data . In Fig. D1(b), the working NaOH concentration was 1.25 mM , and the agreement in all three experimental methods was satisfactory . As the caustic concentration was raised to 2.50 mM , we see in Fig. D1(c) that the data obtained by ring tensiometry deviated considerably from the other two , while SDT IFT data calculated by the method of Princen et al. [62] were closest to those obtained by micropendography . Fig. D1(d) shows that at the higher caustic concentration of 12.5 mM , the ring tensiometer data were completely off , while the agreement between micropendography and

spinning drop tensiometer data got even better . At NaOH levels beyond 12.50 mM , the oil drops were sufficiently long to permit IFT calculation with the Vonnegut's equation and the agreement with the data obtained by micropendography was also quite satisfactory .

14.4 Precision of Tension Measurements

The reason for carrying out all our measurements in replicates was to justify the precision expected from the micropendographic system. On the average, the precison of the experimental technique is about 5% . As can be seen from Figs. 19-31 and also from the data presented in Appendix B, the precision in the reported tension values decreases as the IFT drops due mainly to hydrodynamic instabilities associated with the pendant drop. For the same reason, precision is also poorer at longer contact times between the two phases especially when high NaOH concentrations were employed. As expected, the use of widely different drop sizes would lead to loss of precision particularly when the drop size is not appropriate for the applicable range of tension values. In all cases encountered in this study, bigger drops always gave more consistent tension values.

With regards to accuracy, the comparative measurements obtained with the ring and spinning drop tensiometers confirmed that the micropendographic technique is as good if not better than other available methods used for dynamic tension studies. The uncertainty in the tension values reported in Appendix B is within 10%. Here again, the error in the measurement increases at longer contact times and when relatively low tensions are involved. Indeed ,as can be seen from the SDT data in Appendix D, the spinning drop tensiometer is grossly inaccurate when tensions are above 20 mN/m and the viscosity of the oleic phase is not substantially different from that of water.

14.5 Evaluation of SDT Alternative Solution Schemes

Ordinarily , the best and perhaps the easiest way to obtain accurate SDT tension data is to use infinitely long oil droplets so that the simple Vonnegut's solution will readily apply . However , in some instances such as the systems involved in this study , the tensions are not low enough for infinitely long oil droplets to be obtained even at very high angular velocities . Thus , the alternative solution schemes which involve finite drops will have to be used . Having examined a number of proposed solutions , we found that a scheme based on the procedure outlined by Princen et al. [62] gave the most consistent and reasonably accurate tension values over a wide range of droplet length and width measurements . The data presented in Tables D1–D3 attest to the reliability of this scheme . Fig. D2 is a simplified flow diagram of our proposed solution scheme based on the analysis of Princen et al. [62] . The flow chart also contains the requisite experimental data which are V, $2\mathcal{X}_o$, $2\mathcal{Y}_o$, and ω . According to Fig. D2 , the radius r is first calculated , then followed by the ratios $\frac{\mathcal{X}_o}{r}$, $\frac{\mathcal{Y}_o}{r}$, and $\frac{\mathcal{Y}_o}{\mathcal{Y}_o}$. In order to calculate the parameter cr^3 , data from Table 1 of reference 62 are needed . A sixth degree polynomial fit of the cr^3 vs $\frac{\mathcal{X}_o}{r}$ data taken from Table 1[62] , was employed as indicated in Fig. D2 . With this polynomial expression , one can readily interpolate for cr^3 using the experimentally-determined value of $\frac{\mathcal{X}_o}{r}$ for values of the latter less than 2.209 . At higher values of $\frac{\mathcal{X}_o}{r}$, equation 32 of reference 62 is then used to obtain cr^3 . Finally , c is obtained from cr^3 and the interfacial tension is finally calculated by the use of the following equation ;

$$\gamma = \frac{\Delta\rho\omega^2}{4c} \tag{14.4}$$

For the oleic acid system which has been investigated , we found that a length to width ratio near 2.5 was satisfactory for the Vonnegut's equation to be used in tension calculation . At length to width ratios below this , our proposed algorithm , namely Fig. D2 , has been found to give sufficiently accurate tension data in nearly all the instances examined in this work .

Chapter 15

Single Component Dynamic Studies

Part II : Model Predictions

15.1 Invariant Quantities of the Dynamic Model

The invariant quantities of the dynamic model are considered to be those constants whose values are independent of the working acid concentration in the oleic phase . For the oleic acid systems , the invariant quantities are listed in Table 6 . In Table 7 , we listed the variant quantities for the oleic acid systems . Since only one working concentration was employed for lauric acid , the acid dissociation constants as well as the sorptive equilibrium constants were considered independent of the acid concentration although some dependence on caustic concentration was manifested . We now examine the values of these quantities in the following subsections .

15.1.1 Nernstian Boundary Layer Thicknesses

The applicable relationships based on the Nernstian convective diffusion theory as perfected by Levich[65] were discussed in chapter 9 . A detailed calculation procedure for the evaluation of

Table 6: Invariant Quantities in the Dynamic Model for the Oleic Acid in HD/Caustic Systems

Quantity	Symbol	Value	Units
Oil side Nernstian film thickness	δ_o	2.60×10^{-10}	m
Water side Nernstian film thickness	δ_w	2.60×10^{-9}	m
Saturation adsorption	Γ_{max}	5.53×10^{-6}	mole/m^2
Acid Diffusivity in oil	D_{HX_o}	9.86×10^{-7}	m^2/hr
Salt Diffusivity in oil	D_{NaX_o}	9.86×10^{-7}	m^2/hr
Anion Diffusivity in water	D_{HX_w}, D_w	1.64×10^{-6}	m^2/hr
Acid dissociation constant	K^D_{HX}	2.14×10^{-4}	mole/m^3
Acid Partition coefficient	K_p	1.43×10^{7}	-

the boundary layer thicknesses , namely , δ_o , and δ_w is presented in Appendix C3 . In Table 6, calculated values of δ_o , and δ_w for oleic acid were 2.6 and 26 Å respectively . Corresponding figures for lauric acid as can be seen from Table 8 were 2.8 and 28 Å respectively . deZabala[18] considered that the water side Henry's law constant should be of the order of the thickness of an adsorbed monolayer film (approximately 20 Å) . Rubin and Radke[60] also showed that due to higher convection currents in the oleic phase , the Nernstian film thickness for the oil side would be much smaller than the value for the water side . The boundary layer thicknesses given in Tables 6 and 8 are abnormally small. However, Levich[65] considers that values of 10^{-3}–10^{-4} cm suggested by Nernst are definitely too large.

15.1.2 Diffusion Coefficients

The applicable correlations which were used for the evaluation of the diffusion coefficients were outlined in chapter 9 . The calculational procedure has been detailed in Appendix C2 . Solute

Table 7: Variant Quantities for the Oleic Acid in HD/Caustic Systems

Oleic Acid Conc. (mM)	Acid Sorptive Equilibrium Constant , $K_{HX,o}$	Salt Sorptive Equilibrium Constant , $K_{NaX,o}$	Acid Dissociation Constant , K_{HX}^{D}
0.10	1.76×10^{-4}	2.95×10^{5}	5.70×10^{-4}
0.20	2.39×10^{-4}	2.44×10^{5}	7.74×10^{-4}
0.3125	6.60×10^{-5}	5.12×10^{5}	2.14×10^{-4}
0.6125	3.73×10^{-5}	7.05×10^{5}	1.21×10^{-4}
1.00	4.99×10^{-5}	4.13×10^{6}	1.62×10^{-4}

molar volumes calculated by the methods of Schroeder and Le Bas[81] differed by more than 20%, thus necessitating the use of the correlation of Tyn and Calus[81] . A close examination of the diffusivities estimated by the use of the correlation of Wilke and Chang[104] for both acids in both working solvents showed that the estimates had the desired relationship with the viscosity of the solvents . Conventional molecular diffusion theory[75,80,81] predicts that the diffusivity should be lower in the more viscous solvent . The correlation of Hayduk and Minhas[105] gave diffusivities within the range of those calculated by the equations of Wilke and Chang except that the diffusivities in hexadecane (viscosity 4 c.stokes) were all higher than the corresponding values in water for both acids . Furthermore , Amoudam and Laddha[112] measured the diffusivity of oleic acid in butanol which was within 98% of the value estimated by using the correlation of Wilke and Chang[104] . Also , the calculated diffusivities in water using this same correlation were generally in the range reported by Weinheimer et al. [113] for sodium dodecyl sulfate . Indeed , in the opinion of Reid et al. [81] , the correlation of Wilke and Chang is probably the most accurate for estimating diffusivities of long chain acids . Thus , the diffusivity values listed in Tables 6 and 8

Table 8: Invariant Quantities in the Dynamic Model for the Lauric acid/Caustic Systems

Quantity	Symbol	Value	Units
Oil side Nernstian film thickness	δ_o	2.80×10^{-10}	m
Water side Nernstian film thickness	δ_w	2.80×10^{-9}	m
Saturation adsorption	Γ_{max}	3.69×10^{-6}	mole/m^2
Acid diffusivity in oil	D_{HX_o}	1.21×10^{-6}	m^2/hr
Salt diffusivity in oil	D_{NaX_o}	1.21×10^{-6}	m^2/hr
Anion diffusivity in water	D_{HX_w} , D_w	2.01×10^{-6}	m^2/hr
Acid partition coefficient	K_p	1.36×10^{4}	-
Acid Sorptive Equilibrium constant ; for NaOH conc. < 2.50 mM	K_{HX_o}	5.25×10^{-7}	-
Acid Sorptive Equilibrium constant, for NaOH conc. > 2.50 mM	K_{HX_o}	2.63×10^{-8}	-
Sodium salt Sorptive Equilibrium constant	K_{NaX_o}	1.43×10^{3}	-
Anion Sorptive Equilibrium constant	K_X	7.14×10^{3}	m^3/mole
Acid dissociation constant , for caustic conc. < 2.50 mM	K^D_{HX}	1.00×10^{-6}	mole/m^3
Acid dissociation constant , for caustic conc. > 2.50 mM	K^D_{HX}	5.0×10^{-8}	mole/m^3

were all determined by the use of the correlation of Wilke and Chang .

15.1.3 Sorptive Equilibrium Constants

In chapter 9 , we outlined the procedure for the evaluation of the sorptive equilibrium constants starting from the equilibrium model parameters , namely , K^D_{HX} , and K^D_{NaX} . The calculated values of K_X for oleic and lauric acids as quoted in Tables 6 and 8 respectively were 4.41×10^6 and 7.14×10^3 m^3/mole . Since values of the acid ionization constants as well as the equilibrium constants for the desorption of the inactive soap species varied with the effective oleic acid concentration , it followed that the sorptive equilibrium constants evaluated therefrom would also differ as can be seen in Table 7 . Just as the dissociation constant decreased with increase in oleic acid concentration , the values of $K_{HX,o}$ also decreased as the oleic acid concentration increased . Table 7 also shows that the values of K_{NaX} followed the same trend as that exhibited by K^D_{NaX} listed in Table 5 .

In Table 8 , the calculated value of $K_{HX,o}$ for lauric acid at NaOH concentrations below 2.5 mM was 5.25×10^{-7} compared to the value of 6.60×10^{-5} given in Table 7 for 0.3125 mM oleic acid . The difference in the calculated sorptive equilibrium constants could be ascribed to the afore-mentioned differences in the values of K_X as well as K_p . Even for the same lauric acid concentration , the calculated values of $K_{HX,o}$ at NaOH concentrations below 2.5 mM differed substantially from the figures obtained at higher caustic concentrations . The reason for this is the difference in the acid dissociation constants over the same caustic concentration range .

15.2 The Sensitivity Coefficients

All the quantities listed in Tables 6–8 , were expressed in S.I. units . However , the working unit of time used in the numerical solution of the model equations was in hours . By working with

such a large unit of time , small time steps could then be used in the solution of the differential equations of the dynamic model . By using small time steps , large round off errors in the overall solution could be substantially reduced . The sensitivity coefficients of interest in this problem are the following ; $\frac{\delta\Gamma}{\delta k_{HX}}$, $\frac{\delta\Gamma}{\delta k_{NaX}}$, and $\frac{\delta\Gamma}{\delta k_X}$. These are the coefficients that directly influence the value of the surfactant surface concentration , namely Γ , and hence the dynamic IFT . As expected , the exact values of these coefficients would depend on the starting acid concentration , the caustic concentration and the interfacial age . We illustrate the nature of the information furnished by the sensitivity analyses by examining the coefficients calculated for 0.3125 mM oleic acid solution in contact with 0.25 mM NaOH over the experimental contact time of 15 minutes . Values of $\frac{\delta\Gamma}{\delta k_{HX}}$ were mostly positive and ranged from 1.2×10^{-10} to 4.7×10^{-12} , all expressed in units of $mole^2.hr/m^5$. On the other hand , values of $\frac{\delta\Gamma}{\delta k_X}$ were all negative and ranged from 5.5×10^{-17} to 1.9×10^{-16} . As for $\frac{\delta\Gamma}{\delta k_{NaX}}$, we obtained also negative values ranging from 3.2×10^{-9} to 2.4×10^{-9}. The sign of the coefficients was as important as the values themselves . A positive coefficient would mean that an increase in the value of the parameter would lead to a higher value of Γ , while a negative sign would have the opposite effect .

Since values of $\frac{\delta\Gamma}{\delta k_X}$ were very small compared to those of the other two coefficients, one could infer that the parameter k_X had the least effect on the magnitude of Γ . A similar conclusion was also reached by Borwankar and Wasan[79] following their modelling of the crude oil/caustic system. It was thus clear that only the acid and salt adsorption rate constants, namely , k_{HX} and k_{NaX} , needed to be varied , though in different directions in order to attain a desired value of Γ . This was the important clue which was needed in order to simultaneously solve the model equations and estimate precisely the parameters of the model .

Table 9: Final Parameter Estimates for the Single Component Dynamic Model

System Identification	Adsorption rate constants , (m^3/mole − hr)		
	k_{HX}	k_{NaX}	k_X
Oleic acid in HD/Caustic for all acid and NaOH concentrations	815.0	800.0	1000.0
0.02 M Lauric acid in HD/Caustic (for NaOH Conc. in the range 0.25–12.50 mM)	880.0	940.0	1000.0
0.02 M Lauric acid in HD/Caustic (for NaOH Conc. in the range 25.0–250.0 mM)	1800.0	600.0	1000.0

15.3 Estimates of the Model Parameters

The final parameter estimates in accordance with the solution scheme described in chapter 9 appear in Table 9 for both acid systems . For reasons advanced in the last section , the value of k_X was fixed at 1000 for all the various systems covered in the study . What is particularly significant in the parameter estimates ,especially for the oleic acid systems, is the fact that the largely disparate set of experimental data could be correlated with one single set of parameter values . In order to demonstrate the agreement between the experimental and predicted dynamic IFT values , comparative plots were prepared as shown in Figs. 33–42 for 0.3125 mM oleic acid in contact with various caustic solutions . Similar plots for the lauric acid systems are given as Figs. 43–56 . These figures contain replicate plots for any given acid concentration and the working NaOH concentration . The differences in the replicate experimental data are highlighted in Appendix B and they arise from the slight variations in the actual drop size used for the given experiment .

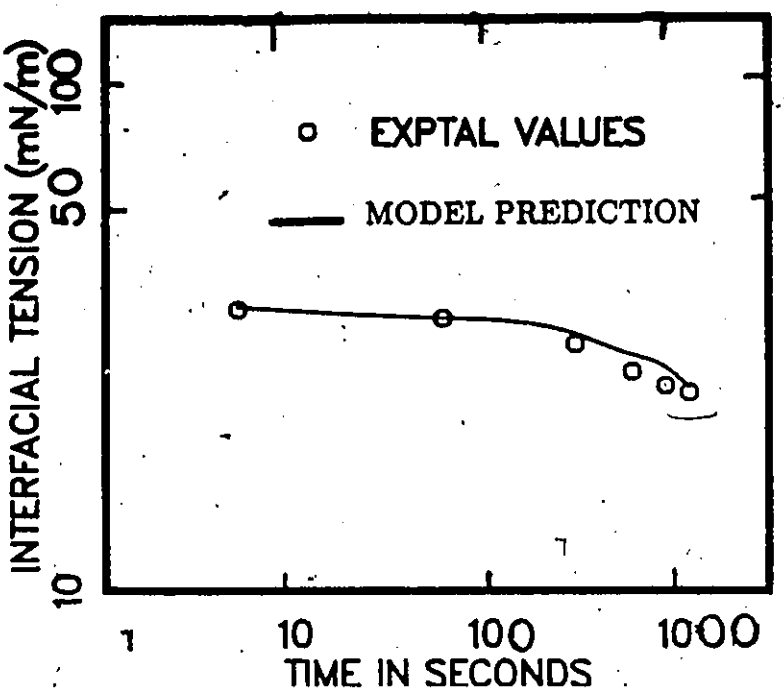

Figure 33 : Exptal Vs Predicted IFT for 0.3125 mM Oleic Acid in HD Vs 0.25 mM NaOH, Drop NO 1

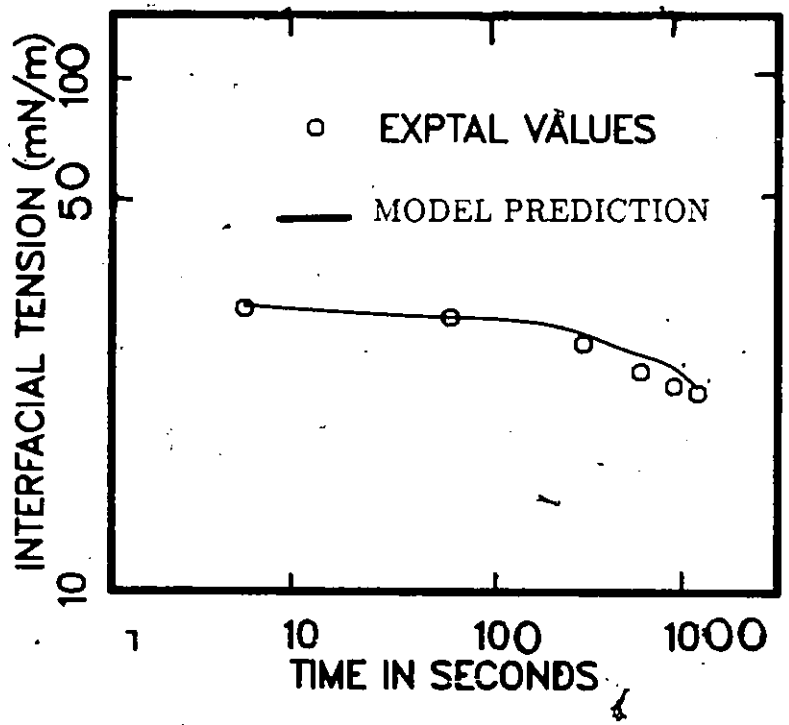

Figure 34 : Exptal Vs Predicted IFT for 0.3125 mM Oleic Acid in HD Vs 0.25 mM NaOH, Drop NO 2

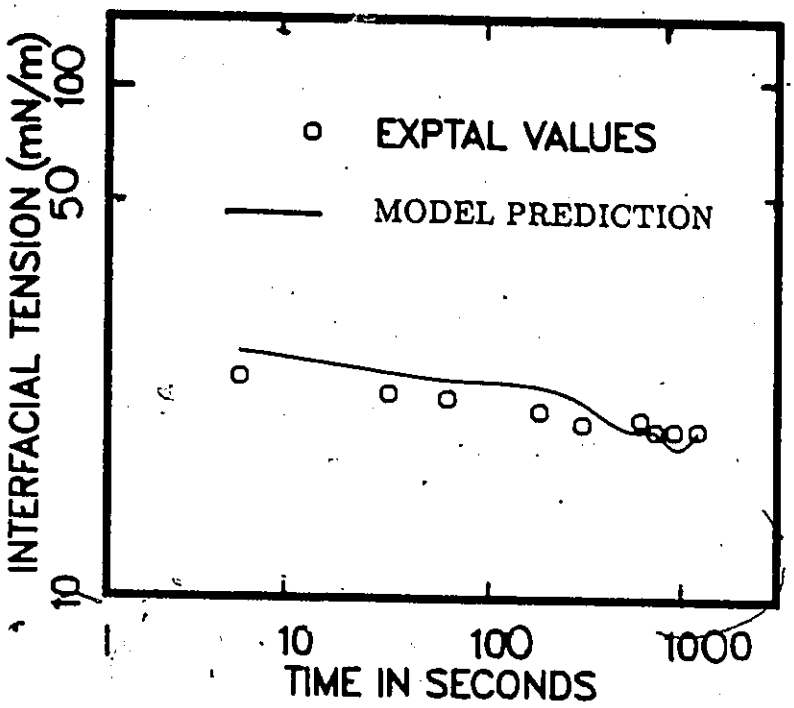

Figure 35 : Exptal Vs Predicted IFT for 0.3125 mM Oleic Acid in HD Vs 1.25 mM NaOH, Drop NO 1

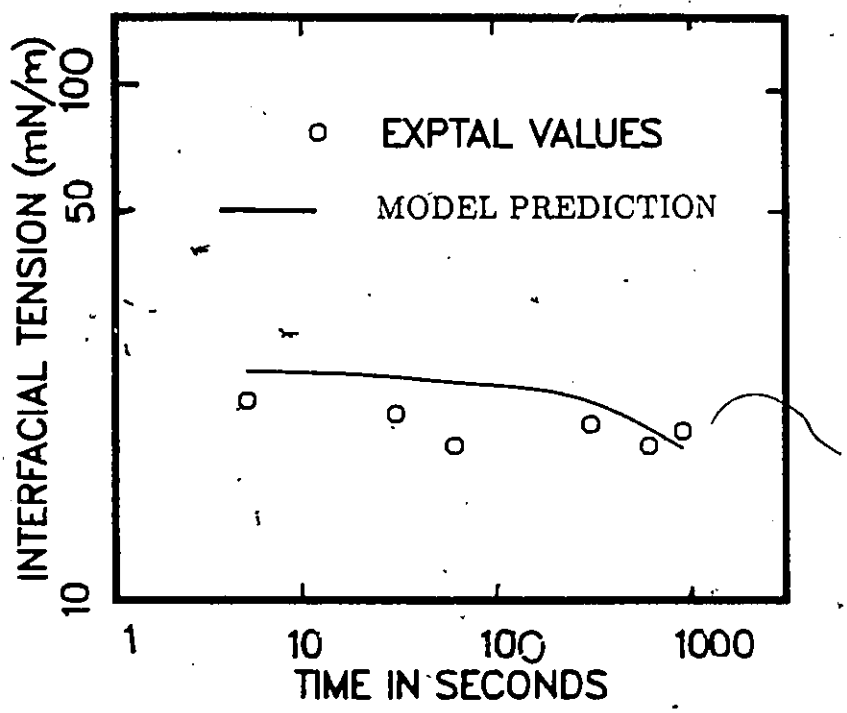

Figure 36 : Exptal Vs Predicted IFT for 0.3125 mM Oleic Acid in HD Vs 1.25 mM NaOH, Drop NO 2

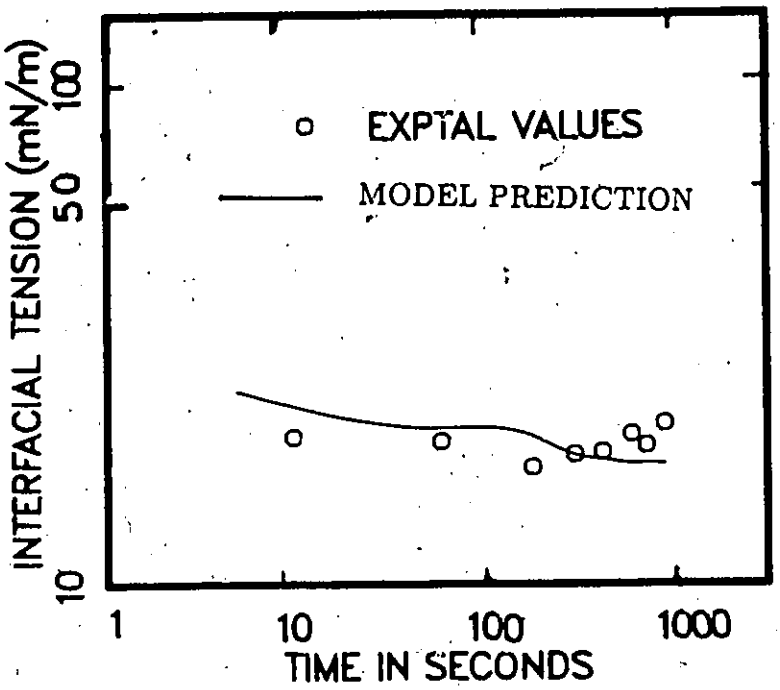

Figure 37 : Exptal Vs Predicted IFT for 0.3125 mM Oleic Acid in HD Vs 2.50 mM NaOH, Drop NO 1

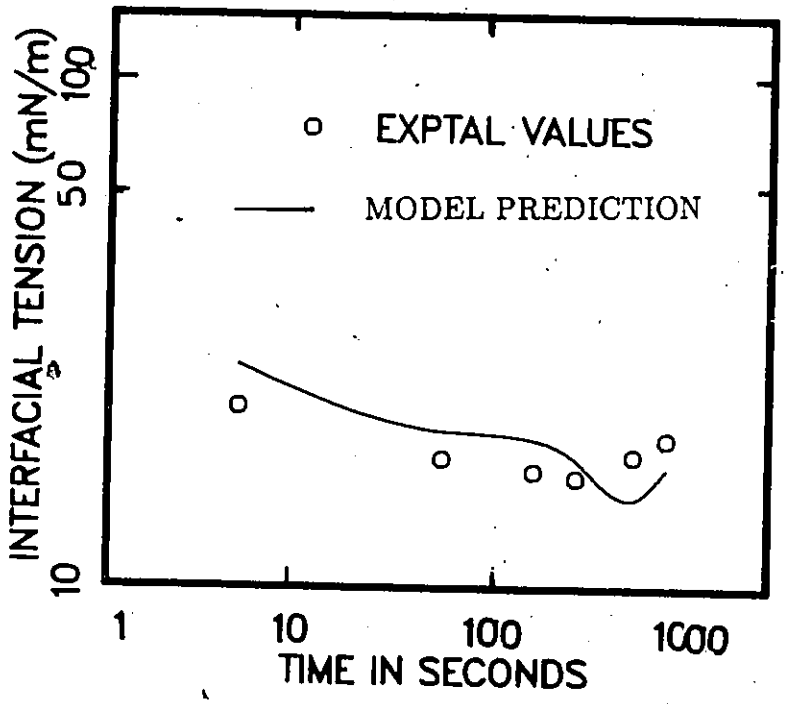

Figure 38 : Exptal Vs Predicted IFT for 0.3125 mM Oleic Acid in HD Vs 2.50 mM NaOH, Drop NO 2

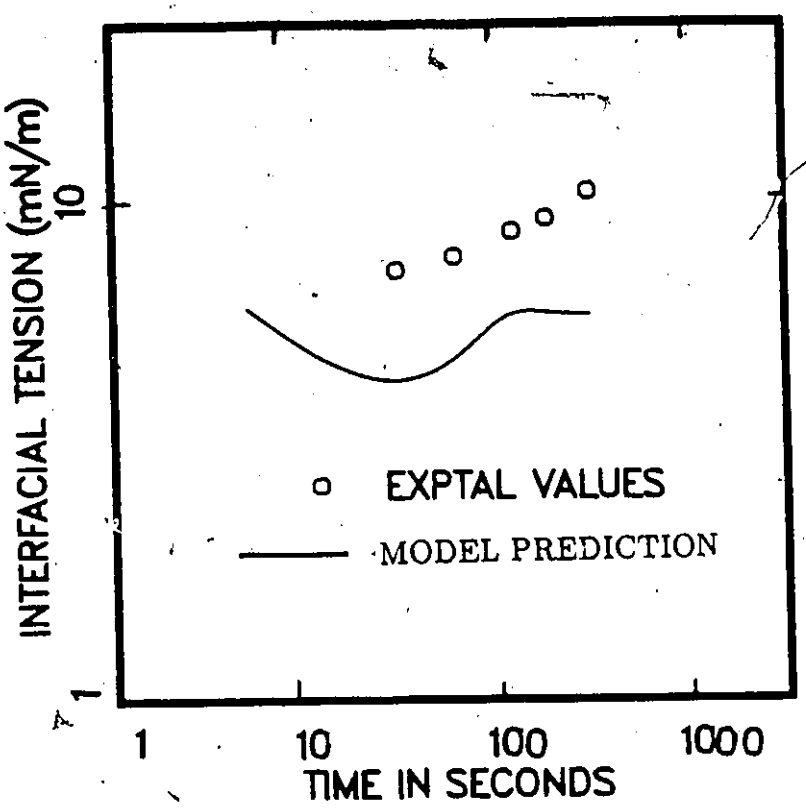

Figure 39 : Exptal Vs Predicted IFT for 0.3125 mM Oleic Acid in HD Vs 12.50 mM NaOH, Drop NO 1

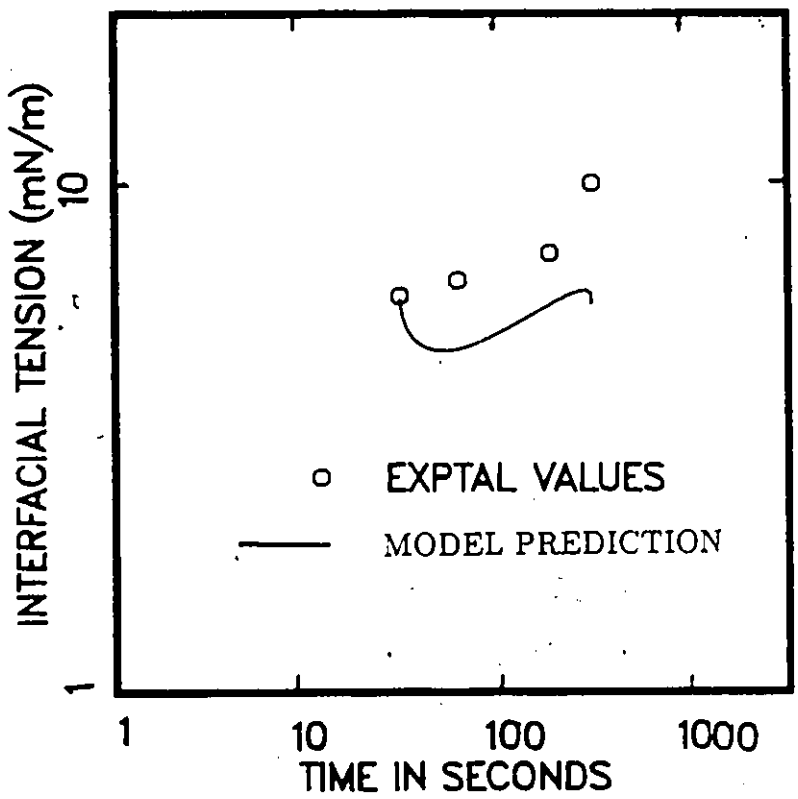

Figure 40 : Exptal Vs Predicted IFT for 0.3125 mM Oleic Acid in HD Vs 12.50 mM NaOH, Drop NO 2

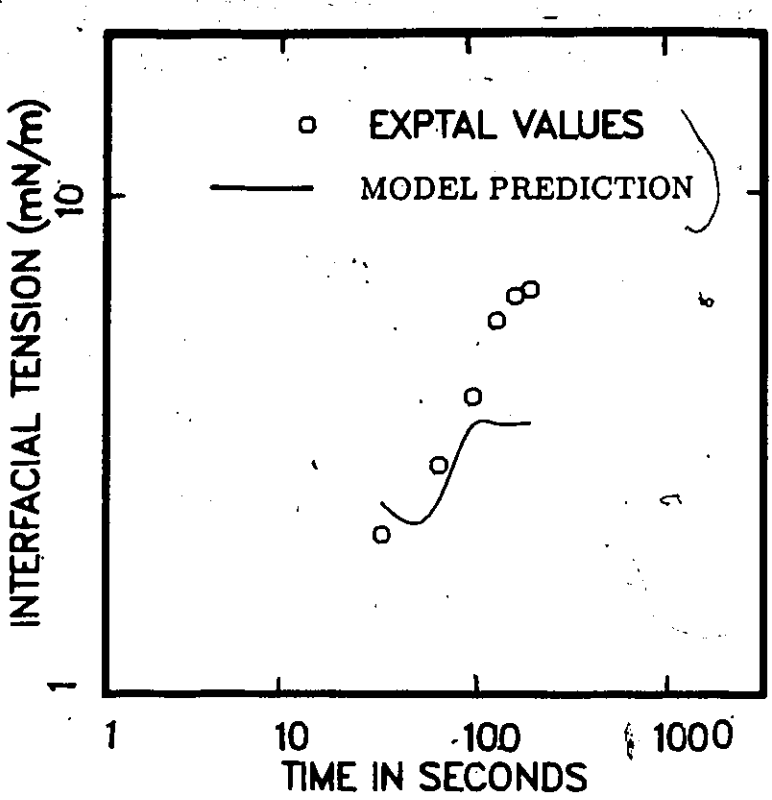

Figure 41 : Exptal Vs Predicted IFT for 0.3125 mM Oleic Acid in HD Vs 25.00 mM NaOH, Drop NO 1

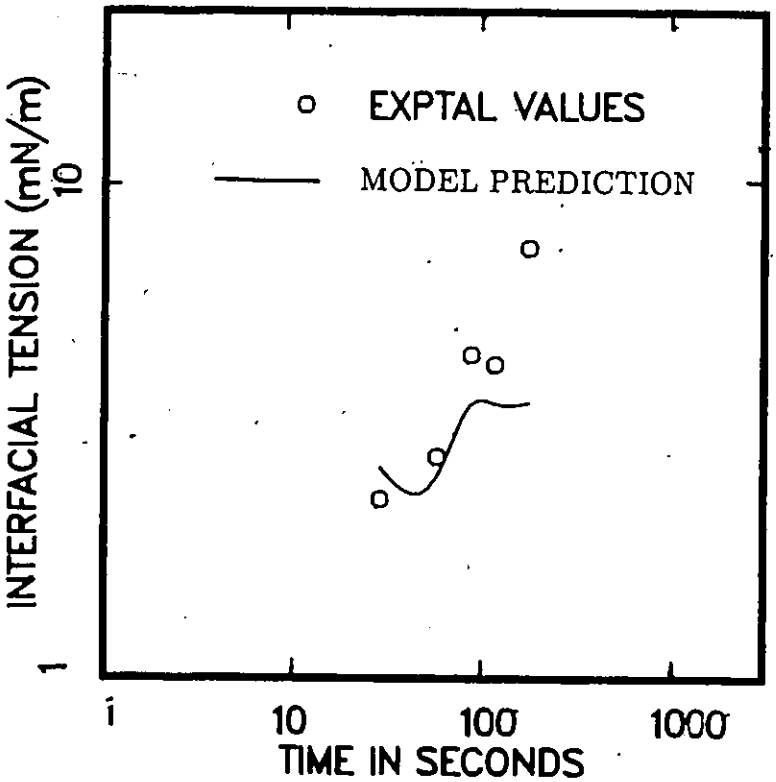

Figure 42 : Exptal Vs Predicted IFT for 0.3125 mM Oleic Acid in HD Vs 25.00 mM NaOH, Drop NO 2

In Table 9 , predicted values of k_{HX} and k_{NaX} for the oleic acid systems were nearly equal and fairly large (approximately 800 m^3/mole.hr) . Large acid adsorption rate constants are necessary in order to accumulate sufficient active anions at the interface subject to the prevailing interfacial potential . The interfacial potential in turn is determined by the effective caustic concentration in the bulk . However , if the desorption rate constant for the inactive soap complex is also high, then the surface concentration of the anion is quickly depreciated ,resulting in a fast increase in IFT at extended contact times . Such was the case with the oleic acid/caustic systems as evident in Figs. 33–42 .

In the case of the lauric acid systems , Table 9 shows one set of parameter values for caustic concentrations less than 25 mM, and a different set of figures when higher NaOH solutions were used . An in-depth examination of the experimental IFT data in the case of this acid will reveal why the parameter estimates turned out to be dependent on the caustic concentration. At the lower end of the caustic concentration spectrum (see Figs. 43–46), the IFT remained relatively constant or dropped very slightly with extended contact time between the two phases. For this lower caustic concentration range, the predicted value of k_{HX} was about half the value obtained at the higher NaOH levels. Table 9 also shows that the predicted value of k_{NaX} at higher NaOH levels was roughly 67% of the value at the lower end of the caustic concentration spectrum. Consequently, the active anions do not accumulate at the interface to any considerable extent due to the relatively high desorption rate constant associated with the inactive soap. Under these circumstances, the IFT remains high and relatively unchanged at extended contact times. The reason why lower IFT values were obtained at higher caustic concentrations is because of the higher acid adsorption rate constant aided by a lesser tendency to desorb in the form of the non-dissociated soap complex.

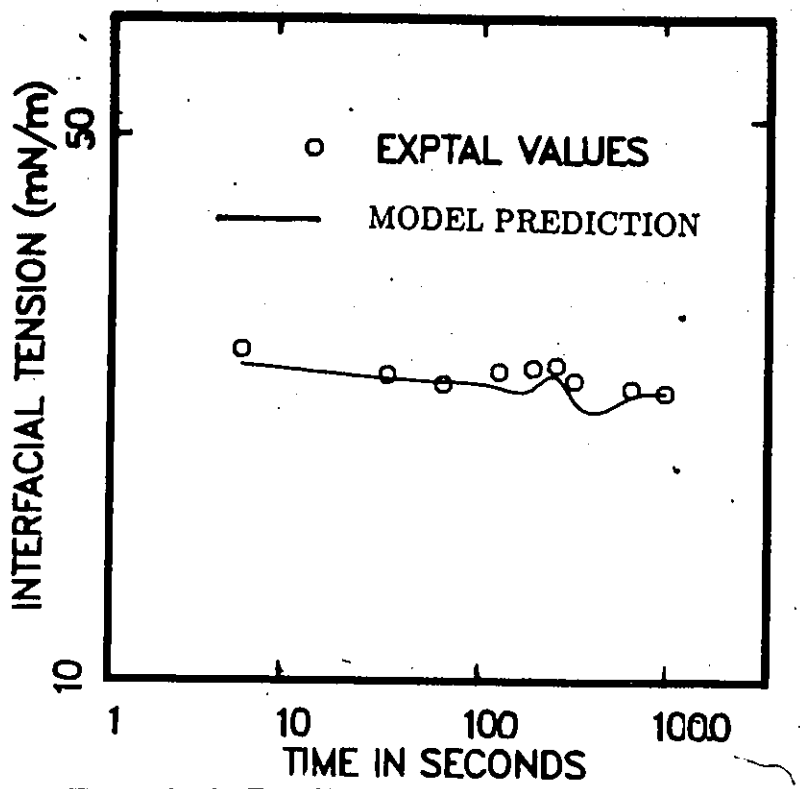

Figure 43 : Exptal Vs Predicted IFT for 0.02 M Lauric Acid in HD Vs 1.25 mM NaOH, Drop NO 1

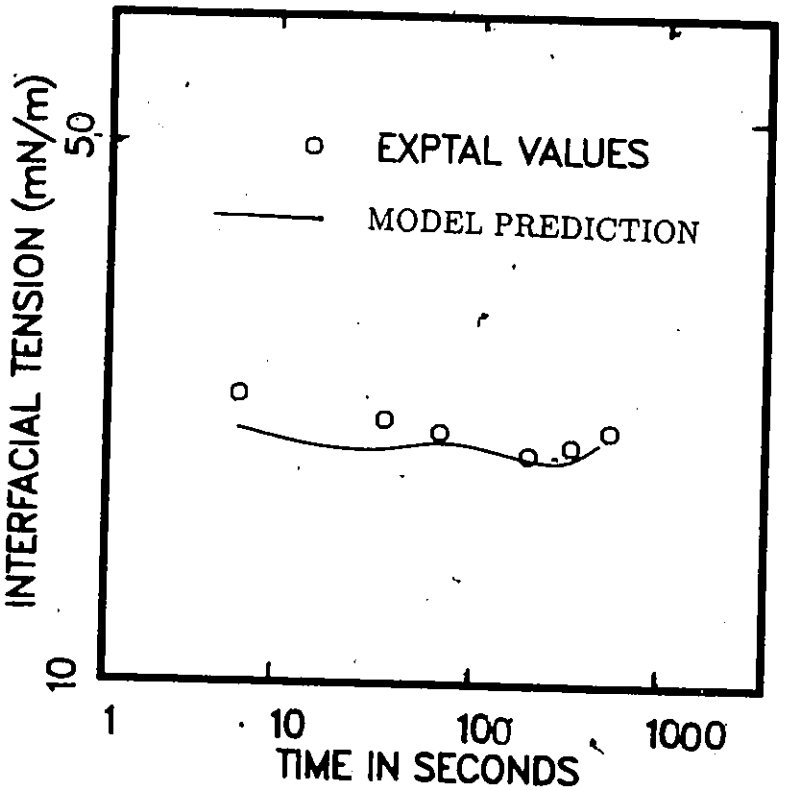

Figure 44 : Exptal Vs Predicted IFT for 0.02 M Lauric Acid in HD Vs 1.25 mM NaOH, Drop NO 2

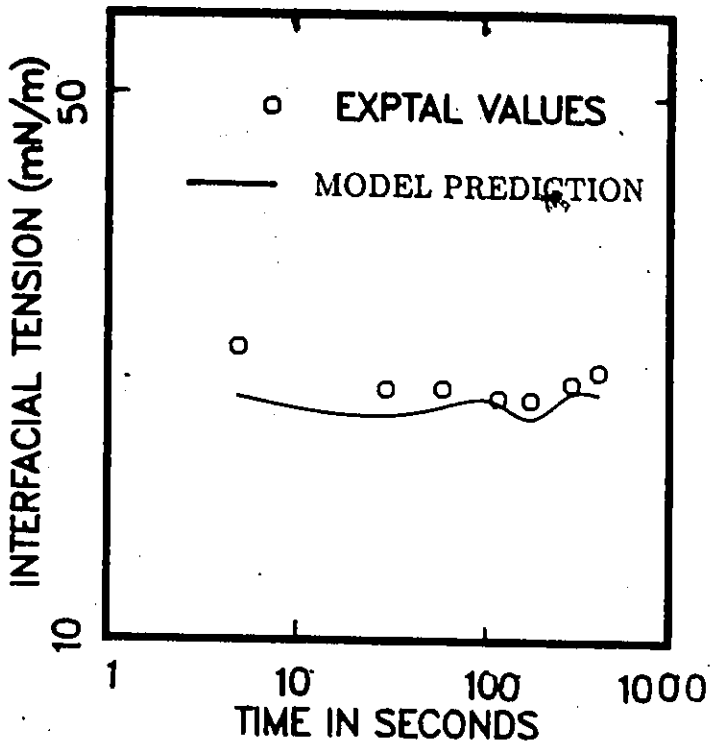

Figure 45 : Exptal Vs Predicted IFT for 0.02 M Lauric Acid in HD Vs 2.50 mM NaOH, Drop NO 1

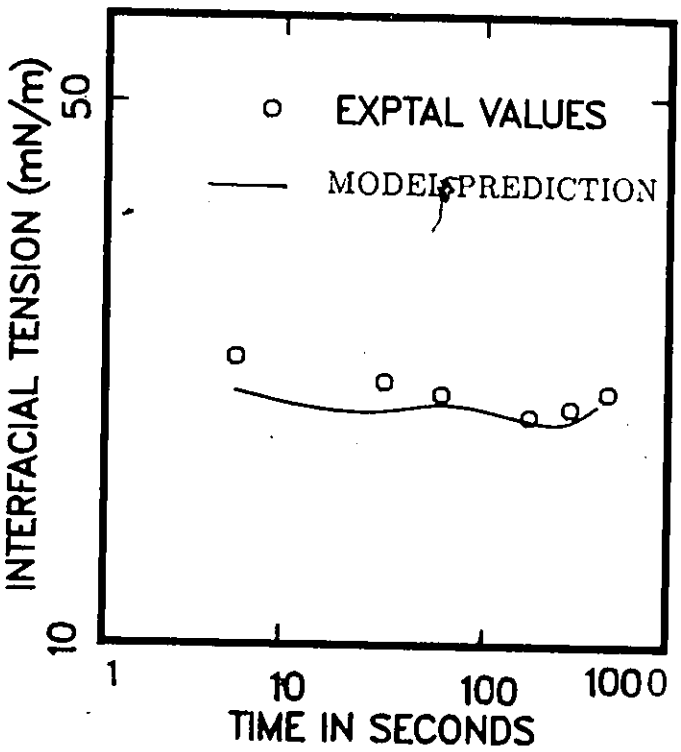

Figure 46 ; Exptal Vs Predicted IFT for 0.02 M Lauric Acid in HD Vs 2.50 mM NaOH, Drop NO 2

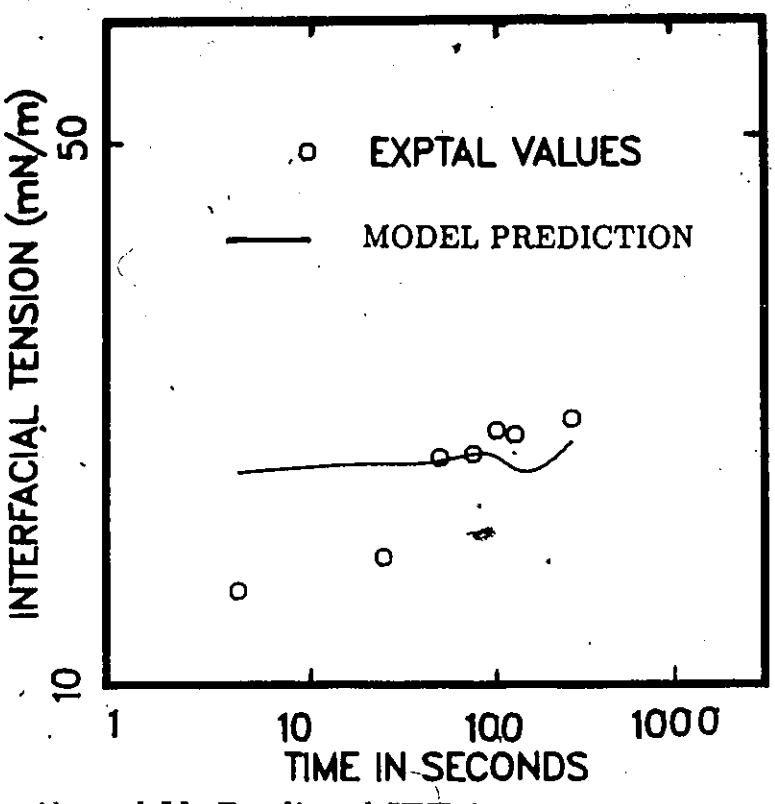

Figure 47 : Exptal Vs Predicted IFT for 0.02 M Lauric Acid in HD Vs 12.50 mM NaOH, Drop NO 1

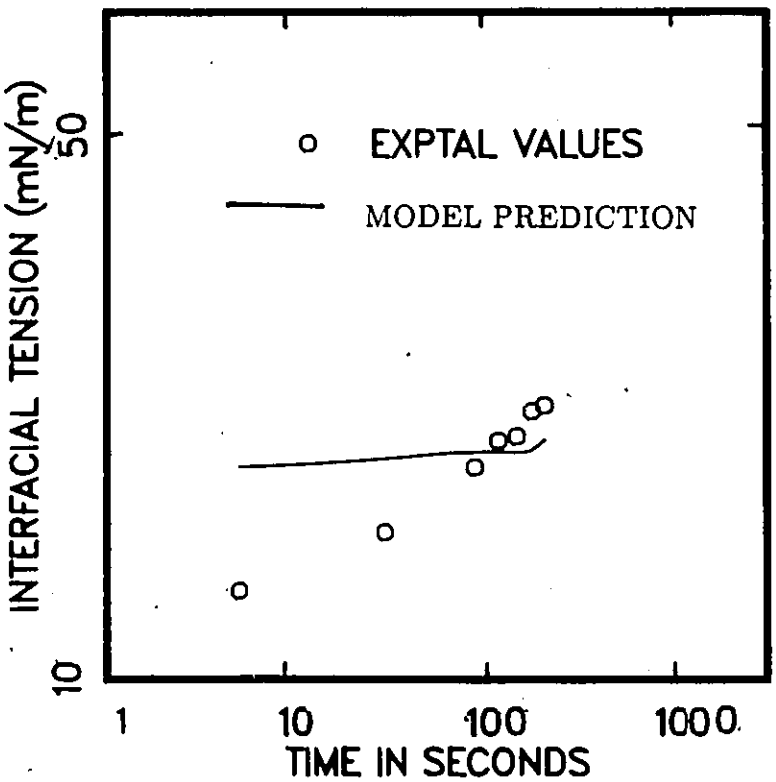

Figure 48 : Exptal Vs Predicted IFT for 0.02 M Lauric Acid in HD Vs 12.50 mM NaOH, Drop NO 2

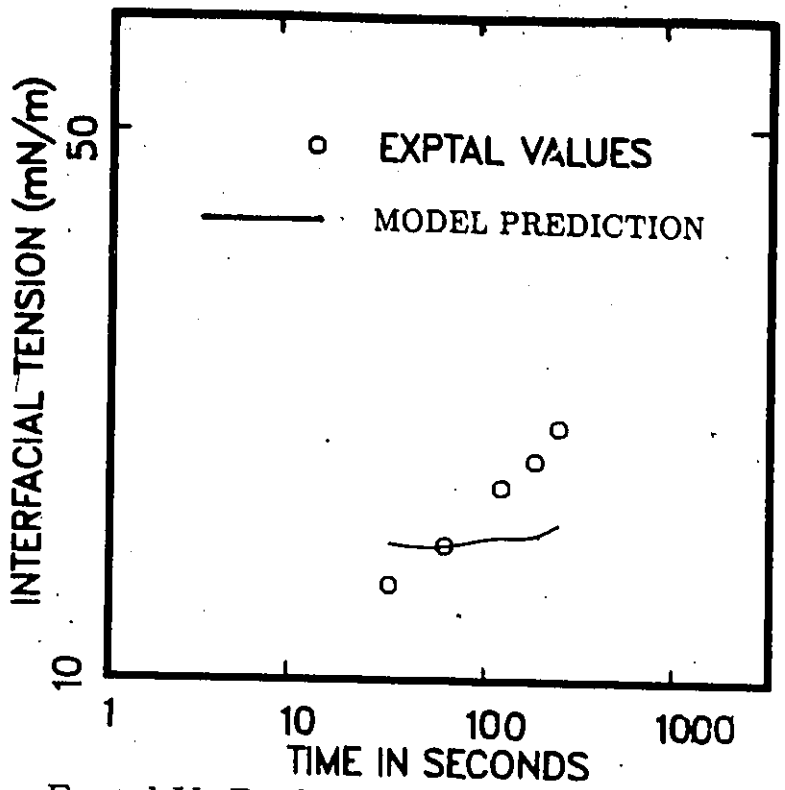

Figure 49 : Exptal Vs Predicted IFT for 0.02 M Lauric Acid in HD Vs 25.00 mM NaOH, Drop NO 1

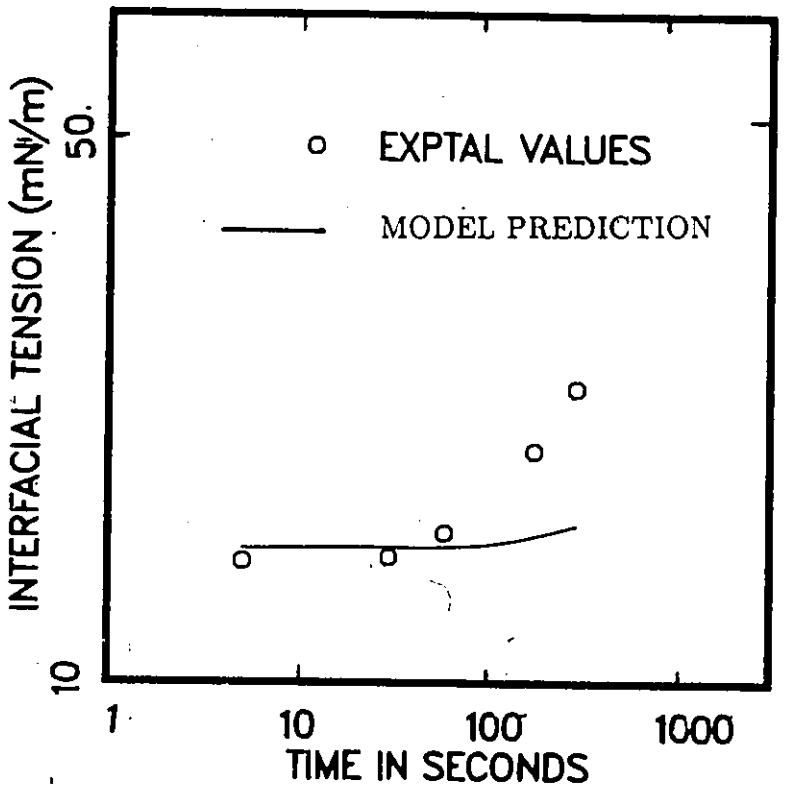

Figure 50 : Exptal Vs Predicted IFT for 0.02 M Lauric Acid in HD Vs 25.00 mM NaOH, Drop NO 2

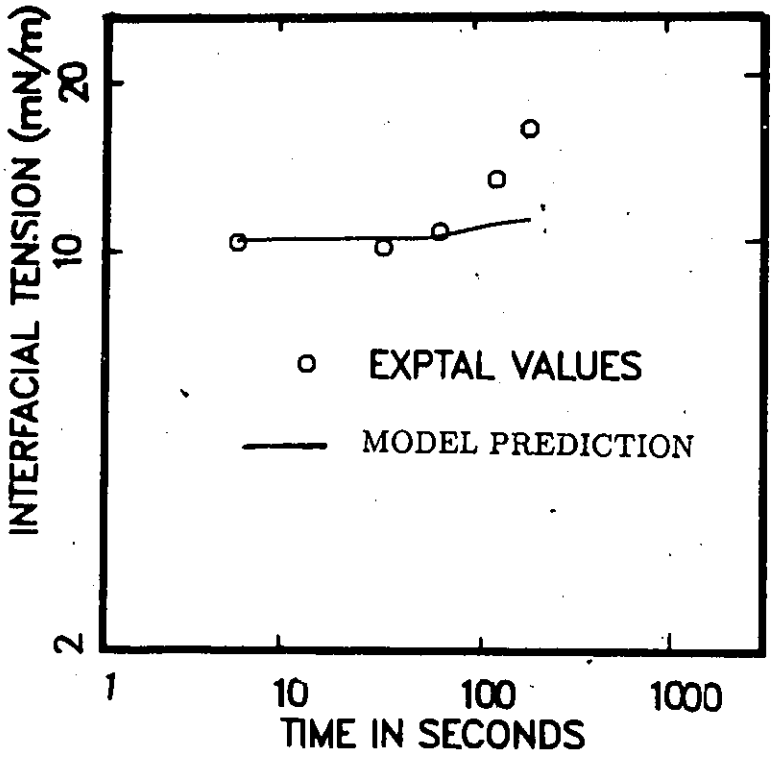

Figure 51 : Exptal Vs Predicted IFT for 0.02 M Lauric Acid in HD Vs 50.00 mM NaOH, Drop NO 1

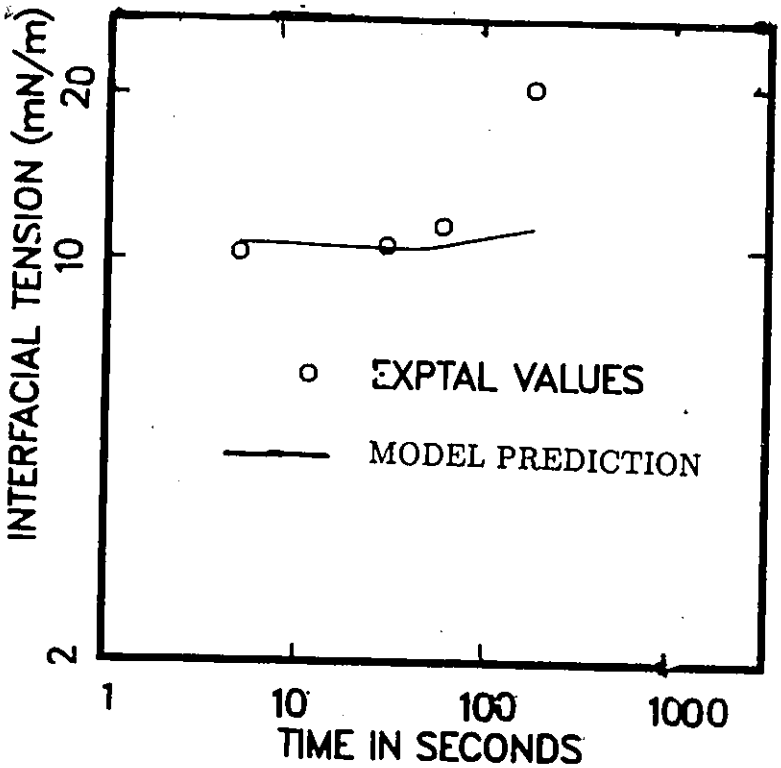

Figure 52 : Exptal Vs Predicted IFT for 0.02 M Lauric Acid in HD Vs 50.00 mM NaOH, Drop NO 2

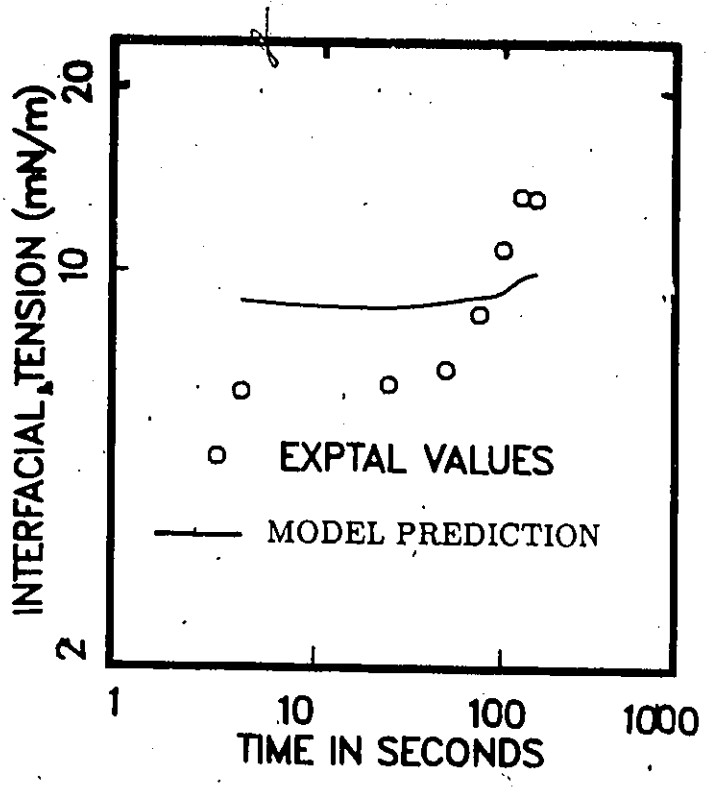

Figure 53 : Exptal Vs Predicted IFT for 0.02 M Lauric Acid in HD Vs 150.00 mM NaOH, Drop NO 1

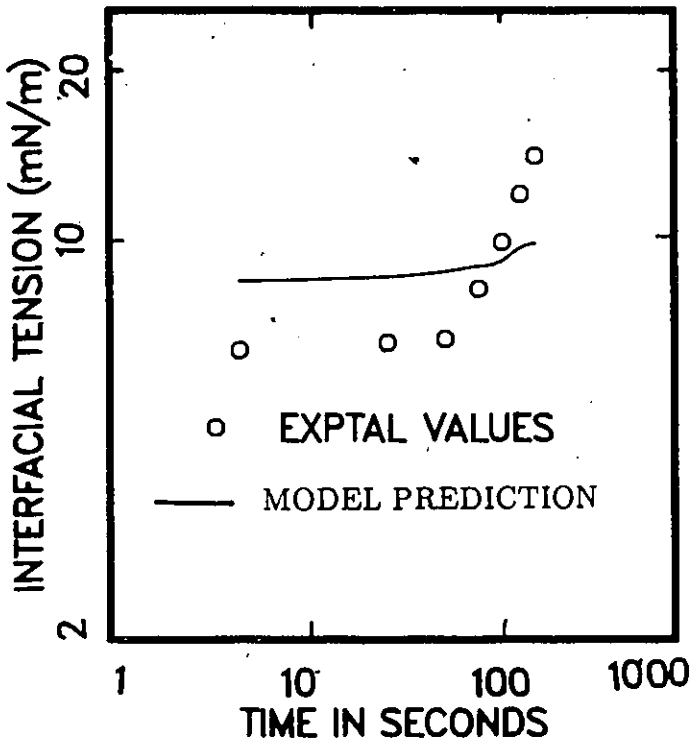

Figure 54 : Exptal Vs Predicted IFT for 0.02 M Lauric Acid in HD Vs 150.00 mM NaOH, Drop NO 2

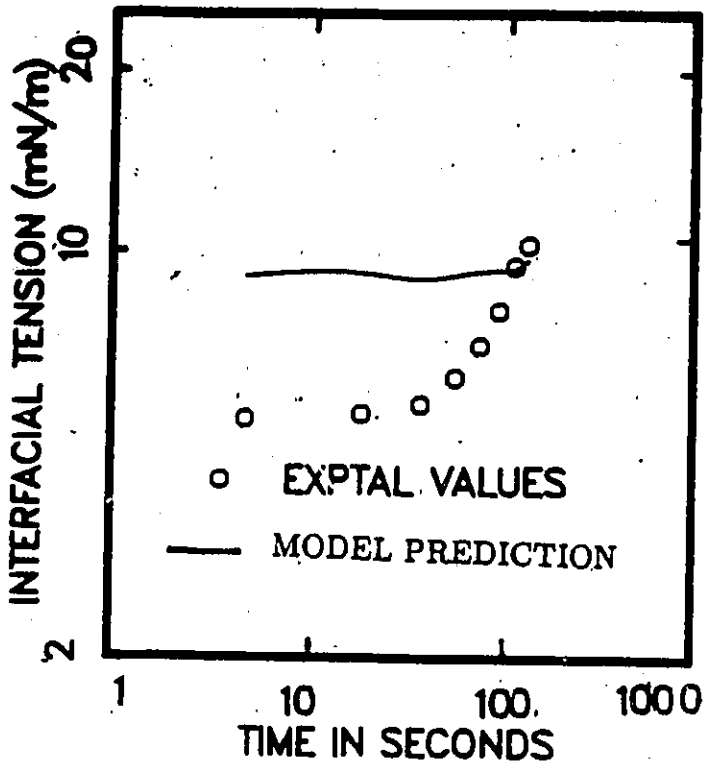

Figure 55 : Exptal Vs Predicted IFT for 0.02 M Lauric Acid in HD Vs 200.00 mM NaOH, Drop NO 1

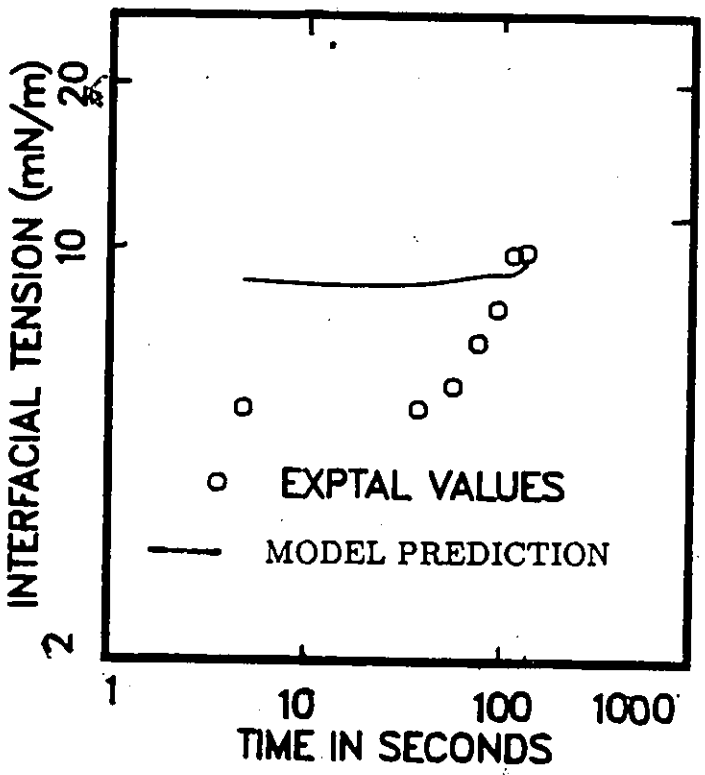

Figure 56 : Exptal Vs Predicted IFT for 0.02 M Lauric Acid in HD Vs 200.00 mM NaOH, Drop NO 2

Figs. 39–42 show a significant discrepancy between the experimental and predicted IFT for the oleic acid system at NaOH concentrations beyond 2.50 mM . This apparent deviation of the experimental from the predicted dynamic tension values may be due in part to a greater uncertainty in the experimental data arising from the hydrodynamic instability of small pendant drops at extended residence times in the aqueous phase . At high caustic concentrations, the initial IFT is quite low . However , as the boundary tension increases at a rather fast rate, the already small and elongated oil droplet becomes increasingly spherical. Because of this sudden change in the shape of the droplet after only a short contact time, the radius of the fitted Laplacian curve becomes relatively bigger and this translates to much higher IFT values than would be obtained in the absence of hydrodynamic instabilities. The onset of this instability problem corresponded to the interfacial age at which measurements of both d_e and d_s (see Fig. 4) could not be obtained from photographs of the pendant drop. Notwithstanding, the agreement between the predicted and experimental IFT values ,as can be seen from Figs. 33- 56 , is satisfactory over the rather short duration in which the dynamic IFT phenomenon could be monitored , for both oleic and lauric acid systems. Within these limits , one can reasonably claim that the proposed mechanisms and models for the interaction of single fatty acids with a spectrum of aqueous caustic solutions are indeed valid. Thus, diffusive-kinetic considerations as demonstrated in this study , hold a lot of promise as we seek to unravel the mysterious way in which crude oil acids interact with caustic reagents in order to reduce oil-water interfacial tensions .

15.4 Interplay of Diffusion , Viscosity and Sorption Kinetics

The work of Rubin and Radke[60] showed among other things that large desorption barriers prevented rapid removal of adsorbed surfactants from the interface separating two immiscible liquids,

and consequently led to the incidence of IFT minima . The authors used a parametric study to show that convective diffusion did not influence IFT to any appreciable extent . In this work , we did not perform a parametric study as such . However, in order to determine if higher values of the Nernstian boundary layer thickness might influence the model predictions, we used δ values three orders of magnitude larger than those given in Tables 6 and 8. There was no significant change in the results obtained with the smaller δ values regardless of which acid or caustic concentration was involved. A similar treatment of other variables such as the sorptive rate constants and the equilibrium parameters resulted in significantly large changes to the predicted IFT values . Thus , the parameters that are associated with sorption kinetics clearly influence the predicted IFT more than the diffusive ones . These are the quantities that need to be properly estimated in dealing with crude oil/caustic interactions .

The effect of viscosity on the dynamic IFT of reactive systems can be quite remarkable from an experimental point of view . In a recent study , Neale et al. [114] found that the addition of polystyrene to augment the oleic phase viscosity slowed down the rate of contraction of the spinning oil droplet and that led to a smaller rate of increase in IFT . Thus, a difference in the viscosity of a given crude oil could lead to substantially different dynamic IFT data . As a matter of fact , a good number of the systems whose interfacial behaviour was studied by using the micropendographic measurement apparatus could not be adequately followed with the spinning drop tensiometer, due to the low viscosity of both phases . The shape of the drop changed so quickly with time especially at higher caustic concentrations that measurements could be made only after freezing the drop photographically . At the moment , there is no direct involvement of viscosity in fundamental equations (such as that of Young and Laplace[41,42]) used for the calculation of interfacial tensions. In the light of this work , there is the need to modify existing theories in order to allow for the effect of viscosity in the determination of boundary tensions .

Chapter 16

Multi-Component Studies: Interfacial Data and Model Predictions

16.1 Interfacial Data

The various binary mixtures of oleic and lauric acids in hexadecane were formulated according to the scheme given in Table 2 . The experimental strategy for this phase of the study was also outlined in chapter 5 . A sequence of tables starting from Table B7.1 to Table B11.6 of Appendix B contains the experimental interfacial data for all the binary mixtures contacted with various caustic solutions . Following an approach similar to that used in the single component dynamic study , we have plotted the experimental IFT as a function of interfacial age for each mixture and for each working NaOH concentration . These plots appear as Figs. 57–61 .

Each of Figs. 57–61 consists of several sub-plots depicting the dynamic IFT obtained when the

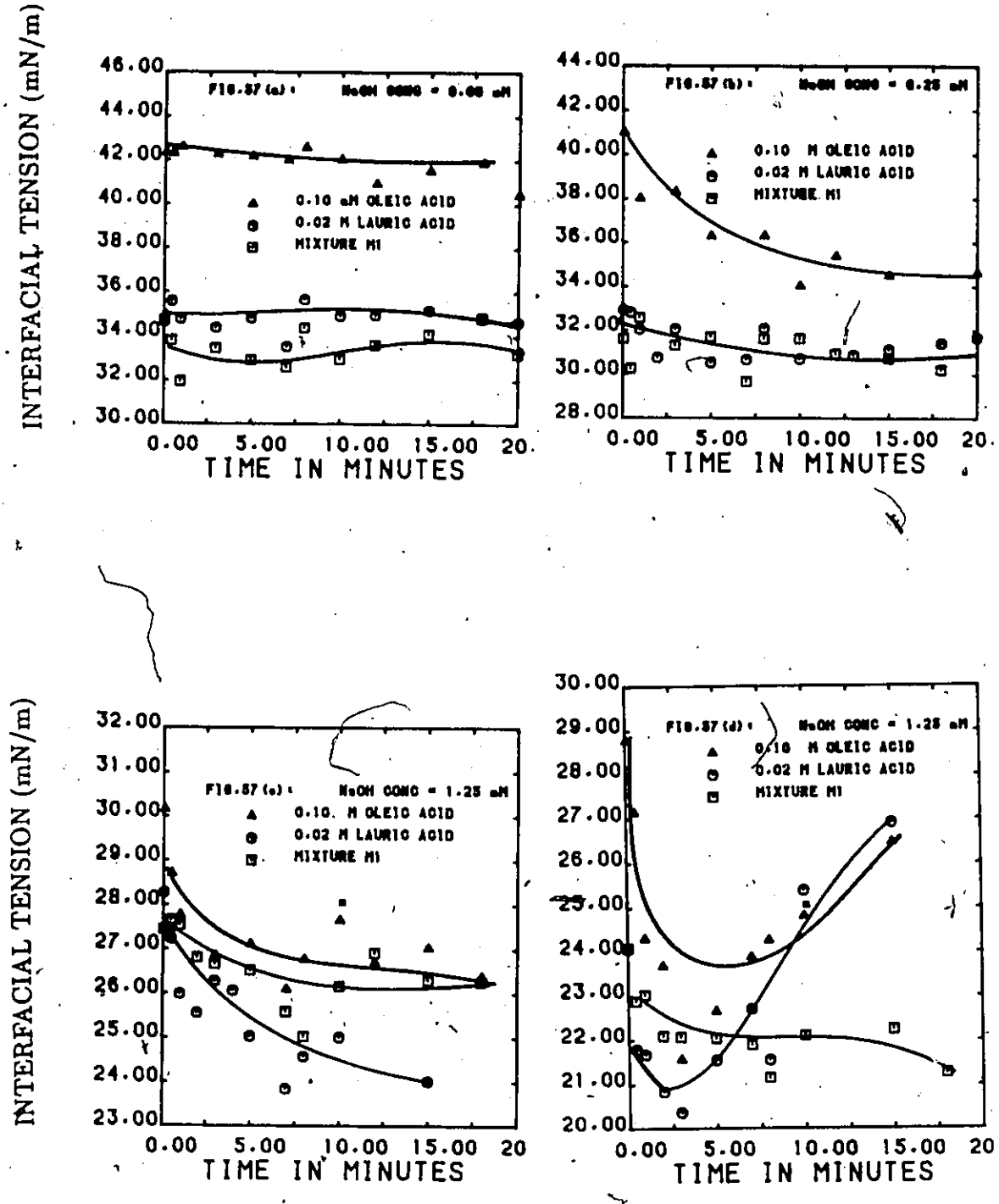

Figure 57 : IFT Vs Time for Mixture M1/NaOH Systems

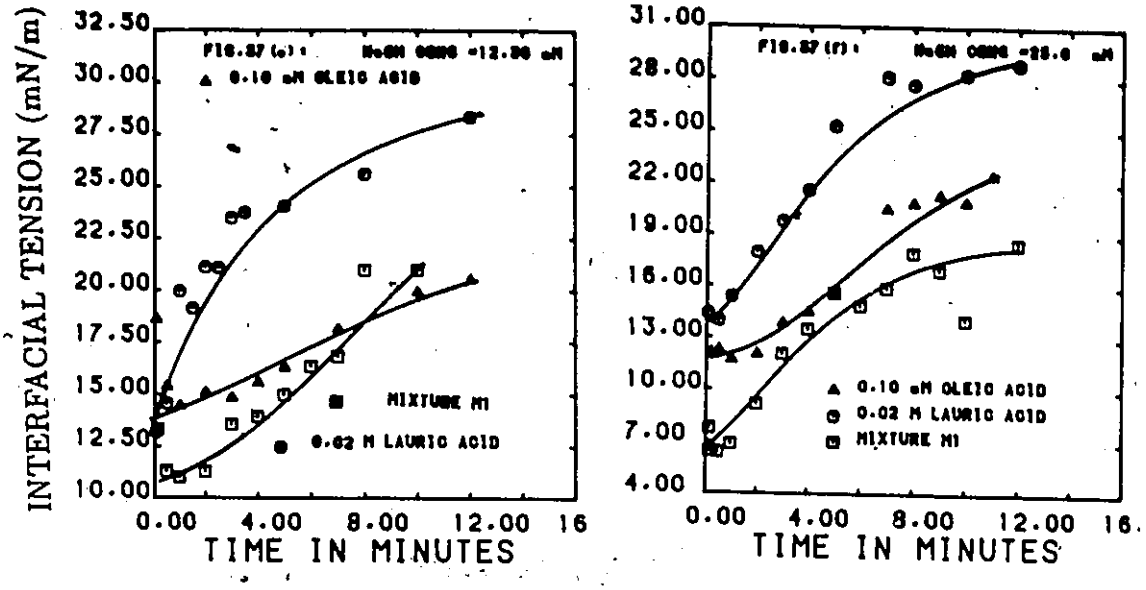

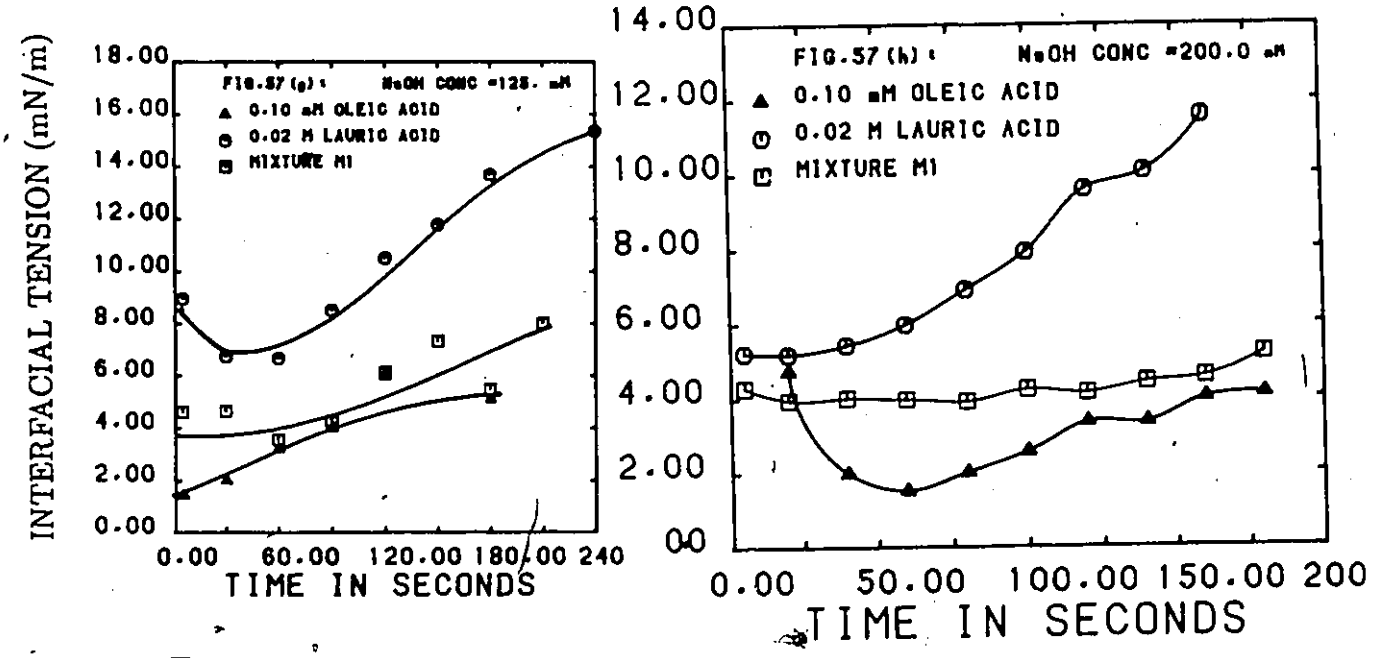

Figure 57 : (Continued)

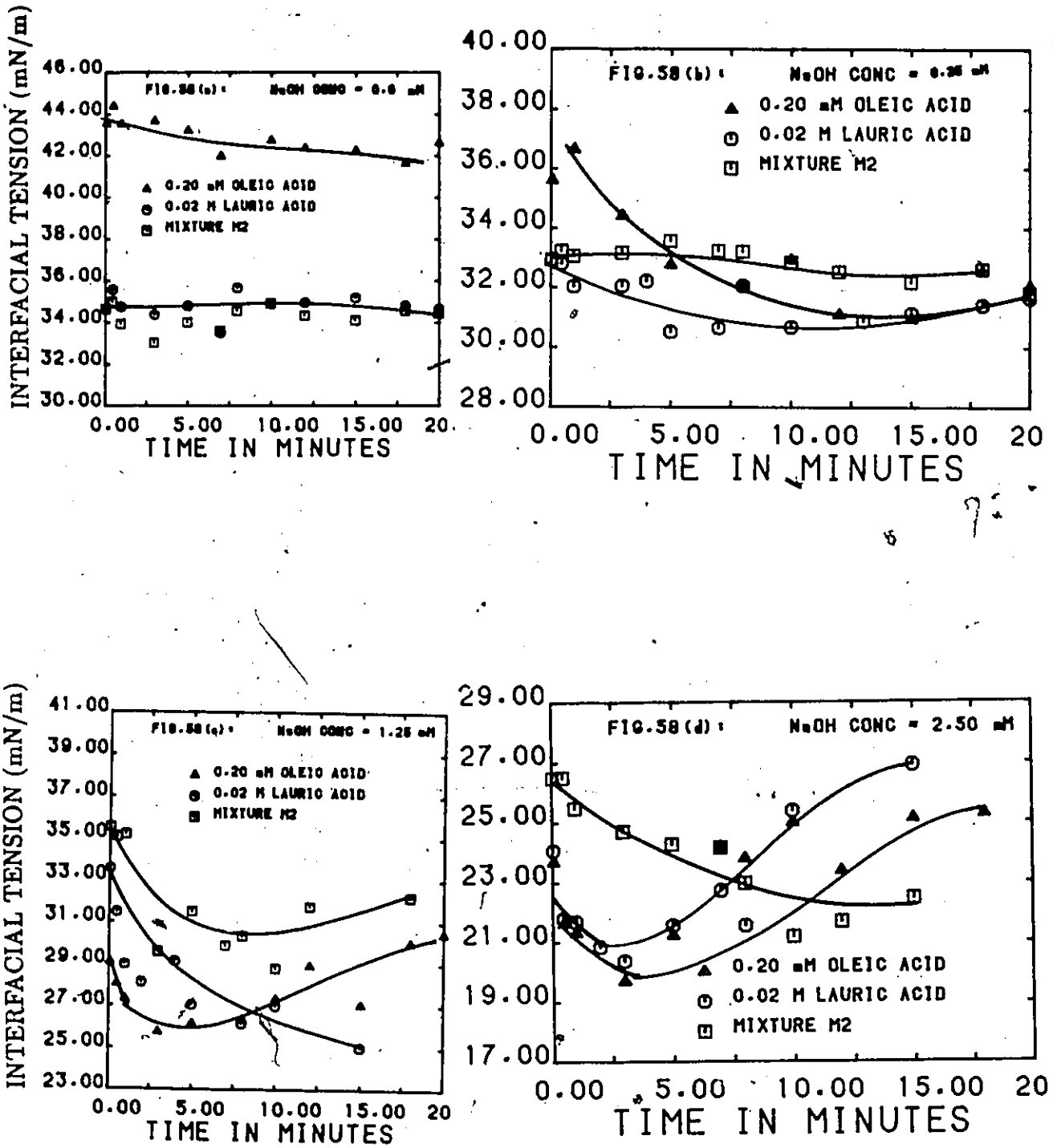

Figure 58 : IFT Vs Time for Mixture M2/NaOH Systems

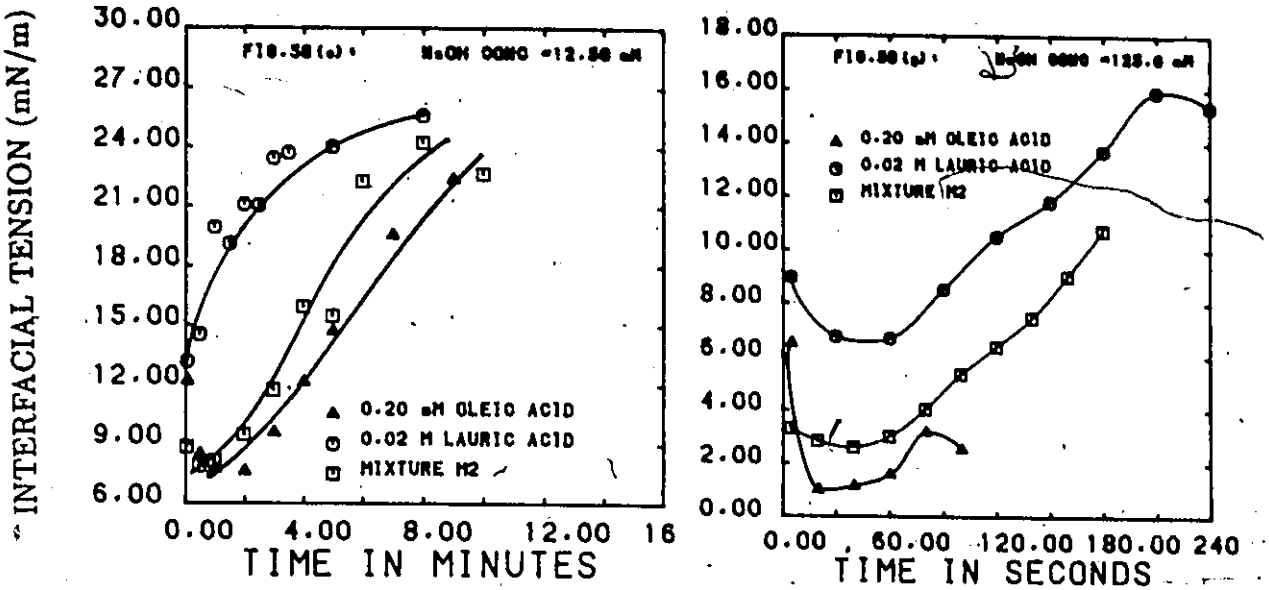

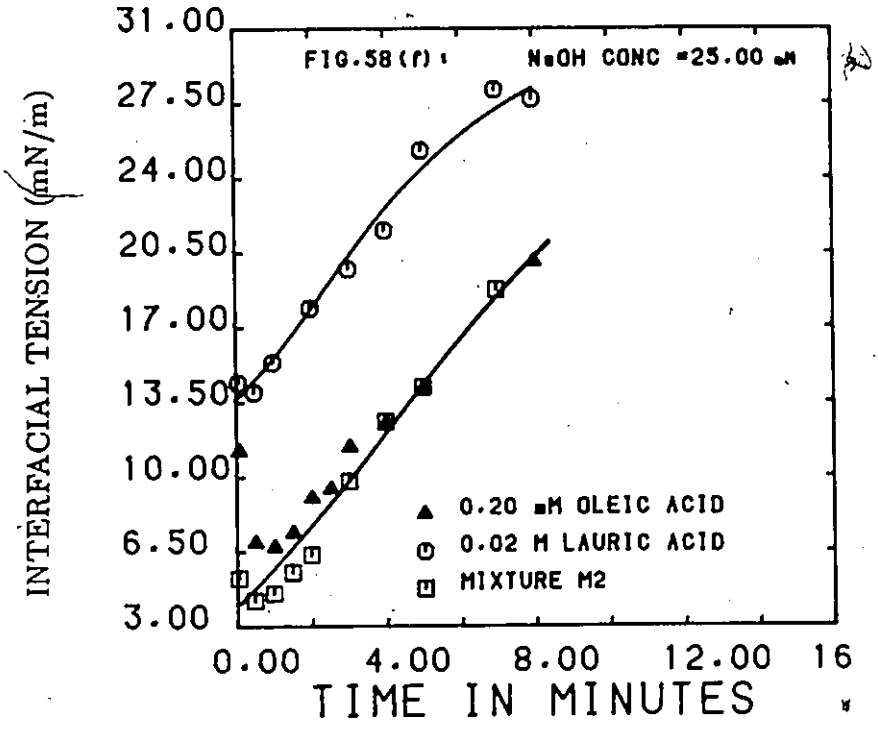

Figure 58 : (Continued)

designated mixture was contacted with a spectrum of NaOH solutions . In addition , we have also interposed the IFT data of the constituent acids as previously obtained in separate single component measurements. Thus , in Fig. 57(a), we have plotted the IFT values for 0.10 mM oleic acid , 0.02 M lauric acid as well as the mixture M1 , all exposed to neutral water . The mixture had a fairly constant IFT of about 33 mN/m which in turn was also the value measured for the 0.02 M lauric acid . On the other hand , the 0.10 mM oleic acid reference system maintained a much higher IFT close to 42 mN/m . One may then conclude that in neutral water , mixture M1 behaved as though it contained only lauric acid . The same conclusion may also be reached based on the IFT trends of Figs. 57(b) and (c) for caustic concentrations of 0.25 and 1.25 mM respectively. When the NaOH concentration was increased to 2.50 mM for the same acid mixture , we see in Fig. 57(d) that the two constituent acids exhibited IFT minima of 21 mN/m at an interfacial age of three minutes . Beyond this minimum , the IFT rose rapidly for both acids while the mixture maintained a constant IFT near 21 mN/m . The 0.10 mM reference oleic acid started to produce markedly lower IFT values than 0.02 M lauric acid when the caustic concentration reached 12.50 mM and beyond (see Fig. 57(e–h)) . At these higher caustic levels , both acids showed a rising trend in IFT with contact time between the phases . So also did the mixture except that its tension values were now close to those exhibited by the more surface active oleic acid .

Fig. 58 gives the IFT data for mixture M2 and the reference acid systems . The trend in the IFT obtained with various NaOH concentrations was similar to that observed for the M1 systems except that the tension values were marginally lower . The reference oleic acid whose effective concentration in the mixture M2 was 0.20 mM , yielded the lowest tension values at caustic concentrations above 2.50 mM and the mixture produced IFT values which were very close to those of the oleic acid . When the oleic acid concentration in the mixture increased to 0.3125 mM as in Fig. 59 , the tension

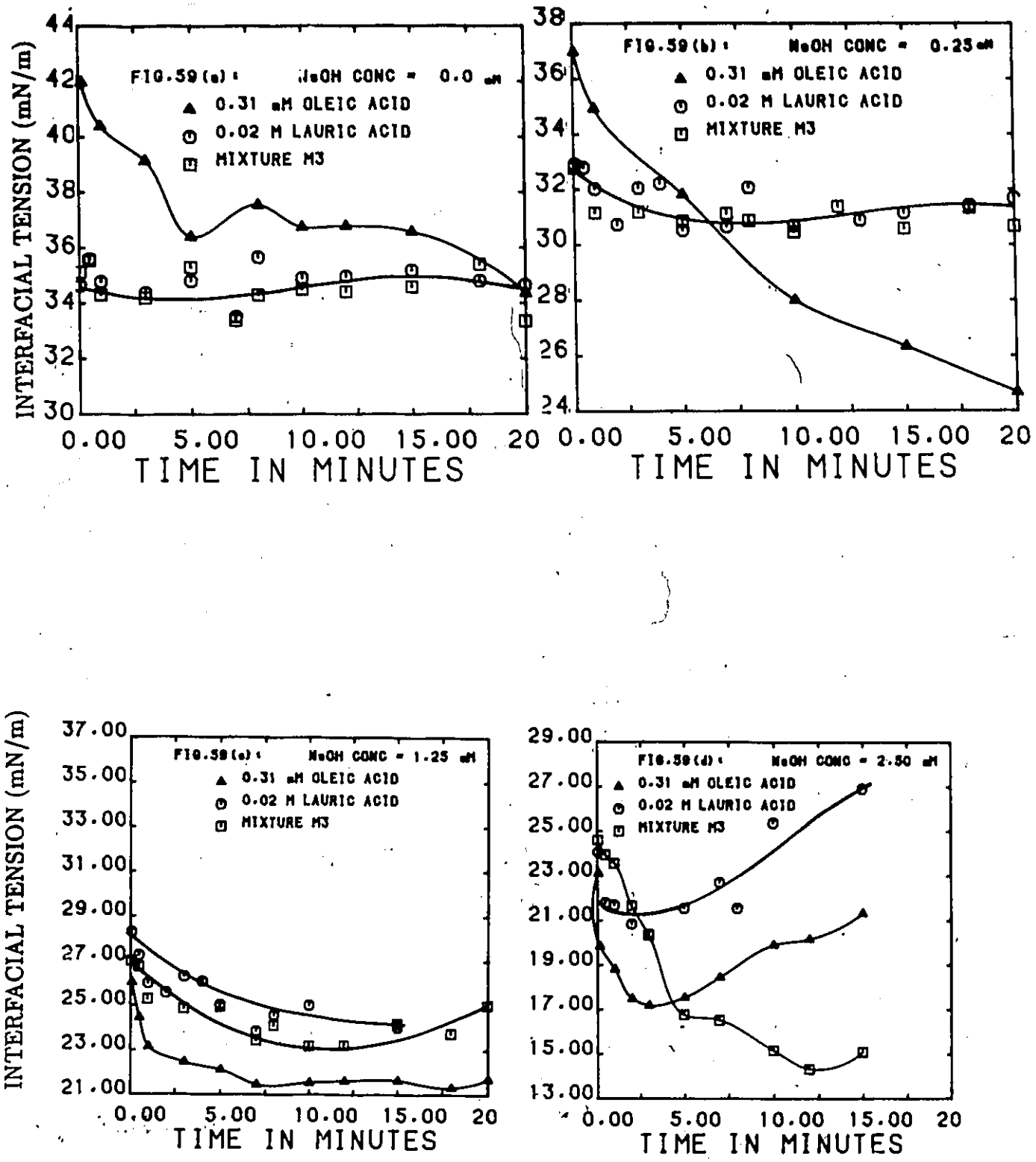

Figure 59 : IFT Vs Time for Mixture M3/NaOH Systems

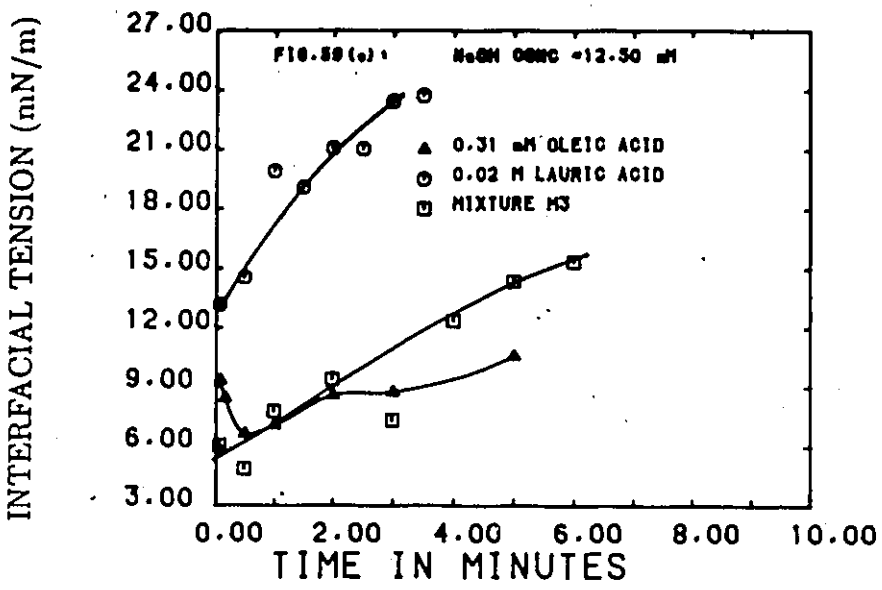

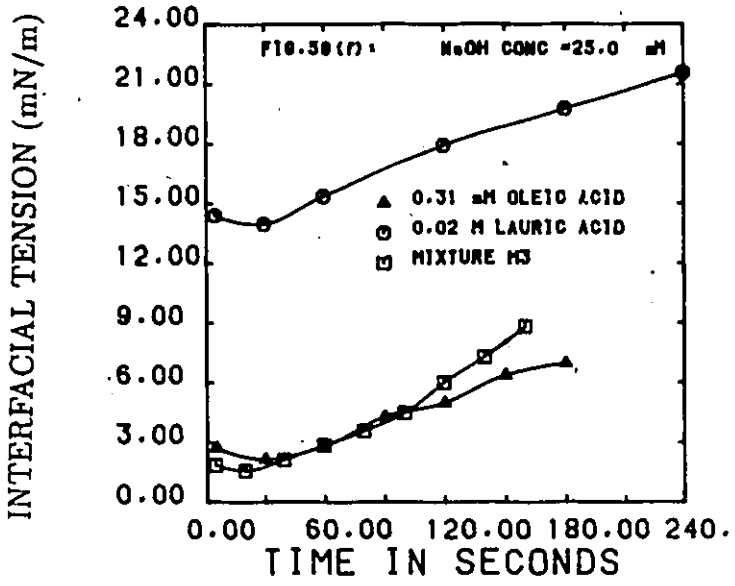

Figure 59 : (Continued)

values given by the reference acid alone dropped appreciably even at lower caustic concentrations. For example , at the NaOH concentration of 1.25 mM , (see Fig. 59(c)) , the drop in IFT for the reference oleic acid was 10 mN/m within 7 minutes contact time of the two phases . The tension lowering efficacy of oleic acid at this working concentration influenced the interfacial behaviour of the mixture to the extent that tensions showed a decreasing trend even though the IFT associated with the lauric acid did not drop appreciably . For this same M3 mixture , we see also in Fig. 59(d–f) that due to the greater interfacial activity of the oleic acid component , the IFT values at higher caustic levels were very close to the values measured for the oleic acid alone . The lauric acid produced tensions that were generally far greater than the values measured for the mixture . The apparent indication here is that the lauric acid has been completely pushed out of the interface by the more surface active oleic acid species .

The reference oleic acid concentration for mixture M4 was 0.6125 mM . The IFT data for the M4 systems were plotted in Fig. 60 . For all working NaOH concentrations , the similarity in IFT trends with the M3 systems is apparent by comparing Figs. 59 and 60 . As noted earlier, the IFT values were generally lower when the oleic acid proportion of the mixture increased. In highly alkaline environments (see Fig. 60(e–f)) , tensions for the M4 systems remained in the range of 0 -10 mN/m, and exhibited the characteristic but gradual increase with extended contact time of the phases. It is important to note that the actual duration of the dynamic IFT phenomenon particularly in high caustic environments is quite short , often less than three minutes. For example, the pendant oil drop of mixture M4 in 25 mM NaOH solution maintained an acceptable shape for only 80 seconds and thereafter the drop became inappropriate for tension calculations by the micropendographic data treatment scheme .

IFT data for mixture M5 systems were plotted in Fig. 61 for the various caustic solutions . The

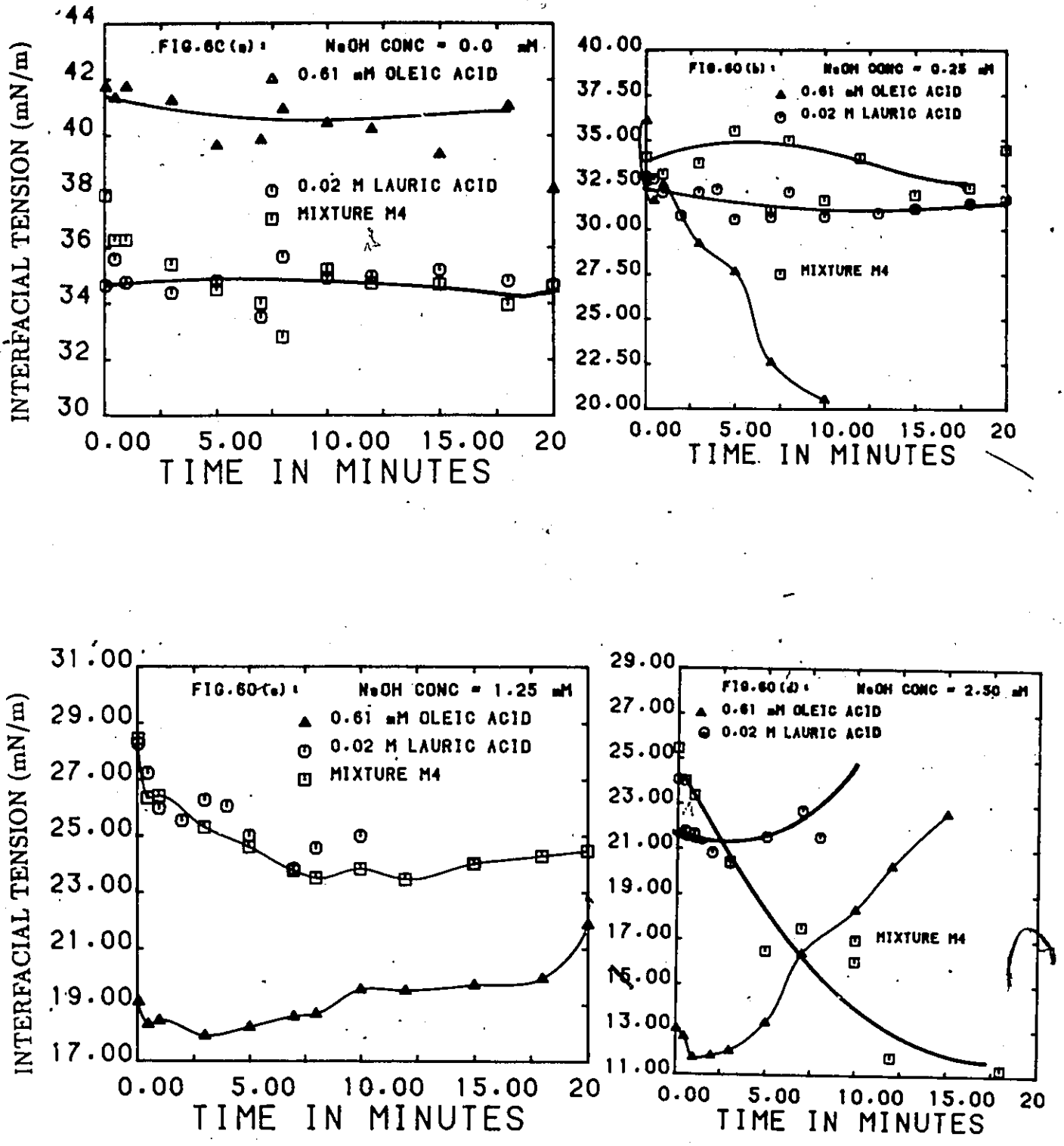

Figure 60 : IFT Vs Time for Mixture M4/NaOH Systems

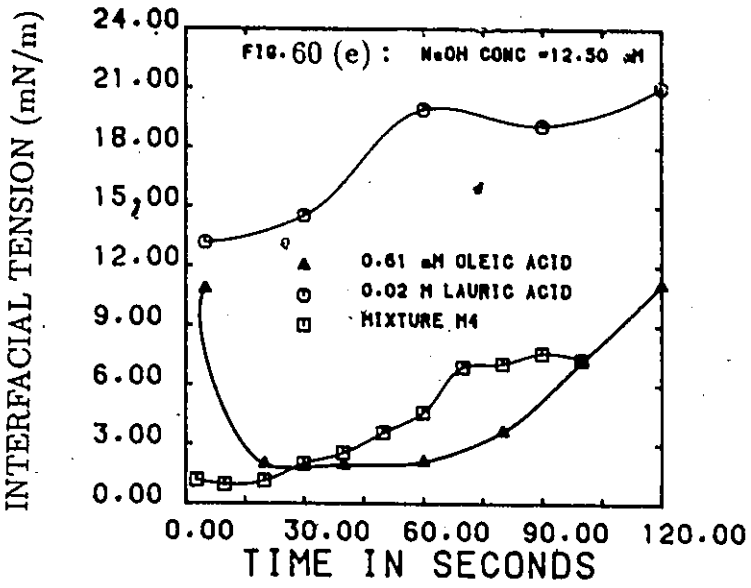

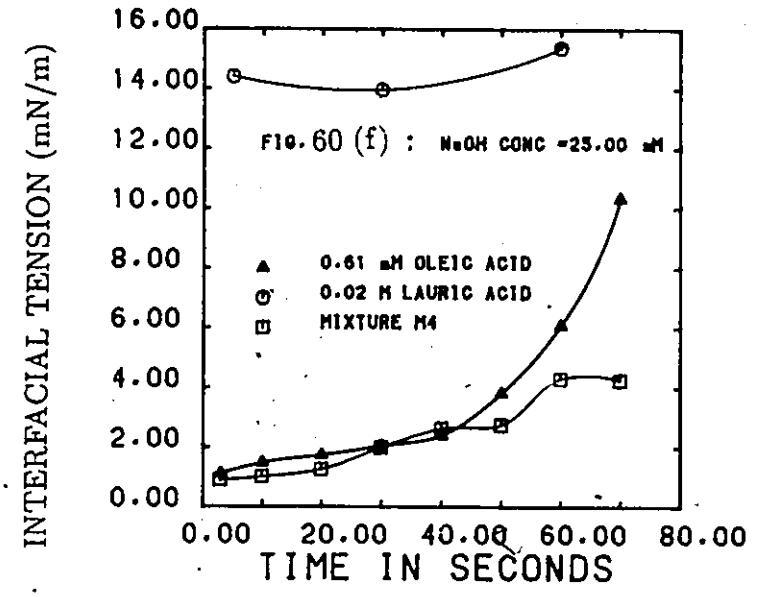

Figure 60 : (Continued)

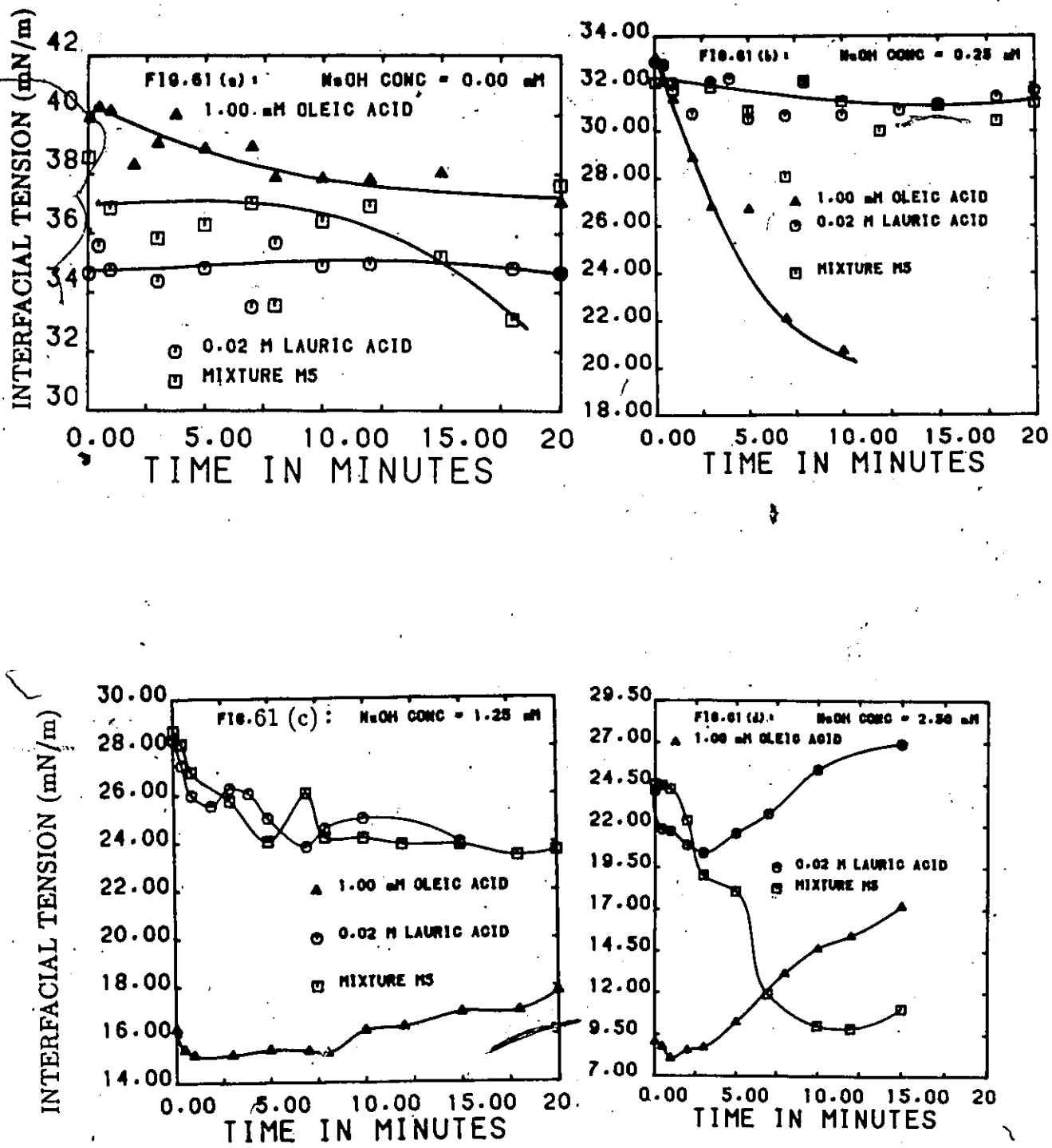

Figure 61 : IFT Vs Time for Mixture M5/NaOH Systems

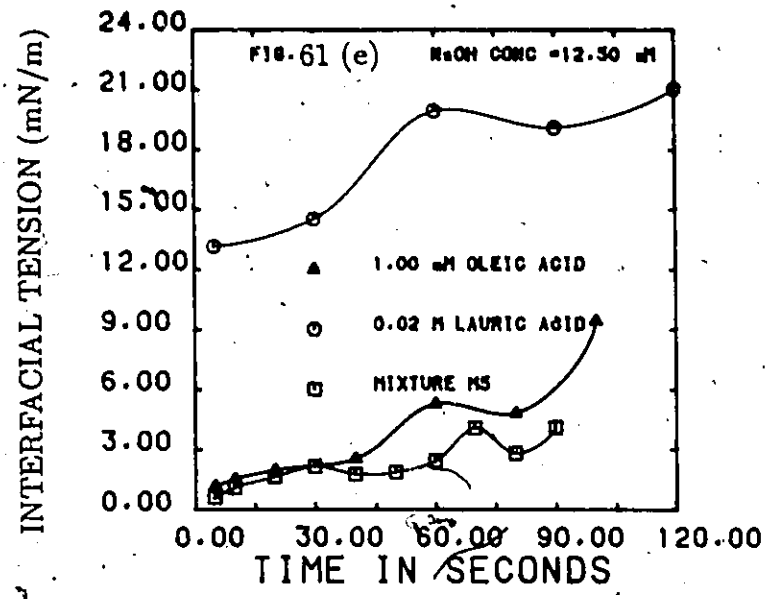

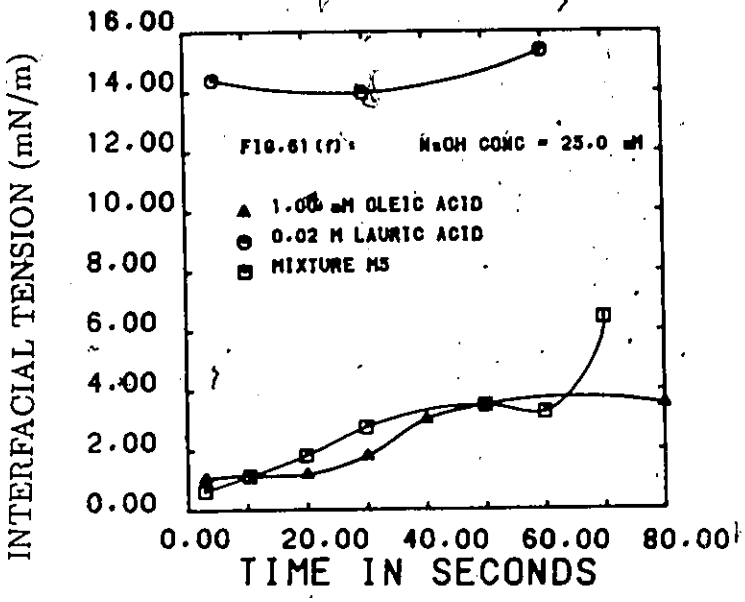

Figure 61 : (Continued)

trends in the data observed for the M3 and M4 systems were also repeated in this particular case . Also at NaOH concentrations above 2.50 mM , the mixture behaved interfacially like the reference oleic acid . Tension values measured for the lauric acid as a single component were markedly higher than the values obtained for the mixture as can be seen in Fig. 61 (d-f) . The pattern which is quite evident in these binary mixture systems is one in which the mixture behaved interfacially like the lauric acid component at caustic levels below 2.5 mM , but at higher caustic levels , the IFT values for the mixture systems were very much the same as for the oleic acid constituent . With further increase in the oleic acid proportion of the mixture , tensions generally edged lower and the mixture tended to follow the pattern set by the more interfacially active oleic acid over all the caustic concentrations investigated . This observation is remarkable because of the extremely high mole ratio of lauric acid compared to oleic acid (200 in M1 and 20 in M5) .

The implication of these acid mixture studies in enhanced oil recovery is that a spectrum of acids is likely to influence oil/water interfacial tensions depending on the prevailing caustic concentration at the leading edge of the caustic flood . If the caustic concentration remains high throughout the life of the flood , then the longer chain , more surface active acids will dominate over shorter chain acids . However , if as will normally be expected , considerable dilution of the caustic solution occurs , then the more abundant but less surface active acids in the crude oil will influence the oil/water interfacial tensions . Since tensions are generally lower when the longer chain acids are dominant , it follows that oil recoveries will be favored under such circumstances .

16.2 Model Predictions

In chapter 11 , we outlined the applicable model equations and the proposed solution procedure for the specific case of a binary acid mixture . The rationale here was to solve the model equations

using parameter values which would have been determined from single component analysis of the constituent acids at the appropriate concentrations . The resulting IFT determined from the model were then compared with the experimental values . Such comparative plots for the mixture systems are given as Figs. 62–87 .

Figs. 62–67 are the comparative IFT plots for mixture M1 exposed to various NaOH solutions. At caustic concentrations below 12.50 mM , (Figs. 62-64) , the agreement between experimental tension values and those predicted by the model is quite good . Some discrepancy between the experimental and predicted IFT values is evident at higher caustic concentrations for the M1 mixture (see Figs. 65–67). However , these discrepancies are well within the limits of experimental errors of the measurement system . The predicted IFT values at early contact times in Figs. 65–67 were generally higher than the measured values , but at extended times , the reverse appears to be the case . The problem may be due in part to the nature of the differential equations themselves as well as to the numerical integration routine . Due to the fact that the IFT changes at a faster rate when higher caustic concentrations are involved, the integration time steps were rather too small for the numerical solution scheme to predict the desired large changes in surfactant surface concentrations and subsequently in the dynamic IFT. This problem does not arise at lower caustic levels where tensions changed rather slowly, thus allowing bigger time steps to be used.

Comparative IFT plots for mixture M2/caustic systems are presented in Figs. 68–73 . Here again the agreement between the experimental and predicted IFT values was good at the lower range of the working NaOH concentration spectrum. There are discrepancies between the predicted and experimental tension values at NaOH concentrations above 2.50 mM. For example, in Fig. 71, at a caustic concentration of 12.50 mM , the predicted IFT values were relatively unchanged at longer contact times whereas the experimental values tended to increase monotonically . In Figs.

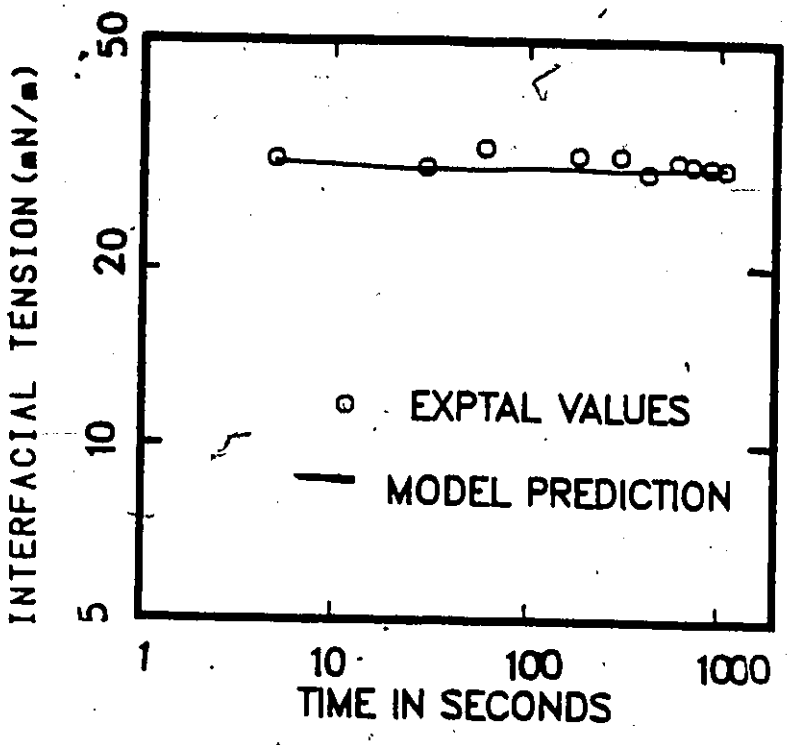

Figure 62 : Exptal Vs Predicted IFT for Mixture M1 in HD Vs 0.25 mM NaOH, Drop NO 1

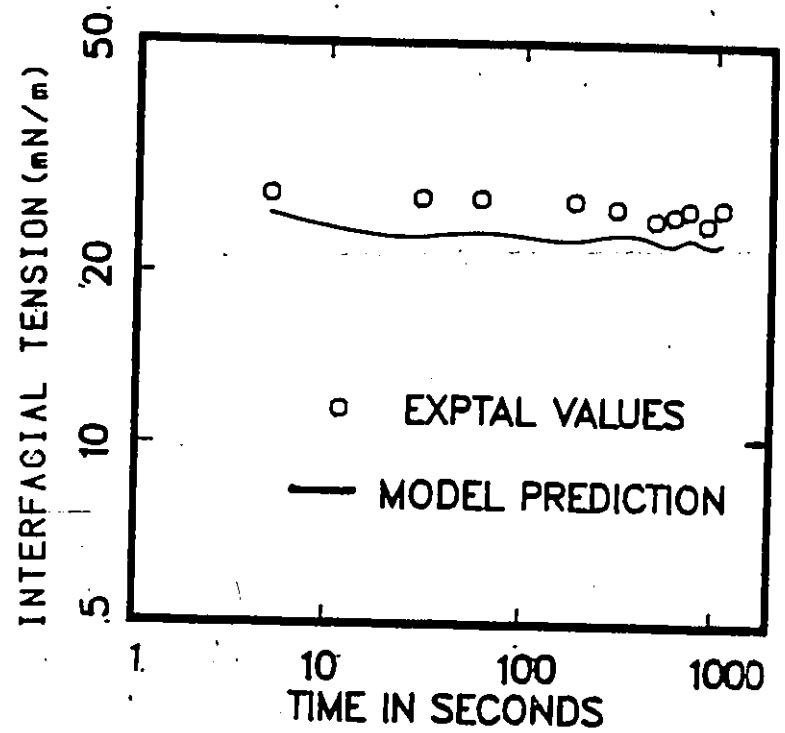

Figure 63 : Exptal Vs Predicted IFT for Mixture M1 in HD Vs 1.25 mM NaOH, Drop NO 2

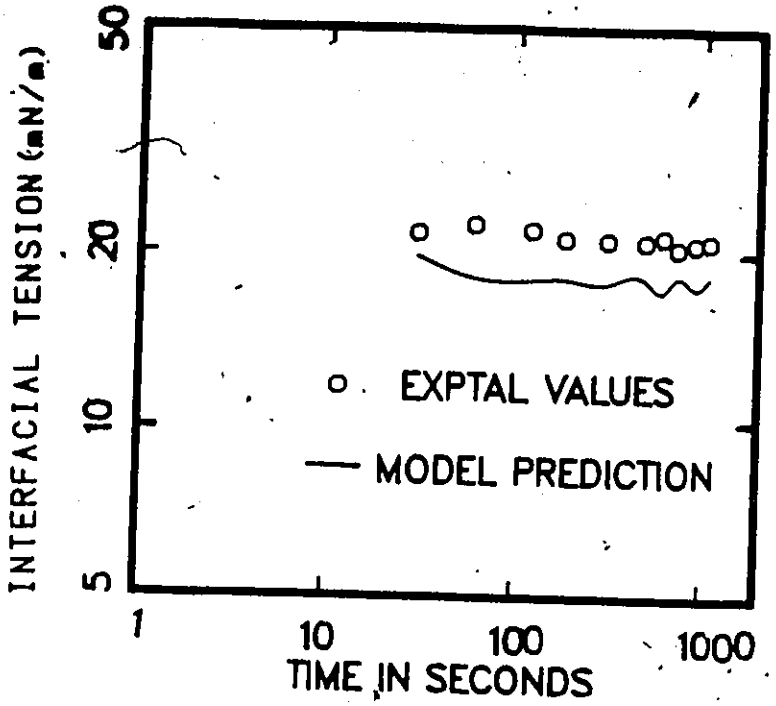

Figure 64 : Exptal Vs Predicted IFT for Mixture M1 in HD Vs 2.50 mM NaOH, Drop NO 2

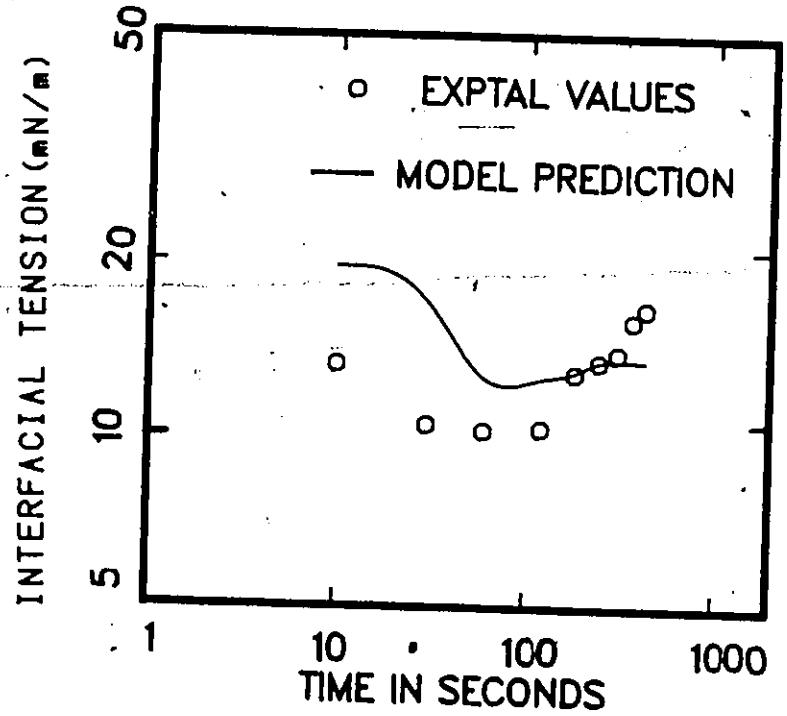

Figure 65 : Exptal Vs Predicted IFT for Mixture M1 in HD Vs 12.50 mM NaOH, Drop NO 1

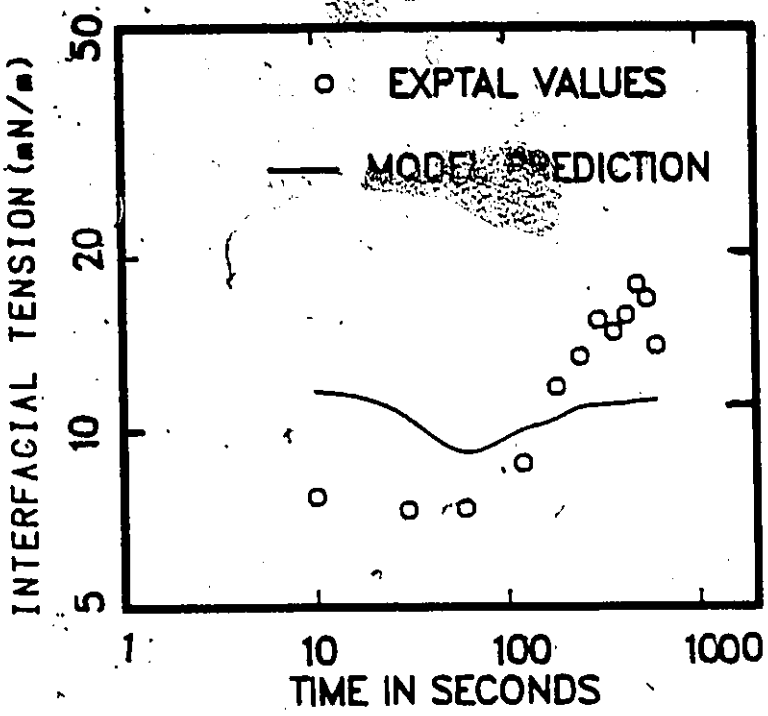

Figure 66 : Exptal Vs Predicted IFT for Mixture M1 in HD Vs 25.00 mM NaOH

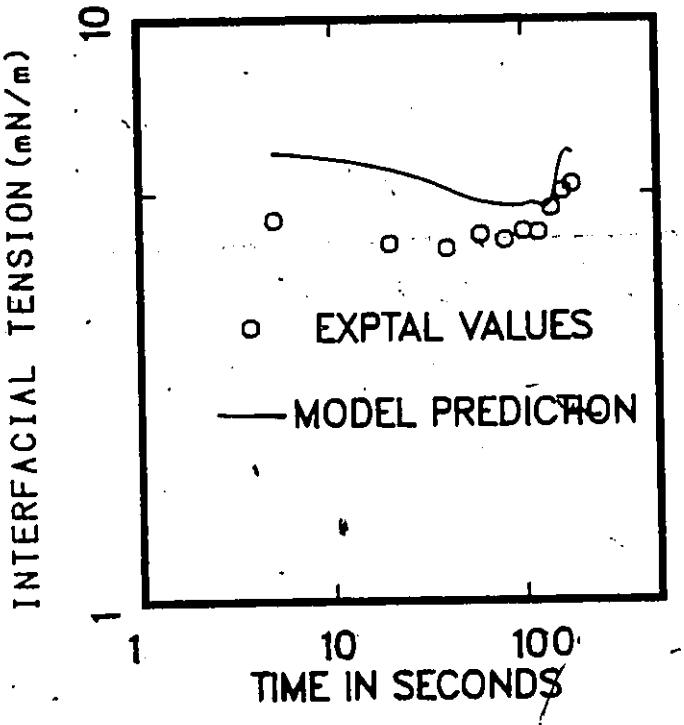

Figure 67 : Exptal Vs Predicted IFT for Mixture M1 in HD Vs 200.0 mM NaOH, Drop No 2

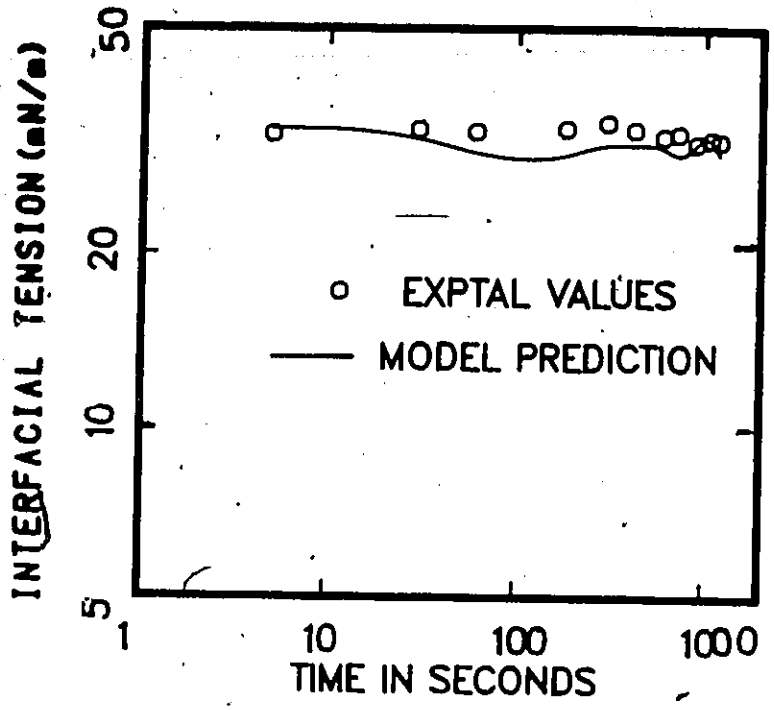

Figure 68 : Exptal Vs Predicted IFT for Mixture M2 in HD Vs 0.25 mM NaOH, Drop No 1

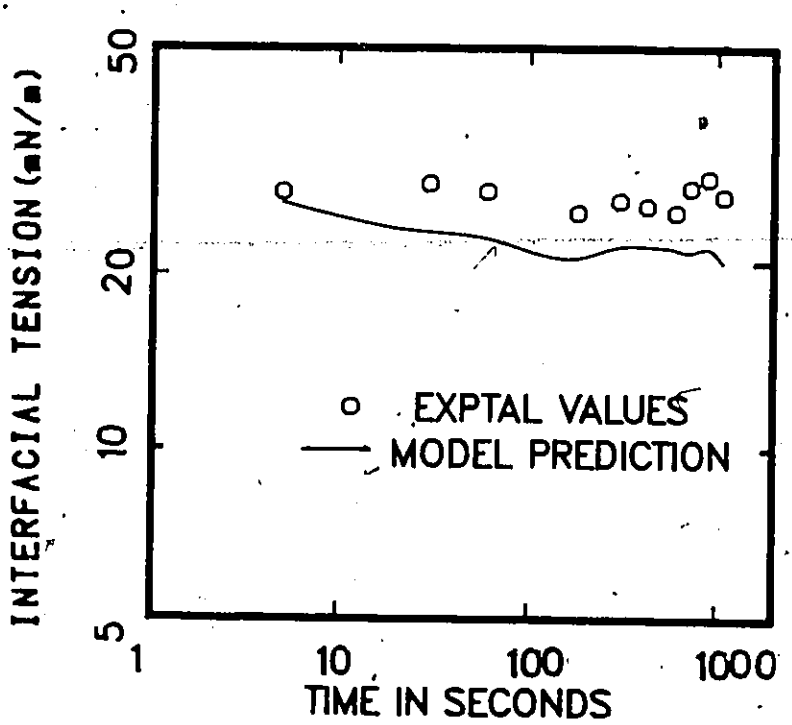

Figure 69 : Exptal Vs Predicted IFT for Mixture M2 in HD Vs 1.25 mM NaOH, Drop No 1

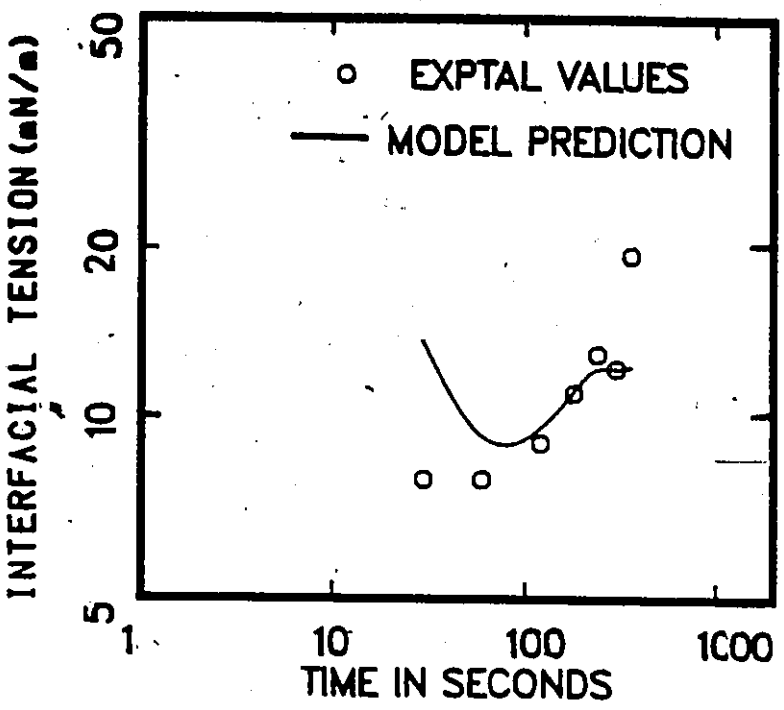

Figure 70 : Exptal Vs Predicted IFT for Mixture M2 in HD Vs 2.50 mM NaOH, Drop No 2

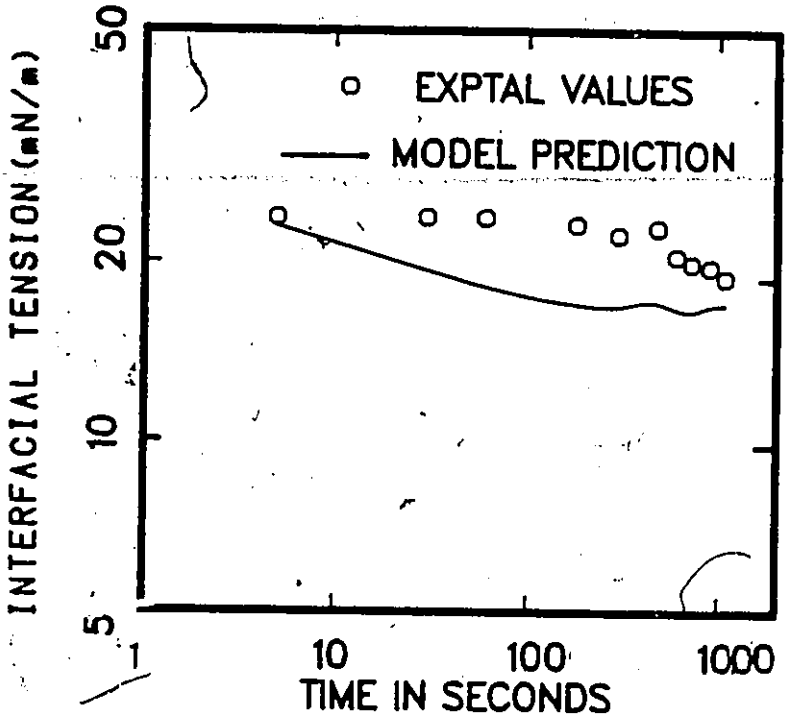

Figure 71 : Exptal Vs Predicted IFT for Mixture M2 in HD Vs 12.50 mM NaOH, Drop NO 2

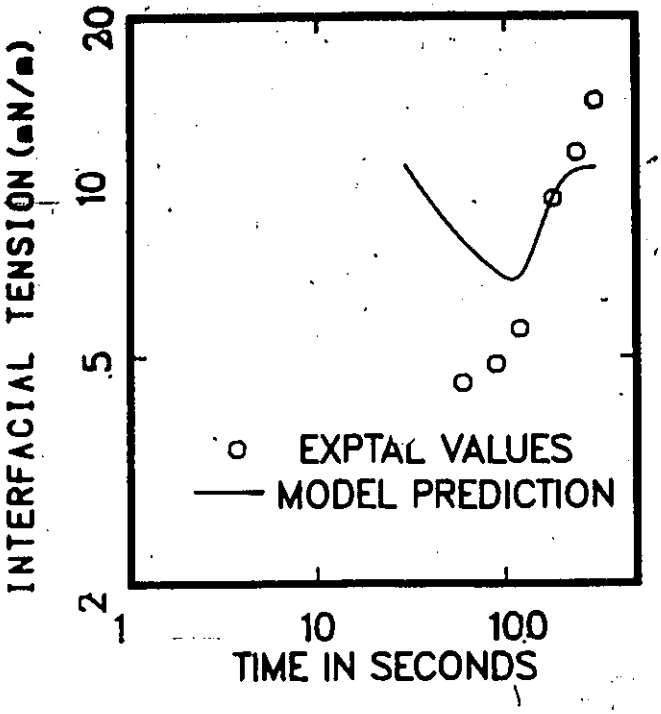

Figure 72 : Exptal Vs Predicted IFT for Mixture M2 in HD Vs 25.00 mM NaOH, Drop No 1

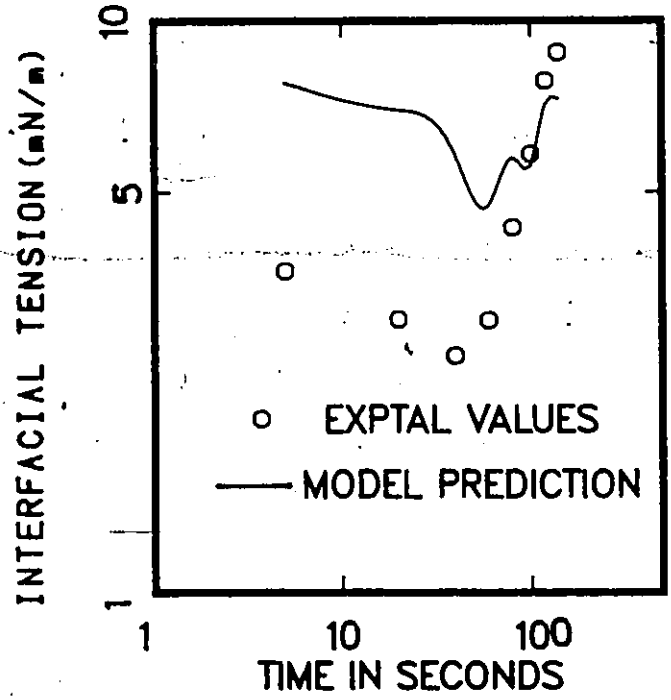

Figure 73 : Exptal Vs Predicted IFT for Mixture M2 in HD Vs 125.00 mM NaOH, Drop No 2

72 and 73 , the departure of the predicted values from the experimental tensions is quite apparent at early contact times but the mismatch is considerably reduced at longer times .

Comparative IFT plots for mixture M3/caustic systems are given in Figs. 74-78 . As with the M1 and M2 systems , the agreement between experimental and predicted IFT values was satisfactory at caustic concentrations below 12.5 mM . In Figs. 77 and 78 , the predicted IFT values for the mixture at NaOH concentrations of 12.5 mM and above varied markedly from the experimentally determined tension values . This considerable variance can be traced to imperfect single component parameter estimates as evident from Figs. 39-42 for 0.3125 mM oleic acid reference system . Since the dynamic model did not correlate the experimental data perfectly well at this oleic acid concentration , it follows that an even greater discrepancy would appear in the binary mixture predictions . The agreement between the predicted and experimental IFT values for M4 and M5 mixtures was better than was found for M4 at higher NaOH concentrations .

The multicomponent acid mixture model as outlined in chapter 10 and demonstrated for a binary system in the present chapter , is indeed simplistic in the sense that ideal behaviour is assumed in both the interface and the bulk of both oleic and aqueous phases . Real systems such as crude oils are not ideal solutions and may not respond very well to the model without applying correction factors to account for departure from ideal behaviour . For the binary mixtures of oleic and lauric acids examined in this study , no correction factors whatsoever were employed . The close agreement between the experimental and predicted tension values for all the various mixture compositions in the presence of a wide spectrum of caustic concentrations , lends a considerable credence not only to the proposed multi-component model but the single component dynamic and equilibrium models as well . After all , the mixture model is merely an extension of the

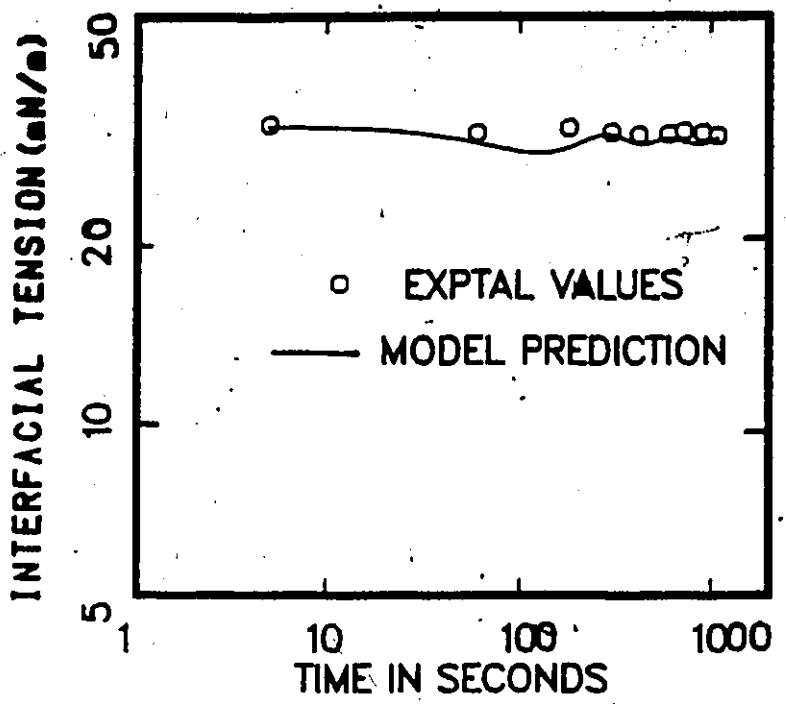

Figure 74 : Exptal Vs Predicted IFT for Mixture M3 in HD Vs 0.25 mM NaOH, Drop No 1

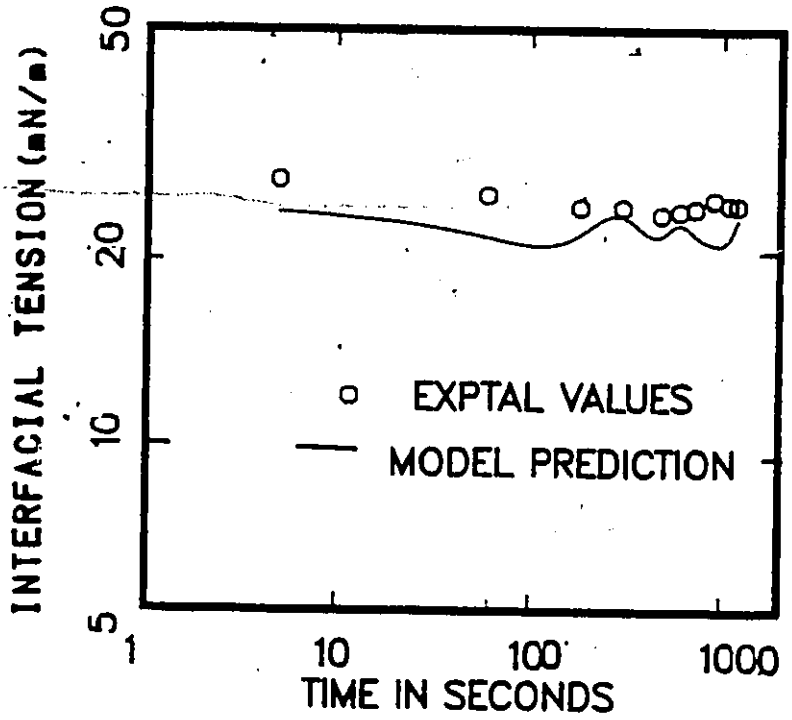

Figure 75 : Exptal Vs Predicted IFT for Mixture M3 in HD Vs 1.25 mM NaOH, Drop No 2

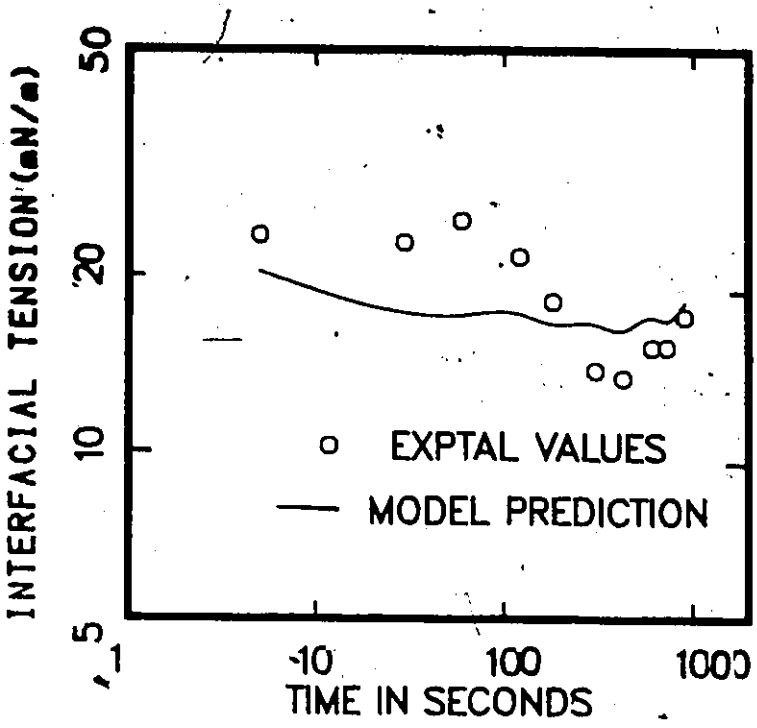

Figure 76 : Exptal Vs Predicted IFT for Mixture M3 in HD Vs 2.50 mM NaOH, Drop No 1

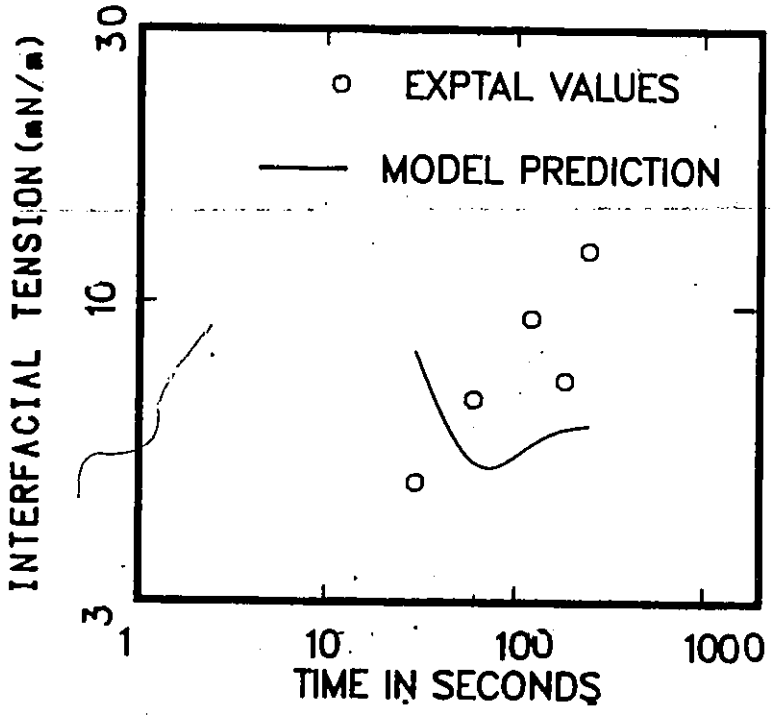

Figure 77 : Exptal Vs Predicted IFT for Mixture M3 in HD Vs 12.50 mM NaOH

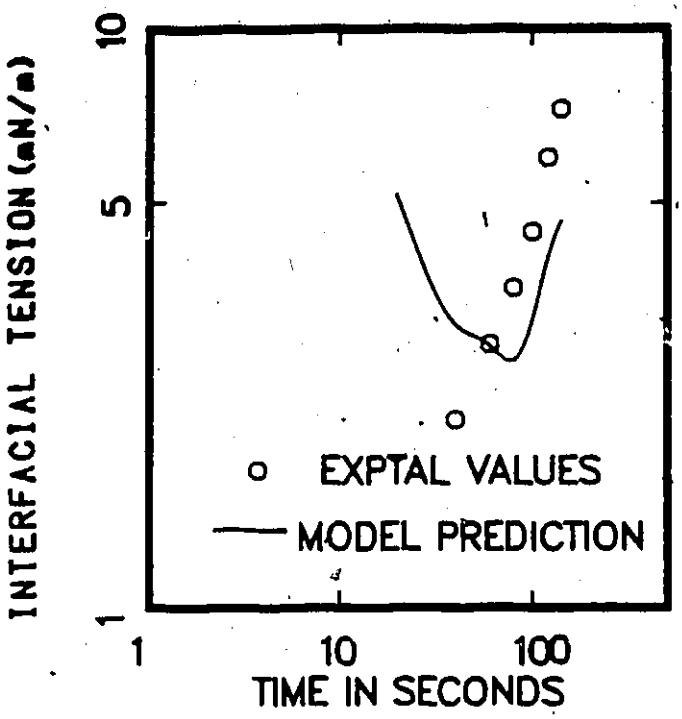

Figure 78 : Exptal Vs Predicted IFT for Mixture M3 in HD Vs 25.00 mM NaOH

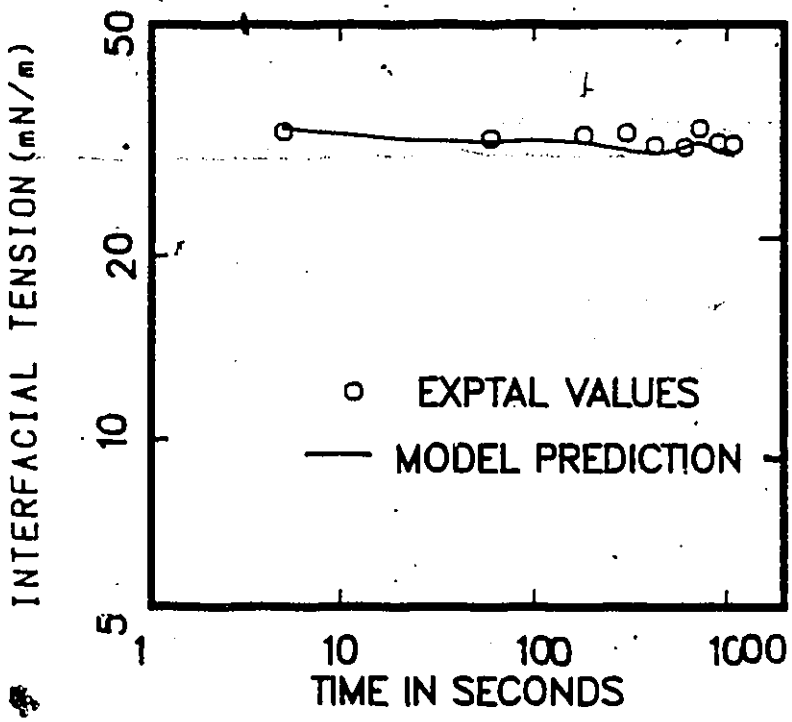

Figure 79 : Exptal Vs Predicted IFT for Mixture M4 in HD Vs 0.25 mM NaOH, Drop No 1

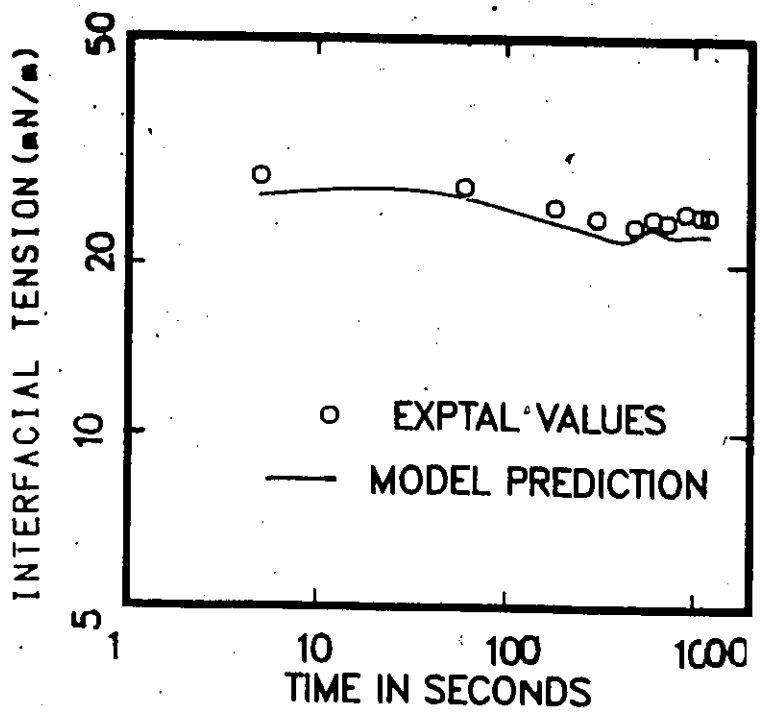

Figure 80 : Exptal Vs Predicted IFT for Mixture M4 in HD Vs 1.25 mM NaOH, Drop No 2

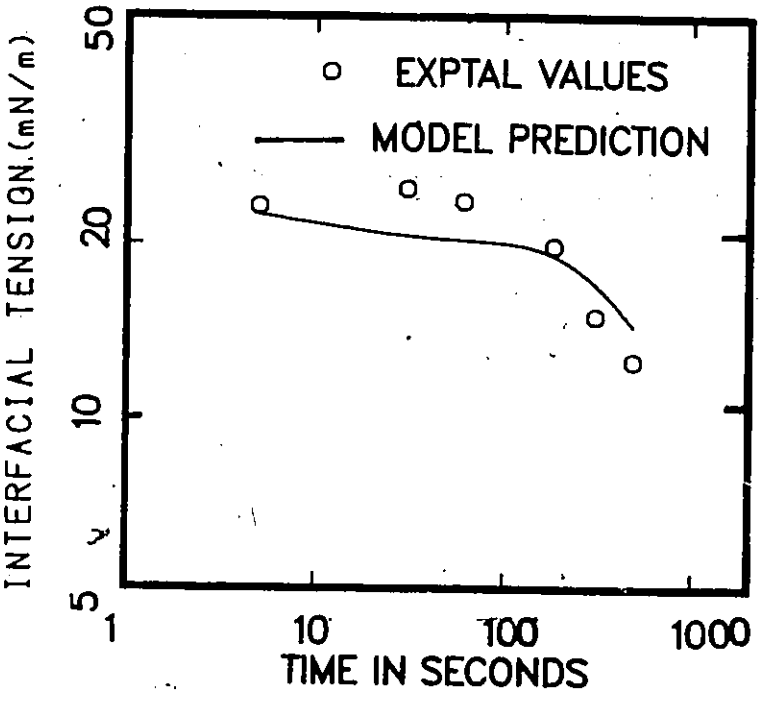

Figure 81 : Exptal Vs Predicted IFT for Mixture M4 in HD Vs 2.50 mM NaOH, Drop No 2

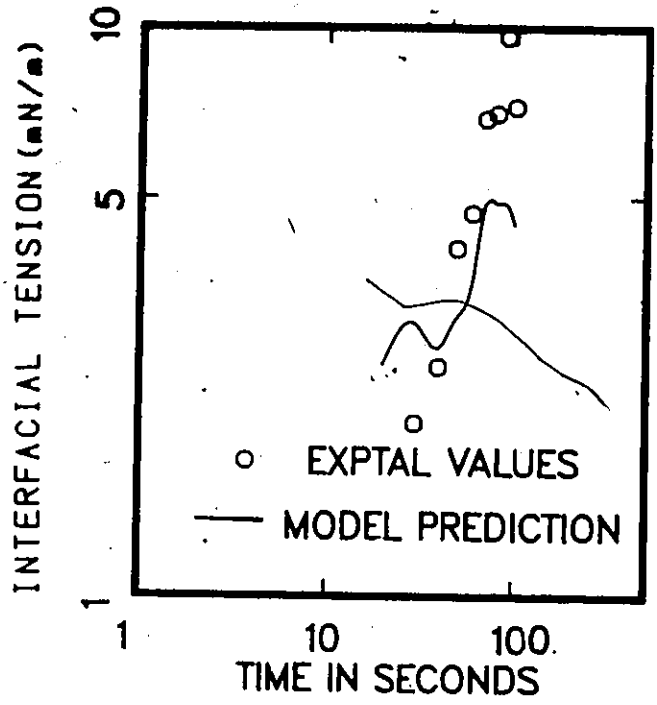

Figure 82 : Exptal Vs Predicted IFT for Mixture M4 in HD Vs 12.50 mM NaOH, Drop No 1

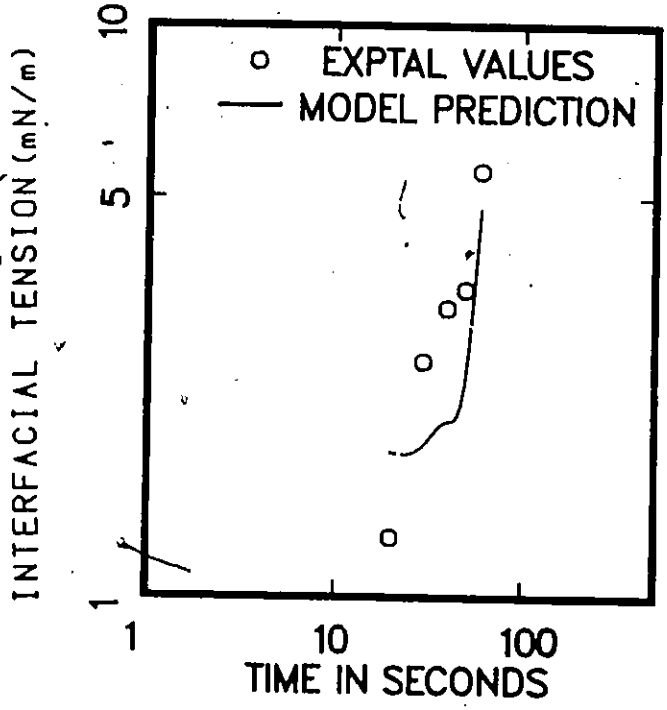

Figure 83 : Exptal Vs Predicted IFT for Mixture M4 in HD Vs 25.00 mM NaOH, Drop No 2

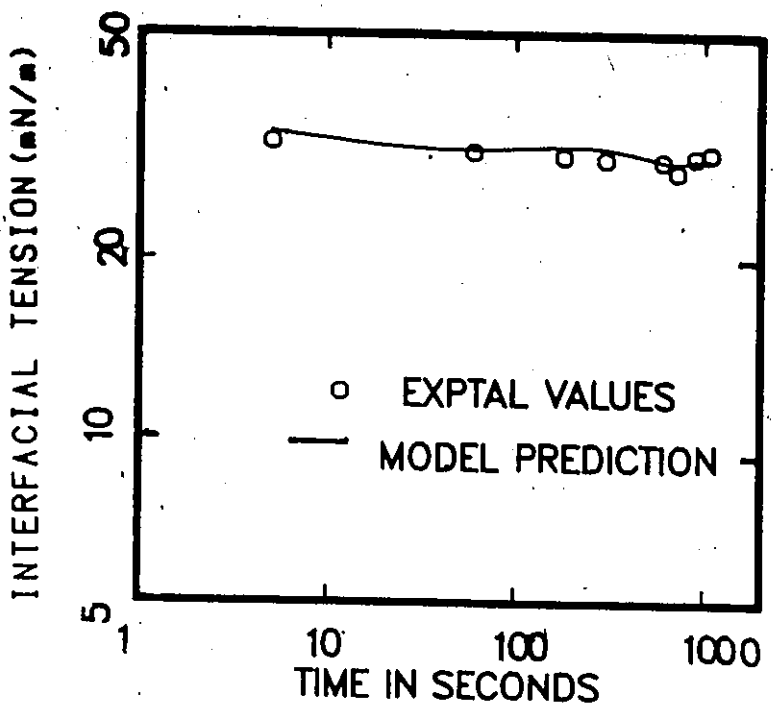

Figure 84 : Exptal Vs Predicted IFT for Mixture M5 in HD Vs 0.25 mM NaOH, Drop No 2

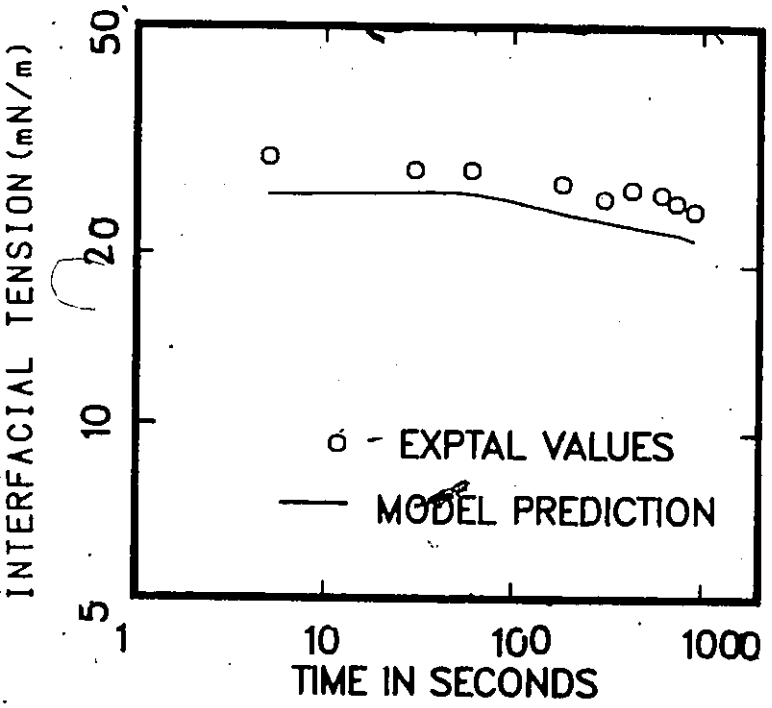

Figure 85 : Exptal Vs Predicted IFT for Mixture M5 in HD Vs 1.25 mM NaOH, Drop No 1

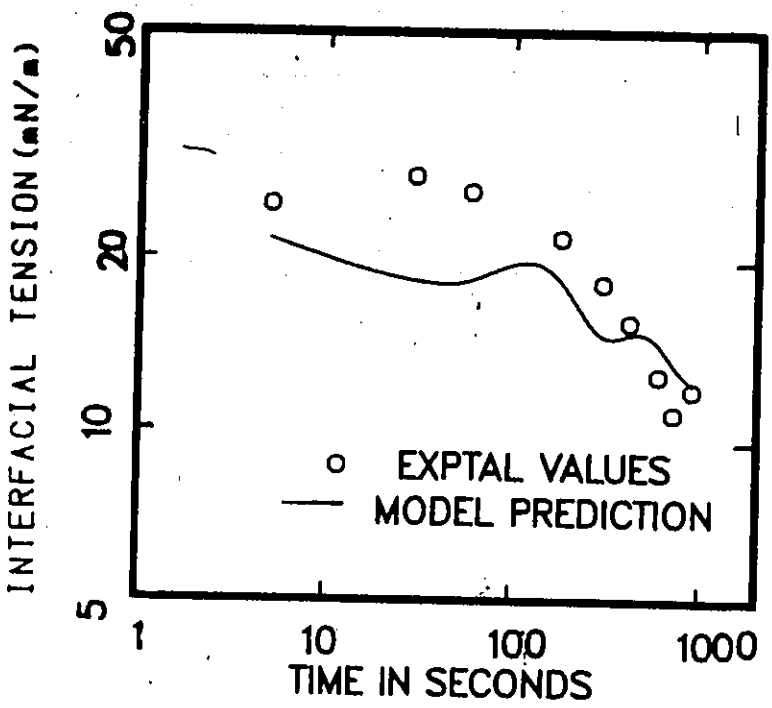

Figure 86 : Exptal Vs Predicted IFT for Mixture M5 in HD Vs 2.50 mM NaOH, Drop No 2

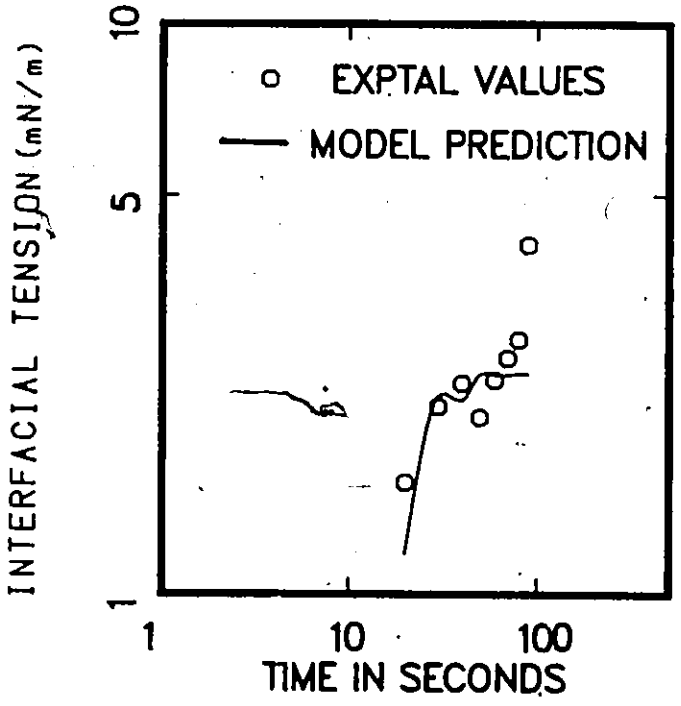

Figure 87 : Exptal Vs Predicted IFT for Mixture M5 in HD Vs 12.50 mM NaOH, Drop No 1

single component dynamic model which in itself leaned heavily on the equilibrium model and the associated theories and mechanisms for the interaction of the fatty acid with different NaOH solutions. Previous models of the dynamic interfacial tension of acidic crudes with caustic solutions had relied on a fictitious representative acid rather than a mixture of acids of different chain lengths and different ionization constants. The unifying approach adopted in this work offers a plausible and novel way of dealing with the complex behaviour of acidic crude/caustic systems. At the same time, currently held theories in classical interfacial phenomena, sorption kinetics and interphase mass transfer have been tested in an attempt to rationalize the mechanisms of dynamic interfacial tensions in reactive systems of special relevance to oil recovery by caustic waterflooding.

Chapter 17

Conclusions and Recommendations

A novel experimental scheme , namely photo-micropendography , has been developed for precise and accurate measurement of dynamic interfacial tensions in reactive systems . Tensions ranging from 1 to 40 mN/m could be accurately measured by this technique for dilute solutions of oleic and lauric acids in hexadecane in contact with a spectrum of NaOH solutions . Phase volume ratios encountered in micropendography were generally in the same range as those obtainable in spinning drop tensiometry (usually 100–1000) . This new experimental scheme affords a more precise and accurate means of monitoring the age of the interface compared to spinning drop tensiometry . In addition , IFT data can be obtained by micropendography at an interfacial age as low as 3 seconds and as high as 30 minutes.

IFT data determined by micropendography were compared with those measured with the ring and spinning drop tensiometers for the same oleic/caustic systems . Reliable measurements could not be easily obtained with the spinning drop tensiometer for tensions above 30 mN/m. Such tensions were readily measured with the ring tensiometer and the agreement between the ring auto-tensiomat's tension data and results obtained by micropendography was satisfactory. On the other hand , when tension values dropped below 20 mN/m , the ring tensiometer gave extremely

low and rather inaccurate results , while the spinning drop tensiometer yielded tension values which were quite close to those measured by micropendography . Hydrodynamic instability associated with small pendant drops severely limits both the range of measurable IFT and the duration over which the dynamic tension behaviour can be accurately followed . When the initial surfactant surface concentration is high , and consequently the IFT is very low , an extremely small pendant drop will be sustained at the tip of the drop forming needle . However , if tensions should drop much further at extended contact times , the drop elongates to the point where it is completely detached. On the other hand , if tensions should increase quickly , then the drop tends to a more spherical and thus unacceptable shape . More work is thus needed to solve this hydrodynamic problem .

An equilibrium model governing the interaction of a single fatty acid dissolved in a known oleic phase and contacted with a spectrum of NaOH aqueous solutions has been proposed . The model specifies the important surface active species which result from the reaction between the acid and the alkali . Also , the effective surface concentration of the active soap anions was determined by Langmuirian sorption kinetics while the FVDH equation of state was used to evaluate the equilibrium surface pressure . The key parameters of the equilibrium model were the acid dissociation constant and the equilibrium constant associated with the formation of the undissociated soap complex. These parameters were precisely estimated by non-linear regression analysis . The calculated ionization constant for oleic acid in the concentration range of 0.10 to 1.00 mM varied from 7.7×10^{-7} at the lower concentration range to 1.2×10^{-7} at higher acid concentrations . For 0.02 M lauric acid , the pK_a value determined from the model at caustic concentrations below 12.5 mM was 9 , and it increased to 10 for higher NaOH levels up to 250 mM .

A dynamic model for single acids in the oleic phase contacting various caustic concentrations in

the aqueous phase was also proposed . This was a diffusive-kinetic treatment in which convective diffusion was modelled by the use of Nernst's theory , while sorption kinetics was treated by the Langmuirian approach . Interfacial potentials associated with the adsorbed soap anions were calculated by the use of the Gouy-Chapman model . The equations that comprised the proposed dynamic model were a set of first order , non-linear ordinary differential equations combined with another set of algebraic relationships . The former accounted for the variation in the concentration of the interfacial species with time , while the latter related the instantaneous surfactant surface concentration to surface pressure via the FVDH equation of state . Sensitivity analysis was used to facilitate the solution of the model equations and at the same time obtain good estimates of the model parameters . The parameters of particular significance in the dynamic model were the adsorption rate constants for the various surface active species . The final parameter estimates correlated the experimental data reasonably well .

In extending the proposed dynamic model to the case of mixtures of several acids in the oleic phase , it was assumed that ideal behaviour prevailed both in the interface and in the main bulk of the phases in contact . Furthermore , we assumed that all relevant interfacial parameters of all constituent acids of the mixture determined from separate single component analysis, would be valid in the mixture . In other words , the dynamic IFT exhibited by the mixture at any given caustic concentration would simply be a summation of the contributions from the constituent acids and their associated interfacial species . This broad hypothesis was then put to test by solving the multi-component model equations for the special case of binary mixtures of oleic and lauric acids contacting a spectrum of caustic solutions . The agreement between predicted and experimental IFT values was surprisingly very close though not perfect. Because such a close agreement was obtained over a wide range of mixture compositions and different caustic concentrations, the proposed multi-

component model as well as the single component equilibrium and dynamic models have been validated. The success of the entire modelling effort is of particular significance in enhanced oil recovery by caustic waterflooding . The extension of the analyses carried out in this study to the crude oil system can be readily effected once the key surface active acids present in a given crude are quantitatively identified. Since a wide range of probable caustic concentrations of the flood water have been taken into account in our treatment, it is thus possible to predict realistic oil-water interfacial tensions that will apply throughout the life of a projected alkaline flood .

Bibliography

[1] Chiwetelu , C.I. : *Development and Evaluation of Lignosulfonate-based Surfactant Systems for EOR Operatons* , MASc Thesis , University of Ottawa , 1979.

[2] Gogarty , W.B.: *Status of Surfactant or Micellar Methods* , J. Pet. Tech. , (Jan 1976), pp 93–102 .

[3] Campbell , T.C.: *The Role of Alkaline Chemicals in Oil Displacement Mechanisms* in *Surface Phenomena in Enhanced Oil Recovery* , Shah D.O.(Editor) , Plenum Press , N.Y., 1981 , pp 293–306.

[4] Campbell ,T.C.: *The Role of Alkaline Chemicals in the Recovery of Low-Gravity Crude Oils* , J. Pet. Tech. , (Nov 1982) , pp 2510–2516.

[5] Mayer , E.H., Berg , R.L., Carmichael , J.D. and Weinbrandt , R.M. : *Alkaline Injection for Enhanced Oil Recovery-A Status Report* , J. Pet. Tech. , (Jan 1983) , pp 209–221 .

[6] Reisberg , J. and Doscher , T.M.: *Interfacial Phenomena in Crude Oil-Water Systems*, Producers' Monthly , (Nov 1956) , pp 45–50.

[7] Jennings , H.Y.Jr.: *A Study of Caustic Solution -Crude Oil Interfacial Tensions* , Soc. Pet. Eng. J., (June 1975), pp 197–202 .

[8] Jennings , H.Y., Johnson ,C.E.Jr. and McAuliffe ,C.D.: *A Caustic Waterflooding Process for Heavy Oils* , J. Pet. Tech. , (Dec 1974) , pp 1365-1374.

[9] Melrose , J.C., and Brandner , C.F.: *Role of Capillary Forces in Determining Microscopic Displacement Efficiency for Oil Recovery by Waterflooding* , J. Can. Pet. Tech., (Oct-Dec 1974) , pp 54-62 .

[10] Cooke , C.E.Jr., Williams , R.E. and Kolodzie , P.A.: *Oil Recovery by Alkaline Waterflooding* , J. Pet. Tech. , (Dec 1974) , pp 1365-1374 .

[11] Castor , T.P., Somerton , W.H. and Kelly , J.F.: *Recovery Mechanisms of Alkaline Flooding* , in *Surface Phenomena in Enhanced Oil Recovery* , Shah , D.O. (Editor) , Plenum Press , N.Y., 1981 , pp 249-291.

[12] McCaffery , F.G.: *Interfacial Tensions and Aging Behaviour of some Crude Oils against Caustic Solutions* , J. Can. Pet. Tech. , (Jul-Sep 1976) , pp 71-74.

[13] Trujillo , E.M.: *The Static and Dynamic Interfacial Tensions between Crude Oils and Caustic Solutions* , Soc. Pet. Eng. J., (Aug 1983) , pp 645-656.

[14] Babu , D.R. , Hornof , V. and Neale , G.H.: *Evaluation of Aqueous Chemical Systems for Heavy Oil Recovery Processes* , Fuel , Vol. 65 , (Jan 1986), pp 4-7.

[15] Khulbe , K.C., Hornof , V. and Neale , G.: *Interfacial Activity of Heavy Oil and Its Maltene Constituents against Caustic Solutions* , AOSTRA J. Research , Vol. 2 , No. 2 , 1985 , pp 95-101 .

[16] Babu , D.R., Hornof ,V. and Neale , G.: *Effects of Temperature and Time on Interfacial Tension Behaviour between Heavy Oils and Alkaline Solutions* , Can. J. Chem.

Eng. , Vol. 62 , (Feb 1984) , pp 156–159 .

[17] Pasquarelli , C.H. and Wasan , D.T. : *The Effect of Film-forming Materials on the Dynamic Interfacial Properties in Crude Oil-Aqueous Systems* , in *Surface Phenomena in Enhanced Oil Recovery* , Shah ,D.O. (Editor) , Plenum Press , N.Y., 1981 , pp 237–238.

[18] deZabala , E.F.: *Tertiary Recovery of Acidic Crudes from Oilsands. Mechanisms and Modelling* , PhD Thesis, University of California , Berkeley , 1984.

[19] deZabala , E.F., and Radke , C.J.: *The Role of Interfacial Resistances in Alkaline Waterflooding of Acid Oils* , SPE paper No. 11213 , presented at the 57th Annual Fall Technical Conference of SPE of AIME , New Orleans , LA , Sept 26–29 , 1982.

[20] Johnson , C.E. Jr.: *Status of Caustic and Emulsion Methods* , J. Pet. Tech. , (Jan 1976) , pp 85–92.

[21] Subkow , P.: *Process for the Removal of Bitumen from Bituminous Deposits* , U.S.Patent No. 2,288,857 , (Jul 7,1942).

[22] Wagner , O.R. and Leach , R.O.: *Improving Oil Displacement Efficiency by Wettability Adjustment* , AIME Pet. Trans. , Vol. 216 , (1959) , pp 63–72.

[23] Mungan , N.: *Certain Wettability Effects in Laboratory Waterfloods* , J. Pet. Tech. , (Feb 1966) , pp 247–252.

[24] Michaels , A.S. and Timmins , R.S.: *Chromatographic Transport of Reverse-Wetting Agents and its Effects on Oil Displacement in Porous Media* , AIME Pet. Trans. , Vol. 219 , (1960) , pp 150–157 .

[25] Dodd , C.G. , Moore , J.W. and Denekas , M.O.: *Metalliferous Substances Adsorbed at Crude Petroleum-Water Interfaces* , Ind. Eng. Chem. , Vol. 44 , No. 11 , (Nov 1952) , pp 2585–2590.

[26] Bunge , A.L. and Radke , C.J.: *Divalent Ion Exchange with Alkali* , Soc. Pet. Eng. J., (Aug 1983) , pp 657–668 .

[27] Dormani , N.A.: *Effect of Divalent Ions in Enhanced Oil Recovery* , MASc Thesis , University of Ottawa , 1986.

[28] Sharma , M.M. and Yen , T.F.: *A Thermodynamic Model for Low Interfacial Tensions in Alkaline Flooding* , Soc. Pet. Eng. J., (Feb 1983) , pp 125–134.

[29] Chan , M. and Yen , T.F.: *A Chemical Equilibrium Model for Interfacial Activity of Crude Oil in Aqueous Alkaline Solution : The Effects of pH , Alkali and Salt* , Can. J. Chem. Eng. , Vol. 60 , (April 1982) , pp 305–308.

[30] Bansal , V.K., Chan , K.S., McCallough , R. and Shah , D.O. : *The Effect of Caustic Concentration on Interfacial Charge,Interfacial Tension and Droplet Size;a Simple Test for Optimum Caustic Concentration for Crude Oils* , J. Can. Pet Tech. , (Jan-Mar 1978) , pp 69–72.

[31] Chan , M. and Yen ,T.F.: *Role of Sodium Chloride in the Lowering of Interfacial Tension between Crude Oil and Alkaline Aqueous Solution* , Fuel , Vol. 60 , (Jun 1981) , pp 552–553.

[32] Lochte , H.L.: *Petroleum Acids and Bases* , Ind. Eng. Chem. , Vol. 44 , No. 11 , (Nov 1952) , pp 2597–2601.

[33] Seifert , W.K. and Teeter , R.M.: *Preparative Thin Layer Chromatography and High Resolution Mass Spectrometry of Crude Oil Carboxylic Acids* , Anal. Chem. , Vol. 41, No. 6 , (May 1969), pp 786–795 .

[34] Seifert , W.K. ,Teeter , R.M. , Howells , W.G. and Cantow , M.J.R.: *Analysis of Crude Oil Carboxylic Acids after Conversion to their Corresponding Hydrocarbons* , Anal. Chem. , Vol. 41 , No. 12 , (Oct. 1969) , pp 1638–1647.

[35] Seifert , W.K. and Teeter , R.M.: *Identification of Polycyclic Naphthenic , Mono- and Di-Aromatic Crude Oil Carboxylic Acids* , Anal. Chem. , Vol. 42 , No. 2 , (Feb 1970), pp 180–189 .

[36] Seifert , W.K. and Teeter , R.M.: *Identification of Polycyclic Aromatic and Heterocyclic Crude Oil Carboxylic Acids* , Anal. Chem. , Vol. 42 , No. 7 , (Jun 1970) , pp 750–758.

[37] Seifert, W.K., Gallegos , E.J. and Teeter , R.M.: *Proof of Structure of Steroid Carboxylic Acids in a California Petroleum by Deuterium Labelling , Synthesis and Mass Spectrometry* , J. Am. Chem. Soc. , Vol. 94 , No. 16 , (Aug 1972) , pp 5880–5887.

[38] Jang , L.K., Chang , Y.I., Chan , M. and Yen , T.F.: *Correlation of Petroleum Component Properties for Caustic Flooding* , AIChE Symposium Series , Vol. 78 , No. 212 , 1982 , pp 97–104.

[39] Dunning , H.N., Moore , J.W. and Denekas , M.O.: *Interfacial Activities and Porphyrin Contents of Petroleum Extracts* , Ind. Eng. Chem. , Vol. 45 , No. 8 , (Aug. 1953) , pp 1759–1765.

[40] Markley , K.S., (Editor) , *Fatty Acids-Their Chemistry , Properties , Production and Uses* , Parts 1–5 , 2nd Edition , Interscience Publishers , N.Y., 1968.

[41] Tanford , C.: *The Hydrophobic Effect: Formation of Micelles and Biological Membranes*, John Wiley and Sons , N.Y., 1980.

[42] Adamson , A. W.: *Physical Chemistry of Surfaces* , 3rd Edition, John Wiley and Sons, N.Y., 1976.

[43] Davies , J.T. and Rideal , E.K.: *Interfacial Phenomena* , 2nd Edition , Academic Press , N.Y., 1963.

[44] Goddard , E.D., (Editor), *Monolayers- Advances in Chemistry Series 144* , ACS , Washington DC , 1975.

[45] Welles , H.L., Zografi , G., Scrimgeour , G.M. and Gunstone , F.D.: *The Effect of Ethylenic and Acetylenic Groups on the Properties of Fatty Acid Monolayers* , Chapter 10 of Ref. [44], pp 135–151 .

[46] Patil , G.S., Mathews , R.H and Cornwall , D.G.: *Estimation of Ionization in Unstable Fatty Acid Monolayers from Desorption Kinetics* , Chapter 5 of Ref. [44] , pp 44–66 .

[47] Spink , J.A.: *Ionization of Monolayers of Fatty Acids from C14 to C18* , J. Colloid Science, Vol. 18 , 1963 , pp 512–525.

[48] Pagano , R.E. and Gershfeld , N.L.: *Physical Chemistry of Lipid Films at the Air-Water Interface. II Binary Lipid- The Principle governing Miscibility of Lipids in Surfaces* , J. Phys. Chem. , Vol. 76 , No. 9 , 1972 , pp 1238–1249.

[49] Kortum , G., Vogel, W. and Andrussow , K.: *Dissociation Constants of Organic Acids in Aqueous Solutions* , Butterworths , London , 1961.

[50] Albert , A. and Serjeant , E.P.:*The Determination of Ionization Constants; A Laboratory Manual* , 3rd Edition , Chapman and Hall , N.Y., 1984.

[51] Ramakrishnan , T.S. and Wasan , D.T.: *A Model for Interfacial Activity of Acidic Crude Oil/Caustic Systems for Alkaline Flooding* , Soc. Pet. Eng. J., (Aug 1983) , pp 602–612.

[52] Cratin , P.D.: *A Quantitative Characterization of pH-Dependent Systems* , Ind. Eng. Chem. , Vol. 61 , No. 2 , (Feb 1969) , pp 35–45 .

[53] Hejl , V. and Levorova , V.: *Stanovcni disociační konstanty kyseliny olejove pro flotační účely* , Rudy , Vol. 24 , No. 1 , 1976 , pp 13–16 .

[54] England , D.C. and Berg , J.C.: *Transfer of Surface-Active Agents across a Liquid-Liquid Interface* , AIChE J., Vol. 17 , No. 2 , (Mar 1971) , pp 313–322.

[55] Sherwood , T.K. and Wei , J.C.: *Interfacial Phenomena in Liquid-Liquid Extraction*, Ind. Eng. Chem. , Vol. 49 , No. 6 ,(June 1957) , pp 1030–1031. .

[56] Clift , R. and Weber , M.E.: *Bubbles , Drops , and Particles* , Academic Press , N.Y., 1978.

[57] Hansen , C., (Editor), *Recent Advances in Liquid-Liquid Extraction* , Pergamon Press, Oxford , 1971.

[58] Sawistowiski , H.: *Interfacial Phenomena* Chapter 9 of Ref[57].

[59] Sternling , C.V. and Scriven , L.E.: *Interfacial Turbulence: Hydrodynamic Instability and the Marangoni Effect* , AIChE J. , Vol. 5 , No. 4 , (Dec 1959) , pp 514–523.

[60] Rubin , E. and Radke , C.J.: *Dynamic Interfacial Tension Minima in Finite Systems*, Chem. Eng. Sci. , Vol. 35 , 1980 , pp 1129–1138.

[61] Brown , J.B. and Radke , C.J.: *Area Effects in Spinning Drop Dynamic Interfacial Tensions* , Chem. Eng. Sci. , Vol. 35 , 1980 , pp 1458–1460.

[62] Princen , H.M., Zia , I.Y.Z., and Mason , S.G.: *Measurement of Interfacial Tension from the Shape of a Rotating Drop* , J. Colloid Interface Sci. , Vol. 23 , 1967 , pp 99–107.

[63] Cayias , J.L., Schechter , R.S. and Wade , W.H.: *The Measurement of Low Interfacial Tension via the Spinning Drop Technique*, in *Adsorption at Interfaces* , ACS Symposium Series , No. 8 , (Mittal, K.L., Editor), Washington DC , 1975 , pp 234–247.

[64] Slattery , J.C. and Chen , J.D.: *Alternative Solution for Spinning Drop Interfacial Tensiometer* , J. Colloid Interface Sci. , Vol. 64 , No. 2 , (Apr 1978) , pp 371–373.

[65] Levich , V.G.: *Physico-chemical Hydrodynamics*, Prentice-Hall , N.J., 1962.

[66] Borwankar , R.P.: *Surfactant Adsorption at Fluid-Fluid Interfaces with Application to Alkaline Flooding* , PhD Thesis , Illinois Institute of Technology , Chicago , Illinois, Aug 1984.

[67] Sharma , M.M., Jang , L.K. and Yen , T.F.: *Transient Interfacial Tension Behaviour of Crude Oil-Caustic Interfaces* , paper No. 12669 , presented at the SPE/DOE 4th Symposium on Enhanced Oil Recovery , Tulsa , Oklahoma , (Apr 15–18, 1984).

[68] Lucassen , J.: *Hydrolysis and Precipitates in Carboxylate Soap Solutions* , J. Phys. Chem. , Vol. 70 , No. 6 , (Jun. 1966) , pp 1824-1830.

[69] Gardner , J.E. and Hayes , M.E.: *Instruction Manual* of the University of Texas Spinning Drop Tensiometer , Model 500.

[70] Hammett , L.P.: *Physical Organic Chemistry* , 2nd Edition , McGraw-Hill Book Co., N.Y., 1970.

[71] Gostisa , M.B. and Vielstich , W.: *Determination of Rate Constants of Weak Acids by Rotating Electrodes: Influence of the Electric Field in the Double Layer* , Ber. Bunsenges. Phys. Chem., Vol. 77 , No. 7 , 1973 , pp 476–483.

[72] Nuernberg , H.W. and Duerbeck , H.W.: *Relations between Structure of Carboxylic Acids and the Kinetics of their Dissociation and Recombination* , Z. Anal. Chem. , Vol. 205 , No. 1 , 1964 , pp 217–237.

[73] Laidler , K.J.: *Personal Communications* , University of Ottawa , 1985.

[74] Smith , J.M.: *Chemical Engineering Kinetics* , 3rd Edition , McGraw-Hill Book Co., N.Y. 1981.

[75] Perry , R.H., Green , D.W. and Maloney , J.O.: *Chemical Engineers' Handbook* , 6th Edition , McGraw-Hill Book Co. , N.Y., 1984.

[76] Smith , J.M. and Van Ness , H.C.:*Introduction to Chemical Engineering Thermodynamics* , 3rd Edition , McGraw-Hill Book Co. , N.Y., 1975.

[77] Denbigh , K.: *The Principles of Chemical Equilibrium with Application in Chemistry and Chemical Engineering* , 4th Edition , Cambridge University Press , 1981.

[78] Borwankar , R.P. and Wasan , D.T.: *Dynamic Interfacial Tensions in Acidic Crude/Caustic Systems Part I: A Chemical Diffusion-Kinetic Model* , AIChE J., Vol. 32 , No. 3 , (Mar 1986) , pp 455–466.

[79] Borwankar , R.P. and Wasan , D.T.: *Dynamic Interfacial Tensions in Acidic Crude Oils/Caustic Systems PartII: Role of Dynamic Effects in Alkaline Flooding for Enhanced Oil Recovery* , AIChE J., Vol. 32 , No. 3 , (Mar 1986) , pp 467–476.

[80] Bird , R.B., Stewart , W.E. and Lightfoot , E.N.: *Transport Phenomena* , John Wiley, N.Y., 1960.

[81] Reid , R.C., Prausnitz , J.M. and Sherwood , T.K.: *The Properties of Gases and Liquids* , 3rd Edition , McGraw-Hill Book Coy. , N.Y., 1977.

[82] Hayduk , W. : *Personal Communications*, University of Ottawa , 1985.

[83] Rotenberg , Y., Boruvka , L. and Neumann , A.W.: *Determination of Surface Tension and Contact Angle from the Shapes of Axisymmetric Fluid Interfaces* , J. Colloid Interface Sci. , Vol. 93 , No. 1 , (May 1983) , pp 169–183.

[84] IMSL Corporation , *The IMSL Libraries: Problem-Solving Software Systems for Numerical Fortran Programming* , IMSL , Houston , Texas , (Nov 1984) , Vols. 1–4.

[85] SAS Institute , *SAS Users' Guide: Statistics* , SAS Institute , Cary , North Carolina, 1982 Edition.

[86] Andreas , J.M., Hauser , E.A. and Tucker, W.B.: *Boundary Tensions by Pendant Drops* , J. Phys. Chem. , Vol. 42 , 1938 , pp 1001–1017.

[87] Stauffer , C.E.: *The Measurement of Surface Tension by the Pendant Drop Technique*, J. Phys. Chem. , Vol. 69 , No. 6 , (Jun 1965) , pp 1933–1938.

[88] Bashforth , F. and Adams , J.C.: *An Attempt to Test the Theories of Capillary Action*, Cambridge University Press , Cambridge , England , 1883.

[89] Ambwani , D.S.and Tomlinson , F.: *Pendant Drop Technique for Measuring Liquid Boundary Tensions* , in *Surface and Colloid Science* , Good , R.J. and Stromberg, R.R., (Editors) , Plenum Press , N.Y., 1979 , Vol. 11 , pp 93–119.

[90] Vos , H. and Los , J.M.: *Interfacial Tensions from Sessile-Drop Profiles. The Interface Hg/0.116 KCl at 25 ° C* , J. Colloid Interface Sci. , Vol. 74 , 1980 , pp 360–369.

[91] Girault , H.H., Schriffrin , D.J. and Smith , B.D.V.: *Drop Image Processing for Surface and Interfacial Tension Measurements*, J. Electroanal. Chem. , Vol. 137 , 1982 , pp 207–217.

[92] Girault , H.H., Schriffrin , D.J. and Smith , B.D.V.: *The Measurement of Interfacial Tension of Pendant Drops Using Video Image Profile Digitizer* , J. Colloid Interface Sci. , Vol. 101 , No. 1 , (Sept. 1984) , pp 257–266.

[93] Haydon , D.A., and Taylor , F.H.:*On Adsorption at the Oil-Water Interface and the Calculation of Electrical Potentials in the Aqueous Surface Phase I: Neutral Molecules and a Simplified Treatment for Ions* , Philosophical Trans. , Vol. 252 , (Feb. 18 , 1960), pp 225–248.

[94] Davies , J.T.: *The Distribution of Ions Under a Charged Monolayer , and a Surface Equation of State for Charged Films*, Proc. Royal Soc. , Series A , Vol. 208 , 1951 , pp 224–247.

[95] Hachisu , S.: *Equation of State of Ionized Monolayers* , J. Colloid Interface Sci. , Vol. 33 , No. 3 , (Jul 1970) , pp 445–454.

[96] Bacon , D.W.: *Collection and Interpretation of Industrial Data* , Dept. of Chemical Eng. , Queen's University , Kingston , Ontario.

[97] Draper , N.R. and Smith , H.: *Applied Regression Analysis* , John Wiley , N.Y., 1966.

[98] Bard , Y.: *NonLinear Parameter Estimation* , Academic Press , N.Y., 1974 .

[99] McLean , D.D.: *Personal Communications* , University of Ottawa , 1985 .

[100] van Voorst Vader , F.: *Adsorption of Detergents at the Liquid-Liquid Interface Part 1.* , Trans. Faraday Soc. , Vol. 56 , 1960 , pp 1067–1079 .

[101] Marquardt , D.W.: *Solution of Nonlinear Chemical Engineering Models* , Chem. Eng. Progress , Vol. 55 , No. 6 , (Jun 1959) , pp 65–70 .

[102] Marquardt , D.W.: *An Algorithm for Least Squares Estimation of Nonlinear Parameters* , J. Soc. Indust. Appl. Math. , Vol. 11 , No. 2 , (Jun 1963) , pp 431–441.

[103] Kittrell , J.R., Mezaki , R.and Watson , C.C.: *Estimation of Parameters for Nonlinear Least Squares Analysis* , Ind. Eng. Chem. , Vol. 57 , No. 12 , (Dec 1965) , pp 19–27 .

[104] Wilke , C.R. and Chang , P.: *Correlation of Diffusion Coefficients in Dilute Solutions*, AIChE J. , Vol. 1 , No. 2 , (Jun 1955) , pp 264–270 .

[105] Hayduk , W. and Minhas , B.S.: *Correlations for the Prediction of Molecular Diffusivities in Liquids* , Can. J. Chem. Eng. , Vol. 60 , No. 2 , 1982 , pp 295–299 .

[106] Tyn , M.T. and Calus , W.F.: *Diffusion Coefficients in Dilute Binary Mixtures* , J. Chem. Eng. Data , Vol. 20 , No. 1 , (Jan 1975), pp 106–109 .

[107] Cheremisinoff , N.P. (Editor) , : *Encyclopedia of Fluid Mechanics* , Vol. 1 , Gulf Publishing , Houston , Texas , 1986 .

[108] Sohn , H.Y. and Wadsworth , M.C., (Editors), *Rate Processes of Extractive Metallurgy*, Plenum Press , N.Y. , 1979 .

[109] Hildebrand , J.H. and Scott , R.L. : *The Solubility of Nonelectrolytes*, Dover Publications Inc. , N.Y., 1964.

[110] Neumann , A.W. : *Personal Communications*, 1988.

[111] Reive , D. M. : *Interfacial Behaviour of a Canadian Heavy Oil against Caustic Solutions* , MASc. Thesis , University of Ottawa , 1985 .

[112] Amourdam , M.J. and Laddha , G.S. : *Diffusivities of Some Binary Liquid Systems using a Diaphragm Cell* , J. Chem. Eng. Data , Vol. 12 , No. 3 , (Jul 1967) , pp 389–391 .

[113] Weinheimer , R.M., Evans , D.F. and Cussler , E.L.: *Diffusion in Surfactant Solutions*, J. Colloid Interface Science , Vol. 80 , No. 2 , (Apr 1981) , pp 357–368 .

[114] Neale , G.H., Khulbe , K.C. and Hornof , V. : *Effects of Oil Phase Viscosity on Interfacial Tension Behaviour of Oil/ Alkaline Systems as Measured by the Spinning Drop Tensiometer* , Can. J. Chem. Eng. , Vol. 65 , August 1987 , pp 700–703 .

[115] Hornbeck , R. W. : *Numerical Methods* , Prentice-Hall , N.Y., 1975 .

Part VI

Appendices

Appendix A

Physical Properties of Solutions

Table A1: Physical Properties of Aqueous Solutions at 25° C

Identification	pH	Density (kg/m^3)	Viscosity (mPa. s)
Double distilled Water	7.06	997.0292	0.8904
0.25 mM NaOH	10.34	997.0627	0.8905
1.25 mM NaOH	11.10	997.1002	0.8905
2.50 mM NaOH	11.40	997.1590	0.8919
12.50 mM NaOH	12.06	997.5988	0.8948
25.0 mM NaOH	12.33	998.1345	0.8961
50.0 mM NaOH	12.64	999.2361	0.9006
100.0 mM NaOH	12.95	1001.4251	0.9119
125.0 mM NaOH	12.98	1002.5016	0.9142
150.0 mM NaOH	13.09	1003.5625	0.9269
200.0 mM NaOH	13.14	1005.6123	0.9513
250.0 mM NaOH	13.17	1007.6435	0.9859

Table A2: Physical Properties of Oleic Solutions at 25° C

Identification	Density (kg/m^3)	Viscosity (mPa. s)
Vacuum redistilled Hexadecane	770.1094	3.0206
0.10 mM Oleic Acid in Hexadecane	770.1109	3.0206
0.20 mM Oleic Acid in Hexadecane	770.1124	3.0237
0.3125 mM Oleic Acid in Hexadecane	770.1253	3.0256
0.6125 mM Oleic Acid in Hexadecane	770.1348	3.0282
1.00 mM Oleic Acid in Hexadecane	770.1715	3.0300
10.00 mM Oleic Acid in Hexadecane	770.3041	3.0434
10.00 mM Lauric Acid in Hexadecane	770.3487	3.0213
20.00 mM Lauric Acid in Hexadecane	770.6251	3.0370
Mixture M1(0.10 mM Oleic + 0.02 M Lauric in Hexadecane)	770.6250	3.0293
Mixture M2(0.20 mM Oleic + 0.02 M Lauric in Hexadecane)	770.6262	3.0306
Mixture M3(0.3125 mM Oleic + 0.02 M Lauric in Hexadecane)	770.6308	3.0430
Mixture M4(0.6125 mM Oleic + 0.02 M Lauric in Hexadecane)	770.6323	3.0443
Mixture M5(1.00 mM Oleic + 0.02 M Lauric in Hexadecane)	770.6733	3.0472

Appendix B

Dynamic Interfacial Data

B.1 Interfacial Data for 0.3125 mM Oleic in Hexadecane/Caustic Solutions

Table B1.1: Interfacial Data for the System: 0.3125 mM Oleic in HD /Distil Water

Time in (Secs)	DROP NO 1			DROP NO 2		
	IFT (mN/m)	Surf Area ($m^2 \times 10^4$)	Drop Vol ($m^3 \times 10^7$)	IFT (mN/m)	Surf Area ($m^2 \times 10^4$)	Drop Vol ($m^3 \times 10^7$)
5.0	44.46	0.321	0.230	41.80	0.334	0.242
5.0	42.17	0.321	0.230	39.30	0.328	0.234
60.0	40.00	0.316	0.223	41.30	0.336	0.244
60.0	39.18	0.318	0.226	-	-	-
180.0	39.15	0.317	0.224	-	-	-
300.0	37.67	0.319	0.224	37.11	0.329	0.235
300.0	35.46	0.318	0.222	35.35	0.326	0.231
480.0	-	-	-	38.75	0.331	0.238
480.0	-	-	-	36.33	0.327	0.232
600.0	37.45	0.312	0.226	-	-	-
600.0	36.03	0.321	0.226	-	-	-
720.0	-	-	-	37.21	0.329	0.234
720.0	-	-	-	36.33	0.327	0.232
900.0	37.07	0.320	0.226	36.65	0.330	0.235
900.0	36.07	0.320	0.225	28.88	0.322	0.224
1200.0	36.46	0.323	0.228	36.89	0.330	0.235
1200.0	33.80	0.318	0.222	30.25	0.325	0.226
EQUBR	36.52	-	-	36.60	-	-

Table B1.2: Interfacial Data for the System:0.3125 mM Oleic in HD / 0.25 mM NaOH

Time in (Secs)	DROP NO 1			DROP NO 2		
	IFT (mN/m)	Surf Area ($m^2 \times 10^4$)	Drop Vol ($m^3 \times 10^7$)	IFT (mN/m)	Surf Area ($m^2 \times 10^4$)	Drop Vol ($m^3 \times 10^7$)
5.0	37.14	0.227	0.139	36.82	0.242	0.153
60.0	34.50	0.227	0.139	35.36	0.245	0.154
300.0	31.78	0.229	0.140	31.86	0.246	0.154
600.0	28.42	0.233	0.142	27.58	0.245	0.152
900.0	26.81	0.235	0.143	25.85	0.248	0.153
1200.0	24.33	0.235	0.141	25.03	0.249	0.154
EQUBR	25.57	-	-	25.44	-	-

Table B1.3: Interfacial Data for the System: 0.3125 mM Oleic in HD / 1.25 mM NaOH

Time in (Secs)	DROP NO 1			DROP NO 2		
	IFT (mN/m)	Surf Area ($m^2 \times 10^4$)	Drop Vol ($m^3 \times 10^7$)	IFT (mN/m)	Surf Area ($m^2 \times 10^4$)	Drop Vol ($m^3 \times 10^7$)
5.0	27.43	0.216	0.128	24.82	0.214	0.124
5.0	25.79	0.215	0.126	-	-	-
30.0	25.47	0.217	0.128	23.40	0.214	0.124
60.0	24.94	0.218	0.128	21.21	0.213	0.122
60.0	23.28	0.215	0.125	-	-	-
180.0	23.61	0.218	0.127	-	-	-
180.0	21.30	0.215	0.124	-	-	-
300.0	22.30	0.215	0.124	22.33	0.219	0.127
300.0	21.72	0.215	0.124	-	-	-
420.0	21.78	0.215	0.124	-	-	-
420.0	21.13	0.213	0.122	-	-	-
600.0	22.76	0.216	0.125	20.25	0.217	0.124
600.0	21.63	0.214	0.123	-	-	-
720.0	21.62	0.214	0.123	-	-	-
900.0	21.64	0.213	0.122	21.64	0.217	0.125
1200.0	21.70	0.213	0.122	-	-	-
EQUBR	21.63	-	-	21.64	-	-

Table B1.4: Interfacial Data for the System: 0.3125 mM Oleic in HD /2.50 mM NaOH

Time in (Secs)	DROP NO 1			DROP NO 2		
	IFT (mN/m)	Surf Area ($m^2 \times 10^5$)	Drop Vol ($m^3 \times 10^8$)	IFT (mN/m)	Surf Area ($m^2 \times 10^5$)	Drop Vol ($m^3 \times 10^8$)
5.0	19.84	0.879	0.340	23.10	0.970	0.396
60.0	19.42	0.886	0.344	18.20	0.958	0.386
120.0	17.74	0.878	0.338	18.02	0.968	0.391
120.0	16.96	0.877	0.337	17.14	0.957	0.384
180.0	17.20	0.867	0.332	17.19	0.963	0.384
240.0	18.25	0.867	0.332	-	-	-
240.0	16.78	0.861	0.328	-	-	-
300.0	18.26	0.861	0.329	16.70	0.959	0.384
300.0	18.08	0.862	0.330	16.32	0.959	0.384
420.0	19.16	0.855	0.326	-	-	-
420.0	17.78	0.850	0.328	-	-	-
600.0	20.28	0.854	0.327	20.81	0.963	0.390
600.0	20.06	0.853	0.326	18.50	0.944	0.377
720.0	21.28	0.859	0.330	-	-	-
720.0	19.04	0.844	0.320	-	-	-
900.0	21.68	0.875	0.340	20.00	0.957	0.388
900.0	21.11	0.872	0.337	22.49	0.946	0.381
EQUBR	21.48	-	-	21.64	-	-

Table B1.5: Interfacial Data for the System: 0.3125 mM Oleic in HD /12.50 mM NaOH

Time in (Secs)	DROP NO 1			DROP NO 2		
	IFT (mN/m)	Surf Area ($m^2 \times 10^5$)	Drop Vol ($m^3 \times 10^8$)	IFT (mN/m)	Surf Area ($m^2 \times 10^5$)	Drop Vol ($m^3 \times 10^8$)
5.0	9.33	0.712	0.243	-	-	-
10.0	-	-	-	8.43	0.836	0.301
60.0	7.62	0.745	0.254	6.57	0.862	0.305
120.0	8.60	0.743	0.255	-	-	-
120.0	8.54	0.742	0.255	-	-	-
180.0	9.11	0.731	0.251	8.42	0.836	0.301
180.0	9.08	0.730	0.250	6.47	0.806	0.280
300.0	10.28	0.695	0.237	10.82	0.800	0.289
EQUBR	9.33	-	-	9.62	-	-

Table B1.6 : Interfacial Data for the System: 0.3125 mM Oleic in HD /25.0 mM NaOH

Time in (Secs)	DROP NO 1			DROP NO 2		
	IFT (mN/m)	Surf Area ($m^2 \times 10^5$)	Drop Vol ($m^3 \times 10^9$)	IFT (mN/m)	Surf Area ($m^2 \times 10^5$)	Drop Vol ($m^3 \times 10^9$)
5.0	-	-	-	2.73	0.209	0.400
30.0	2.05	0.277	0.572	2.27	0.218	0.419
60.0	2.85	0.281	0.602	2.79	0.217	0.423
90.0	3.99	0.280	0.613	4.56	0.219	0.436
120.0	5.67	0.287	0.646	4.32	0.222	0.445
180.0	6.57	0.291	0.659	7.37	0.214	0.427
EQUBR	6.97	-	-	7.63	-	-

B.2 Interfacial Data for the 0.02 M Lauric Acid/Caustic Systems

Table B2.1: Interfacial Data for the System: 0.02 M Lauric in HD /Distilled Water

Time in (Secs)	DROP NO 1			DROP NO 2		
	IFT (mN/m)	Surf Area ($m^2 \times 10^4$)	Drop Vol ($m^3 \times 10^7$)	IFT (mN/m)	Surf Area ($m^2 \times 10^4$)	Drop Vol ($m^3 \times 10^7$)
5.0	34.13	0.355	0.258	32.68	0.344	0.246
30.0	33.88	0.357	0.260	-	-	-
60.0	32.82	0.355	0.257	33.91	0.344	0.247
120.0	32.32	0.352	0.254	33.41	0.343	0.246
180.0	32.35	0.357	0.258	-	-	-
300.0	32.92	0.355	0.257	31.88	0.343	0.245
420.0	33.60	0.359	0.262	-	-	-
600.0	32.07	0.355	0.256	32.86	0.345	0.247
720.0	32.54	0.360	0.262	32.41	0.344	0.246
900.0	32.06	0.361	0.262	33.41	0.348	0.251
1200.0	31.52	0.362	0.263	33.97	0.349	0.252
EQUBR	32.06	-	-	33.21	-	-

Table B2.2: Interfacial Data for the System: 0.02 M Lauric in HD /0.25 mM NaOH

Time in (Secs)	DROP NO 1			DROP NO 2		
	IFT (mN/m)	Surf Area ($m^2 \times 10^4$)	Drop Vol ($m^3 \times 10^7$)	IFT (mN/m)	Surf Area ($m^2 \times 10^4$)	Drop Vol ($m^3 \times 10^7$)
5.0	33.12	0.289	0.195	32.72	0.290	0.195
30.0	33.05	0.289	0.194	32.55	0.289	0.194
60.0	31.81	0.290	0.195	32.26	0.290	0.194
120.0	30.99	0.290	0.195	30.50	0.289	0.193
180.0	31.55	0.290	0.194	32.57	0.290	0.194
300.0	31.97	0.291	0.195	29.09	0.287	0.190
600.0	30.08	0.285	0.188	31.30	0.288	0.192
900.0	31.15	0.287	0.190	-	-	-
1200.0	31.68	0.288	0.191	-	-	-
EQUBR	30.77	-	-	31.21	-	-

Table B2.3: Interfacial Data for the System: 0.02 M Lauric in HD /1.25 mM NaOH

Time in (Secs)	DROP NO 1			DROP NO 2		
	IFT (mN/m)	Surf Area ($m^2 \times 10^4$)	Drop Vol ($m^3 \times 10^7$)	IFT (mN/m)	Surf Area ($m^2 \times 10^4$)	Drop Vol ($m^3 \times 10^7$)
5.0	27.30	0.231	0.139	29.25	0.235	0.144
30.0	25.29	0.230	0.138	29.18	0.236	0.145
60.0	24.61	0.230	0.138	27.36	0.235	0.143
120.0	25.56	0.232	-	-	-	-
180.0	25.83	0.232	0.139	26.74	0.238	0.145
300.0	24.90	0.229	0.136	25.14	0.237	0.144
600.0	24.29	0.228	0.136	25.71	0.236	0.143
900.0	24.01	0.226	-	-	-	-
EQUBR	24.15	-	-	-	-	-

Table B2.4: Interfacial Data for the System: 0.02 M Lauric in HD /2.50 mM NaOH

Time in (Secs)	DROP NO 1			DROP NO 2		
	IFT (mN/m)	Surf Area ($m^2 \times 10^4$)	Drop Vol ($m^3 \times 10^7$)	IFT (mN/m)	Surf Area ($m^2 \times 10^4$)	Drop Vol ($m^3 \times 10^7$)
5.0	24.25	0.208	0.119	23.87	0.235	0.140
30.0	21.39	0.205	0.205	22.20	0.235	0.139
30.0	20.72	0.206	0.116	21.13	0.235	0.139
60.0	22.50	0.207	0.118	22.07	0.238	0.142
60.0	21.43	0.207	0.117	20.71	0.238	0.142
180.0	20.73	0.206	0.116	20.02	0.238	0.141
300.0	22.62	0.207	0.118	22.03	0.243	0.146
300.0	21.00	0.206	0.116	20.56	0.237	0.139
420.0	22.79	0.205	0.116	-	-	-
600.0	-	-	-	23.47	0.238	0.143
EQUBR	24.45	-	-	22.83	-	-

Table B2.5: Interfacial Data for the System: 0.02 M Lauric in HD / 12.50 mM NaOH

Time in (Secs)	DROP 1			DROP NO 2		
	IFT (mN/m)	Surf Area ($m^2 \times 10^4$)	Drop Vol ($m^3 \times 10^8$)	IFT (mN/m)	Surf Area ($m^2 \times 10^4$)	Drop Vol ($m^3 \times 10^8$)
5.0	13.26	0.119	0.518	13.05	0.122	0.533
30.0	14.68	0.118	0.518	15.60	0.126	0.555
30.0	13.78	0.118	0.514	14.05	0.121	0.534
60.0	19.86	0.120	0.539	-	-	-
90.0	20.09	0.118	0.530	18.99	0.122	0.548
120.0	21.59	0.117	0.523	20.56	0.123	0.562
150.0	22.95	0.117	0.524	22.01	0.122	0.556
210.0	-	-	-	22.86	0.120	0.543
300.0	22.37	0.112	0.492	25.69	0.120	0.541
EQUBR	22.66	-	-	22.44	-	-

Table B2.7: Interfacial Data for the System: 0.02 M Lauric in HD /50.0 mM NaOH

Time in (Secs)	DROP NO 1			DROP NO 2		
	IFT (mN/m)	Surf Area ($m^2 \times 10^5$)	Drop Vol ($m^3 \times 10^8$)	IFT (mN/m)	Surf Area ($m^2 \times 10^5$)	Drop Vol ($m^3 \times 10^8$)
5.0	10.45	0.742	0.257	10.41	0.689	0.232
30.0	10.24	0.737	0.255	10.72	0.689	0.232
60.0	10.94	0.724	0.249	11.62	0.677	0.228
120.0	13.51	0.708	0.244	-	-	-
180.0	16.65	0.682	0.233	20.19	0.639	0.214
300.0	20.28	0.650	0.218	27.23	0.609	0.200
EQUBR	21.36	-	-	26.05	-	-

Table B2.6: Interfacial Data for the System: 0.02 M Lauric in HD /25.0 mM NaOH

Time in (Secs)	DROP NO 1			DROP NO 2		
	IFT (mN/m)	Surf Area ($m^2 \times 10^5$)	Drop Vol ($m^3 \times 10^8$)	IFT (mN/m)	Surf Area ($m^2 \times 10^5$)	Drop Vol ($m^3 \times 10^8$)
5.0	-	-	-	14.40	0.796	0.291
30.0	13.32	0.998	0.400	14.62	0.788	0.286
60.0	15.05	0.994	0.400	15.70	0.768	0.277
120.0	17.93	0.978	0.395	-	-	-
180.0	19.44	0.966	0.389	20.06	0.711	0.250
240.0	21.55	0.958	0.386	-	-	-
300.0	26.22	0.959	0.389	24.34	0.665	0.227
EQUBR	22.19	-	-	22.20	-	-

Table B2.8: Interfacial Data for the System: 0.02 M Lauric in HD /100.0 mM NaOH

Time (Secs)	IFT (mN/m)	Surf Area ($m^2 \times 10^5$)	Drop Vol ($m^3 \times 10^8$)
5.0	6.41	0.594	0.180
30.0	6.88	0.590	0.180
60.0	6.84	0.585	0.178
90.0	7.62	0.571	0.173
120.0	9.48	0.561	0.172
150.0	11.12	0.551	0.168
180.0	13.17	0.542	0.166
210.0	14.20	0.531	0.162
240.0	17.99	0.531	0.162
EQUBR	18.27	-	-

Table B2.9: Interfacial Data for the System: 0.02 M Lauric in HD /125.0 mM NaOH

Time (Secs)	IFT (mN/m)	Surf Area ($m^2 \times 10^5$)	Drop Vol ($m^3 \times 10^8$)
5.0	8.94	0.602	0.190
30.0	6.74	0.560	0.168
60.0	6.68	0.544	0.161
90.0	8.51	0.534	0.160
120.0	10.50	0.518	0.154
150.0	11.79	0.506	0.150
180.0	13.70	0.500	0.148
210.0	15.92	0.492	0.145
240.0	15.35	0.481	0.141
EQUBR	15.64	-	-

Table B2.10: Interfacial Data for the System: 0.02 M Lauric in HD /150.0 mM NaOH

Time in (Secs)	DROP NO 1			DROP NO 2		
	IFT (mN/m)	Surf Area ($m^2 \times 10^5$)	Drop Vol ($m^3 \times 10^8$)	IFT (mN/m)	Surf Area ($m^2 \times 10^5$)	Drop Vol ($m^3 \times 10^8$)
5.0	6.07	0.459	0.126	6.37	0.501	0.143
30.0	6.32	0.454	0.124	6.57	0.500	0.141
60.0	6.70	0.449	0.123	6.67	0.480	0.134
90.0	8.39	0.431	0.117	8.22	0.453	0.126
120.0	10.93	0.418	0.113	9.89	0.436	0.120
150.0	13.50	0.405	0.109	12.00	0.421	0.115
180.0	13.38	0.392	0.104	14.01	0.408	0.110
EQUBR	13.44	-	-	13.01	-	-

Table B2.11: Interfacial Data for the System: 0.02 M Lauric in HD / 200.0 mM NaOH

Time in (Secs)	DROP NO 1			DROP NO 2		
	IFT (mN/m)	Surf Area ($m^2 \times 10^5$)	Drop Vol ($m^3 \times 10^8$)	IFT (mN/m)	Surf Area ($m^2 \times 10^5$)	Drop Vol ($m^3 \times 10^8$)
5.0	5.07	0.413	0.106	5.37	0.432	0.114
20.0	5.18	0.403	0.103	-	-	-
40.0	5.41	0.400	0.102	5.43	0.423	0.111
60.0	6.06	0.395	0.101	5.89	0.415	0.109
80.0	6.81	0.387	0.099	7.02	0.409	0.107
100.0	7.85	0.380	0.097	7.99	0.399	0.104
120.0	9.29	0.375	0.096	9.92	0.392	0.102
140.0	10.15	0.368	0.094	10.02	0.380	0.098
EQUBR	9.72	-	-	9.97	-	-

B.3 Interfacial Data for Binary Mixture Reference Systems

B.3.1 Data for 0.10 mM Oleic Acid in Hexadecane/Caustic Systems

Table B3.1: Interfacial Data for the System: 0.10 mM Oleic in HD /Double Distilled Water

Time in (Secs)	DROP NO 1			DROP NO 2		
	IFT (mN/m)	Surf Area ($m^2 \times 10^4$)	Drop Vol ($m^3 \times 10^7$)	IFT (mN/m)	Surf Area ($m^2 \times 10^4$)	Drop Vol ($m^3 \times 10^7$)
5.0	43.65	0.302	0.211	43.67	0.297	0.207
30.0	42.29	0.301	0.210	-	-	-
60.0	42.40	0.304	0.213	42.74	0.292	0.201
180.0	42.16	0.303	0.212	42.37	0.293	0.203
300.0	42.96	0.303	0.212	41.46	0.292	0.201
420.0	42.01	0.304	0.213	-	-	-
480.0	-	-	-	41.40	0.294	0.203
600.0	42.48	0.304	0.213	41.57	0.292	0.203
720.0	40.94	0.303	0.211	-	-	-
900.0	41.17	0.303	0.212	41.90	0.294	0.203
1080.0	41.89	0.304	0.214	-	-	-
1200.0	40.55	0.302	0.211	41.17	0.291	0.201
EQUBR	40.54	-	-	41.76	-	-

Table B3.2: Interfacial Data for the System: 0.10 mM Oleic in HD /0.25 mM NaOH

Time in (Secs)	DROP NO 1			DROP NO 2		
	IFT (mN/m)	Surf Area ($m^2 \times 10^4$)	Drop Vol ($m^3 \times 10^7$)	IFT (mN/m)	Surf Area ($m^2 \times 10^4$)	Drop Vol ($m^3 \times 10^7$)
5.0	39.91	0.265	0.174	42.09	0.271	0.182
60.0	36.48	0.264	0.172	39.55	0.269	0.180
180.0	36.93	0.263	0.172	39.70	0.271	0.180
300.0	35.31	0.263	0.171	37.47	0.273	0.182
480.0	35.10	0.262	0.170	37.48	0.273	0.182
600.0	35.13	0.264	0.172	36.22	0.273	0.182
720.0	35.37	0.265	0.173	-	-	-
900.0	33.43	0.264	0.171	35.62	0.275	0.184
1200.0	34.93	0.266	0.173	34.34	0.272	0.180
EQUBR	35.25	-	-	34.98	-	-

Table B3.3: Interfacial Data for the System: 0.10 mM Oleic in HD /1.25 mM NaOH

Time in (Secs)	DROP NO 1			DROP NO 2		
	IFT (mN/m)	Surf Area ($m^2 \times 10^4$)	Drop Vol ($m^3 \times 10^7$)	IFT (mN/m)	Surf Area ($m^2 \times 10^4$)	Drop Vol ($m^3 \times 10^7$)
5.0	31.41	0.241	0.149	28.89	0.247	0.154
30.0	29.52	0.242	0.150	27.89	0.249	0.155
60.0	28.88	0.241	0.148	26.65	0.247	0.153
180.0	26.58	0.240	0.148	27.15	0.247	0.154
300.0	27.61	0.242	0.149	26.62	0.245	0.151
420.0	26.09	0.241	0.148	-	-	-
480.0	-	-	-	26.77	0.243	0.149
600.0	26.78	0.241	0.148	28.53	0.247	0.153
720.0	27.18	0.242	0.149	26.23	0.242	0.148
900.0	25.77	0.241	0.147	28.30	0.244	0.151
1080.0	-	-	-	26.38	0.243	0.149
1200.0	26.71	0.241	0.147	-	-	-
EQUBR	26.95	-	-	27.16	-	-

Table B3.4: Interfacial Data for the System: 0.10 mM Oleic in HD /2.50 mM NaOH

Time in (Secs)	DROP NO 1			DROP NO 2		
	IFT (mN/m)	Surf Area ($m^2 \times 10^4$)	Drop Vol ($m^3 \times 10^8$)	IFT (mN/m)	Surf Area ($m^2 \times 10^4$)	Drop Vol ($m^3 \times 10^7$)
5.0	29.23	0.167	0.887	28.34	0.197	0.111
30.0	27.15	0.169	0.895	-	-	-
60.0	25.57	0.169	0.891	23.04	0.197	0.110
120.0	23.68	0.168	0.883	-	-	-
180.0	22.31	0.168	0.878	20.83	0.196	0.110
300.0	22.88	0.167	0.870	22.44	0.198	0.110
420.0	23.88	0.165	0.860	-	-	-
480.0	-	-	-	24.26	0.194	0.107
600.0	25.31	0.163	0.850	24.29	0.192	0.106
EQUBR	27.61	-	-	24.30	-	-

Table B3.5: Interfacial Data for the System: 0.10 mM Oleic in HD /12.50 mM NaOH

Time in (Secs)	DROP NO 1			DROP NO 2		
	IFT (mN/m)	Surf Area ($m^2 \times 10^4$)	Drop Vol ($m^3 \times 10^8$)	IFT (mN/m)	Surf Area ($m^2 \times 10^4$)	Drop Vol ($m^3 \times 10^8$)
5.0	20.27	0.160	0.800	16.90	0.134	0.618
30.0	15.46	0.161	0.794	15.25	0.136	0.627
60.0	14.76	0.161	0.788	14.07	0.136	0.620
120.0	15.05	0.162	0.794	-	-	-
180.0	15.25	0.160	0.789	14.40	0.135	0.618
240.0	15.55	0.160	0.778	-	-	-
300.0	16.34	0.158	0.776	16.21	0.133	0.610
420.0	17.67	0.157	0.778	18.57	0.132	0.610
600.0	19.46	0.155	0.776	20.37	0.131	0.610
720.0	20.07	0.155	0.770	20.98	0.131	0.603
EQUBR	19.76	-	-	20.68	-	-

Table B3.6: Interfacial Data for the System: 0.10 mM Oleic in HD /25.00 mM NaOH

Time in (Secs)	DROP NO 1			DROP NO 2		
	IFT (mN/m)	Surf Area ($m^2 \times 10^5$)	Drop Vol ($m^3 \times 10^8$)	IFT (mN/m)	Surf Area ($m^2 \times 10^5$)	Drop Vol ($m^3 \times 10^8$)
5.0	18.47	0.857	0.328	17.25	0.878	0.338
30.0	11.99	0.866	0.326	12.51	0.893	0.340
60.0	12.02	0.867	0.325	11.37	0.884	0.339
120.0	12.09	0.863	0.323	11.98	0.877	0.332
180.0	13.12	0.864	0.326	14.57	0.872	0.332
240.0	14.08	0.860	0.325	14.90	0.861	0.327
300.0	14.53	0.853	0.322	16.67	0.856	0.326
420.0	-	-	-	20.45	0.854	0.327
EQUBR	17.66	-	-	18.56	-	-

Table B3.7: Interfacial Data for the System: 0.10 mM Oleic in HD /125.00 mM NaOH

Time in (Secs)	DROP NO 1			DROP NO 2		
	IFT (mN/m)	Surf Area ($m^2 \times 10^5$)	Drop Vol ($m^3 \times 10^9$)	IFT (mN/m)	Surf Area ($m^2 \times 10^5$)	Drop Vol ($m^3 \times 10^9$)
5.0	1.76	-	-	1.10	-	-
30.0	2.35	0.270	0.580	1.63	-	-
60.0	4.08	0.265	0.578	2.37	0.238	0.490
90.0	4.22	0.250	0.532	3.81	0.225	0.457
120.0	6.25	0.244	0.522	5.70	0.215	0.434
150.0	10.10	0.240	0.520	-	-	-
EQUBR	10.23	-	-	-	-	-

Table B3.8: Interfacial Data for the System: 0.10 mM Oleic in HD /200.00 mM NaOH

Time in (Secs)	DROP NO 1			DROP NO 2		
	IFT (mN/m)	Surf Area ($m^2 \times 10^5$)	Drop Vol ($m^3 \times 10^9$)	IFT (mN/m)	Surf Area ($m^2 \times 10^5$)	Drop Vol ($m^3 \times 10^9$)
20.0	6.98	0.311	0.730	2.50	0.257	0.542
40.0	2.87	0.317	0.721	1.10	-	-
60.0	1.97	-	-	1.06	-	-
80.0	2.91	0.335	0.781	1.12	-	-
100.0	2.61	0.312	0.702	2.52	0.262	0.554
120.0	-	-	-	3.35	0.253	0.533
140.0	3.09	0.300	0.661	3.62	0.243	0.507
160.0	3.99	0.304	0.698	-	-	-
180.0	4.10	0.300	0.670	-	-	-

B.3.2 Data for 0.20 mM Oleic Acid in HD /Caustic Systems

Table B4.1: Interfacial Data for the System: 0.20 mM Oleic in HD /Double Distilled Water

Time in (Secs)	DROP NO 1			DROP NO 2		
	IFT (mN/m)	Surf Area ($m^2 \times 10^4$)	Drop Vol ($m^3 \times 10^7$)	IFT (mN/m)	Surf Area ($m^2 \times 10^4$)	Drop Vol ($m^3 \times 10^7$)
5.0	43.98	0.287	0.196	43.12	0.279	0.190
30.0	44.35	0.285	0.194	-	-	-
60.0	42.45	0.285	0.194	44.78	0.273	0.183
180.0	43.20	0.284	0.192	44.97	0.270	0.180
300.0	43.53	0.284	0.193	44.08	0.267	0.177
420.0	42.28	0.280	0.188	-	-	-
480.0	-	-	-	45.45	0.261	0.171
600.0	42.54	0.280	0.188	44.87	0.259	0.169
720.0	41.88	0.278	0.187	42.41	0.257	0.168
900.0	41.21	0.280	0.188	43.25	0.255	0.166
1080.0	41.65	0.280	0.189	-	-	-
1200.0	41.23	0.280	0.188	44.02	0.256	0.164
EQUBR	40.02	-	-	43.25	0.256	0.164

Table B4.2: Interfacial Data for the System: 0.20 mM Oleic in HD /0.25 mM NaOH

Time in (Secs)	DROP NO 1			DROP NO 2		
	IFT (mN/m)	Surf Area ($m^2 \times 10^4$)	Drop Vol ($m^3 \times 10^7$)	IFT (mN/m)	Surf Area ($m^2 \times 10^4$)	Drop Vol ($m^3 \times 10^7$)
5.0	35.67	0.254	0.162	35.55	0.248	0.157
60.0	37.23	0.254	0.163	36.05	0.247	0.156
180.0	35.07	0.253	0.162	33.77	0.242	0.151
300.0	31.40	0.248	0.157	34.15	0.240	0.149
480.0	32.99	0.251	0.159	31.19	0.235	0.144
600.0	34.45	0.253	0.161	31.46	0.234	0.143
720.0	33.23	0.253	0.161	29.00	0.233	0.141
900.0	32.75	0.253	0.160	29.17	0.233	0.142
1200.0	32.07	0.255	0.161	-	-	-
EQUBR	32.07	-	-	30.32	-	-

Table B4.3: Interfacial Data for the System: 0.20 mM Oleic in HD /1.25 mM NaOH

Time in (Secs)	DROP NO 1			DROP NO 2		
	IFT (mN/m)	Surf Area ($m^2 \times 10^4$)	Drop Vol ($m^3 \times 10^7$)	IFT (mN/m)	Surf Area ($m^2 \times 10^4$)	Drop Vol ($m^3 \times 10^7$)
5.0	24.91	0.216	0.125	27.15	0.217	0.127
30.0	25.35	0.217	0.126	25.67	0.215	0.125
60.0	24.86	0.216	0.125	25.45	0.216	0.125
180.0	24.25	0.214	0.124	24.50	0.215	0.125
300.0	24.82	0.214	0.124	24.33	0.214	0.124
420.0	23.31	0.211	0.121	-	-	-
480.0	-	-	-	24.68	0.210	0.121
600.0	24.56	0.211	0.121	25.77	0.210	0.120
720.0	25.76	0.211	0.121	26.16	0.210	0.121
900.0	24.76	0.210	0.120	25.29	0.208	0.119
1080.0	-	-	-	26.51	0.209	0.121
EQUBR	25.75	-	-	25.99	-	-

Table B4.4: Interfacial Data for the System: 0.20 mM Oleic in HD /2.50 mM NaOH

Time in (Secs)	DROP NO 1			DROP NO 2		
	IFT (mN/m)	Surf Area ($m^2 \times 10^4$)	Drop Vol ($m^3 \times 10^8$)	IFT (mN/m)	Surf Area ($m^2 \times 10^4$)	Drop Vol ($m^3 \times 10^8$)
5.0	24.15	0.153	0.790	23.22	0.160	0.810
30.0	21.63	0.154	0.780	-	-	-
60.0	21.48	0.154	0.770	21.12	0.158	0.800
180.0	20.57	0.150	0.740	18.81	0.154	0.760
300.0	21.01	0.150	0.720	21.41	0.153	0.760
420.0	24.15	0.145	0.710	-	-	-
480.0	-	-	-	23.78	0.150	0.740
600.0	24.70	0.144	0.700	25.25	0.148	0.730
720.0	23.13	0.141	0.700	23.61	0.146	0.730
900.0	24.24	0.141	0.680	25.97	0.145	0.720
1080.0	23.08	0.140	0.670	-	-	-
EQUBR	23.79	-	-	24.65	-	-

Table B4.5: Interfacial Data for the System: 0.20 mM Oleic in HD /12.50 mM NaOH

Time in (Secs)	DROP NO 1			DROP NO 2		
	IFT (mN/m)	Surf Area ($m^2 \times 10^5$)	Drop Vol ($m^3 \times 10^8$)	IFT (mN/m)	Surf Area ($m^2 \times 10^5$)	Drop Vol ($m^3 \times 10^8$)
5.0	11.96	0.820	0.300	12.40	0.860	0.320
30.0	8.53	0.820	0.300	8.43	0.860	0.320
60.0	7.79	0.830	0.300	7.72	0.870	0.320
120.0	-	-	-	7.63	0.840	0.301
180.0	9.21	0.780	0.280	9.95	0.820	0.294
240.0	-	-	-	12.13	0.800	0.290
300.0	14.80	0.760	0.274	14.58	0.780	0.290
EQUBR	14.80	-	-	13.36	-	-

Table B4.6: Interfacial Data for the System: 0.20 mM Oleic in HD /25.00 mM NaOH

Time in (Secs)	DROP NO 1			DROP NO 2		
	IFT (mN/m)	Surf Area ($m^2 \times 10^5$)	Drop Vol ($m^3 \times 10^8$)	IFT (mN/m)	Surf Area ($m^2 \times 10^5$)	Drop Vol ($m^3 \times 10^8$)
5.0	10.13	0.540	0.164	12.32	0.430	0.110
30.0	5.95	0.550	0.163	7.89	0.435	0.120
60.0	6.24	0.550	0.163	7.21	0.430	0.116
90.0	6.97	0.540	0.163	7.79	0.420	0.113
120.0	7.93	0.541	0.163	10.09	0.410	0.112
150.0	8.19	0.530	0.160	10.67	0.410	0.110
180.0	10.03	0.540	0.162	12.77	0.410	0.110
EQUBR	11.37	-	-	11.51	-	-

Table B4.7: Interfacial Data for the System: 0.20 mM Oleic in HD /125.00 mM NaOH

Time in (Secs)	DROP NO 1			DROP NO 2		
	IFT (mN/m)	Surf Area ($m^2 \times 10^5$)	Drop Vol ($m^3 \times 10^9$)	IFT (mN/m)	Surf Area ($m^2 \times 10^5$)	Drop Vol ($m^3 \times 10^9$)
5.0	5.77	0.160	0.280	7.19	0.160	0.300
20.0	0.98	-	-	1.05	-	-
40.0	1.13	0.160	0.260	1.05	-	-
60.0	1.58	0.150	0.250	1.56	0.160	0.280
80.0	3.16	0.140	0.220	1.78	0.150	0.250
100.0	4.78	0.146	0.250	1.91	0.140	0.210

B.3.3 Data for 0.6125 mM Oleic Acid/Caustic Systems

Table B5.1: Interfacial Data for the System: 0.6125 mM Oleic in HD /Double Distilled Water

Time in (Secs)	DROP NO 1			DROP NO 2		
	IFT (mN/m)	Surf Area ($m^2 \times 10^4$)	Drop Vol ($m^3 \times 10^7$)	IFT (mN/m)	Surf Area ($m^2 \times 10^4$)	Drop Vol ($m^3 \times 10^7$)
5.0	39.26	0.280	0.188	44.16	0.293	0.204
30.0	41.33	0.281	0.190	-	-	-
60.0	41.30	0.281	0.190	42.16	0.293	0.203
180.0	40.73	0.281	0.190	41.75	0.292	0.203
300.0	39.50	0.281	0.190	39.77	0.293	0.202
420.0	39.83	0.282	0.191	-	-	-
480.0	-	-	-	40.94	0.294	0.204
600.0	38.16	0.284	0.193	41.62	0.293	0.203
720.0	36.66	0.285	0.194	40.25	0.295	0.205
900.0	37.37	0.284	0.193	40.54	0.295	0.205
1080.0	-	-	-	41.05	0.296	0.206
EQUBR	36.86	0.285	0.194	40.94	-	-

Table B5.2: Interfacial Data for the System: 0.6125 mM Oleic in HD /0.25 mM NaOH

Time in (Secs)	DROP NO 1			DROP NO 2		
	IFT (mN/m)	Surf Area ($m^2 \times 10^4$)	Drop Vol ($m^3 \times 10^7$)	IFT (mN/m)	Surf Area ($m^2 \times 10^4$)	Drop Vol ($m^3 \times 10^7$)
5.0	33.25	0.207	0.121	38.92	0.219	0.133
30.0	31.58	0.206	0.120	-	-	-
60.0	31.60	0.207	0.121	33.35	0.217	0.130
180.0	28.23	0.206	0.120	30.18	0.218	0.130
300.0	25.50	0.207	0.120	29.73	0.220	0.131
420.0	22.59	0.208	0.120	-	-	-
480.0	-	-	-	24.31	0.223	0.131
600.0	19.67	0.210	0.120	21.36	0.224	0.131
EQUBR	19.94	-	-	20.03		-

Table B5.3: Interfacial Data for the System: 0.6125 mM Oleic in HD /1.25 mM NaOH

Time in (Secs)	DROP NO 1			DROP NO 2		
	IFT (mN/m)	Surf Area ($m^2 \times 10^4$)	Drop Vol ($m^3 \times 10^8$)	IFT (mN/m)	Surf Area ($m^2 \times 10^4$)	Drop Vol ($m^3 \times 10^7$)
5.0	19.29	0.181	0.964	18.92	0.199	0.110
30.0	18.30	0.181	0.961	-	-	-
60.0	18.87	0.182	0.970	18.02	0.199	0.110
180.0	17.64	0.180	0.960	18.17	0.200	0.110
300.0	18.35	0.181	0.960	18.07	0.198	0.109
420.0	18.58	0.180	0.950	-	-	-
480.0	-	-	-	18.67	0.195	0.107
600.0	19.50	0.181	0.964	19.59	0.195	0.107
720.0	19.27	0.180	0.950	19.74	0.195	0.107
900.0	19.50	0.180	0.960	19.90	0.194	0.106
1080.0	19.89	0.184	0.980	20.00	0.193	0.106
EQUBR	19.53	-	-	19.81	-	-

Table B5.4: Interfacial Data for the System: 0.6125 mM Oleic in HD /2.50 mM NaOH

Time in (Secs)	DROP NO 1			DROP NO 2		
	IFT (mN/m)	Surf Area ($m^2 \times 10^4$)	Drop Vol ($m^3 \times 10^8$)	IFT (mN/m)	Surf Area ($m^2 \times 10^4$)	Drop Vol ($m^3 \times 10^8$)
5.0	12.93	0.123	0.546	13.10	0.156	0.760
30.0	12.53	0.125	0.550	12.79	0.156	0.758
60.0	11.55	0.124	0.547	11.96	0.155	0.745
120.0	-	-	-	11.84	0.155	0.743
180.0	12.44	0.123	0.546	11.67	0.156	0.740
300.0	13.80	0.123	0.546	12.83	0.153	0.740
420.0	15.70	0.122	0.545	17.09	0.154	0.760
600.0	17.93	0.121	0.542	18.76	0.152	0.760
EQUBR	18.39	-	-	18.80	-	-

Table B5.5: Interfacial Data for the System: 0.6125 mM Oleic in HD /12.50 mM NaOH

Time in (Secs)	DROP NO 1			DROP NO 2		
	IFT (mN/m)	Surf Area ($m^2 \times 10^5$)	Drop Vol ($m^3 \times 10^9$)	IFT (mN/m)	Surf Area ($m^2 \times 10^5$)	Drop Vol ($m^3 \times 10^9$)
5.0	2.18	0.280	0.600	1.48	-	-
20.0	2.42	0.271	0.580	1.56	-	-
40.0	2.53	0.261	0.560	1.36	-	-
60.0	2.73	0.242	0.500	1.51	-	-
80.0	-	-	-	3.65	0.280	0.620
100.0	-	-	-	7.02	0.270	0.600
EQUBR	7.39	-	-	9.04	-	-

Table B5.6: Interfacial Data for the System: 0.6125 mM Oleic in HD /25.00 mM NaOH

Time in (Secs)	DROP NO 1			DROP NO 2		
	IFT (mN/m)	Surf Area ($m^2 \times 10^5$)	Drop Vol ($m^3 \times 10^9$)	IFT (mN/m)	Surf Area ($m^2 \times 10^5$)	Drop Vol ($m^3 \times 10^9$)
3.0	1.05	-	-	1.16	-	-
10.0	1.12	-	-	1.84	0.198	0.370
20.0	1.58	0.220	0.440	1.90	0.197	0.371
30.0	1.86	0.218	0.422	2.25	0.199	0.380
40.0	2.26	0.210	0.400	2.55	0.185	0.340
50.0	3.45	0.200	0.380	4.62	0.182	0.340
60.0	6.08	0.196	0.377	-	-	-
EQUBR	10.33	-	-	-	-	-

B.3.4 Data for 1.00 mM Oleic Acid in HD /Caustic Systems

Table B6.1: Interfacial Data for the System: 1.00 mM Oleic in HD /Double Distilled Water

Time in (Secs)	DROP NO 1			DROP NO 2		
	IFT (mN/m)	Surf Area ($m^2 \times 10^4$)	Drop Vol ($m^3 \times 10^7$)	IFT (mN/m)	Surf Area ($m^2 \times 10^4$)	Drop Vol ($m^3 \times 10^7$)
5.0	40.26	0.284	0.193	40.83	0.279	0.188
30.0	40.40	0.284	0.193	40.93	0.278	0.186
60.0	39.62	0.283	0.191	-	-	-
120.0	-	-	-	38.29	0.276	0.184
180.0	38.68	0.281	0.188	39.28	0.276	0.184
300.0	39.05	0.280	0.187	38.61	0.274	0.183
420.0	38.54	0.279	0.186	-	-	-
480.0	-	-	-	37.49	0.274	0.182
600.0	37.44	0.278	0.184	37.76	0.273	0.181
720.0	37.66	0.278	0.184	35.93	0.272	0.180
900.0	37.56	0.278	0.186	36.99	0.272	0.180
EQUBR	34.19	-	-	36.06	-	-

Table B6.2: Interfacial Data for the System: 1.00 mM Oleic in HD /0.25 mM NaOH

Time in (Secs)	DROP NO 1			DROP NO 2		
	IFT (mN/m)	Surf Area ($m^2 \times 10^4$)	Drop Vol ($m^3 \times 10^7$)	IFT (mN/m)	Surf Area ($m^2 \times 10^4$)	Drop Vol ($m^3 \times 10^7$)
5.0	35.64	0.193	0.111	35.12	0.250	0.158
30.0	33.72	0.191	0.110	30.38	0.246	0.154
60.0	32.44	0.192	0.110	30.24	0.245	0.154
180.0	26.78	0.192	0.110	26.82	0.249	0.157
300.0	26.55	0.195	0.110	27.77	0.250	0.156
420.0	-	-	-	25.69	0.252	0.156
600.0	-	-	-	22.38	0.253	0.155
EQUBR	22.81	-	-	20.26	-	-

Table B6.3: Interfacial Data for the System: 1.00 mM Oleic in HD /1.25 mM NaOH

Time in (Secs)	DROP NO 1			DROP NO 2		
	IFT (mN/m)	Surf Area ($m^2 \times 10^4$)	Drop Vol ($m^3 \times 10^8$)	IFT (mN/m)	Surf Area ($m^2 \times 10^4$)	Drop Vol ($m^3 \times 10^8$)
5.0	17.18	0.180	0.950	15.27	0.170	0.880
30.0	15.36	0.178	0.920	-	-	-
60.0	15.28	0.178	0.923	15.01	0.172	0.880
180.0	14.74	0.177	0.912	15.56	0.172	0.879
300.0	15.19	0.177	0.912	15.52	0.171	0.870
420.0	15.32	0.175	0.900	-	-	-
480.0	-	-	-	15.22	0.170	0.850
600.0	16.56	0.175	0.905	15.71	0.168	0.852
720.0	16.12	0.174	0.900	16.49	0.168	0.857
900.0	16.99	0.174	0.900	16.81	0.168	0.852
1080.0	16.77	0.174	0.903	17.15	0.167	0.850
EQUBR	16.88	-	-	16.82	-	-

Table B6.4: Interfacial Data for the System: 1.00 mM Oleic in HD /2.50 mM NaOH

Time in (Secs)	DROP NO 1			DROP NO 2		
	IFT (mN/m)	Surf Area ($m^2 \times 10^5$)	Drop Vol ($m^3 \times 10^8$)	IFT (mN/m)	Surf Area ($m^2 \times 10^5$)	Drop Vol ($m^3 \times 10^8$)
5.0	8.52	0.970	0.380	9.54	0.990	0.390
30.0	8.14	0.987	0.385	9.35	0.991	0.392
60.0	7.85	0.981	0.381	8.27	0.995	0.392
120.0	-	-	-	8.54	0.987	0.387
180.0	8.76	0.960	0.374	8.67	0.961	0.374
300.0	10.33	0.940	0.370	10.13	0.940	0.362
420.0	14.05	0.930	0.370	-	-	-
480.0	-	-	-	13.14	0.920	0.360
600.0	14.05	0.900	0.360	15.24	0.900	0.360
EQUBR	14.05	-	-	14.35	-	-

Table B6.5: Interfacial Data for the System: 1.00 mM Oleic in HD /12.50 mM NaOH

Time in (Secs)	DROP NO 1			DROP NO 2		
	IFT (mN/m)	Surf Area ($m^2 \times 10^5$)	Drop Vol ($m^3 \times 10^9$)	IFT (mN/m)	Surf Area ($m^2 \times 10^5$)	Drop Vol ($m^3 \times 10^9$)
5.0	0.97	-	-	1.29	0.160	0.280
10.0	-	-	-	1.51	0.167	0.290
20.0	1.77	0.189	0.350	2.15	0.164	0.290
30.0	-	-	-	5.39	0.163	0.294
40.0	2.80	0.181	0.340	2.27	0.161	0.291
60.0	5.28	0.180	0.340	-	-	-
80.0	4.80	0.180	0.330	-	-	-
EQUBR	9.42	-	-	8.23	-	-

Table B6.6: Interfacial Data for the System: 1.00 mM Oleic in HD /25.00 mM NaOH

Time in (Secs)	DROP NO 1			DROP NO 2		
	IFT (mN/m)	Surf Area ($m^2 \times 10^5$)	Drop Vol ($m^3 \times 10^9$)	IFT (mN/m)	Surf Area ($m^2 \times 10^5$)	Drop Vol ($m^3 \times 10^9$)
3.0	1.01	0.140	0.226	1.18	0.160	0.268
10.0	1.11	0.140	0.224	1.20	0.160	0.267
20.0	1.31	0.140	0.230	1.06	0.154	0.250
30.0	1.67	0.140	0.230	1.94	0.157	0.260
40.0	2.80	0.143	0.240	3.21	0.152	0.260
50.0	2.13	0.134	0.220	4.88	0.152	0.260
60.0	3.52	0.140	0.230	2.26	0.144	0.240
70.0	2.72	0.138	0.230	2.70	0.144	0.240
EQUBR	5.20	-	-	-	-	-

B.4 Interfacial Data for the Binary Mixture Systems

B.4.1 Data for M1/Caustic Systems

Table B7.1: Interfacial Data for the System: M1/Double Distilled Water

Time in (Secs)	DROP NO 1			DROP NO 2		
	IFT (mN/m)	Surf Area ($m^2 \times 10^4$)	Drop Vol ($m^3 \times 10^7$)	IFT (mN/m)	Surf Area ($m^2 \times 10^4$)	Drop Vol ($m^3 \times 10^7$)
5.0	34.47	0.283	0.189	34.95	0.283	0.191
30.0	33.78	0.282	0.188	-	-	-
60.0	31.19	0.280	0.186	32.62	0.282	0.188
180.0	33.20	0.283	0.189	32.62	0.282	0.189
300.0	32.13	0.281	0.187	33.63	0.283	0.189
420.0	32.56	0.281	0.186	-	-	-
480.0	-	-	-	34.34	0.283	0.189
600.0	32.30	0.281	0.186	33.53	0.283	0.187
720.0	33.26	0.282	0.188	33.88	0.281	0.186
900.0	32.90	0.282	0.188	35.27	0.283	0.189
1080.0	34.55	0.284	0.190	35.11	0.282	0.189
1200.0	33.19	0.284	0.190	34.60	0.283	0.189

Table B7.2: Interfacial Data for the System: M1/0.25 mM NaOH

Time in (Secs)	DROP NO 1			DROP NO 2		
	IFT (mN/m)	Surf Area ($m^2 \times 10^4$)	Drop Vol ($m^3 \times 10^7$)	IFT (mN/m)	Surf Area ($m^2 \times 10^4$)	Drop Vol ($m^3 \times 10^7$)
5.0	31.15	0.263	0.170	32.04	0.272	0.178
30.0	30.23	0.262	0.168	-	-	-
60.0	32.69	0.265	0.172	32.41	0.273	0.179
180.0	31.75	0.263	0.170	30.83	0.270	0.176
300.0	31.73	0.264	0.170	31.63	0.271	0.177
420.0	29.64	0.260	0.166	-	-	-
480.0	-	-	-	31.59	0.271	0.177
600.0	31.04	0.262	0.168	32.17	0.272	0.178
720.0	30.68	0.264	0.170	31.17	0.271	0.177
900.0	30.42	0.261	0.167	31.03	0.271	0.176
1080.0	30.21	0.261	0.167	-	-	-

Table B7.3: Interfacial Data for the System: M1/1.25 mM NaOH

Time in (Secs)	DROP NO 1			DROP NO 2		
	IFT (mN/m)	Surf Area ($m^2 \times 10^4$)	Drop Vol ($m^3 \times 10^7$)	IFT (mN/m)	Surf Area ($m^2 \times 10^4$)	Drop Vol ($m^3 \times 10^7$)
5.0	-	-	-	27.44	0.243	0.150
30.0	28.25	0.245	0.151	27.03	0.243	0.150
60.0	27.96	0.244	0.151	27.08	0.242	0.148
120.0	26.79	0.243	0.150	-	-	-
180.0	26.43	0.245	0.151	26.86	0.242	0.149
300.0	26.89	0.244	0.151	26.12	0.242	0.148
420.0	25.57	0.243	0.149	-	-	-
480.0	-	-	-	25.01	0.241	0.146
600.0	26.82	0.244	0.150	25.46	0.240	0.146
720.0	27.70	0.244	0.150	26.10	0.241	0.147
900.0	27.90	0.244	0.151	24.67	0.240	0.145
1080.0	-	-	-	26.25	0.240	0.146

Table B7.4: Interfacial Data for the System: M1/2.50 mM NaOH

Time in (Secs)	DROP NO 1			DROP NO 2		
	IFT (mN/m)	Surf Area ($m^2 \times 10^4$)	Drop Vol ($m^3 \times 10^7$)	IFT (mN/m)	Surf Area ($m^2 \times 10^4$)	Drop Vol ($m^3 \times 10^8$)
5.0	24.89	0.200	0.114	23.26	0.168	0.880
30.0	23.98	0.200	0.113	21.78	0.167	0.870
60.0	23.49	0.200	0.112	22.56	0.168	0.880
120.0	-	-	-	22.09	0.168	0.881
180.0	22.78	0.200	0.111	21.36	0.168	0.875
300.0	22.81	0.200	0.112	21.28	0.167	0.866
420.0	21.89	0.198	0.110	-	-	-
480.0	-	-	-	21.14	0.166	0.860
600.0	22.62	0.198	0.111	21.57	0.167	0.870
720.0	21.96	0.197	0.110	20.60	0.166	0.852
900.0	23.46	0.198	0.111	21.01	0.166	0.862
1080.0	-	-	-	21.24	0.167	0.864

Table B7.5: Interfacial Data for the System: M1/12.50 mM NaOH

Time in (Secs)	DROP NO 1			DROP NO 2		
	IFT (mN/m)	Surf Area ($m^2 \times 10^4$)	Drop Vol ($m^3 \times 10^8$)	IFT (mN/m)	Surf Area ($m^2 \times 10^4$)	Drop Vol ($m^3 \times 10^8$)
10.0	13.26	0.106	0.430	-	-	-
30.0	10.42	0.104	0.420	12.74	0.113	0.470
60.0	10.18	0.104	0.410	11.74	0.114	0.470
120.0	10.29	0.100	0.400	12.19	0.109	0.450
180.0	12.86	0.100	0.403	14.16	0.108	0.450
240.0	13.48	0.099	0.395	14.31	0.105	0.440
300.0	13.93	0.096	0.380	15.96	0.104	0.430
360.0	15.89	0.095	0.376	16.72	0.104	0.430
420.0	16.79	0.094	0.370	-	-	-
480.0	-	-	-	20.94	0.103	0.425

Table B7.6: Interfacial Data for the System: M1/25.00 mM NaOH

Time in (Secs)	DROP NO 1			DROP NO 2		
	IFT (mN/m)	Surf Area ($m^2 \times 10^5$)	Drop Vol ($m^3 \times 10^9$)	IFT (mN/m)	Surf Area ($m^2 \times 10^5$)	Drop Vol ($m^3 \times 10^9$)
5.0	6.40	0.350	0.870	-	-	-
10.0	-	-	-	7.72	0.620	0.196
30.0	5.38	0.347	0.851	7.33	0.620	0.195
60.0	6.29	0.340	0.824	7.37	0.612	0.192
120.0	9.44	0.330	0.806	8.81	0.589	0.184
180.0	12.13	0.324	0.787	11.92	0.591	0.188
240.0	-	-	-	13.46	0.581	0.185
300.0	-	-	-	15.56	0.574	0.182
360.0	-	-	-	14.82	0.563	0.180
420.0	-	-	-	15.85	0.565	0.178
480.0	-	-	-	17.90	0.565	0.179

Table B7.7: Interfacial Data for the System: M1/125.00 mM NaOH

Time in (Secs)	DROP NO 1			DROP NO 2		
	IFT (mN/m)	Surf Area ($m^2 \times 10^5$)	Drop Vol ($m^3 \times 10^9$)	IFT (mN/m)	Surf Area ($m^2 \times 10^5$)	Drop Vol ($m^3 \times 10^9$)
5.0	4.59	0.240	0.500	-	-	-
30.0	3.69	0.240	0.490	5.57	0.350	0.850
60.0	3.77	0.234	0.477	3.34	0.320	0.700
90.0	4.87	0.225	0.455	3.65	0.302	0.680
120.0	6.83	0.221	0.450	5.37	0.300	0.673
150.0	8.46	0.213	0.430	6.15	0.283	0.640
210.0	-	-	-	7.97	0.260	0.560

Table B7.8: Interfacial Data for the System: M1/200.00 mM NaOH

Time in (Secs)	DROP NO 1			DROP NO 2		
	IFT (mN/m)	Surf Area ($m^2 \times 10^5$)	Drop Vol ($m^3 \times 10^9$)	IFT (mN/m)	Surf Area ($m^2 \times 10^5$)	Drop Vol ($m^3 \times 10^9$)
5.0	4.03	0.240	0.500	4.50	0.380	0.950
20.0	3.76	0.240	0.500	4.10	0.380	0.940
40.0	3.94	0.240	0.500	4.03	0.372	0.920
60.0	3.64	0.240	0.481	4.25	0.360	0.880
80.0	3.62	0.234	0.470	4.16	0.355	0.860
100.0	4.12	0.231	0.465	4.31	0.350	0.840
140.0	4.10	0.222	0.440	4.72	0.340	0.802
160.0	4.06	0.220	0.430	5.04	0.330	0.782
180.0	-	-	-	5.18	0.331	0.782

B.4.2 Data for M2/Caustic Systems

Table B8.1: Interfacial Data for the System: M2/Double Distilled Water

Time in (Secs)	DROP NO 1			DROP NO 2		
	IFT (mN/m)	Surf Area ($m^2 \times 10^4$)	Drop Vol ($m^3 \times 10^8$)	IFT (mN/m)	Surf Area ($m^2 \times 10^4$)	Drop Vol ($m^3 \times 10^7$)
5.0	35.00	0.169	0.900	34.25	0.270	0.180
30.0	34.70	0.167	0.887	35.30	0.270	0.180
60.0	33.24	0.166	0.882	34.61	0.270	0.177
180.0	32.78	0.164	0.860	33.27	0.270	0.177
300.0	33.92	0.163	0.858	34.08	0.270	0.177
420.0	33.57	0.161	0.843	-	-	-
480.0	-	-	-	34.54	0.269	0.176
600.0	36.51	0.162	0.852	33.29	0.269	0.177
720.0	35.47	0.160	0.840	33.18	0.268	0.175
900.0	-	-	-	34.08	0.269	0.177
1080.0	-	-	-	33.40	0.270	0.177

Table B8.2: Interfacial Data for the System: M2/0.25 mM NaOH

Time in (Secs)	DROP NO 1			DROP NO 2		
	IFT (mN/m)	Surf Area ($m^2 \times 10^4$)	Drop Vol ($m^3 \times 10^7$)	IFT (mN/m)	Surf Area ($m^2 \times 10^4$)	Drop Vol ($m^3 \times 10^7$)
5.0	32.50	0.246	0.154	33.36	0.262	0.170
30.0	33.21	0.246	0.155	-	-	-
60.0	32.94	0.247	0.155	33.15	0.263	0.171
180.0	33.38	0.245	0.153	32.94	0.261	0.169
300.0	34.17	0.243	0.152	32.96	0.260	0.167
420.0	33.23	0.241	0.150	-	-	-
480.0	-	-	-	33.21	0.257	0.166
600.0	32.39	0.239	0.148	33.32	0.258	0.166
720.0	32.77	0.239	0.149	32.31	0.258	0.166
900.0	31.48	0.238	0.147	32.88	0.257	0.165
1080.0	32.03	0.239	0.148	33.21	0.261	0.170
1200.0	31.83	0.239	0.148	-	-	-

Table B8.3: Interfacial Data for the System: M2/1.25 mM NaOH

Time in (Secs)	DROP NO 1			DROP NO 2		
	IFT (mN/m)	Surf Area ($m^2 \times 10^4$)	Drop Vol ($m^3 \times 10^7$)	IFT (mN/m)	Surf Area ($m^2 \times 10^4$)	Drop Vol ($m^3 \times 10^7$)
5.0	27.92	0.234	0.142	30.59	0.238	0.146
30.0	28.90	0.235	0.144	29.14	0.238	0.146
60.0	28.03	0.234	0.142	30.11	0.238	0.147
180.0	25.72	0.231	0.138	26.85	0.234	0.141
300.0	26.97	0.231	0.139	27.51	0.232	0.140
420.0	26.43	0.228	0.136	-	-	-
480.0	-	-	-	26.66	0.231	0.139
600.0	25.78	0.225	0.134	26.00	0.228	0.137
720.0	28.45	0.227	0.136	26.29	0.229	0.137
900.0	29.58	0.227	0.137	27.24	0.228	0.136
1080.0	27.51	0.224	0.134	27.69	0.227	0.136

Table B8.4: Interfacial Data for the System: M2/2.50 mM NaOH

Time in (Secs)	DROP NO 1			DROP NO 2		
	IFT (mN/m)	Surf Area ($m^2 \times 10^4$)	Drop Vol ($m^3 \times 10^8$)	IFT (mN/m)	Surf Area ($m^2 \times 10^4$)	Drop Vol ($m^3 \times 10^7$)
5.0	29.11	0.160	0.860	23.86	0.193	0.107
30.0	29.11	0.160	0.854	23.87	0.191	0.106
60.0	27.09	0.161	0.830	23.84	0.191	0.106
180.0	26.20	0.156	0.800	23.22	0.190	0.104
300.0	26.20	0.153	0.770	22.33	0.188	0.102
420.0	24.15	0.150	0.750	-	-	-
480.0	-	-	-	22.96	0.188	0.103
600.0	21.81	0.147	0.720	20.53	0.186	0.101
720.0	23.38	0.147	0.730	19.96	0.187	0.100
900.0	-	-	-	19.68	0.187	0.101

Table B8.5: Interfacial Data for the System: M2/12.50 mM NaOH

Time in (Secs)	DROP NO 1			DROP NO 2		
	IFT (mN/m)	Surf Area ($m^2 \times 10^5$)	Drop Vol ($m^3 \times 10^8$)	IFT (mN/m)	Surf Area ($m^2 \times 10^5$)	Drop Vol ($m^3 \times 10^8$)
5.0	8.63	0.670	0.220	9.03	0.698	0.230
30.0	7.75	0.663	0.216	8.02	0.707	0.236
60.0	8.24	0.650	0.211	8.02	0.700	0.232
120.0	9.64	0.623	0.200	9.28	0.700	0.232
180.0	12.11	0.588	0.188	11.32	0.672	0.230
240.0	18.60	0.581	0.186	13.20	0.664	0.224
300.0	18.38	0.550	0.180	12.46	0.652	0.222
360.0	-	-	-	19.54	0.656	0.222

Table B8.6: Interfacial Data for the System: M2/25.00 mM NaOH

Time in (Secs)	DROP NO 1			DROP NO 2		
	IFT (mN/m)	Surf Area ($m^2 \times 10^5$)	Drop Vol ($m^3 \times 10^8$)	IFT (mN/m)	Surf Area ($m^2 \times 10^5$)	Drop Vol ($m^3 \times 10^8$)
5.0	4.88	0.557	0.163	5.62	0.440	0.118
30.0	3.65	-	-	4.76	0.439	0.117
60.0	4.50	0.564	0.163	4.59	0.439	0.117
90.0	4.86	0.556	0.163	6.21	0.428	0.116
120.0	5.61	0.550	0.162	7.09	0.427	0.115
180.0	9.53	0.541	0.164	10.02	0.423	0.115
240.0	11.50	0.540	0.165	13.64	0.420	0.114
300.0	14.19	0.537	0.165	-	-	-

Table B8.7 : Interfacial Data for the System: M2/125.00 mM NaOH

Time in (Secs)	DROP NO 1			DROP NO 2		
	IFT (mN/m)	Surf Area ($m^2 \times 10^5$)	Drop Vol ($m^3 \times 10^9$)	IFT (mN/m)	Surf Area ($m^2 \times 10^5$)	Drop Vol ($m^3 \times 10^9$)
5.0	2.95	0.190	0.340	3.64	0.212	0.410
20.0	2.65	0.200	0.374	3.00	0.220	0.430
40.0	2.58	0.207	0.389	2.59	0.223	0.431
60.0	2.98	0.205	0.389	2.99	0.216	0.416
80.0	3.68	0.210	0.407	4.34	0.215	0.420
100.0	4.80	0.214	0.423	5.84	0.213	0.419
120.0	4.86	0.216	0.428	7.85	0.214	0.426
140.0	6.07	0.220	0.440	8.80	0.214	0.426

B.4.3 Data for M3/Caustic Systems

Table B9.1: Interfacial Data for the System: M3/Double Distilled Water

Time in (Secs)	DROP NO 1			DROP NO 2		
	IFT (mN/m)	Surf Area ($m^2 \times 10^4$)	Drop Vol ($m^3 \times 10^7$)	IFT (mN/m)	Surf Area ($m^2 \times 10^4$)	Drop Vol ($m^3 \times 10^7$)
5.0	34.76	0.269	0.176	35.47	0.292	0.198
30.0	35.53	0.269	0.176	-	-	-
60.0	33.85	0.268	0.175	34.73	0.291	0.197
180.0	34.21	0.266	0.173	34.18	0.290	0.195
300.0	34.66	0.266	0.173	35.91	0.292	0.197
420.0	33.36	0.264	0.172	-	-	-
480.0	-	-	-	34.28	0.289	0.194
600.0	33.79	0.264	0.171	35.18	0.290	0.195
720.0	33.82	0.264	0.171	34.97	0.289	0.195
900.0	34.41	0.265	0.172	34.74	0.289	0.194
1080.0	-	-	-	35.40	0.291	0.196
1200.0	33.33	0.265	0.172	-	-	-

Table B9.2: Interfacial Data for the System: M3/0.25 mM NaOH

Time in (Secs)	DROP NO 1			DROP NO 2		
	IFT (mN/m)	Surf Area ($m^2 \times 10^4$)	Drop Vol ($m^3 \times 10^7$)	IFT (mN/m)	Surf Area ($m^2 \times 10^4$)	Drop Vol ($m^3 \times 10^7$)
5.0	32.46	0.202	0.117	33.08	0.240	0.149
60.0	31.40	0.202	0.117	30.91	0.239	0.148
180.0	32.04	0.202	0.117	30.32	0.238	0.147
300.0	31.45	0.201	0.116	30.23	0.237	0.146
420.0	31.12	0.200	0.115	-	-	-
480.0	-	-	-	30.86	0.237	0.146
600.0	31.22	0.200	0.115	29.69	0.237	0.144
720.0	31.58	0.201	0.116	31.16	0.237	0.146
900.0	31.40	0.200	0.115	29.74	0.235	0.144
1080.0	31.07	0.200	0.115	31.54	0.236	0.145
1200.0	-	-	-	30.66	0.235	0.144

Table B9.3: Interfacial Data for the System: M3/1.25 mM NaOH

Time in (Secs)	DROP NO 1			DROP NO 2		
	IFT (mN/m)	Surf Area ($m^2 \times 10^4$)	Drop Vol ($m^3 \times 10^7$)	IFT (mN/m)	Surf Area ($m^2 \times 10^4$)	Drop Vol ($m^3 \times 10^7$)
5.0	26.34	0.213	0.124	27.58	0.218	0.128
30.0	26.71	0.214	0.125	-	-	-
60.0	24.60	0.213	0.124	25.93	0.218	0.128
180.0	24.92	0.215	0.126	24.77	0.216	0.126
300.0	25.07	0.216	0.126	24.77	0.216	0.126
420.0	23.42	0.213	0.123	-	-	-
480.0	-	-	-	24.09	0.215	0.125
600.0	21.93	0.212	0.122	24.40	0.215	0.125
720.0	21.72	0.212	0.122	24.68	0.215	0.125
900.0	22.79	0.215	0.124	25.56	0.216	0.126
1080.0	22.40	0.215	0.124	25.06	0.214	0.124

Table B9.4: Interfacial Data for the System: M3/2.50 mM NaOH

Time in (Secs)	DROP NO 1			DROP NO 2		
	IFT (mN/m)	Surf Area ($m^2 \times 10^4$)	Drop Vol ($m^3 \times 10^8$)	IFT (mN/m)	Surf Area ($m^2 \times 10^4$)	Drop Vol ($m^3 \times 10^8$)
5.0	23.54	0.100	0.420	25.64	0.153	0.770
30.0	22.86	0.100	0.421	25.01	0.153	0.770
60.0	25.03	0.102	0.430	22.07	0.152	0.760
120.0	21.65	0.099	0.411	-	-	-
180.0	18.05	0.099	0.407	22.61	0.151	0.756
300.0	13.66	0.099	0.401	19.86	0.149	0.740
420.0	13.27	0.099	0.405	19.78	0.149	0.740
600.0	15.03	0.100	0.412	15.30	0.151	0.740
720.0	15.05	0.098	0.403	13.58	0.152	0.735

Table B9.5: Interfacial Data for the System: M3/12.50 mM NaOH

Time (Secs)	IFT (mN/m)	Surf Area ($m^2 \times 10^5$)	Drop Vol ($m^3 \times 10^8$)
5.0	5.23	0.620	0.195
30.0	4.85	0.640	0.200
60.0	6.77	0.631	0.200
120.0	9.37	0.622	0.200
180.0	7.31	0.600	0.189
240.0	12.31	0.604	0.195
300.0	14.31	0.589	0.189
360.0	15.30	0.580	0.185

Table B9.6 : Interfacial Data for the System: M3/25.00 mM NaOH

Time (Secs)	IFT (mN/m)	Surf Area ($m^2 \times 10^5$)	Drop Vol ($m^3 \times 10^9$)
5.0	1.39	-	-
20.0	1.29	-	-
40.0	1.52	-	-
60.0	2.05	-	-
80.0	3.56	0.310	0.730
100.0	4.45	0.305	0.710
120.0	5.99	0.308	0.722
140.0	7.27	0.305	0.713
160.0	8.80	0.300	0.703

B.4.4 Data for M4/Caustic Systems

Table B10.1: Interfacial Data for the System: M4/Double Distilled Water

Time in (Secs)	DROP NO 1			DROP NO 2		
	IFT (mN/m)	Surf Area ($m^2 \times 10^4$)	Drop Vol ($m^3 \times 10^7$)	IFT (mN/m)	Surf Area ($m^2 \times 10^4$)	Drop Vol ($m^3 \times 10^7$)
5.0	39.23	0.280	0.190	36.54	0.280	0.190
30.0	36.26	0.280	0.188	-	-	-
60.0	37.93	0.281	0.189	34.61	0.281	0.187
180.0	35.68	0.273	0.180	35.10	0.280	0.186
300.0	34.48	0.270	0.176	34.50	0.277	0.184
420.0	33.99	0.266	0.174	-	-	-
480.0	-	-	-	32.79	0.275	0.181
600.0	35.38	0.266	0.174	34.98	0.276	0.183
720.0	35.65	0.264	0.173	33.76	0.275	0.181
900.0	34.71	0.262	0.170	34.61	0.275	0.182
1080.0	-	-	-	33.94	0.274	0.180
1200.0	34.60	0.261	0.170	-	-	-

Table B10.2: Interfacial Data for the System: M4/0.25 mM NaOH

Time in (Secs)	DROP NO 1			DROP NO 2		
	IFT (mN/m)	Surf Area ($m^2 \times 10^4$)	Drop Vol ($m^3 \times 10^7$)	IFT (mN/m)	Surf Area ($m^2 \times 10^4$)	Drop Vol ($m^3 \times 10^7$)
5.0	32.75	0.215	0.128	33.16	0.224	0.136
60.0	31.84	0.214	0.127	31.93	0.224	0.136
180.0	32.27	0.214	0.127	32.65	0.224	0.136
300.0	32.57	0.215	0.128	32.88	0.224	0.136
420.0	31.02	0.213	0.125	-	-	-
480.0	-	-	-	31.25	0.222	0.132
600.0	30.81	0.212	0.125	32.38	0.220	0.132
720.0	33.13	0.213	0.126	31.52	0.221	0.133
900.0	31.30	0.211	0.124	32.52	0.220	0.132
1080.0	31.10	0.211	0.124	33.50	0.220	0.132
1200.0	-	-	-	32.74	0.220	0.132

Table B10.3: Interfacial Data for the System: M4/1.25 mM NaOH

Time in (Secs)	DROP NO 1			DROP NO 2		
	IFT (mN/m)	Surf Area ($m^2 \times 10^4$)	Drop Vol ($m^3 \times 10^7$)	IFT (mN/m)	Surf Area ($m^2 \times 10^4$)	Drop Vol ($m^3 \times 10^7$)
5.0	28.32	0.206	0.119	28.57	0.189	0.105
30.0	26.34	0.205	0.118	-	-	-
60.0	25.43	0.204	0.117	27.40	0.188	0.104
180.0	25.30	0.206	0.118	25.31	0.187	0.104
300.0	22.96	0.203	0.115	26.25	0.188	0.104
420.0	23.76	0.205	0.117	-	-	-
480.0	-	-	-	23.50	0.184	0.101
600.0	23.34	0.204	0.116	24.30	0.186	0.102
720.0	22.97	0.205	0.116	23.94	0.186	0.102
900.0	23.14	0.204	0.116	24.88	0.186	0.102
1080.0	24.02	0.205	0.117	24.55	0.186	0.102
1200.0	-	-	-	24.47	0.185	0.101

Table B10.4: Interfacial Data for the System: M4/2.50 mM NaOH

Time in (Secs)	DROP NO 1			DROP NO 2		
	IFT (mN/m)	Surf Area ($m^2 \times 10^4$)	Drop Vol ($m^3 \times 10^8$)	IFT (mN/m)	Surf Area ($m^2 \times 10^4$)	Drop Vol ($m^3 \times 10^8$)
5.0	27.58	0.159	0.820	23.33	0.147	0.730
30.0	22.97	0.156	0.800	25.06	0.148	0.740
60.0	22.91	0.158	0.800	23.81	0.147	0.732
180.0	20.94	0.158	0.802	19.90	0.146	0.720
300.0	17.93	0.157	0.790	15.03	0.148	0.720
420.0	17.50	0.158	0.792	-	-	-
480.0	-	-	-	12.54	0.151	0.721
600.0	16.04	0.158	0.789	-	-	-
720.0	11.79	0.160	0.776	-	-	-
1080.0	11.27	0.162	0.785	-	-	-

Table B10.5: Interfacial Data for the System: M4/12.50 mM NaOH

Time in (Secs)	DROP NO 1			DROP NO 2		
	IFT (mN/m)	Surf Area ($m^2 \times 10^5$)	Drop Vol ($m^3 \times 10^9$)	IFT (mN/m)	Surf Area ($m^2 \times 10^5$)	Drop Vol ($m^3 \times 10^9$)
3.0	1.15	-	-	-	-	-
10.0	0.89	-	-	0.99	-	-
20.0	1.05	-	-	1.22	-	-
30.0	2.01	0.230	0.460	1.98	0.240	0.490
40.0	2.52	0.230	0.440	2.56	0.233	0.470
50.0	4.07	0.224	0.455	3.05	0.227	0.460
60.0	4.70	0.220	0.441	4.46	0.224	0.460
70.0	6.89	0.220	0.444	6.83	0.227	0.474
80.0	7.04	0.220	0.435	5.50	0.220	0.450
90.0	9.64	0.220	0.437	7.06	0.221	0.452

Table B10.6: Interfacial Data for the System: M4/25.00 mM NaOH

Time in (Secs)	DROP NO 1			DROP NO 2		
	IFT (mN/m)	Surf Area ($m^2 \times 10^5$)	Drop Vol ($m^3 \times 10^9$)	IFT (mN/m)	Surf Area ($m^2 \times 10^5$)	Drop Vol ($m^3 \times 10^9$)
3.0	0.88	-	-	-	-	-
10.0	1.14	-	-	0.87	-	-
20.0	1.23	-	-	1.27	-	-
30.0	1.40	-	-	2.58	0.193	0.360
40.0	2.04	0.240	0.490	3.20	0.180	0.331
50.0	2.03	0.234	0.470	3.45	0.170	0.304
60.0	3.01	0.235	0.485	5.56	0.166	0.301
70.0	4.23	0.235	0.486	-	-	-

B.4.5 Data for M5/Caustic Systems

Table B11.1: Interfacial Data for the System: M5/Double Distilled Water

Time in (Secs)	DROP NO 1			DROP NO 2		
	IFT (mN/m)	Surf Area ($m^2 \times 10^4$)	Drop Vol ($m^3 \times 10^7$)	IFT (mN/m)	Surf Area ($m^2 \times 10^4$)	Drop Vol ($m^3 \times 10^7$)
5.0	40.49	0.283	0.191	36.63	0.262	0.170
60.0	37.94	0.285	0.192	35.77	0.261	0.170
180.0	36.85	0.283	0.190	34.81	0.261	0.169
300.0	37.23	0.284	0.191	35.31	0.261	0.169
420.0	37.01	0.285	0.192	-	-	-
480.0	-	-	-	33.54	0.260	0.168
600.0	37.71	0.287	0.194	35.08	0.264	0.172
720.0	38.79	0.288	0.196	35.04	0.264	0.172
900.0	36.08	0.288	0.195	34.29	0.263	0.171
1080.0	-	-	-	33.07	0.263	0.170
1200.0	37.61	0.290	0.199	34.31	0.265	0.172

Table B11.2: Interfacial Data for the System: M5/0.25 mM NaOH

Time in (Secs)	DROP NO 1			DROP NO 2		
	IFT (mN/m)	Surf Area ($m^2 \times 10^4$)	Drop Vol ($m^3 \times 10^7$)	IFT (mN/m)	Surf Area ($m^2 \times 10^4$)	Drop Vol ($m^3 \times 10^7$)
5.0	31.87	0.196	0.112	32.24	0.214	0.127
60.0	32.45	0.197	0.112	30.97	0.213	0.126
180.0	33.24	0.198	0.113	30.47	0.214	0.126
300.0	31.61	0.197	0.113	30.12	0.214	0.126
420.0	28.05	0.195	0.111	-	-	-
480.0	-	-	-	32.12	0.216	0.128
600.0	32.52	0.198	0.114	29.99	0.215	0.127
720.0	31.31	0.197	0.113	28.69	0.213	0.125
900.0	31.66	0.198	0.113	30.50	0.213	0.126
1080.0	29.90	0.197	0.113	30.95	0.215	0.127

Table B11.3: Interfacial Data for the System: M5/1.25 mM NaOH

Time in (Secs)	DROP NO 1			DROP NO 2		
	IFT (mN/m)	Surf Area ($m^2 \times 10^4$)	Drop Vol ($m^3 \times 10^8$)	IFT (mN/m)	Surf Area ($m^2 \times 10^4$)	Drop Vol ($m^3 \times 10^7$)
5.0	29.58	0.177	0.967	27.80	0.190	0.106
30.0	28.12	0.178	0.967	-	-	-
60.0	28.12	0.178	0.970	25.78	0.190	0.106
180.0	26.66	0.180	0.980	24.81	0.191	0.106
300.0	25.08	0.179	0.970	22.99	0.189	0.105
420.0	26.05	0.180	0.980	-	-	-
480.0	-	-	-	24.19	0.189	0.105
600.0	25.57	0.180	0.987	22.77	0.188	0.104
720.0	24.71	0.180	0.981	23.09	0.189	0.104
900.0	23.89	0.180	0.981	23.87	0.188	0.103
1080.0	24.01	0.182	0.991	22.83	0.188	0.103
1200.0	-	-	-	23.64	0.190	0.105

Table B11.4: Interfacial Data for the System: M5/2.50 mM NaOH

Time in (Secs)	DROP NO 1			DROP NO 2		
	IFT (mN/m)	Surf Area ($m^2 \times 10^4$)	Drop Vol ($m^3 \times 10^8$)	IFT (mN/m)	Surf Area ($m^2 \times 10^4$)	Drop Vol ($m^3 \times 10^8$)
5.0	24.13	0.111	0.486	24.85	0.120	0.550
30.0	20.99	0.110	0.478	27.82	0.119	0.542
60.0	22.29	0.111	0.484	26.12	0.119	0.539
120.0	22.30	0.111	0.488	-	-	-
180.0	16.41	0.111	0.481	21.66	0.118	0.535
300.0	9.21	0.116	0.490	18.06	0.120	0.538
420.0	8.37	0.119	0.499	15.46	0.121	0.542
600.0	7.54	0.119	0.487	12.48	0.124	0.552
720.0	9.01	0.119	0.503	10.70	0.124	0.547
900.0	10.27	0.115	0.487	11.77	0.132	0.545

Table B11.5: Interfacial Data for the System: M5/12.50 mM NaOH

Time in (Secs)	DROP NO 1			DROP NO 2		
	IFT (mN/m)	Surf Area ($m^2 \times 10^5$)	Drop Vol ($m^3 \times 10^9$)	IFT (mN/m)	Surf Area ($m^2 \times 10^5$)	Drop Vol ($m^3 \times 10^9$)
3.0	0.61	-	-	0.57	-	-
10.0	0.96	-	-	1.23	0.180	0.318
20.0	1.57	0.168	0.294	1.72	0.180	0.331
30.0	2.13	0.170	0.305	2.18	0.173	0.310
40.0	2.34	0.171	0.306	1.17	0.160	0.260
50.0	2.04	0.168	0.300	1.69	0.160	0.275
60.0	2.37	0.171	0.306	2.45	0.161	0.281
70.0	2.59	0.169	0.304	5.54	0.162	0.288
90.0	4.09	0.168	0.303	-	-	-

Table B11.6: Interfacial Data for the System: M5/25.00 mM NaOH

Time in (Secs)	DROP NO 1			DROP NO 2		
	IFT (mN/m)	Surf Area ($m^2 \times 10^5$)	Drop Vol ($m^3 \times 10^9$)	IFT (mN/m)	Surf Area ($m^2 \times 10^5$)	Drop Vol ($m^3 \times 10^9$)
3.0	0.62	-	-	0.66	-	-
10.0	1.32	0.140	0.240	0.95	-	-
20.0	2.16	0.140	0.242	1.46	0.180	0.330
30.0	4.00	0.138	0.233	1.53	0.173	0.310
40.0	-	-	-	1.58	0.164	0.287
50.0	3.77	0.130	0.220	3.22	0.164	0.299
60.0	-	-	-	3.25	0.160	0.260

Appendix C

Model Calculations

C.1 Standard Errors of the Equilibrium Model Estimates

C.1.1 Calculation of Pure Error Variance

Pure error variance is defined as follows [96,97];

$$\hat{\sigma^2} = \sum_{u=1}^{m} (y_u - \bar{y})^2/m - 1 \qquad (C.1)$$

Since we have two replicates per run, $m = 2$, and the associated pure error variances for each run become ;

(Run 1) for 0.3125 mM Oleic in HD / 0.25 mM NaOH ;

$$\begin{aligned} y_u &= 10.99, 11.11 \quad mN/m \\ \bar{y} &= 11.05 \quad mN/m \end{aligned}$$

from equation C.1 , we then have that ;

$$\hat{\sigma_1^2} = 0.0072 \qquad (C.2)$$

(Runs 2&3) C_{OH} = 1.25, 2.50 mM respectively . For Run No 2 , the following obtains ;

$$\begin{aligned} y_u &= 14.92, 14.92 \quad mN/m \\ \text{and hence,} \quad \hat{\sigma_2^2} &= 0.0 \end{aligned}$$

however for Run No 3 , we have the following ;

$$\begin{aligned} y_u &= 15.08, 15.53 \quad mN/m \\ \bar{y} &= 15.305 \quad mN/m \\ \hat{\sigma_3^2} &= 0.10125 \end{aligned}$$

(Run 4) C_{OH} = 12.50 mM

$$\begin{aligned} y_u &= 27.23, 26.94 \quad mN/m \\ \bar{y} &= 27.085 \quad mN/m \\ \hat{\sigma_4^2} &= 0.04205 \end{aligned}$$

The global pure error variance is given by ;

$$\hat{\sigma}_p^2 = \sum_{i=1}^{l}(m_i - 1)\hat{\sigma}_i^2 / \sum_{i=1}^{l} m_i - 1 \qquad (C.3)$$

since, $l = 4$,

$$\begin{aligned}\hat{\sigma}_p^2 &= \sum_{i=1}^{4}\hat{\sigma}_i^2/4 \\ &= 0.1505/4 \\ &= 0.0376\end{aligned}$$

C.1.2 Calculation of Residual Sum of Squares Less Pure Error

The residual sum of squares corrected for pure error is given by Bacon[96] as the following ;

$$\begin{aligned}\sum_{u=1}^{N}(\bar{y_u} - \hat{y_u})^2 &= \sum_{u=1}^{N} e_u^2 - \sum_{u=1}^{N}(y_u - \bar{y_u})^2 \\ &= SSR - \hat{\sigma}_p^2 \sum_{i=1}^{l} m_i - 1 \qquad (C.4)\end{aligned}$$

The value of SSQ determined from our parameter estimation routine was 52.5077 ; thus the corrected residual sum of squares becomes ;

$$\sum(\bar{y_u} - \hat{y_u})^2 = 52.3572$$

C.1.3 Calculation of R

The ratio R , is given by the following ;

$$R = \sum(\bar{y_u} - \hat{y_u})^2 / (N - p - \sum_{i=1}^{l} m_i - 1) \qquad (C.5)$$

plugging the already calculated quantities , the result becomes ;

$$\begin{aligned}R &= 52.3572/(8 - 2 - 4) \\ &= 26.18\end{aligned}$$

We now compute the degrees of freedom for the F-distribution as follows ;

$$\begin{aligned}\nu_1 &= N - p - \sum_{i=1}^{l}(m_i - 1) \\ &= 2 \\ \nu_2 &= \sum_{i=1}^{l}(m_i - 1) \\ &= 4\end{aligned}$$

The F-distribution at 1% level , $F_{\nu_1,\nu_2} = 18.00$.

C.1.4 The Covariance Matrix

In linear least square regression , the covariance matrix is given as ;

$$V(\hat{\theta}) = (X^T X)^{-1}\hat{\sigma}^2 \qquad (C.6)$$

with $\hat{\sigma}$ defined as follows ;

$$\hat{\sigma}^2 = SSR/(N - p) \qquad (C.7)$$

substituting previously determined values in equation C.7 we finally obtain the value of the pure error variance as follows ;

$$\begin{aligned}\hat{\sigma}^2 &= 52.5077/6 \\ &= 8.7513\end{aligned}$$

Bard[98] has suggested that for nonlinear regression, $(X^T X)$ may be approximated by the Hessian, $H_i(\hat{\theta})$. In the IMSL's Levenberg-Marquardt algorithm , ZSSQ , the Hessian is approximated by $2J_i^T J_i$, for small values of SSR [84] . The matrix $J_i^T J_i$ as determined from our parameter estimation routine had very large elements . Thus matrix inversion was done manually employing the procedure outlined by Hornbeck[115] . The inverse Hessian thus becomes ;

$$H_i^{-1} = 10^{-9}\begin{bmatrix} 0.336838 & -0.113085 \\ -0.113085 & 0.209634 \end{bmatrix}$$

Substituting into equation C.6 , we obtain the covariances for the parameters thus ;

$$\begin{aligned} V(\theta_1) &= 0.33683810^{-9} \times 8.75128 \\ S.E.(\theta_1) &= \sqrt{V(\theta_1)} \\ &= 5.429 \times 10^{-5}\end{aligned}$$

similarly for θ_2 , the result is as follows ;

$$\begin{aligned} S.E.(\theta_2) &= \sqrt{V(\theta_2)} \\ &= 4.283 \times 10^{-5}\end{aligned}$$

C.1.5 Confidence Intervals

For each parameter, the confidence interval is given as follows ;

$$\theta_i \pm t(\nu, 1 - 1/2\alpha)S.E.(\theta_i) \qquad (C.8)$$

where ν is defined as ;

$$\nu = N - p \qquad (C.9)$$

The 95% confidence level of the t- distribution gives ;

$$t(6, 0.05) = 2.447 \qquad (C.10)$$

Thus , substituting in equation C.8 , we obtain the following ;

$$\begin{aligned} \theta_1 &\equiv 10^{-3}[\theta_1 \pm 2.447(5.429 \times 10^{-5})] \\ \theta_1 &= 10^{-3}[\theta_1 \pm 1.3285 \times 10^{-4}] \end{aligned}$$

in other words , the 95% confidence limits for K^D_{HX} becomes ;

$$K^D_{HX} = [2.14 \pm 1.33] \times 10^{-7} \quad M \tag{C.11}$$

similarly the confidence interval based on θ_2 becomes ;

$$K^D_{NaX} = [1.16 \pm 1.05] \times 10^{-4} \quad M \tag{C.12}$$

C.2 Calculation of Diffusion Coefficients

C.2.1 Estimation of Molar Volumes

By Schroeder's Method

Pertinent group contributions for the elements that make up the molecular structure of each acid are taken from Table 11 of Ref[81] . Thus for lauric acid , Schroeder's method gives the following result ;

$$\begin{aligned} V_b &= 12 \times 7 + 24 \times 7 + 2 \times 7 \\ &= 226 \quad cm^3/mole \end{aligned}$$

similarly for oleic acid , the molar volume becomes ;

$$\begin{aligned} V_b &= 18 \times 7 + 34 \times 7 + 2 \times 7 + 7 \\ &= 385 \quad cm^3/mole \end{aligned}$$

By the Method of Le Bas

Group contributions were also taken from Reid et al. [81] and for lauric acid , the molar volume estimated by this method is as follows ;

$$\begin{aligned} V_b &= 12 \times 14.8 + 24 \times 3.7 + 2 \times 24 \\ &= 314.4 \quad cm^3/mole \end{aligned}$$

for oleic acid , Le Bas method yields the following result ;

$$\begin{aligned} V_b &= 18 \times 14.8 + 34 \times 3.7 + 12 \times 2 \\ &= 416.2 \quad cm^3/mole \end{aligned}$$

Since there is a significant disparity in the above estimates of molar volumes of the acids , we now employ the correlation of Tyn and Calus (see equation [9.1]) as detailed below.

Group	ΔV_i	M_i	$\Delta V_i M_i$
$-CH_3-$	3.360	15.03	50.50
$-CH_2-$	3.360	14.03	47.14
-CHOOH	1.652	45.02	74.37

Group	ΔV_i	M_i	$\Delta V_i M_i$
$-CH_3-$	3.360	15.03	50.50
$-CH_2-$	3.360	14.03	47.14
$-CH=$	2.940	13.02	38.28
-CHOOH	1.652	45.02	74.37

The Correlation of Tyn and Calus

We begin by estimating the critical volumes of the acids by the Vetere's method[81] as follows ; For lauric acid, the table of property values is as follows ; The contributing groups for oleic acid are necessarily different from those of lauric and the pertinent table becomes the following ; The expression for the critical volume then becomes ;

$$V_c = 33.04 + [\sum \Delta V_i M_i]^{1.029} \qquad (C.13)$$

By substituting values obtained from the above tables in equation C.13 , the critical volume of lauric acid becomes ;

$$\begin{aligned} V_c &= 33.04 + 596.27^{1.029} \\ &= 750.7199 \quad cm^3/mole \end{aligned}$$

and for oleic acid , the critical volume is given as follows ;

$$\begin{aligned} V_c &= 33.04 + 823.11^{1.029} \\ &= 1033.0542 \quad cm^3/mole \end{aligned}$$

Finally in accordance with equation 9.1 , the solute molar volume for lauric acid is given by ;

$$\begin{aligned} V_b &= 0.285 \times 750.7199^{1.048} \\ &= 294.0 \quad cm^3/mole \end{aligned}$$

the corresponding value for oleic acid becomes ;

$$\begin{aligned} V_b &= 0.285 \times 1033.0542^{1.048} \\ &= 410.81 \quad cm^3/mole \end{aligned}$$

C.2.2 Calculation of Diffusivities by the Wilke-Chang Correlation

Diffusivity in Hexadecane

The correlation had already been presented as equation 9.2 . The requisite quantities for the evaluation of the diffusivity are as follows;

$$\begin{aligned} M_B &= 226.45 \\ \eta_B &= 3.271 \quad cp \\ \omega_d &= 1.0 \\ T &= 298 \quad K \end{aligned}$$

The molar volume of lauric acid as estimated in the previous section was 294.0 cm^3/mole , while the corresponding value for oleic acid was 410.81 cm^3/mole . We now substitute all the quantities into equation 9.2 and the acid diffusivities are evaluated as ;

$$D^{\circ}_{lauric-HD} = 3.351 \times 10^{-6} \quad cm^2/s$$
$$D^{\circ}_{oleic-HD} = 2.742 \times 10^{-6} \quad cm^2/s$$

Diffusivities in Water

For water the relevant parameter values are as follows ;

$$\omega_d = 2.6$$
$$M_B = 18.02$$
$$\eta_B = 0.8937 \quad cp$$

A similar substitution in equation 9.2 yields the diffusivities as ;

$$D^{\circ}_{lauric-water} = 5.577 \times 10^{-6} \quad cm^2/s$$
$$D^{\circ}_{oleic-water} = 4.562 \times 10^{-6} \quad cm^2/s$$

C.2.3 Calculation of Diffusivities with the Hayduk-Minhas Correlation

Diffusivities in Hexadecane

The Hayduk-Minhas correlation[105] applicable to paraffinic hydrocarbons was given in chapter 9 as equations 9.3 and 9.4 . Firstly , we evaluate molar volume function, ϵ , which for lauric acid takes the value of -0.7563, while the corresponding value for oleic acid is -0.7662 . Equation 9.3 can then be solved and the resulting diffusivity of lauric acid , namely , $D^{\circ}_{lauric-HD}$, is 4.161×10^{-6}, cm^2/s . The corresponding value for oleic acid , $D^{\circ}_{oleic-HD}$, becomes 3.242×10^{-6} , cm^2/s .

Diffusivity in Water

For diffusivities in water , Hayduk and Minhas[105] proposed a different set of equations which was presented as equations 9.5 and 9.6 . The function ϵ^* was evaluated for lauric acid as -1.0874, while the corresponding value for oleic acid became -1.09668 . Plugging the values of all relevant quantities in equation 9.5 , we obtain the acid diffusivities thus ;

$$D^{\circ}_{lauric-water} = 3.879 \times 10^{-6} \quad cm^2/s$$
$$D^{\circ}_{oleic-water} = 2.178 \times 10^{-6} \quad cm^2/s$$

C.3 Calculation of Nernstian Film Thicknesses

In chapter 9 , a simplified relationship , (equation 9.23), for the estimation of Nernstian boundary layer thicknesses , namely , δ_o and δ_w, was derived. Reference values of the boundary layer thicknesses can be calculated on the basis of the work done by Rubin and Radke[60] and the analysis

of deZabala[18] . Two dimensionless rate parameters were proposed by Rubin and Radke[60] as follows;

$$\lambda_1 = \delta_1/H_{c,1} \quad (C.14)$$

$$\lambda_2 = \delta_2/H_{c,2} \quad (C.15)$$

The value of these rate parameters used consistently by the authors throughout their work was 0.10 . deZabala[18] also rationalized that for oil-water systems , the Henry's law constants should have roughly the following values ;

$$H_{c,1} = 10^{-7} \text{ cm}$$

$$H_{c,2} = 2 \times 10^{-6} \text{ cm}$$

By substituting into equations C.14 and C.15 , we obtain the following ;

$$\delta_o = 10^{-8} \text{ cm}$$

$$\delta_w = 2 \times 10^{-7} \text{ cm}$$

For water difffusivity , D_w , deZabala[18] used the value of 2×10^{-6} , cm^2/s . The crude oil studied by deZabala was 40 times more viscous than water . Its diffusivity, D_o, was quoted as 5.0×10^{-8}, cm^2/s . Thus, we have completely specified the reference system which will then enable the use of equation 9.23 to calculate the boundary layer thickness for our system .

Film Thicknesses for the Oleic Acid System

The diffusivity and viscosity for the working oleic acid system are as follows;

$$D_{oleic-HD} = 2.742 \times 10^{-6} \text{ cm}^2/s$$

$$D_{oleic-water} = 4.562 \times 10^{-6} \text{ cm}^2/s$$

$$\nu^*_{oil} = 4.06196 \text{ c. stokes}$$

$$\nu^*_{water} = 1.00 \text{ c. stokes}$$

by a simple substitution into equation 9.23 , the results are as follows,

$$\delta_{o,oleic}/\delta_{o,crude} = 2.60$$

$$\text{thus } \delta_{o,oleic} = 2.60 \times 10^{-8} \text{ cm}$$

In a similar manner , the result for the aqueous phase is given by ;

$$\delta_{w,oleic} = 2.63 \times 10^{-7} \text{ cm}$$

Film Thicknesses for the Lauric Acid System

The transport parameters determined in Appendix C2 were as follows ;

$$D_{lauric-HD} = 3.351 \times 10^{-6} \text{ cm}^2/s$$

$$D_{lauric-water} = 5.577 \times 10^{-6} \text{ cm}^2/s$$

Using the same procedure as was employed in the oleic acid case , we then obtain the corresponding values for lauric acid as follows ;

$$\delta_{o,lauric} = 2.77 \times 10^{-8} \text{ cm}$$

$$\delta_{w,lauric} = 2.81 \times 10^{-7} \text{ cm}$$

Appendix D

Comparative IFT Data from Micropendography, Ring and Spinning Drop Tensiometries

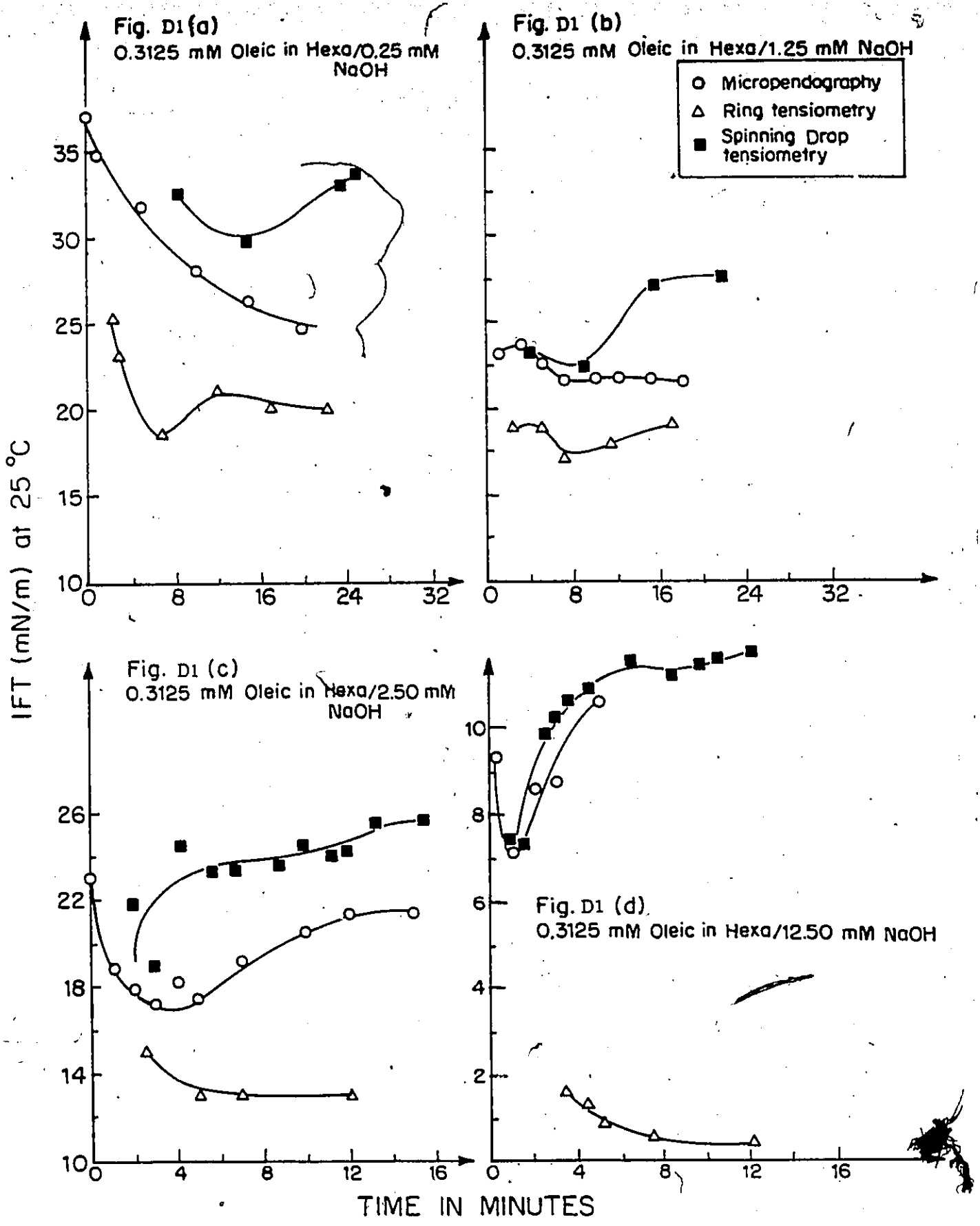

Figure D1 : IFT Data obtained by Micropendography, Ring and Spinning Drop Tensiometries

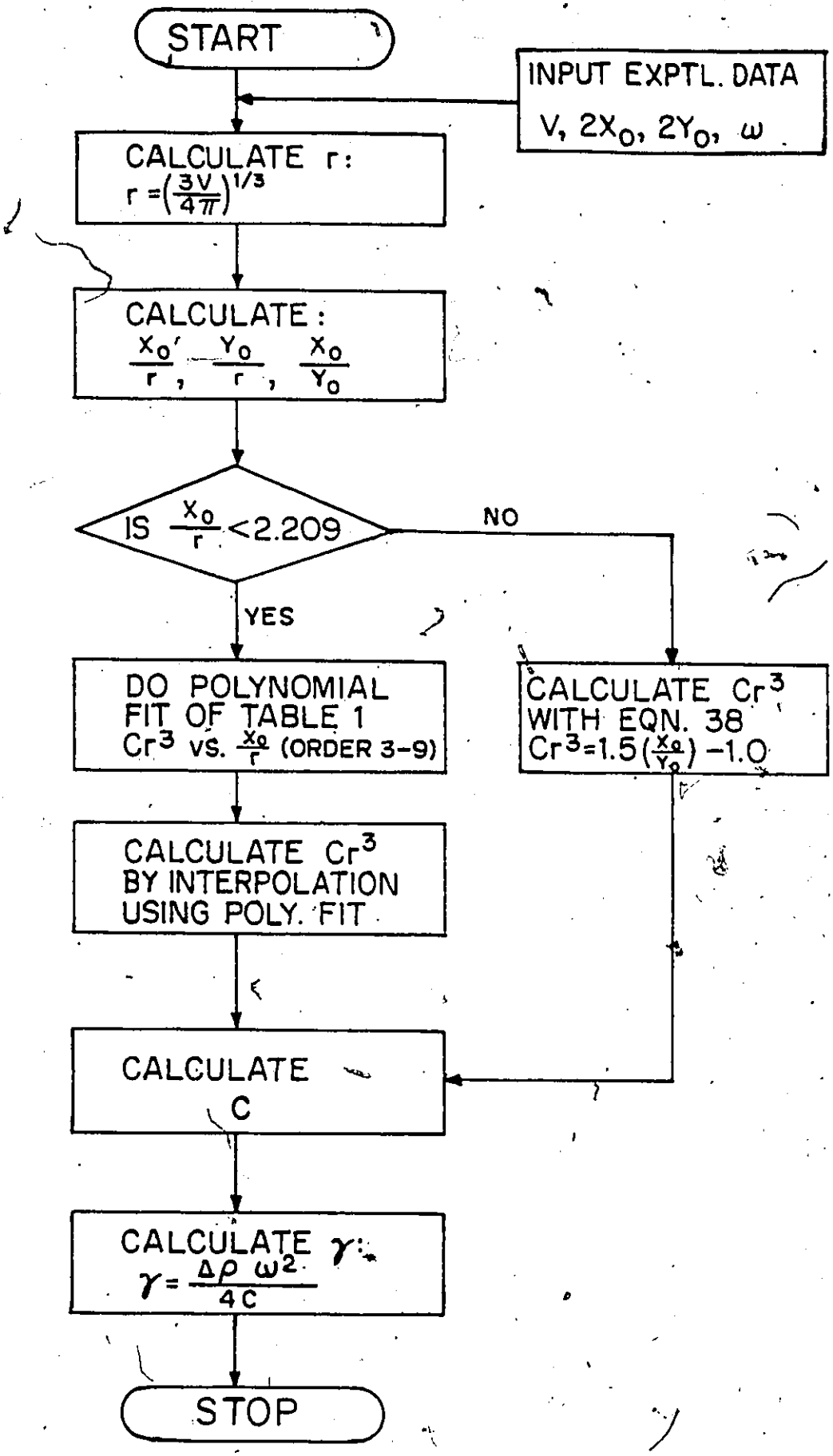

Figure D2 : Flowchart Showing Calculation of IFT with the Solution Scheme of Princen et al.

Table D1: SDT IFTs using various solution schemes for the System: 0.3125 mM Oleic acid/0.25 mM NaOH, Droplet Volume = 1.5 μL, Temp = 26.0 $\pm$0.2° C

Time in Secs	Droplet Dimensions		Period T	IFT Calculated by			
	Length $\times 10^2$ cm	Width $\times 10^2$ cm	msec/rev	Vonnegut's Equation	Slattery & Chen's Soln	Princen et al Table 1	Princen et al Equation 38
500	23.106	17.603	6.59	14.88	32.52	8.57	19.08
900	23.818	17.615	6.59	14.91	29.78	7.89	17.98
1300	23.211	17.699	6.60	15.08	33.06	8.44	19.05
1500	23.359	17.799	6.60	15.33	33.55	8.29	19.03

Table D2: SDT IFTs using various solution schemes for the System: 0.3125 mM Oleic acid/1.25 mM NaOH, Droplet Volume = 1.5 μL, Temp = 27.2 $\pm$0.2° C

Time in Secs	Droplet Dimensions		Period T	IFT Calculated by			
	Length $\times 10^2$ cm	Width $\times 10^2$ cm	msec/rev	Vonnegut's Equation	Slattery & Chen's Soln	Princen et al Table 1	Princen et al Equation 38
240	19.834	16.480	6.58	12.25	37.20	23.03	14.07
530	20.000	16.363	6.59	11.95	33.77	22.18	13.60
930	18.681	16.666	6.60	12.59	59.75	27.05	17.85
1140	18.665	17.788	6.60	15.57	167.09	32.11	17.92
1320	18.768	16.800	6.60	12.90	62.94	27.28	17.49

Table D3: SDT IFTs using various solution schemes for the System: 0.3125 mM Oleic acid/2.50 mM NaOH, Droplet Volume = 2.5 μL, Temp = 27.4 $\pm$0.1° C

Time in Secs	Droplet Dimensions		Period T	IFT Calculated by			
	Length $\times 10^2$ cm	Width $\times 10^2$ cm	msec/rev	Vonnegut's Equation	Slattery & Chen's Soln	Princen et al Table 1	Princen et al Equation 38
120	24.020	17.829	6.57	15.56	31.36	21.76	30.37
180	24.974	16.991	6.60	13.34	22.37	18.87	25.50
250	23.175	17.299	6.60	14.08	28.87	24.65	30.43
340	23.530	17.312	6.60	14.11	27.86	23.26	29.58
400	23.511	17.386	6.61	14.25	28.47	23.26	29.78
470	23.499	17.399	6.61	14.27	28.54	23.30	29.86
530	23.426	17.442	6.61	14.39	29.40	23.58	30.19
600	23.189	17.409	6.61	14.31	29.87	24.52	30.69
670	23.307	16.518	6.61	12.22	22.25	24.04	27.43
720	23.256	16.455	6.61	12.08	21.92	24.24	27.35
800	22.970	17.645	6.61	14.90	33.46	25.45	32.15
870	22.815	17.502	6.61	14.54	32.05	26.16	32.06
930	22.948	17.658	6.61	14.93	33.72	25.55	32.26
1000	22.880	17.478	6.61	14.48	31.94	25.86	31.79